Global Hydroelastic Response of Catamarans due to Wetdeck Slamming

A thesis submitted in partial fulfillment of the
requirements for the degree of Doktor Ingeniør
by

Chunhua Ge

Trondheim, November 2, 2002

Department of Marine Technology
Faculty of Engineering Science and Technology
Norwegian University of Science and Technology

Acknowledgements

This thesis is an interdisciplinary research work in hydroelasticity. It was initiated by one of my supervisors, professor Torgeir Moan at the Department of Marine Technology, Norwegian University of Science and Technology. He has served as my main supervisor and has supervised in the aspects of hydroelasticity and structural mechanics for which he has an outstanding competence. I appreciate his guidance, support and constructive discussions.

Professor Odd M. Faltinsen at the Department of Marine Technology has been my co-supervisor. His vast experience and knowledge in the hydrodynamic and hydroelastic aspects has made it possible to focus deeply into the slamming studies. In the last 1.5 years, professor Faltinsen has been deeply involved in the day-to-day guidance and has supervised most of the details in the thesis. I appreciate his incomparable contribution to this work and unlimited time for guiding me. His encouragement and help in non-academic fields have been invaluable.

I would like to thank Ole D. Økland and Jan V. Aarsnes for their clarification and helpful discussions of the experiments analyzed in this thesis.

Thanks should also be given to Jan R. Hoff in Marintek for his patient help in applying VERES in this work. Discussions about structural dynamics with Mingkang Wu at Marintek also proved helpful to me.

I thank Olav F. Rognebakke and Rolf J. Baarholm for helpful talks regarding wetdeck slamming and programming problems. Abuu K. Mohammed, Gro S. Baarholm and Hanne T. Wist helped me to familiarize with Latex quickly. I also thank Svein Ersdal, Marit Ronæss, Haibo Chen and Rolf J. Baarholm for proof reading this thesis.

The faculty staff and my fellow Ph.D students at the Department of Marine Technology have been offering me a lot of academic and non-academic supports. Their friendship have made the time here memorable. Qinzheng Yang, Naiquan Ye, Kjetil Skaugset, as well as Dongmei Wang should also be mentioned at this aspect.

Comments and questions from Committee members Finn Gunnar Nilsen, Jørgen Juncher Jensen and Svein Skjørdal before final printing have helped in making the thesis clearer. Their work is acknowledged.

Deep thanks go to my beloved husband, Binghua Zhang. His patience, tolerance and love have been supporting and encouraging me ever since we met. This work must also be dedicated to my parents and family members in China. Their devoted supports are always present no matter where I am.

This work has been financially supported by the Strong Point Center on Hydroelasticity funded by NTNU and Marintek. This support is acknowledged.

Abstract

Global hydroelastic effects due to wetdeck slamming on a catamaran at Froude numbers between 0.30 and 0.33 in regular head waves are studied theoretically and experimentally.

The wetdeck has a horizontal transverse cross-section. The important elastic properties of the experimental model are theoretically accounted for by using small elastic beam elements connecting three rigid bodies. The hydrodynamic loads on the side hulls are based on the strip theory by Salvesen *et al.* (1970) without hull interaction. The forward speed causes end terms at the forward ends of the second and third body counted from forward perpendicular (FP). A modal based method is used to include heave, pitch, two-node and three-node vertical bending modes.

The three-body theoretical model without wetdeck slamming agrees well with experimental eigenvalues, relative vertical motions at the bow, vertical shear forces and bending moments at two transverse cuts. Mode shapes agree with Finite Element Method (FEM) results. Five analytically based wetdeck slamming models are presented. The structure is locally rigid and the flow due to slamming is two-dimensional in a longitudinal cross-sectional plane. It is shown sufficient from a global response point of view, to use a Von Karman type of method and a linear approximation of the relative impact velocity. The effect of high forward speed on the slamming loads is investigated by modifying the dynamic free surface condition and including a Kutta condition at the aft end of the wetted deck. The flow is mathematically equivalent to the 2D linear unsteady lifting problem of a thin foil in infinite fluid. An important difference is that the wetted length is time dependent. The Kutta condition model may matter. Both the water entry and exit phases during the slamming are important for global response. The theory gives generally good agreement with experimental results for slamming loads and wetdeck slamming induced global vertical shear forces and bending moments at the two transverse cuts. However, there is one slamming case with unsatisfactory agreement. This is believed to be due to the neglection of piston mode resonance of the fluid motion between the two side hulls. Both theory and experiments show a strong influence of two-node bending on global loads. There is also some influence of the three-node bending, but this is not satisfactorily predicted.

An error analysis in the experiments is made for the most severe slamming case. Since the experiments were not done as a part of this thesis and each test condition was done only once, random errors can not be identified. Systematic errors are discussed and error estimates of experimentally predicted vertical shear forces and bending moments are made by extensively

using the theoretical model. It is shown that the trim angle is the most important error source. The changing incident wave amplitudes along the track of the model and the wave measurement inaccuracies are equally the second most important error source for vertical bending moment at the two transverse cuts investigated in the experiments. The error associated with roll, yaw and sway is the second most important for vertical shear force at the two cuts. The estimated combined relative errors in experimentally predicted vertical shear forces and bending moments are between 0.17 and 0.29.

Error sources in the theory are also discussed. Since no benchmark theoretical model that properly includes all physical effects exists, we must to some extent rely on experimental results. The discussion covers side hull hydrodynamics and hull interaction, slamming modelling, structural modelling and effect of transient phase. It is shown that hydrodynamic hull interaction may matter.

A future perspective is to develop a numerical method that can predict wetdeck slamming induced global response of multihull vessels in any sea state and at any forward speed. This involves long term statistical description of combined load effects due to both transient slamming induced whipping and steady state linear and nonlinear wave loads.

Nomenclature

General Rules

- Symbols are generally defined where they appear in the text for the first time.
- Only the frequently used symbols are listed in this chapter.
- Matrices are represented by bold characters, *e.g.* $\mathbf{A}$.
- Overdots signify differentiation with respect to time, *e.g.* $\ddot{\eta}$, $\dot{\eta}$.

Subscripts

gen	Matrices for the 6 degree-of-freedom three-body system
$j, k = 1, \cdots, 6$	jth or kth degree of freedom for a rigid body
A, B, C, D	Four consecutive ends of the beam connections from the bow towards the stern

Superscripts

$i, j, k = 1, 2, 3$	For ith or jth or kth body in the three-body system
0	Speed independent term
U	Speed dependent term

Roman Letters

a_{jk}	Sectional added mass coefficients for the side hulls
$a(t)$	Ship-fixed x-coordinate of upstream deck-water intersection
A_{jk}	Added mass coefficients
A_n	Fourier coefficients used in expressing V_R as $\sum_0^\infty A_n \cos(n\theta)$ on the wetted length
$\mathbf{A}$	Added mass matrix
b_{jk}	Sectional damping coefficients for the side hulls
$b(t)$	Ship-fixed x-coordinate of downstream deck-water intersection

$B(x)$	Breadth of the wetted deck
B_{jk}	Damping coefficients
$\mathbf{B}$	Damping matrix
$\mathbf{B}_{gen}$	Damping matrix for the three-body system
$c(t)$	Half length of the wetted deck area
C_A	Aft mean submerged cross-sectional curve of one of the three bodies representing a side hull
C_F	Forward mean submerged cross-sectional curve of one of the three bodies representing a side hull
$d(x)$	Time independent wetdeck height above calm water
DT	Time step
E	Young's modulus
$f_3(x)$	Sectional Froude-Krylov force on the side hulls in vertical direction
$F_{3,buoy}$	Sum of the vertical nonlinear Froude-Krylov and hydrostatic restoring forces over the wetted area on the wetdeck
F_j	jth mode excitation force or moment
F_j^I	Froude-Krylov force or moment in direction j
F_j^D	Diffraction force or moment in direction j
F_n	Froude number
F_3	Slamming induced vertical force
F_5	Slamming induced pitch moment about the mid point of the wetted deck
$\mathbf{F}$	Excitation force vector
g	Gravitational acceleration
$h_3(x)$	Sectional diffraction force on the side hulls in vertical direction
H	Wave height of incident waves
i	Complex unit, $i = \sqrt{-1}$
I	Area moment of inertia of cross section of a beam about its neutral axis
J_n	Bessel functions of the first kind
k	Wave number, $k = 2\pi/\lambda$, where λ is the wave length
k_{ij}	Restoring coefficients due to the beam connections between rigid body segments
K_{jk}	Hydrostatic restoring coefficients
$\mathbf{K}$	Hydrostatic restoring matrix
$\mathbf{K}_{gen}$	Restoring matrix for the three-body system
$l(t)$	Ship-fixed x-coordinate of the mid point of wetted length of the deck
L	Length of a connecting beam between two adjacent rigid body segments
L_{PP}	Length between fore and aft perpendiculars
M	Structural mass
$M(x)$	Bending moment in a connecting beam between two adjacent rigid body segments
$\mathbf{M}$	Structural mass matrix
$\mathbf{M}_{gen}$	Mass matrix containing both structural mass and added mass

$\vec{n}$	Unit surface normal vector, $\vec{n} = (n_1, n_2, n_3)$, positive direction towards the fluid domain
(n_4, n_5, n_6)	$(n_4, n_5, n_6) = \vec{r} \times \vec{n}$, where $\vec{r} = x\vec{i} + y\vec{j} + z\vec{k}$
O	Center of gravity of the vessel
O_i	Center of gravity of ith segment of the three-body model
O_iX	Distance from local O_i to the adjacent connecting beam end X
p	Fluid pressure (atmospheric pressure excluded)
p_{inc}	Pressure due to incident regular waves
$Q(x)$	Vertical shear force in the connecting beams
$\mathbf{r}$	6 degrees of freedom of the three-body system
R	Radius of curvature of the incident waves
t	Time variable
T	Incident wave period
T_e	Encounter wave period
T_N	Natural period
T_d	Time duration of wetdeck slamming
u	Horizontal fluid velocity due to incident waves
U	Ship forward speed
V_1, V_2	Velocity components when $V_R = V_1 + V_2X$
V_1, V_2, V_3, V_4	Velocity components when V_R is Fourier expanded
V_{deck}	Vertical velocity of the deck
V_R	Relative impact velocity normal to the deck during wetdeck slamming
w	Vertical fluid velocity due to incident waves
(x, y, z)	Coordinate system, fixed relative to the mean oscillating position of the ship. See Fig. 2.3.
(x_i, y_i, z_i)	Local coordinate system for ith segment of the three-body model. See Fig. 2.4.
(X, Z)	Local $2D$ coordinate system for the wetted part of the deck. See Fig. 3.1.

Greek Letters

α	Phase difference between ship motions and incident waves
α	Angle between the center plane of a monohull and the outer part of the wave system generated by the monohull. See Fig. 7.1.
β	Incident wave heading angle. $\beta = 0^0$ refers to head sea.
γ	Vortex density
δ	Phase difference
Δc_{j+1}	A prescribed wetted length change during Δt_{j+1}
Δt_{j+1}	Time step from time instant No.j to No.$j+1$
ΔZ_{j+1}	Vertical distance that a free surface particle should travel vertically during Δt_{j+1}
ζ	Free surface elevation
ζ_a	Incident wave amplitude
η_B	Vertical body motion
$\ddot{\eta}_i$, $\dot{\eta}_i$ and η_i	Acceleration, velocity and displacement in degree of freedom i

η_R	Relative vertical displacement between wetdeck and water
θ	Parametric coordinate for longitudinal position X on the wetted deck length, defined by $X = c(t)\cos\theta$.
λ	Wave length
λ	Eigenvalue
ρ	Mass density of the fluid
τ	Local trim angle of the wetdeck relative to the mean free surface
ϕ	Velocity potential due to wetdeck slamming
ϕ_{add}	Velocity potential with $\phi_{add} = Ux + \phi_I + \phi_{sh}$
ϕ_D	Diffraction potential
ϕ_i	Eigenvector for the ith mode shape
ϕ_I	Velocity potential of incident waves
ϕ_k	Radiation velocity potential due to kth motion mode
ϕ_{sh}	Velocity potential due to the ship hulls
ϕ_{slm}	Velocity potential due to wetdeck slamming
Φ	Total fluid velocity potential, $\Phi = \phi_{add} + \phi_{slm}$
ω_0	Wave frequency (rad/s)
ω_e	Encounter frequency (rad/s)

Abbreviations

2D	Two-dimensional
2modes	The lowest 2 eigenmodes in the three-body system; including the two coupled heave & pitch modes
3D	Three-dimensional
3modes	The lowest 3 eigenmodes in the three-body system; including the two coupled heave & pitch modes and the two-node bending mode
4modes	The lowest 4 eigenmodes in the three-body system; including the two coupled heave & pitch modes, two-node and three-node bending modes
AP	Aft perpendicular
COG	Center of gravity
Cut1, Cut2	Transverse cuts of catamaran at respectively $1.48m$ and $2.68m$ from the bow of the catamaran. See Fig. 2.1.
DNV	Det Norske Veritas
FP	Forward perpendicular
ISSC	International ship and offshore structures conference
ITTC	International towing tank conference
MRU	'Motion response unit' measurement system
VBM	Vertical bending moment
VERES	VEssel RESponse; computer program by Marintek
VSF	Vertical shear force

Contents

Chapter 1

Introduction

1.1 General background and motivation

Wetdeck slamming causes important global and local structural response of multihull vessels. Global longitudinal bending effects should be considered for vessels of lengths larger than 50m, while local effects matter for all ship lengths. DNV rules for high speed and light craft express the slamming loads in terms of the vertical accelerations at the center of gravity of the vessel and also specify a minimum wetdeck height for wetdeck slamming to occur. Aarsnes and Hoff (1998) and Faltinsen (1999) demonstrated by full scale experiments of the 30m long Ulstein test catamaran that this minimum height was not sufficient to avoid slamming. Actually, local slamming induced bending stress in longitudinal stiffeners corresponding to approximately half the yield stress was recorded in a head sea condition with a significant wave height $H_{1/3} = 1.5m$. The ship speed was 18 knots. The vessel was allowed to operate up to $H_{1/3} = 3.5m$.

The full scale measurements on the Ulstein test vessel demonstrated even for a small vessel the clear effect of wetdeck slamming induced transient vertical accelerations with a period corresponding to the global two-node bending. This phenomenon is called whipping. The maximum measured vertical acceleration in the bow, in the condition causing local wetdeck slamming induced maximum strains close to half the yield stress, was about $20m/s^2$. The whipping contribution was about $5m/s^2$. This acceleration level is higher than operability limiting criteria presented by NORDFORSK (1987) for merchant vessels of lengths less than $100m$. This specifies a Root-Mean-Square (RMS) value of $0.275g$ as a limit for vertical accelerations at FP. The corresponding maximum amplitude would be less than four times the RMS value.

An important matter regarding wetdeck slamming is the operational aspects. A ship master may change course or reduce speed when slamming represents a danger. This is likely to occur for a passenger vessel, which is the most common type of catamarans. This may be the reason why few accidents due to wetdeck slamming were reported. However, the oceanographic research vessel USN Hayes of length 220ft (67.0m) experienced local deformations of the shell

plating due to wetdeck slamming. This also caused shock loading on sensitive oceanographic instruments and reduced the effective operating time by 50% (Hadler *et al.* (1974)). This was the consequence of bad seakeeping behaviour causing large relative vertical motions between the ship and the water. The ship design was altered by introducing foils between the side hulls in the forward part of the ship. This reduced the relative vertical motions by 30%. The ship was then found to be an efficient oceanographic research vessel according to Hadler *et al.* (1974). Some other high speed catamarans also encountered damages due to wetdeck slamming, *e.g.* Stena Discovery in 1997.

A future trend may be that larger and faster multihull vessels for cargo transportation are built. Slamming may not be that strongly sensed by the ship master for larger vessels as for smaller vessels. His or her concern may be less for cargo transportation than for passenger transportation. This implies that change of ship course and ship speed may not be so actively used to avoid wetdeck slamming. However, hull surveillance systems may be introduced and combined with control systems. This requires simplified and physically based mathematical models that describe the slamming load effects. There are no appropriate simple criteria for operational limits due to wetdeck slamming like Ochi's (1964) criterion for bottom slamming on monohulls, that can be used in computational operational studies.

Since wetdeck slamming may represent an important safety problem, there is a need to improve present rules due to wetdeck slamming. This is not a simple task. Introducing too conservative rules may have important negative economic consequences. This illustrates the need for design by 'direct analysis' using 'first principles' to calculate loads and load effects. This means the use of physically based and experimentally validated computer programs. DNV opened the possibility to base design on such rules in early 1990s, but the complexity of the matter makes the introduction of this approach slow. The work in this thesis provides a step towards this goal.

1.2 Slamming physics and previous studies

The occurrence and severity of wetdeck slamming depend on the relative vertical motions and velocities between the ship and the water. Head sea conditions are considered to be the most severe cases. If regular incident waves are assumed, the largest relative vertical motions and velocities occur for frequencies of encounter in the vicinity of heave and pitch resonance frequencies. This means for wave lengths that are the order of the ship length and longer. The incident wave lengths causing resonance for head sea increase with ship speed. Since a linear irregular sea is the sum of regular waves, information from regular waves can be used to evaluate which sea states are most critical.

DNV rules state simply that wetdeck slamming is avoided when the wetdeck height above calm water is larger than 5% of the ship length. The ship length is certainly an important parameter for ship motions, but there are also other hull parameters that matter (Faltinsen (1990)). An example is the beam-draft ratio of each hull. If this is chosen very small, like it can be done for multihull vessels but not for monohulls due to metacentric height requirements, large vertical

motions will occur in resonant conditions for a ship without damping devices at forward speed. Foils are effective in damping heave and pitch for high speed ships. The associated damping can be explained by the lift force on the foils caused by circulation and shed vorticity. If the relative vertical velocity of the foil is small relative to the forward speed, the damping increases linearly with ship speed. It means that decreased vertical motions can be obtained by increasing the ship speed for a high speed vessel (Haugen *et al.* (1997)).

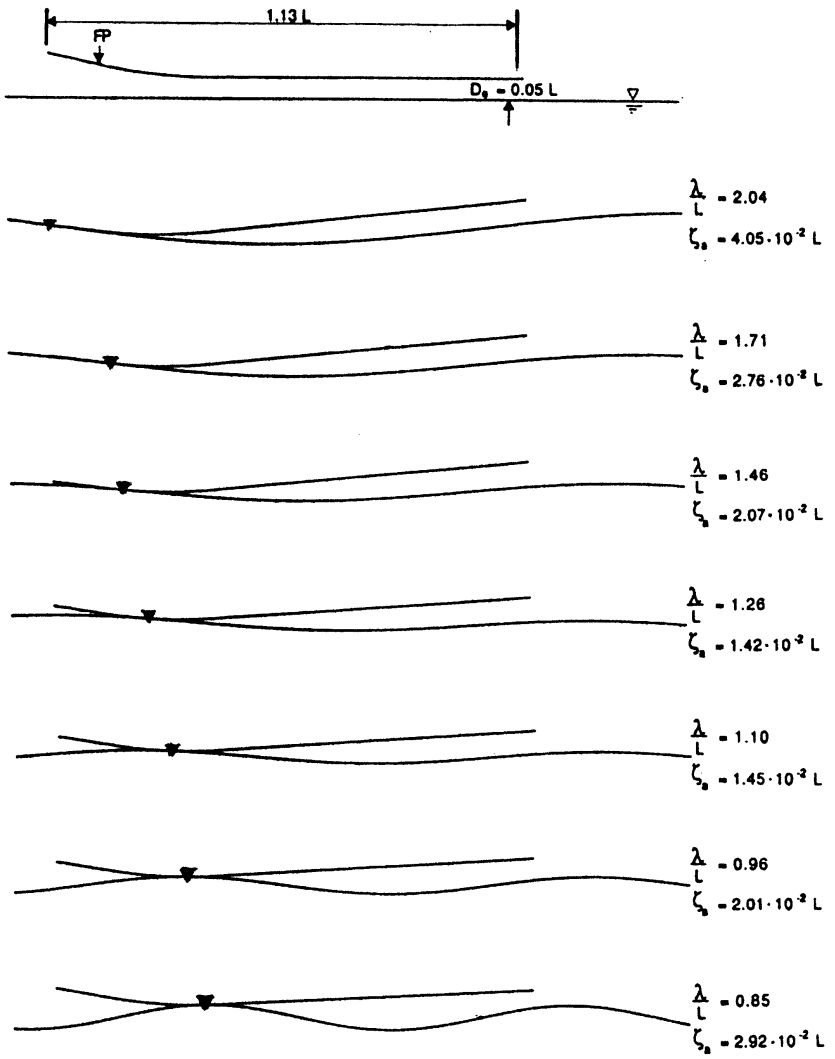

Figure 1.1 Position of slamming on the wetdeck of a catamaran in regular head sea waves as a function of wavelength λ. The figure shows a longitudinal cross-section at the center-plane of the catamaran. $F_n = 0.5$, $\zeta_a = \zeta_{slam}$ =lowest incident wave amplitude when slamming occurs. L =length between perpendiculars. Zhao and Faltinsen (1992)

It matters how the water hits the wetdeck. Figure 1.1 from Zhao and Faltinsen (1992) shows how the impact position depends on the wave period in regular head sea waves for a given catamaran

and Froude number. The water hits always in the forward part of the deck. This follows from that the relative vertical motions of a ship are always largest in the forward part for a ship at forward speed in head sea. Figure 1.1 shows that the longer the wave length is, the closer to the bow the initial impact occurs. If the initial impact occurs in the bow ramp region, it means that the relative vertical motion for impact has to increase with wave length. The figure presents also the minimum wave amplitude ζ_a for slamming to occur for a given incident wave length λ. Disregarding that the impact position is wave length dependent Fig. 1.1 shows that the maximum relative vertical motion divided by ζ_a occurs when $\lambda/L = 1.26$ for the presented cases. When the water does not initially hit at the end of the deck, the water surface has to be initially tangential to the wetdeck surface at the impact position. Let us consider a wetdeck with a plane horizontal cross-section, long-crested incident head waves and a forward speed which is not small. The water surface at the initial impact position can then be approximated by the incident waves and the flow due to slamming can be assumed two-dimensional in the longitudinal cross-sectional plane of the vessel. By using Wagner's (1932) theory, it can be shown that the initial slamming force F_3 is equal to

$$F_3 = \rho\pi V_R^2 RB \tag{1.1}$$

Here V_R is the relative velocity normal to the deck surface at initial impact, R is the radius of curvature of the incident waves at the impact position and B is the breadth of the wetdeck at the impact position. R can for linear incident regular waves be expressed as $1/(k^2\zeta_a)$ at the wave crest. Here k and ζ_a are respectively wave number and wave amplitude. If V_R is proportional to ζ_a, it implies that F_3 is proportional to ζ_a.

If the water instead hits initially at the end of the deck, there will initially be a small angle α between the free surface and the deck surface. This implies initially zero slamming force. The increase in the slamming force with time would be sensitive to α in a similar way as water entry forces on wedges are sensitive to the deadrise angle β for small β. If the wetdeck has a wedge-shaped transverse cross-section, the slamming loads are for the same reason smaller than for a plane horizontal cross-section. It is also beneficial with a bow ramp. This reduces the probability of slamming. A mean trim angle has a similar effect. This can be significantly increased at Froude numbers larger than 0.35 (Molland *et al.* (1995)). By increased trim is meant that the bow rises. This is physically caused by the increased importance of the velocity square term in Bernoulli's equation for the pressure relative to the hydrostatic pressure. Another way of saying this is that the increased trim is associated with the wave making of the ship in calm water. Nonlinear unsteady wave-body interaction will also cause a mean trim angle. The same physical effects cause also a mean sinkage.

1.2.1 Local slamming effects

There are two frequently referred methods in slamming studies, that is a Wagner (1932) and a Von Karman (1929) type of method. A Wagner method means that the flow caused by the impact is accounted for in finding the body-water intersection while a Von Karman method neglects this effect. Normally the slamming period is divided into the water entry and exit phase. This means respectively that the wetted surface increases and decreases. The Wagner method

is physically correct and numerically feasible only in the water entry phase.

Slamming is a complicated physical process where compressibility of the water, air cushions, air bubbles and hydroelasticity may influence. The practical relevance of these effects must be considered in the framework of structural dynamic response. The time scales for structural response are associated with the natural periods of structural vibrations. A representative time scale of local wetdeck slamming is $10^{-2}s$, while it is the order of $1s$ for global effects. Since the time scales of compressibility of the water, air cushions and air bubbles are typically much smaller, we may assume incompressible water and neglect interaction between water and air. Since significant viscous effects do not have time to develop, the flow can be assumed irrotational. The fluid accelerations associated with the initial impact is generally much larger than the gravitational acceleration in the vicinity of the impacting body. If in addition the time durations of the water entry and water exit phase are small relative to typical wave periods, we may neglect gravity when evaluating slamming loads.

Verhagen (1967) and Haugen (1999) have for instance studied details of air cushions. Korobkin (1996) gave a review of compressibility effects. Zhao and Faltinsen (1993) provided benchmark numerical results by a Boundary Element Method and by Dobrovol'skaya's (1969) similarity solution for water entry of rigid wedges with constant velocity. Incompressible fluid and irrotational flow are assumed. Exact nonlinear free surface conditions without gravity are used. Kvålsvold (1994), Faltinsen (1997) and Haugen (1999) studied theoretically the effect of hydroelasticity on local slamming induced stresses. Kvålsvold tried originally to use a Boundary Element Method, but found that too large numerical errors were introduced. This led him to follow a more analytically based method. The same is true in the studies by Faltinsen (1997) and Haugen (1999). A Boundary Element Method was also used in a preliminary stage in this work to calculate the slamming loads. Since also in this case numerical errors occurred, it was decided to follow more analytically based methods.

Aarsnes (1994) reported experimental drop tests with horizontal or nearly horizontal elastic plates. The scaling accounted for representative local structural dimensions of wetdecks. Kvålsvold *et al.* (1995), Faltinsen (1997) and Haugen (1999) demonstrated generally good agreement with the experiments by Aarsnes. An earlier theoretical local hydroelastic study was presented by Meyerhoff (1965). A review article on slamming was presented by Faltinsen (2000). It illustrates the many applications for ships, sloshing in tanks, offshore structures and marine operations associated with lowering of objects through the free surface. Slamming loads are also of concern for coastal structures.

The importance of hydroelasticity can be related to the duration of the loading. This was exemplified by Faltinsen (1999) for local impact (See also Faltinsen (2000) for a review of local hydroelastic slamming). He studied wedge-shaped cross-sections penetrating an initially calm water surface (See Fig. 1.2). A hydroelastic theory based on orthotropic plate theory, strip theory and Wagner type of flow model was used. One application was a wetdeck with non-horizontal cross-section. A stiffened plate between two rigid transverse stiffeners or frames was examined.

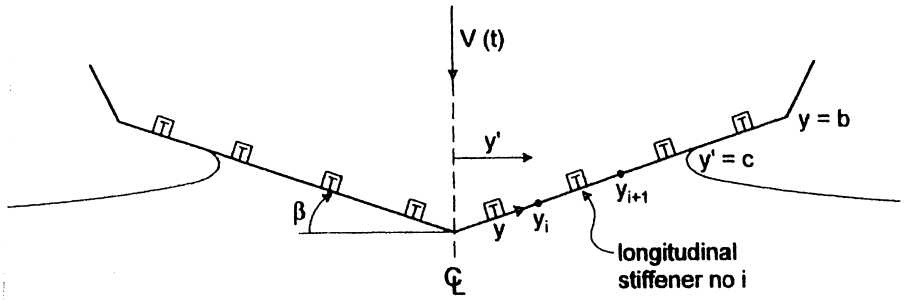

Figure 1.2 Water entry of a wedge-shaped elastic cross section between two rigid transverse frames (Faltinsen (1999))

Figure 1.3 shows the important parameters in the problem. The horizontal axis is proportional to the ratio between wetting time (loading time) and the highest natural period of a longitudinal stiffener based on beam theory. The calculations are made with specific structural data given by Faltinsen (1999) and show nearly no influence of the dimensionless impact velocity V_{ND}. Figure 1.3 illustrates that hydroelasticity matters when $\tan\beta <\sim 0.25V(\rho L^3/EI)^{0.5}$. If realistic impact velocities and structural properties of wetdecks are considered, it means that local hydroelastic effects on the local maximum strains due to impact should be considered when $\beta <\sim 5^o$.

Haugen (1999) demonstrated also this limiting angle by numerical and experimental drop tests of elastic plates with different inclination angles and structural properties representative for wetdecks. When local hydroelastic effects are dominant, *i.e.* $\beta \sim 0^o$, the slamming pressures may be very high and concentrated in time and space. They are very sensitive to small changes in environmental conditions and angular positions of the impacting body. These high pressures are a bad measure of what is the resulting local maximum strains. The force impulse during an initial stage is what matters. This causes an initial vibratory velocity of the structure with a space-averaged velocity that completely counteracts the rigid body drop velocity. This initial velocity leads to a free vibration of the local structure. It is during this free vibration phase that maximum local strains occur.

Faltinsen (1999) compared his theory with fullscale measurements of local strains due to wetdeck impact on the Ulstein test catamaran. Fair agreement between theory and experiments was recorded, but the predicted strains were sensitive to the time varying relative impact velocity caused by global ship motions and fluid motion.

Local hydroelasticity effects due to slamming can also be sensitive to how the horizontal velocity of the flow at the water-body intersecting points is simulated (Ulstein (1995)). Ulstein considered impact loads on the stern seal bag of a Surface Effect Ship (SES) at high forward speed. Gravity is neglected. His concern is coupling with cobblestone oscillations. This is high-frequency unpleasant vertical accelerations of a SES in small sea states associated with resonance oscillations in the air cushion between the two side hulls of the SES. Ulstein (1995) accounts for the flexibility of the bag. This is mainly due to membrane effects. The theoretical

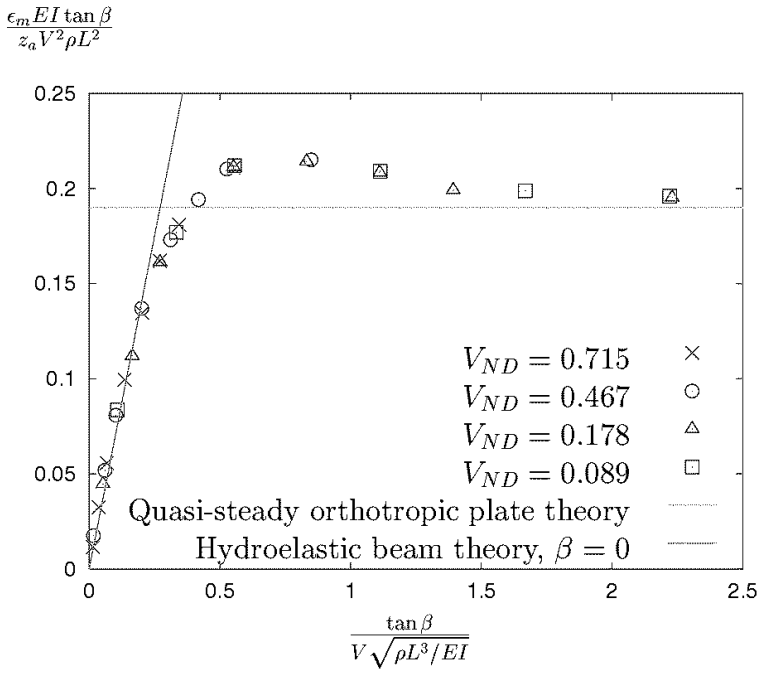

Figure 1.3 ε_m = Maximum strain in the middle of the second longitudinal stiffener from the keel, β = deadrise angle, V = impacting constant rigid body velocity, L = length of a longitudinal stiffener, EI = bending stiffness based on a beam model of a longitudinal stiffener and its effective flange, ρ = mass density of water, z_a = distance from neutral axis of the equivalent beam to maximum strain, $V_{ND} = V(\rho L^3/EI)^{0.5}$. (Faltinsen (1999))

flow model separates from the lowest point of the bag in its static configuration. The impact problem is equivalent to the 2D linear unsteady lifting problem of a thin foil in infinite fluid. This implies that a Kutta condition is applied at the separation point on the bag. Physically the Kutta condition means smooth detachment of the flow from the wetted surface. The other previously mentioned methods imply spray at the intersection points. Further, the dynamic free surface condition over a distance Ut aft of the separation point differs from the high frequency free surface condition typically used in slamming models.

Ulstein's slamming model is similar to one of the slamming models studied in this thesis. However, we account for the time dependence of the aft intersection point between the free surface and the body surface. Further, we use a Von Karman method to find the body-water intersection points. Ulstein uses a Wagner method to find the upstream intersection point. This is numerically more complicated and physically more correct than a Von Karman method during the water entry phase. However, a Wagner type method can not be used during the water exit phase. Ulstein (1995) assumes that the flow is then ventilating and sets the hydrodynamic force equal to zero. This can not be done in the analysis of wetdeck slamming induced global response, where the water exit phase plays an important role. It is also shown in this thesis that the difference in global response is minor between using a Von Karman method and Wagner method during the water entry phase. Ulstein (1995) has further simplified the impact problem

for very high forward speed. The problem is then equivalent to the steady lifting problem of a thin foil in infinite fluid. This approximation is not appropriate for the studies in this thesis.

1.2.2 Global effects

When global effects are considered, the local structure can be considered rigid. The reason is the very different natural periods for local and global behaviour and that local vibrations have died out on the time scale of the global natural periods. Kaplan (1987) analyzed slamming on the bow ramp of a SES in hull borne condition. The SES is then similar to a catamaran. The vessel was assumed locally and globally rigid and head sea was considered. A linear strip theory was used for the hydrodynamic loads on the side hulls. Kaplan (1987) (1991) expressed the impact loads as the sum of a buoyancy force due to nonlinear Froude-Krylov and hydrostatic restoring loads and the vertical force term

$$F_3 = -(\frac{\partial}{\partial t} + U\frac{\partial}{\partial x})(A_{33}V_R) \tag{1.2}$$

Here t is the time variable, U is the forward speed and x is the longitudinal coordinate. Increasing x along the ship is towards the aft end of the ship. A_{33} is the high-frequency added mass in heave for the wetted part of the deck and V_R is the relative velocity normal to the deck surface. An important part of F_3 is the slamming term associated with the time rate of change of A_{33}. This term can be related to the time derivative of the wetted area. This slamming term is proportional to V_R^2, *i.e.* like in Eq. (1.1). This term is always positive upwards and is by Kaplan (1987) set equal to zero during the water exit phase. A dominant term during the water exit phase is the added mass term $-A_{33}dV_R/dt$. This term is negative with an absolute value of the same order as the maximum force during the water entry phase. The loads during both the water entry and exit phase are important for the global response of the vessel. Kaplan demonstrated small influence of slamming on motions while the effect on vertical accelerations and vertical shear forces and bending moments was important. Numerically predicted shear forces and bending moments showed an overall good agreement with experiments, but the numerical results were sensitive to the phasing between the ship motions and the incident waves.

Zhao and Faltinsen (1992) used an analytically based Wagner-type method to predict wetdeck slamming loads during the water entry phase. The emphasis was on global effects and the catamaran was rigid. This method can not be used during the water exit phase and this phase was neglected. Very large initial slamming induced vertical accelerations were predicted.

Økland (2002) studied numerically and experimentally the global effect of wetdeck slamming on an elastic catamaran model at zero forward speed and head sea. Other wave headings were only studied experimentally. The catamaran model consists of rigid body segments connected by elastic beam elements. The same model is used in the experimental and numerical studies in this thesis and will be described in later chapters. However, the mass distribution differs, and we consider forward speed. A similar elastic model with softer spring connections was used by Hermundstad (1996) in his springing studies. The springing was excited by linear high-frequency hydrodynamic loads on the side hulls. Faltinsen *et al.* (1992) used the same hull geometry in

their theoretical and experimental studies of linear global wave induced loads in regular oblique sea at forward speed. The catamaran model was then rigid.

Økland (2002) solved the high frequency boundary value problem for slamming loads by a boundary element method with the wetted surface determined by a Von Karman (1929) method. The important elastic global effects in head sea are in terms of two-node and three-node longitudinal bending. These modes are shown in Fig. 1.4 based on Økland's FEM calculations for a similar model as in this thesis.

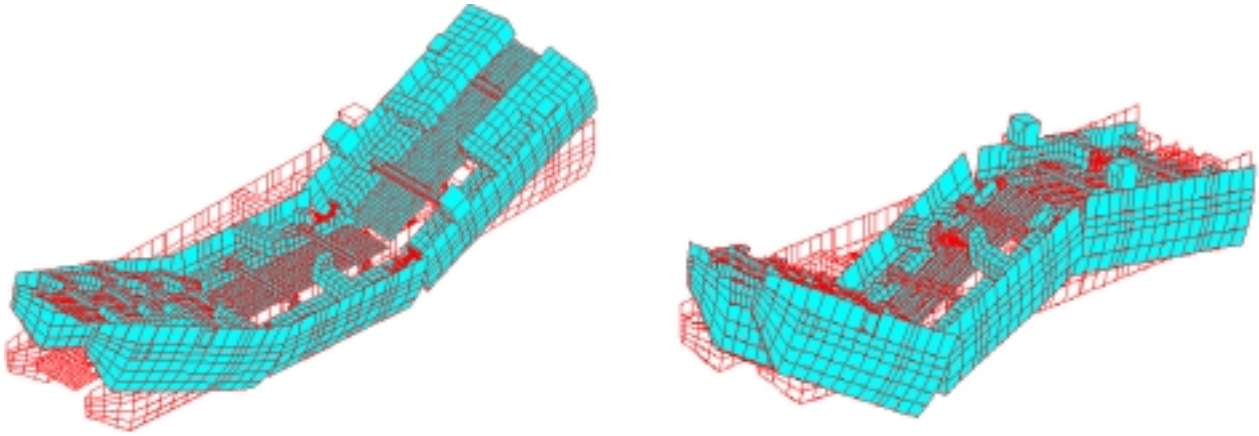

(a) Two-node longitudinal bending (b) Three-node longitudinal bending

Figure 1.4 Calculated shapes of eigenmodes, by Økland (2002)

Both Hermundstad *et al.* (1999) and Økland (2002) used the Finite Element Method, while we will incorporate the elastic properties in a three-body model developed specifically for comparisons with the model tests. Økland described the side hull forces by linear strip theory without accounting for hull interactions. He demonstrated reasonable agreement between experimentally and numerically determined vertical shear forces and bending moments, as well as slamming forces.

The wetdeck slamming studies by Kaplan, Økland and in this thesis use linear strip theory to describe the hydrodynamic loads on the side hulls. Zhao and Faltinsen (1992) used the high-speed theory by Faltinsen and Zhao (1991) without hull interaction. Strip theory is considered as a reliable and practical method for monohulls as long as the Froude number is less than $0.4 \sim 0.5$. However, strip theory can give unreliable results for catamaran hulls if hull interaction is accounted for (Hadler *et al.* (1974)).

The hull interaction is strongly frequency dependent and there are eigenmodes for the fluid motion between the two hulls. For heave and pitch, a piston mode, as well as a sloshing mode (standing waves) resonance may occur between the hulls. The most relevant mode is the piston mode (Ronæss (2002)). The forward speed and three-dimensionality of the flow will in reality cause less wave interaction than strip theory with hull interaction predicts. The forward speed effect can be illustrated schematically by Fig. 1.5 from Ronæss (2002). Steady state harmonic

oscillations with circular frequency ω_e were assumed.

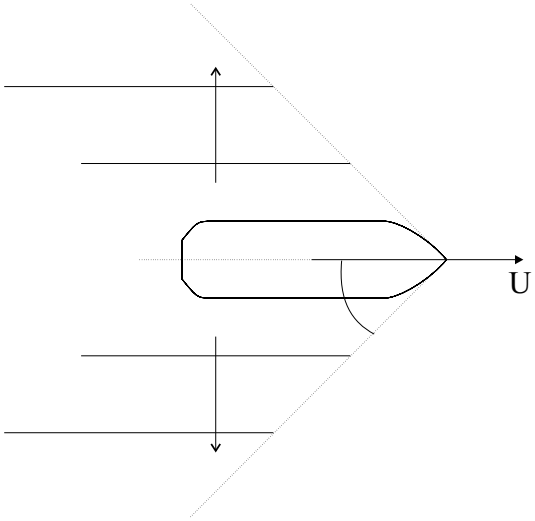

Figure 1.5 Wave pattern based on combining strip theory with forward speed effect. The strip theory wave front propagates with the group velocity $0.5g/\omega$, where ω is the forced oscillation frequency of the body. This in combination with the forward speed determines α. Ronæss (2002)

Figure 1.5 shows the general features of the important wave patterns generated by a single hull. Ronæss (2002) represented the ship in the far-field by a longitudinal line distribution of 3D forward speed dependent oscillating sources along the ship's center plane. The source strengths were determined by using the unified theory by Newman (1978). It was verified that Fig. 1.5 is a reasonable approximation. The angle α between the outer part of the wave system and the longitudinal center line of the ship can be expressed as

$$\tan\alpha = \frac{0.5gt/\omega_e}{Ut} = \frac{g}{2U\omega_e} \tag{1.3}$$

This can be physically explained by first considering waves based on strip theory. These waves have crests parallel to the center plane of the ship, as shown in Fig. 1.5. The group velocity *i.e.* the velocity of the wave front is $g/(2\omega_e)$ in deep water. Equation (1.3) follows now by accounting for that the ship due its forward speed will run away from these waves. This means that the wave front during a time t has moved a transverse distance $\frac{g}{2\omega_e}t$ while the ship has moved a forward distance Ut. If a catamaran is considered, we can as a first approximation consider wave systems generated by each hull as shown in Fig. 1.5. These waves generated by one hull can then, dependent on α, be incident to the other hull and cause hull interaction. The most important frequencies to consider are in the vicinity of heave and pitch resonance frequencies. Equation (1.3) shows that, for a given ω_e, the angle α and the importance of hull interaction decrease with increasing speed.

Since the wetdeck slamming occurs at the forward part of the wetdeck for a catamaran at forward speed in head sea, the hull generated waves do not influence the ambient waves in the

impact area. However, there are local effects due to run-up at the side hulls. These local effects can for instance be explained by the $2\frac{1}{2}D$ high speed theory by Faltinsen and Zhao (1991) even if the Froude number is less than $0.4 \sim 0.5$. What matters is a local Froude number based on the length parameter equal to the distance from the bow. This must be higher than $0.4 \sim 0.5$, and the hull must be slender. This is relevant for the ship length studied in this thesis.

If the local Froude number is higher than approximately 1.0, 2D water entry theories without gravity can be used to assess the run-up. Zhao *et al.* (1997) used this to study steady flow around a planning boat. The numerical results for water entry of wedges by Zhao and Faltinsen (1993) for large deadrise analysis is useful in our context. Even if the flow caused by the impact of the run-up on the wetdeck is 3D, 2D impact of wedge-flow with small interior angles (Greco (2001)) can be used to assess the relative importance for global wetdeck slamming induced response. However, the effect is believed to be small and is not further pursued in this thesis.

Wetdeck slamming can also be important for offshore structures. Baarholm (2001) studied global impact loads on a fixed horizontal wetdeck in incident regular waves and 2-D flow conditions. A boundary element method that accounted for gravity and nonlinearities in the free surface condition was used. This was combined with a Kutta condition at the aft intersection point between the deck and the free surface both when the flow separated from the aft edge and during the water exit phase. Experimental observations were the basis for applying the Kutta condition. Baarholm (2001) demonstrated a good agreement between theoretical and experimental time histories of vertical force. The water exit phase lasted much longer than a Von Karman method would predict. There is an important difference between Baarholm's case and the studies in this thesis and the other previously mentioned wetdeck studies. The deck wetting in Baarholm's case lasted considerable longer so that gravity effects may matter and cause wave generation due to the impact.

Figure 1.6 presents a schematic view based on video recordings of the free surface behaviour in Baarholm's experiments. The free surface hits initially at the front end of the deck causing uprise of the water at the front end of the deck. The water will subsequently turn rapidly around the front edge with local high curvature of the free surface. This is probably amplified by a vortex created due to the cross flow past the sharp edge. This rapid cross-flow was artificially handled in Baarholm's numerical method. The whole deck is subsequently wetted with the flow leaving the aft end tangentially to the deck surface. When the wetted area later diminishes, there is smooth detachment from the aft body-water intersection point until the final stages of the wetting. The free surface slope is then high at the intersection points (See Fig. 1.6).

Baarholm *et al.* (2001) studied numerically the global wetdeck slamming induced vertical motions of a semi-submersible. 3D slamming load effects were accounted for by using a 3D-correction to the high-frequency heave added mass proposed by Blagovenschensky (1962). This has an important effect when a large part of the deck is wetted. 3D flow effects due to the incident flow field caused by wave diffraction and scattering effects of the platform wave were neglected, but ought to be studied in the future. Baarholm *et al.* (2001) demonstrated a significant global vertical impact force on the deck by using realistic environment conditions. A large

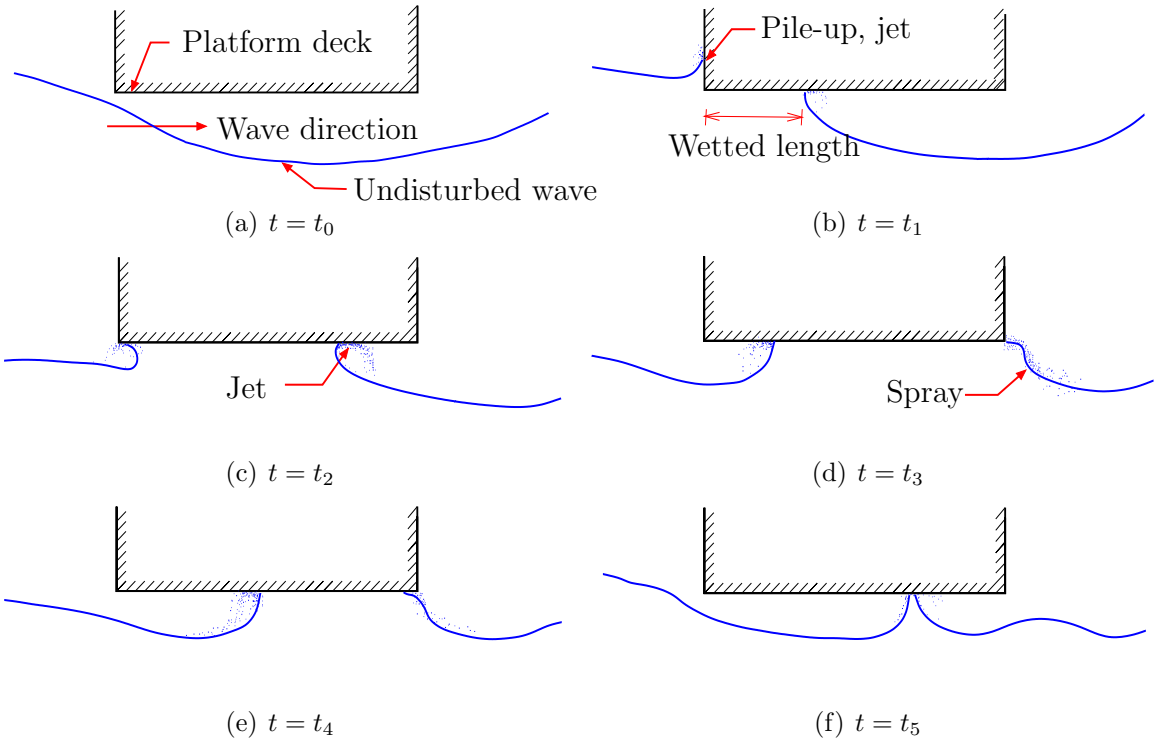

Figure 1.6 Sketches of free surface at different time instants of water impact on a horizontal deck. Incident regular waves, 2D flow. Based on video recordings of model tests. Baarholm (2001)

influence on the heave motion was also found.

1.3 Objectives

The ultimate aim is to develop a numerical method that can predict wetdeck slamming induced global response of multihull vessels in any sea state and at any forward speed. This involves long term statistical description of combined load effects due to both transient slamming induced whipping and steady state linear and nonlinear wave loads. Since this most likely requires very long time simulations with different stochastic realizations of different short term sea states for given operational areas, the combined hydrodynamic and structural model has to be simplified by proper physical approximations and experimental validation. It would be impossible today from a CPU point of view, to solve the 3D potential flow with exact nonlinear boundary conditions. Another matter is that numerical solutions like this are still at the research stage with several unsolved challenges (Jensen *et al.* (2000)). Using Navier Stokes equation to represent the effect of viscosity is still in its infancy relative to a potential flow model.

The studies in this thesis are steps towards the final objectives. Regular incident head waves on a catamaran at forward speed is analyzed theoretically. The wetdeck is assumed to have a horizontal cross-section. The theoretical model is validated by comparisons with model tests.

Since the elastic test model consisted of rigid body parts, a structural model was developed specifically for the test model. A major challenge in this thesis is to properly approximate the wetdeck slamming loads and calculate the globally induced response. Also an error analysis is made of the experiments and a partly qualitative and partly quantitative discussion of the accuracy of the theory is provided. Potential improvements are then pointed out.

1.4 Outline of the thesis

Chapter 1 is the introduction. It gives the background, describes earlier relevant research and presents the objectives and contents of this thesis.

Chapter 2 presents the theoretical three-body model of the catamaran needed in comparisons with model tests. Each of the three bodies is assumed to be rigid. Regular head sea waves and forward speed are considered. The hydrodynamic loads on the side hulls are based on the linear strip theory by Salvesen *et al.* (1970). Important modifications are needed in terms of forward speed dependent end terms at the front ends of the second and third body from the bow. This is derived by Stokes theorem. Hydrodynamic hull interaction is neglected. The global elasticity of the catamaran is accounted for by small beam elements between the three rigid bodies. It is shown how this introduces restoring terms in the equations of motions. The unknowns are the local heave and pitch for the three rigid bodies.

Chapter 3 deals with the different 2D slamming models by considering different ways to determine wetted length, to approximate relative impact velocity, and to consider the forward speed effect on the free surface condition and a Kutta condition at the aft end of the wetted part. Detailed solution procedures are presented.

It is assumed that the wetdeck has a horizontal transverse cross-section and that the slamming induced flow is 2D in a longitudinal cross-sectional plane. Gravity is neglected in the free surface conditions and boundary conditions are transferred to a horizontal line. Since neither a Wagner nor a Von Karman based impact model with high frequency dynamic free surface condition and a general representation of the relative impact velocity in the boundary condition is known from the open literature, a detailed analytical derivation is presented. The flow is represented by a vortex distribution along the instantaneous wetted part of the wetdeck. The solution of the resulting singular integral equation is based on Newman (1977). The Wagner based method can only be used during the water entry phase. Even if Ulstein (1995) has applied a similar Kutta condition model as in this thesis, there are important differences associated with the changing wetted length and the water exit phase. Details of the solution procedure are therefore given both in Chapter 3 and Appendix B. Gravity is considered for all models in terms of nonlinear Froude-Krylov and hydrostatic loads. By Froude-Krylov loads are meant integrated pressure loads due to the undisturbed incident waves.

Chapter 4 compares five slamming models based on different theories presented in Chapter 3, by investigating the wetted length, impact loads, global motions and accelerations of a rigid

catamaran. It concludes that a Wagner method does not influence the global response greatly relative to using a Von Karman method. Various approximation of relative impact velocity over the wetted area in the body boundary condition is investigated. It shows that linear expression is sufficient. The importance of the Kutta condition is demonstrated. The water exit phase, where the added mass force is dominant and causes negative loads, is shown to be important for the global response. The negative impact loads in our studies do not cause ventilation. This will typically be started by cavitation, *i.e.* that the total pressure is close to zero (vapor pressure) somewhere along the wetted part of the deck.

In Chapter 5, the three-body model is used to investigate the global hydroelastic effect caused by wetdeck slamming. A modal based method is introduced to avoid unphysical effects of the two highest modes. One reason is that structural damping is neglected. Further, since the two highest modes have relatively high natural frequencies, introduction of the modal based method reduces the CPU time significantly. The modal based method used includes two coupled heave and pitch modes, as well as vertical two-node and three-node vertical bending. It is verified that the modal based method and direct solution of the equations of motions give consistent results.

Numerical verification and experimental validation are done systematically. The experiments contained five cases with high incident wave amplitudes. Both theory and experiments agree that wetdeck slamming does not occur in one of the cases. The agreement between theory and experiments of the vertical shear force and bending moment as well as the slamming force on the wetdeck between experiments and theory is reasonable for most severe slamming case and in one moderate slamming case. Both theory and experiments demonstrate that the slamming force is in general positive during the water entry phase and negative during the water exit phase. The duration of the water exit phase is well predicted with Von Karman method which is contrary to what a similar method will do in the previously discussed case of Baarholm (2001). A reason may be that the water exit phase lasted longer relative to the wave period in Baarholm's example. Two-node bending is shown in general to be dominant in the response. The prediction of three-node bending is unsatisfactory. The case with largest wave period does not show good agreement between theory and experiments. A thorough investigation is made and the reason is suggested to be piston mode resonance between the two hulls. One of the test cases show relatively small slamming effect. The wave amplitude in the theoretical predictions has to be increased 20% to cause slamming in this case.

In Chapter 6, experimental error sources are systematically and extensively investigated. Based on an error analysis of the experiments, relative errors of the global load response are given for the most severe slamming case. Since the experiments were not done as part of this thesis and each test was only done once, random errors can not be estimated. It is shown that the trim angle is the most important error source. The changing incident wave amplitudes along the track of the model and the wave measurement inaccuracies are equally the second most important error source for vertical bending moment at the two transverse cuts studied in the experiments. The errors associated with roll, yaw and sway is the second most important for vertical shear force at the two cuts. This roll, yaw and sway effect is partly due to an unintended mass distribution causing a small mean roll angle. Table 1.1 lists the importance of the different error sources

investigated. The error analysis combines estimated uncertainties for each error source with the theoretical model to find errors in wetdeck slamming induced global vertical shear forces and bending moments. The estimated relative errors vary between 0.17 and 0.29 depending on the response variable.

Theoretical error sources are investigated in Chapter 7. The numerical related and physical related error sources are investigated separately. The numerical error sources show negligible influence on the final results. Among the physical errors, the most important theoretical error source is believed to be neglection of hydrodynamic hull interaction. It is shown that neglection of transverse bending in the theoretical model causes negligible errors in predicting longitudinal global response. Table 1.2 lists the relative importance of the different physical error sources in the theory investigated in Chapter 7.

Finally, conclusions and future perspectives are given in Chapter 8.

Part of this thesis work has been presented in Ge *et al.* (2002a), Ge *et al.* (2002b) as well as in Faltinsen *et al.* (2002).

Table 1.1 Importance of error sources in the experiments of global wetdeck slamming on a catamaran at forward speed in head sea; investigated in Chapter 6

Error sources in experiments	Importance
Speed	No
Changing wave amplitude along the track	Yes
Seiching in the tank	No
Inaccuracies in wave measurements	Yes
Roll, yaw and sway	Yes
Sinkage	No
Trim	Yes
Mass distribution	Yes/No
Wetdeck geometry	Yes

Table 1.2 Importance of physical error sources in theoretical modelling of global wetdeck slamming on a catamaran at forward speed in head sea; investigated in Chapter 7

Physical error sources in the theory	Importance
Incident wave nonlinearities	No
Hull interaction	Yes
Nonlinear hydrodynamics on side hulls	??
3D slamming	No
Kutta condition in slamming model	No
Transverse bending	No
Transient phase	No

1.5 Major contributions of this thesis

- A theoretical three-body model for analyzing global wetdeck slamming induced elastic response based on a tested catamaran has been developed;
- New wetdeck slamming models are presented. These include an analytical model where the relative impact velocity is described by a Fourier series. Another model appropriate for high speed and accounting for smooth detachment of the flow (Kutta condition) at the aft end of the wetted deck is also developed;
- Error analysis of experiments on global wetdeck slamming induced vertical shear forces and bending moments are performed. This has to our knowledge not been done systematically before. However, since the experiments were done by others and each test condition was only done once, we were not able to account for random errors.

Chapter 2

Theoretical Three-Body Model

2.1 Introduction

In order to study slamming effects on global response of catamarans, model tests in regular head sea waves have been performed in the Ocean Basin at the Marine Technology Center in Trondheim. The test model is geometrically the same as used by Økland and Moan (1998). However, the structural mass distribution differs. The experimental results were obtained by Aarsnes and Økland in 1996, but they did not publish the results for forward speed. The objective was to study the global hydroelastic effects of wetdeck slamming on large catamarans. So the tested model was cut into pieces connected by softer materials. In details, each side hull was divided into three sections longitudinally, with an aluminum frame mounted in each section. The hull sections are connected by steel springs and aluminum transducers longitudinally and transversely, as illustrated in Fig. 2.1. The wetdeck in the tested catamaran consisted of four sections, notated consecutively as Deck1, 2, 3, 4 from the bow towards the stern.

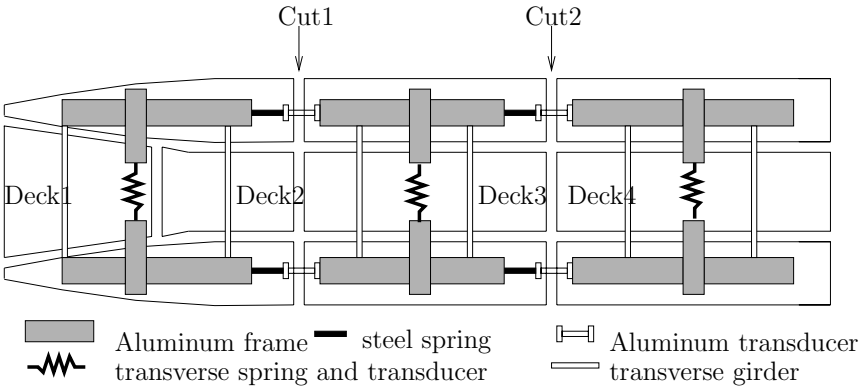

Figure 2.1 Outline of the experimental hull arrangements (top view)

The basic geometrical data and body plan of the model catamaran are given in Appendix A. The vertical shear forces (VSF) and bending moments (VBM) were measured at the transverse

cuts denoted as Cut1 and Cut2. These cuts are respectively 1.48m and 2.68m from the bow. Here the bow refers to the forward end of the Deck1. Cut1 and Cut2 do not necessarily coincide with where maximum VSF and VBM occur. Figures 2.2 illustrate the calculated longitudinal distribution of the linear transfer function of VSF and VBM by assuming a rigid vessel. The body plan and mass distribution are the same as for the test model. Head sea conditions without wetdeck slamming are considered. Results in Fig. 2.2 are for the case with wave period $1.8s$ and the forward speed $1.9m/s$. The strip theory by Salvesen *et al.* (1970) is applied. Since the mass distribution was presented by very few points (See Appendix A), there are large variations in vertical shear force in Fig. 2.2(a). This is not believed to be a problem when we are examining VSF and VBM at Cut1 and Cut2, where the loads do not show large jumps like it does for VSF between $x = -0.34m$ to $0.14m$.

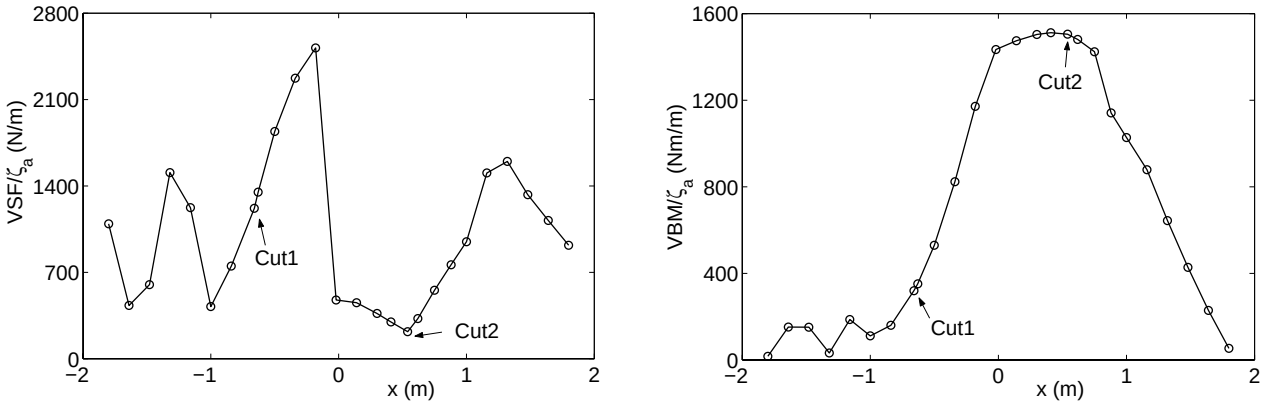

(a) VSF along ship length

(b) VBM along ship length

Figure 2.2 Longitudinal distribution of amplitudes of Vertical Shear Force (VSF) and Vertical Bending Moment (VBM) divided by wave amplitude ζ_a along the catamaran length; $x = 0$ refers to the position of $L_{PP}/2$, $x = -2.14m$ is the bow end. Rigid catamaran with forward speed $U = 1.9m/s$ in regular head waves with period $T = 1.8s$.

This catamaran model has also been the basis for the experimental and theoretical studies by Økland (2002), and Hermundstad (1996) but with softer spring connections. Hermundstad (1996) investigated springing due to linear hydrodynamic side-hull forces at high forward speed while Økland (2002) studied wetdeck slamming induced global response at zero forward speed. A modal superposition method as presented by Bishop and Price (1979) was applied in their studies, and the dry modes were found by using the Finite Element Method. Hermundstad (1996) modified the high-speed $2\frac{1}{2}D$ theory by Faltinsen and Zhao (1991) to find linear hydrodynamic forces on the side hulls. Hydrodynamic interaction between the side hulls was considered. Økland (2002) applied the commercial computer code VERES based on the strip theory by Salvesen *et al.* (1970) to calculate the side hull forces. The slamming loads were found by solving numerically the boundary value problem due to slamming. The 'high frequency' dynamic free surface condition $\phi = 0$ was used with the wetted length determined by the Von Karman method. Here ϕ is the velocity potential due to wetdeck slamming. The flow due to the wetdeck slamming was assumed two-dimensional in a longitudinal cross-sectional plane of the vessel. A boundary element method based on representing the velocity potential by Green's

second identity was used. The pressure was found by $-\rho\partial\phi/\partial t$. Here ρ means mass density of the fluid.

In the present work a three-body model connected by quasi-static elastic beams is established to account for the global flexibility and to investigate the global response due to wetdeck slamming. The linear wave induced forces on the side hulls in the time domain are based on a frequency domain solution. Hull interaction is neglected. The strip theory by Salvesen *et al.* (1970) has been used separately for the three bodies. An important modification is needed when the pressure term $-\rho U\frac{\partial\phi}{\partial x}$ is integrated to find the heave force and pitch moment on each body. Here U is the forward speed, ϕ is the velocity potential caused by the vessel and x is the longitudinal coordinate with positive direction aftwards. In Salvesen *et al.* (1970) Stokes theorem is used to integrate this pressure term. Part of the expressions are line integrals which in our case give important contributions not only from the aft end cross-section of each ship segment but also from the front cross-section of the mid and aft segments. The relevant details will be presented in the coming sections.

2.2 Governing system equations

A rigid catamaran is first considered. To describe the motions, a right-handed global coordinate system (x, y, z) is used. It is fixed with respect to the mean oscillatory position of the catamaran, with positive x from bow to stern, positive z vertically upwards through the center of gravity of the catamaran in its mean oscillatory position. The origin of the coordinate system is in the plane of the undisturbed free surface. The translatory displacements in the x-, y- and z-directions are defined as surge, sway and heave respectively, and denoted as η_1, η_2 and η_3. The angular displacements of the rotational motion about x-, y- and z-axis are roll, pitch and yaw respectively, and denoted as η_4, η_5 and η_6. The catamaran is assumed to be symmetric about the x-z plane (See Fig. 2.3).

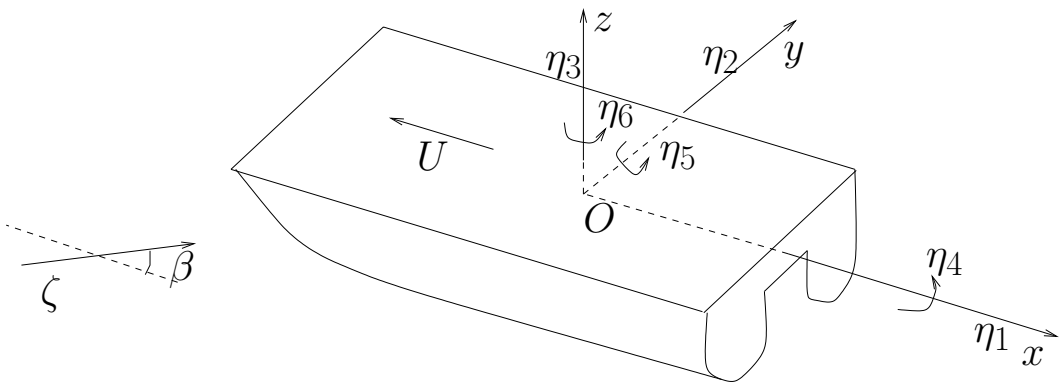

Figure 2.3 Global coordinate and degree-of-freedom system of the catamaran

We focus now on the test catamaran as presented in Fig. 2.1 and on head sea cases. The

flexibility in the test catamaran is mainly controlled by the connecting parts of the rigid hull segments. The transverse connecting springs and beams are longer and therefore softer than the longitudinal ones. Also for the longcrested head sea wave cases, the longitudinal bending modes will be dominant relative to transverse bending and torsional modes (*e.g.* Faltinsen *et al.* (1992)). So a three-body model of the test model was made as shown in Fig. 2.4.

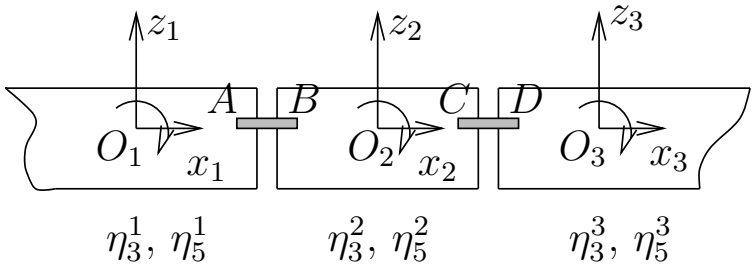

Figure 2.4 Degrees of freedom of segmented model (side view)

The catamaran is modelled as three rigid bodies (fore, mid & aft) with longitudinal connections of quasi-static elastic beams, without accounting for the transverse flexibility between the two side hulls. For each rigid ship segment, there are two degrees of freedom, namely heave and pitch. So totally there are six degrees of freedom in this system, and each degree of motion is referred to its local COG. The connecting equivalent beams are denoted as AB and CD respectively.

The general equation system that will be used to study the global effects of wetdeck slamming in head sea regular waves is given by

$$\mathbf{M}_{gen}\ddot{\mathbf{r}} + \mathbf{B}_{gen}\dot{\mathbf{r}} + \mathbf{K}_{gen}\mathbf{r} = \mathbf{F}_{gen}(\mathbf{r}, \dot{\mathbf{r}}, \ddot{\mathbf{r}}, t) \tag{2.1}$$

Here $\mathbf{r}$ is the displacement matrix of this 6 degrees of freedom system, containing the heave and pitch for each segment. $\mathbf{M}_{gen}$ and $\mathbf{B}_{gen}$ are the mass and damping matrices. Here mass means both structural and added mass. $\mathbf{K}_{gen}$ is the restoring matrix, including the hydrostatic restoring terms from the ship segments and also the coupling terms from the spring beams. $\mathbf{F}_{gen}$ includes the forces due to wetdeck slamming and linear wave excitation loads on the side hulls. Dot means time derivative. In the following sections we will discuss the components of the matrices. Only the force and moment contributions from the linear wave loading are discussed in this chapter. The detailed derivations of slamming loads will be described in Chapter 3.

2.3 Linear strip theory

We here consider the linear frequency domain solution of a catamaran operating in regular incident waves in deep water of infinite horizontal extent. As illustrated in Fig. 2.4, each segment contains contributions from the two side hulls, each of which can be dealt with as a monohull. The basis for deriving the hydrodynamic loads on each rigid body is the strip theory by Salvesen *et al.* (1970) for a rigid monohull. We will therefore first describe essential parts of that theory from our perspective.

2.3.1 Linear strip theory for a rigid monohull

The coordinate system is parallel to the (x, y, z) system in Fig. 2.3, with z going through the mean position of the COG of this side hull. $z = 0$ is in the mean free surface. Following the procedure in Faltinsen (1990), the frequency domain equation of rigid body motions for a monohull in incident regular waves can be expressed as

$$(\mathbf{M} + \mathbf{A})\ddot{\mathbf{r}} + \mathbf{B}\dot{\mathbf{r}} + \mathbf{K}\mathbf{r} = \mathbf{F} \tag{2.2}$$

Here $\mathbf{M}$ is the structural mass matrix. $\mathbf{A}$, $\mathbf{B}$ and $\mathbf{K}$ are respectively hydrodynamic added mass, damping and restoring matrices. $\mathbf{F}$ contains the wave excitation load components and dot means time derivative. We can express $\mathbf{r}$ as $\mathbf{r} = [\eta_1,\, \eta_2,\, \eta_3,\, \eta_4,\, \eta_5,\, \eta_6]^T$.

The structural mass matrix is then

$$\mathbf{M} = \begin{bmatrix} \rho\nabla & 0 & 0 & 0 & \rho\nabla_{Z_G} & 0 \\ 0 & \rho\nabla & 0 & -\rho\nabla_{Z_G} & 0 & 0 \\ 0 & 0 & \rho\nabla & 0 & 0 & 0 \\ 0 & -\rho\nabla_{Z_G} & 0 & I_{44} & 0 & -I_{46} \\ \rho\nabla_{Z_G} & 0 & 0 & 0 & I_{55} & 0 \\ 0 & 0 & 0 & -I_{64} & 0 & I_{66} \end{bmatrix} \tag{2.3}$$

Here z_G is the $z-$coordinate of the center of gravity, ∇ is the displacement of the vessel, ρ is the water density and I_{ij} are the structural moment of inertia terms.

The added mass and damping forces, *i.e.* radiation forces, are steady-state hydrodynamic forces caused by forced motions of the vessel when there are no incident waves. The forced motions generate outgoing waves and dynamic pressure on the hull. When the pressure minus the hydrostatic pressure is integrated over the mean wetted surface of the vessel, hydrodynamic forces which can be decomposed into terms that are proportional to the acceleration and velocity are obtained. The hydrodynamic added mass and damping loads due to harmonic mode η_k can formally be expressed by

$$G_j = -A_{jk}\ddot{\eta}_k - B_{jk}\dot{\eta}_k \tag{2.4}$$

Generally speaking in a 6 degree-of-freedom system, (G_1, G_2, G_3) and (G_4, G_5, G_6) mean respectively the force and moment components relative to the (x, y, z) coordinate system. A_{jk} and B_{jk} are added mass and damping coefficients respectively. The subscript jk means induced parameter in jth mode due to forced motion of kth mode. For normal slender hulls, it is appropriate to assume that the variation of the flow in the cross-sectional plane is much larger than the variation of the flow in the longitudinal direction. This means two-dimensional Laplace equation in the cross-sectional plane is assumed. However, the free surface condition at forward speed can cause flow variations in the longitudinal direction that must be accounted for. An example on this is the high-speed theory by Faltinsen and Zhao (1991). We will apply strip theory which neglects the longitudinal flow variation when the velocity potential is found. 2D hydrodynamic coefficients are then calculated for each strip by solving 2D boundary value problems. Following

Salvesen *et al.*'s (1970) strip theory, the added mass and damping coefficients for the whole ship can be expressed as

$$\begin{aligned} A_{jk} &= \frac{\rho}{\omega_e^2}\Re\left\{\int\int_S (i\omega_e + U\frac{\partial}{\partial x})\phi_k n_j ds\right\} \\ &= A_{jk}^{(0)} + UA_{jk}^{(1)} + U^2 A_{jk}^{(2)} \end{aligned} \tag{2.5}$$

$$\begin{aligned} B_{jk} &= -\frac{\rho}{\omega_e}\Im\left\{\int\int_S (i\omega_e + U\frac{\partial}{\partial x})\phi_k n_j ds\right\} \\ &= B_{jk}^{(0)} + UB_{jk}^{(1)} + U^2 B_{jk}^{(2)} \end{aligned} \tag{2.6}$$

Here the time dependence is expressed as $e^{i\omega_e t}$. ω_e is the circular frequency of oscillations, which is the same as the circular frequency of encounter. U is the vessel's forward speed. ϕ_k is the velocity potential due to forced motion in mode k with unit velocity. (n_1, n_2, n_3) are the components of the normal vector $\vec{n}$ to the body surface with positive direction into the fluid domain. (n_4, n_5, n_6) are the components of $\vec{r} \times \vec{n}$ where $\vec{r} = x\vec{i} + y\vec{j} + z\vec{k}$. The integrations in Eqs. (2.5) and (2.6) are over the mean wetted surface S. $\Re$ and $\Im$ means real and imaginary part, and i is the complex unit.

The exciting forces are calculated by integrating the Froude-Krylov and diffraction forces over the mean hull surface. The ship is restrained from oscillating. The Froude-Krylov forces are found by integrating the pressure due to the undisturbed incident wave over the mean wetted body surface. The diffraction potential is needed to satisfy zero flow through the body surface. The exciting forces of jth mode can be expressed as

$$F_j = \rho\int\int_S \left(i\omega_0\phi_I + i\omega_e\phi_D + U\frac{\partial\phi_D}{\partial x}\right)n_j ds \tag{2.7}$$

Here ϕ_I is the undisturbed wave potential and ϕ_D is the diffraction potential. ϕ_I can be expressed as

$$\phi_I = \frac{g\zeta_a}{\omega_0}\, e^{kz}\, e^{i(\omega_e t - kx\cos\beta - ky\sin\beta)} \tag{2.8}$$

where k is the wave number, β is the wave propagation direction with $\beta = 0$ corresponding to head sea (See Fig. 2.3). The frequency of encounter ω_e is related to the frequency of incident wave ω_0 by $\omega_e = \omega_0 + kU\cos\beta$.

The hydrostatic restoring coefficients $\mathbf{K}$ are independent of frequency and forward speed. For a vessel in the free surface symmetric about the $x - z$ plane and considering the heave and pitch only, the coefficients are (*e.g.* Faltinsen (1990))

$$\begin{aligned} K_{33} &= \rho g\int_L b dx = \rho g A_{wp} \\ K_{35} &= K_{53} = -\rho g\int_L bx dx \\ K_{55} &= \rho g\nabla(z_B - z_G) + \rho g\int_L bx^2 dx = \rho g\nabla\overline{GM_L} \end{aligned} \tag{2.9}$$

Here g is the gravitational acceleration, b is the sectional breadth, A_{wp} is the water plane area, and z_B and z_G are the z-coordinates of the center of buoyancy and gravity. $\overline{GM_L}$ is the longitudinal metacentric height.

2.3.2 Modification of 2D strip theory

In Salvesen *et al.* (1970), Stokes theorem was applied to derive the hydrodynamic coefficients in Eqs. (2.5) and (2.6). The Stokes theorem states that (*e.g.* Spiegel (1959))

$$\iint_S (\mathbf{n} \times \nabla) \times \mathbf{q}\, dS = \int_C \vec{dl} \times \mathbf{q} \tag{2.10}$$

where S is the surface situated in the fluid with the closed curve C as its boundary. $\mathbf{n}$ is positive outwards normal to S. Further, $\mathbf{q}$ is any vector function with continuous first order partial derivatives and $\vec{dl}$ is the direction element of C. The closed curve C will consist of C_F, C_A and paths along the mean water plane-body surface intersection between C_A and C_F. The direction of C is called positive if an observer, walking on the boundary of S in this direction, with his head pointing in the direction of the positive normal to S, has the surface on his left, as shown in Fig. 2.5. We will apply Eq. (2.10) to the portion of the hull surface S aft of a cross-sectional curve C_F and forward of cross-sectional curve C_A.

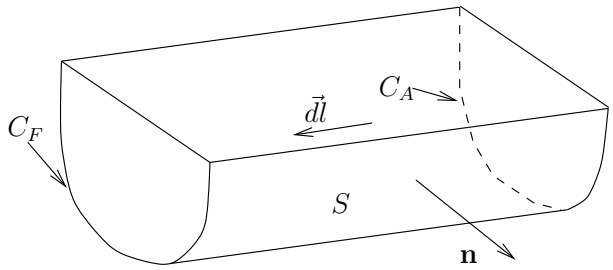

Figure 2.5 Illustration of line integration used in connection with Stokes theorem

Now by letting $\mathbf{q} = \phi U \mathbf{i}$ (for the case $j = 1, 2, 3$) and $\mathbf{q} = \phi U \mathbf{i} \times \mathbf{r}$ (for the case $j = 4, 5, 6$) and applying vector relationships like Ogilvie and Tuck (1969) did, the following variant of Stokes theorem can be derived for $j = 2, \ldots, 6$:

$$\iint_S n_j U \frac{\partial}{\partial x} \phi \, ds = U \iint_S m_j \phi \, ds + U \int_{C_A} n_j \phi \, dl - U \int_{C_F} n_j \phi \, dl \tag{2.11}$$

Here ϕ is a differentiable scalar function. m_j is defined by the body boundary condition $\partial \phi_j / \partial n = i\omega_e n_j - U m_j$, meaning $m_j = 0$ for $j = 2, 3, 4$ and $m_5 = n_3$ and $m_6 = -n_2$. The line integral along the waterline has been ignored by assuming that the angle between the waterline and the x-axis is small.

With Eq. (2.11), the term in the brackets of Eq. (2.5) and (2.6) can then be expressed as:

$$\iint_S (i\omega_e + U\frac{\partial}{\partial x})\phi_k n_j ds = i\omega_e \iint_S n_j\phi_k\, ds + U\iint_S m_j\phi_k\, ds + U\int_{C_A} n_j\phi_k\, dl - U\int_{C_F} n_j\phi_k\, dl \tag{2.12}$$

This is a generalization of the formula by Salvesen *et al.* (1970) by also including a contribution from C_F. In their case C_F corresponded to the bow of the ship. Since ϕ_k is zero by strip theory at C_F, there is no contribution from C_F in their case. Salvesen *et al.* (1970) used the formula both in deriving global load distribution along the vessel as well for the total hydrodynamic loads on the vessel. In the latter case, a contribution from the integral over C_A will only occur if the ship has a transom stern and the flow separates from the stern. ϕ_k is then non-zero at C_A. We here keep both the C_F and C_A contributions because we will later study three rigid bodies elastically linked together and with a negligible gap between them. If Eq. (2.12) is then applied separately for the three rigid bodies, there will be contributions from C_F for the second and third body from the front, while not for the first body.

Stokes theorem can also be generalized from rigid modes to any mode of motion. For example, Skjørdal (1978) applied it for a flexible beam. Hermundstad *et al.* (1999) developed an extension of Stokes theorem to be applied in calculating the springing effects of high speed vessels. This was used to compare with a method where the pressure term $-\rho U\partial\phi/\partial x$ was obtained by direct numerical differentiation.

2.3.3 Hydrodynamic coefficients for a rigid body part

For our three-body system, as illustrated in Fig. 2.4, only heave and pitch are considered. The following text gives the details of the derivation of the modified hydrodynamic coefficients based on the above strip theory.

In strip theory, the oscillatory velocity potential in the kth mode (ϕ_k) is divided into speed dependent and speed independent parts as

$$\phi_k = \phi_k^0 - \frac{U}{i\omega_e}\phi_k^U \tag{2.13}$$

It follows from the body boundary conditions that $\phi_k^U = 0$ for $k = 1, 2, 3, 4$, $\phi_5^U = \phi_3^0$ and $\phi_6^U = -\phi_2^0$. Further, T_{jk} (Eq. 2.14) are introduced to derive the added mass (A_{jk}) and damping (B_{jk}) coefficients, as

$$T_{jk} = \rho\iint_S (i\omega_e + U\frac{\partial}{\partial x})\phi_k n_j ds = \omega_e^2 A_{jk} - i\omega_e B_{jk} \tag{2.14}$$

Physically T_{jk} means the hydrodynamic force or moment in the jth degree of freedom caused by unit oscillatory displacement in the kth mode. T_{jk} can be expressed in terms of T_{jk}^0 and t_{jk},

which are defined as

$$T_{jk}^0 = \rho i\omega_e \iint_S \phi_k^0 n_j ds = \int_L t_{jk} d\xi \tag{2.15}$$

$$t_{jk} = \rho i\omega_e \int_{C_x} n_j \phi_k^0 dl \tag{2.16}$$

Then together with Eq. (2.12) for heave and pitch, T_{jk} can be expressed as follows

$$\begin{aligned}
T_{33} &= T_{33}^0 + \frac{U}{i\omega_e} t_{33}^A - \frac{U}{i\omega_e} t_{33}^F \\
T_{35} &= T_{35}^0 - \frac{U}{i\omega_e} T_{33}^0 + \frac{U}{i\omega_e} t_{35}^A + \frac{U^2}{\omega_e^2} t_{33}^A - \frac{U}{i\omega_e} t_{35}^F - \frac{U^2}{\omega_e^2} t_{33}^F \\
T_{53} &= T_{53}^0 + \frac{U}{i\omega_e} T_{33}^0 + \frac{U}{i\omega_e} t_{53}^A - \frac{U}{i\omega_e} t_{53}^F \\
T_{55} &= T_{55}^0 + \frac{U^2}{\omega_e^2} T_{33}^0 + \frac{U}{i\omega_e} t_{55}^A + \frac{U^2}{\omega_e^2} t_{53}^A - \frac{U}{i\omega_e} t_{55}^F - \frac{U^2}{\omega_e^2} t_{53}^F
\end{aligned} \tag{2.17}$$

where t_{jk}^A and t_{jk}^F refer to the line integral evaluated at the aftmost and foremost sections, respectively. The symmetry relationship $T_{jk}^0 = T_{kj}^0$ can be shown by using Green's second identity in combination with the radiation condition and that ϕ_k satisfies the free surface condition $-\omega_e^2\phi_k + g\frac{\partial \phi_k}{\partial z}$ on $z = 0$ and 2D Laplace equation. Further, by assuming $\partial/\partial x \ll \partial/\partial y$ or $\partial/\partial z$ in the neighborhood of the hull, we can for $k, j = 3, 5$ write

$$\begin{aligned}
T_{33}^0 &= \int_L t_{33} d\xi \\
T_{35}^0 &= T_{35}^0 = -\int_L \xi t_{33} d\xi \\
T_{55}^0 &= \int_L \xi^2 t_{33} d\xi
\end{aligned} \tag{2.18}$$

Here t_{33} can be expressed by the sectional two-dimensional added mass a_{33} and damping coefficient b_{33} as

$$t_{33} = \omega_e^2 a_{33} - i\omega_e b_{33} \tag{2.19}$$

The added mass coefficients can now be expressed as Eq. (2.20) by using the previous expressions and the definition given in Eq. (2.5).

$$\begin{aligned}
A_{33} &= \int_L a_{33} d\xi - \frac{U}{\omega_e^2} b_{33}^A + \frac{U}{\omega_e^2} b_{33}^F \\
A_{35} &= -\int_L \xi a_{33} d\xi + \frac{U}{\omega_e^2} \int_L b_{33} d\xi + \frac{U}{\omega_e^2} x_A b_{33}^A + \frac{U^2}{\omega_e^2} a_{33}^A - \frac{U}{\omega_e^2} x_F b_{33}^F - \frac{U^2}{\omega_e^2} a_{33}^F \\
A_{53} &= -\int_L \xi a_{33} d\xi - \frac{U}{\omega_e^2} \int_L b_{33} d\xi + \frac{U}{\omega_e^2} x_A b_{33}^A - \frac{U}{\omega_e^2} x_F b_{33}^F \\
A_{55} &= \int_L \xi^2 a_{33} d\xi + \frac{U^2}{\omega_e^2} \int_L a_{33} d\xi - \frac{U}{\omega_e^2} x_A^2 b_{33}^A - \frac{U^2}{\omega_e^2} x_A a_{33}^A + \frac{U}{\omega_e^2} x_F^2 b_{33}^F + \frac{U^2}{\omega_e^2} x_F a_{33}^F
\end{aligned} \tag{2.20}$$

Similarly can be done for the damping coefficients, *i.e.*

$$
\begin{aligned}
B_{33} &= \int_L b_{33}d\xi + Ua_{33}^A - Ua_{33}^F \\
B_{35} &= -\int_L \xi b_{33}d\xi - U\int_L a_{33}d\xi - Ux_Aa_{33}^A + \frac{U^2}{\omega_e^2}b_{33}^A + Ux_Fa_{33}^F - \frac{U^2}{\omega_e^2}b_{33}^F \\
B_{53} &= -\int_L \xi b_{33}d\xi + U\int_L a_{33}d\xi - Ux_Aa_{33}^A + Ux_Fa_{33}^F \\
B_{55} &= \int_L \xi^2 b_{33}d\xi + \frac{U^2}{\omega_e^2}\int_L b_{33}d\xi + Ux_A^2a_{33}^A - \frac{U^2}{\omega_e^2}x_Ab_{33}^A - Ux_F^2a_{33}^F + \frac{U^2}{\omega_e^2}x_Fb_{33}^F
\end{aligned}
\tag{2.21}
$$

Here a_{33}^A and a_{33}^F mean the sectional added mass at the aft and start strip respectively. Similarly b_{33}^A and b_{33}^F mean the sectional damping coefficient at the two ends. In our numerical model, only a_{33}^F and b_{33}^F for the first segment are zero. Further, x_A and x_F mean the x-coordinate of the aftmost and foremost section, respectively. The sectional added mass a_{33} and damping b_{33} coefficients can be found by solving a 2D boundary value problem (*e.g.* Salvesen *et al.* (1970)). This has to be done numerically. The commercial computer VERES that is used in this thesis, does that by a Boundary Element Method. The velocity potential is by Green's second identity expressed in terms of distribution of Rankine sources and dipoles over the mean wetted body surface and the mean free surface. The free surface length has to be truncated and a radiation condition requiring 2D outgoing waves is imposed.

2.3.4 Excitation forces and moments for a rigid body part

Equation (2.7) shows that the excitation forces and moments include the incident wave (Froude-Krylov) part F_j^I as

$$F_j^I = \rho\iint_S i\omega_0\phi_I n_j ds \tag{2.22}$$

and diffraction force part F_j^D as

$$F_j^D = \rho\iint_S\left(i\omega_e\phi_D + U\frac{\partial\phi_D}{\partial x}\right)n_j ds \tag{2.23}$$

By applying Stokes theorem in Eq. (2.11), F_j^D can be expressed in a similar form as Eq. (2.12) with contributions both from the foremost section and the aftmost section. This means

$$F_j^D = \rho\iint_S(i\omega_e n_j + Um_j)\phi_D ds + \rho U\int_{C_A} n_j\phi_D dl - \rho U\int_{C_F} n_j\phi_D dl \tag{2.24}$$

Further, by introducing the sectional Froude-Krylov force $f_3(x)$ and sectional diffraction force $h_3(x)$ in vertical direction, the vertical excitation force and pitch excitation moment can be written as

$$F_3 = \rho\zeta_a\int_L (f_3 + h_3)d\xi + \rho\zeta_a\frac{U}{i\omega_e}h_3^A - \rho\zeta_a\frac{U}{i\omega_e}h_3^F \tag{2.25}$$

$$F_5 = -\rho\zeta_a\int_L\left(\xi(f_3 + h_3) - \frac{U}{i\omega_e}h_3\right)d\xi - \rho\zeta_a\frac{U}{i\omega_e}x_Ah_3^A + \rho\zeta_a\frac{U}{i\omega_e}x_Fh_3^F \tag{2.26}$$

Here h_3^A and h_3^F are the sectional diffraction force at the aftmost and foremost section, respectively. Details of the calculation of the sectional forces can be found in Salvesen *et al.* (1970).

2.3.5 Coordinate transformations

When dealing with our three-body problem, we must in Eqs. (2.20), (2.21), (2.25) and (2.26) use X_i relative to the local COG for each body. This means

$$X_i = x_i - x_{cog,i} \tag{2.27}$$

where $x_{cog,i}$ is the x-coordinate of the local COG in the global system. x_i and X_i are the longitudinal coordinates before and after transformation to segment i, respectively. It must be noted that we keep the phasing of the incident waves given by Eq. (2.8) relative to the global coordinate system.

For the whole catamaran, the longitudinal center of buoyancy (LCB) and longitudinal center of gravity (LCG) overlap. However, this is not so for each segment. Further, the restoring terms for each segment found from Eq. (2.9) is based on the local LCB, which should then be transferred to local LCG system for the global response calculations. If X_P is the X-coordinate of LCB in LCG system, there are the following relationships for the restoring terms in the LCB system (C_{ij}) and in the LCG system (C'_{ij}).

$$\begin{aligned} C'_{33} &= C_{33} \\ C'_{35} &= C_{35} - X_P C_{33} \\ C'_{53} &= C_{53} - X_P C_{33} \\ C'_{55} &= C_{55} - X_P C_{53} - X_P C_{35} + X_P^2 C_{33} \end{aligned} \tag{2.28}$$

2.4 Restoring terms due to beam connections

The effective stiffness of the longitudinal steel transducer and aluminum spring are quite close. They were therefore modified as one equivalent beam. Geometry and detailed analysis of this connection are presented in Appendix A.6

To account for the forces from the connecting beams, we start from the static beam equation $EI\frac{\partial^4 w}{\partial x^4} = q$ with $q = 0$. Here EI is the bending stiffness, w is the vertical beam deformation with positive direction upwards and q is the external load per unit length. The connecting beam AB between Body1 and Body2 is used to illustrate the procedure (see Fig. 2.6).

In Figure 2.6, x is the local coordinate along the beam, with $x = 0$ at point A and $x = L$ at point B. The beam equation can be integrated and the solutions are

$$\begin{aligned} w(x) &= \frac{1}{EI}(\frac{1}{6}a\,x^3 + \frac{1}{2}b\,x^2 + c\,x + d) \\ \frac{\partial w(x)}{\partial x} &= \frac{1}{EI}(\frac{1}{2}a\,x^2 + b\,x + c) \end{aligned} \tag{2.29}$$

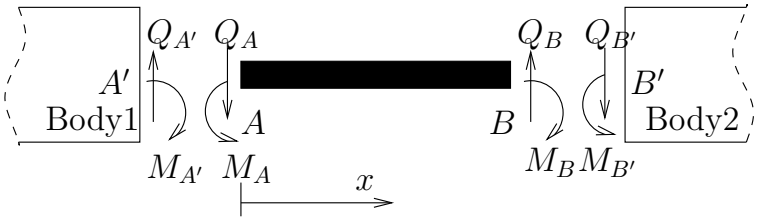

Figure 2.6 Elastic beam connection between two adjacent rigid body segments (side view)

The boundary conditions of the beam require that the vertical and rotational displacements at the ends of A and B should match those at the adjacent ends of Body1 and Body2. Hence,

$$\begin{aligned} w|_A &= \eta_3^1 - \overline{O_1A}\,\eta_5^1 \\ w|_B &= \eta_3^2 + \overline{O_2B}\,\eta_5^2 \\ \frac{\partial w}{\partial x}\Big|_A &= -\eta_5^1 \\ \frac{\partial w}{\partial x}\Big|_B &= -\eta_5^2 \end{aligned} \tag{2.30}$$

where η_3^i and η_5^i are heave of COG and pitch of Body i. Further, $\overline{O_iX}$ denotes the distance from the beam end X to the local COG of the adjacent body i. One should notice the different sign definition between $\partial w/\partial x$ and η_5. This means $\partial w/\partial x = -\eta_5$, as illustrated in Fig. 2.7.

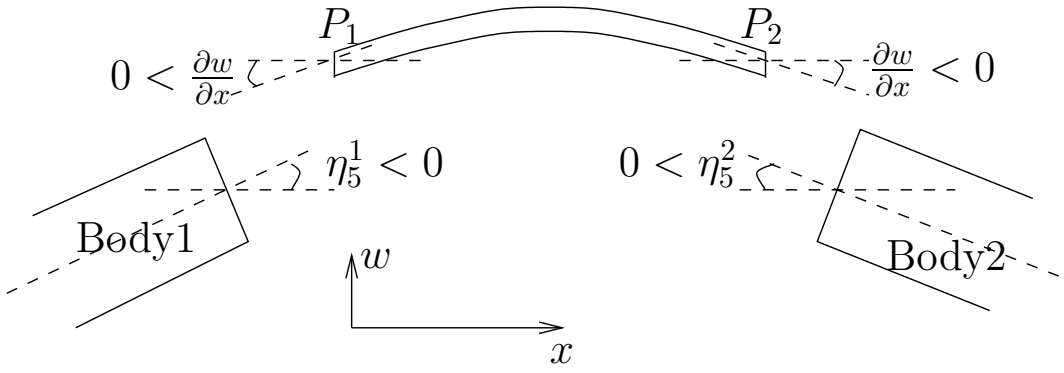

Figure 2.7 Rotational sign illustration for beam and adjacent bodies

The coefficients in Eq. (2.29) can then be expressed in terms of the degrees of freedom of Body1 and Body2.

$$\begin{pmatrix} a \\ b \\ c \\ d \end{pmatrix} = \frac{EI}{L^3} \begin{bmatrix} 12 & -6(L+2\,\overline{O_1A}) & -12 & -(L+2\,\overline{O_2B}) \\ -6L & 2(2L+3\,\overline{O_1A})L & 6L & 2(L+3\,\overline{O_2B})L \\ 0 & -L^3 & 0 & 0 \\ L^3 & -\overline{O_1A}\,L^3 & 0 & 0 \end{bmatrix} \begin{pmatrix} \eta_3^1 \\ \eta_5^1 \\ \eta_3^2 \\ \eta_5^2 \end{pmatrix} \tag{2.31}$$

The longitudinal distribution of vertical shear force $Q(x)$ and bending moment $M(x)$ at the right hand side of the beam cut can be expressed as

$$\begin{aligned} Q(x) &= -EI\frac{\partial^3 w}{\partial x^3} = -a \\ M(x) &= -EI\frac{\partial^2 w}{\partial x^2} = -ax - b \end{aligned} \tag{2.32}$$

The sign definition is given in Fig. 2.6.

By inserting $x = 0$ at A and $x = L$ at B, we get forces and moments at the two ends of the beam AB as follows

$$Q_A = Q_B = \frac{6EI}{L^3}\left(-2\eta_3^1 + 2\eta_3^2 + (L + 2\,\overline{O_1A})\eta_5^1 + (L + 2\,\overline{O_2B})\eta_5^2\right) \tag{2.33}$$

$$M_A = \frac{2EI}{L^2}\left(3\eta_3^1 - 3\eta_3^2 - (2L + 3\,\overline{O_1A})\eta_5^1 - (L + 3\,\overline{O_2B})\eta_5^2\right) \tag{2.34}$$

$$M_B = \frac{2EI}{L^2}\left(-3\eta_3^1 + 3\eta_3^2 + (L + 3\,\overline{O_1A})\eta_5^1 + (2L + 3\,\overline{O_2B})\eta_5^2\right) \tag{2.35}$$

A similar formulation can be obtained for the second connecting beam of Body2 and Body3, with ends named C and D, respectively.

The loads acting on the ship system due to the connecting beams can then be expressed as shown in Eq. (2.36).

$$\begin{pmatrix} F_3^1 \\ F_5^1 \\ F_3^2 \\ F_5^2 \\ F_3^3 \\ F_5^3 \end{pmatrix} = \begin{pmatrix} Q_A \\ M_A - Q_A\,\overline{O_1A} \\ Q_C - Q_B \\ M_C - M_B - Q_B\,\overline{O_2B} - Q_C\,\overline{O_2C} \\ -Q_D \\ -M_D - Q_D\,\overline{O_3D} \end{pmatrix} = \mathbf{kr} \tag{2.36}$$

Here, F_i^j with $i = 3, 5$ represent heave force and pitch moment respectively, and $j = 1, 2, 3$ mean Body1, Body2 and Body3. Q_X and M_X are vertical shear forces and bending moments at point X, as illustrated in Fig. 2.6. The vector $\mathbf{r}$ is $[\eta_3^1\ \eta_5^1\ \eta_3^2\ \eta_5^2\ \eta_3^3\ \eta_5^3]^T$, and $\mathbf{k}$ is a symmetric matrix

of 6×6, with non-zero terms as in Eqs. (2.37), where $\gamma = EI/L^3$.

$$
\begin{aligned}
k_{11} &= -12\,\gamma \\
k_{12} &= 6(L + 2\,\overline{O_1A})\,\gamma \\
k_{13} &= 12\,\gamma \\
k_{14} &= 6(L + 2\,\overline{O_2B})\,\gamma \\
k_{22} &= -4(L^2 + 3L\,\overline{O_1A} + 4\,\overline{O_1A}^2)\,\gamma \\
k_{23} &= -6(L + 2\,\overline{O_1A})\,\gamma \\
k_{24} &= -2(L^2 + 3L\,\overline{O_1A} + 3L\,\overline{O_2B} + 6\,\overline{O_1A}\,\overline{O_2B})\,\gamma \\
k_{33} &= -24\,\gamma \\
k_{34} &= 12(\overline{O_2C} - \overline{O_2B})\,\gamma \\
k_{35} &= 12\,\gamma \\
k_{36} &= 6(L + 2\,\overline{O_3D})\,\gamma \\
k_{44} &= -4(2L^2 + 3L\,\overline{O_2B} + 3L\,\overline{O_2C} + 3\,\overline{O_2B}^2 + 3\,\overline{O_2C}^2)\,\gamma \\
k_{45} &= -6(L + 2\,\overline{O_2C})\,\gamma \\
k_{46} &= -2(L^2 + 3L\,\overline{O_2C} + 3L\,\overline{O_3D} + 6\,\overline{O_2C}\,\overline{O_3D})\,\gamma \\
k_{55} &= -12\,\gamma \\
k_{56} &= -6(L + 2\,\overline{O_3D})\,\gamma \\
k_{66} &= -4(L^2 + 3L\,\overline{O_3D} + 3\,\overline{O_3D}^2)\,\gamma
\end{aligned}
\tag{2.37}
$$

In establishing Eq. (2.36), care should be shown when determining the signs of the forces acting on the ship segments from the spring-transducer connections. The signs were verified by checking the deformation Eq. (2.29) and forces Eq. (2.32) along the beams by giving a unit displacement at the beam ends.

2.5 The complete dynamic system

It should be noted that the structural damping is neglected in our system. Relevant discussions will be presented in Chapter 5. By now introducing all the previously discussed terms, the total matrices of the dynamic system in Eq. (2.1) can be expressed as

$$
\mathbf{M}_{gen} = \begin{bmatrix}
M^1 + A^1_{33} & A^1_{35} & 0 & 0 & 0 & 0 \\
A^1_{53} & I^1_{55} + A^1_{55} & 0 & 0 & 0 & 0 \\
0 & 0 & M^2 + A^2_{33} & A^2_{35} & 0 & 0 \\
0 & 0 & A^2_{53} & I^2_{55} + A^2_{55} & 0 & 0 \\
0 & 0 & 0 & 0 & M^3 + A^3_{33} & A^3_{35} \\
0 & 0 & 0 & 0 & A^3_{53} & I^3_{55} + A^3_{55}
\end{bmatrix}
\tag{2.38}
$$

$$\mathbf{B}_{gen} = \begin{bmatrix} B^1_{33} & B^1_{35} & 0 & 0 & 0 & 0 \\ B^1_{53} & B^1_{55} & 0 & 0 & 0 & 0 \\ 0 & 0 & B^2_{33} & B^2_{35} & 0 & 0 \\ 0 & 0 & B^2_{53} & B^2_{55} & 0 & 0 \\ 0 & 0 & 0 & 0 & B^3_{33} & B^3_{35} \\ 0 & 0 & 0 & 0 & B^3_{53} & B^3_{55} \end{bmatrix} \tag{2.39}$$

$$\mathbf{K}_{gen} = \begin{bmatrix} K^1_{33} - k_{11} & K^1_{35} - k_{12} & -k_{13} & -k_{14} & 0 & 0 \\ K^1_{53} - k_{21} & K^1_{55} - k_{21} & -k_{23} & -k_{24} & 0 & 0 \\ -k_{31} & -k_{32} & K^2_{33} - k_{33} & K^2_{35} - k_{34} & -k_{35} & -k_{36} \\ -k_{41} & -k_{42} & K^2_{53} - k_{43} & K^2_{55} - k_{44} & -k_{45} & -k_{46} \\ 0 & 0 & -k_{53} & -k_{54} & K^3_{33} - k_{55} & K^3_{35} - k_{55} \\ 0 & 0 & -k_{63} & -k_{64} & K^3_{53} - k_{65} & K^3_{55} - k_{66} \end{bmatrix} \tag{2.40}$$

Here A^k_{ij}, B^k_{ij} and K^k_{ij} are the added mass, damping and hydrostatic restoring respectively, in heave ($i, j = 3$) and pitch ($i, j = 5$) directions on Body number k, defined in earlier equations in Section 2.3. k_{ij} are restoring terms due to beam connection as shown in Eq. (2.37). $\mathbf{F}_{gen}$ is the sum of the wave excitation loads on the side hulls and the wetdeck slamming loads. Detailed derivation of slamming forces will be presented in Chapter 3.

In the experiments there is a transient period for ship motions to reach steady-state conditions. An artificial transient period is used in the numerical solution. This is done by expressing the linear wave excitation loads on the side hulls as

$$F'_{exc}(t) = F_{exc}(t) \sin(\frac{\pi}{2nT} t) \tag{2.41}$$

for $0 \leq t < nT$. Here T is the incident wave period. n is typically chosen as 4 in the numerical solutions. This means that the transient period lasts for four incident wave periods. When $t \geq nT$, the excitation load $F_{exc}(t)$ is the same as predicted by the linear strip theory previously outlined. If this transient period is not introduced and the calculations start with $F_{exc}(t)$, too strong wetdeck slamming may occur initially and cause collapse of the numerical solution.

To improve the numerical stability of the dynamic response system when slamming happens, all the terms in the slamming loads that can be explicitly expressed in terms of accelerations, velocities and motions are moved to the left hand side of the dynamic system (See expressions later in Chapter 3 and Appendix B.2).

Fourth order Runge-Kutta method is used in the time integration to find global response. The constant averaged acceleration method, linear acceleration method and the second difference method (See *e.g.* Langen and Sigbjörnsson (1979)) were also found satisfactory. Attempts to use the Euler method were unsuccessful. The algorithm of the fourth order Runge Kutta method can be described as follows by using the reference differential equation $dy/dt = f(t, y)$ with given initial conditions $y(t_0) = y_0$. So given a equidistant integration step h and values t_n, y_n at step N, the value y_{n+1} at step $N + 1$ can be calculated by the following formula (*e.g.* Cheney and

Kincaid (1999))

$$\begin{aligned} k_1 &= hf(t_n,\, y_n) \\ k_2 &= hf(t_n + \frac{1}{2}h,\, y_n + \frac{1}{2}k_1) \\ k_3 &= hf(t_n + \frac{1}{2}h,\, y_n + \frac{1}{2}k_2) \\ k_4 &= hf(t_n + h,\, y_n + k_3) \\ t_{n+1} &= t_n + h \\ y_{n+1} &= y_n + \frac{1}{6}(k_1 + 2k_2 + 2k_3 + k_4) \end{aligned} \tag{2.42}$$

To apply this fourth order Runge-Kutta integration method, the second order differential equations of Eq. (2.1) should be rewritten into a set of first order differential equations. By introducing a new set of variables $\mathbb{X}$, which is defined as

$$\mathbb{X} = \begin{bmatrix} \dot{\mathbf{r}} \\ \mathbf{r} \end{bmatrix} \tag{2.43}$$

we get the following dynamic system

$$\widetilde{\mathbb{M}}\dot{\mathbb{X}} = \widetilde{\mathbb{K}}\mathbb{X} + \widetilde{\mathbb{F}} \tag{2.44}$$

Here $\widetilde{\mathbb{K}}$ and $\widetilde{\mathbb{M}}$ are square matrices in dimensions 12×12 and $\widetilde{\mathbb{F}}$ is a vector in dimensions 12×1. They are defined as

$$\widetilde{\mathbb{K}} = \begin{bmatrix} -\mathbf{B}_{gen} & -\mathbf{K}_{gen} \\ \mathbf{1} & \mathbf{0} \end{bmatrix} \qquad \widetilde{\mathbb{M}} = \begin{bmatrix} \mathbf{M}_{gen} & \mathbf{0} \\ \mathbf{0} & \mathbf{1} \end{bmatrix} \qquad \widetilde{\mathbb{F}} = \begin{bmatrix} \mathbf{F}_{gen} \\ \mathbf{0} \end{bmatrix} \tag{2.45}$$

$\mathbf{M}_{gen}$, $\mathbf{B}_{gen}$, $\mathbf{K}_{gen}$ and $\mathbf{F}_{gen}$ are defined by Eq. (2.1). Further, $\mathbb{X}$ is a column matrix with $\mathbb{X} = [X_1 \cdots X_k \cdots X_{12}]^T$, where X_{2i-1} with $i = 1, 2, 3$ are the heave velocities of body number i and X_{2i} with $i = 1, 2, 3$ are the pitch velocities of body i. Further, X_{2i+5} with $i = 1, 2, 3$ are the heave motions of body number i and X_{2i+6} with $i = 1, 2, 3$ are the pitch motions of body i. Then, the iteration procedure described by Eq. (2.42) can be applied to this 12 dimensional system.

The numerical simulation procedure of combining the linear and slamming induced response is illustrated in the flow chart in Appendix C.

Chapter 3

Slamming Theories

3.1 Introduction

Slamming loads on the wetdeck will be considered in this chapter. Our interest is in predicting global slamming induced response. An important time scale is the natural period of two node bending of the hull. Phenomena happening on a much shorter time scale will not matter in this context. We can then neglect the effect of possible air cushions, the compressibility of the air and the water as well as the local hydroelasticity. The flow can be considered irrotational.

The slamming can be divided into a water entry and exit phase, which means that the wetted surface of the wetdeck increases and decreases, respectively. The water entry phase is characterized by positive upwards force, while the forces are mainly negative during the water exit phase. The magnitude of the initial impact force depends on where the water initially hits. If the impact occurs initially at the front end of the wetdeck, there is a finite angle between the wetdeck and the free surface. If this is not the case and the initial impact occurs at wetdeck positions with continuous slope, the free surface has to be initially tangential to the wetdeck surface. This implies higher initial loads than if there is a finite angle between the wetdeck and the free surface.

The fluid accelerations in the vicinity of the impacting body are initially much larger than the gravitational acceleration. The total slamming duration is assumed sufficiently small for gravity waves not to be generated. This implies that the gravity is only included in the nonlinear Froude-Krylov and hydrostatic restoring loads on the wetdeck.

3.2 High frequency boundary value problem

By assuming incompressible fluid and irrotational flow, a velocity potential that satisfies Laplace equation can be applied. The velocity potential Φ is divided into two main parts, *i.e.*

$$\Phi = \phi_{slm} + \phi_{add} \tag{3.1}$$

Here ϕ_{slm} is the velocity potential due to wetdeck slamming. ϕ_{add} contains the incident wave potential ϕ_I , the disturbance due to the side hulls ϕ_{sh} and a uniform stream with velocity U equal to the steady forward speed of the vessel as observed when moving with a coordinate system propagating with U relative to an earth-fixed coordinate system. This means

$$\phi_{add} = Ux + \phi_I + \phi_{sh} \tag{3.2}$$

where x is a longitudinal coordinate that is positive aftwards (See Fig. 2.3).

3.2.1 Basic equations

Only head sea conditions are studied in this thesis. They are the most severe cases from a wetdeck slamming point of view at forward speed. Regular incident waves are considered. When the forward speed is not small, slamming will occur in the forward part of the wetdeck. ϕ_{add} can then be approximated by Ux and ϕ_I except for in the close vicinity of the side hulls. It is assumed that the transverse cross-section of the wetdeck has a horizontal surface. By neglecting the local run-up along the side hulls two-dimensional flow in the longitudinal cross-sectional plane of the ship can be assumed in solving ϕ_{slm}. This means

$$\nabla^2\phi_{slm} = \frac{\partial^2\phi_{slm}}{\partial x^2} + \frac{\partial^2\phi_{slm}}{\partial z^2} = 0 \tag{3.3}$$

Both free surface conditions and body boundary conditions are required in solving Eq. (3.3).

3.2.2 Free surface conditions

We here first discuss the dynamic free surface condition which states that the pressure is atmospheric on the free surface. The pressure p can be expressed by the Bernoulli's equation as

$$p + \rho g z + \rho\frac{\partial\Phi}{\partial t} + \frac{\rho}{2}\nabla\mathbf{\Phi}\cdot\nabla\mathbf{\Phi} = C \tag{3.4}$$

where C is a constant. Here $z = 0$ corresponds to the mean free surface, and z is a vertical coordinate that is positive upwards. ρ is the mass density of the fluid and g is the acceleration of gravity. By assuming the velocity potential at infinity is Ux, C can be written as $\frac{1}{2}\rho U^2 + p_a$, where p_a is the atmospheric pressure. By using Eq. (3.1), neglecting ϕ_{sh} and denoting p as the excess pressure relative to atmospheric pressure, we can write

$$\begin{aligned} p = &-\rho\frac{\partial\phi_{slm}}{\partial t} - \rho U\frac{\partial\phi_{slm}}{\partial x} \\ &- \rho[\frac{\partial\phi_I}{\partial x}\frac{\partial\phi_{slm}}{\partial x} + \frac{\partial\phi_I}{\partial z}\frac{\partial\phi_{slm}}{\partial z}] - \frac{\rho}{2}[(\frac{\partial\phi_{slm}}{\partial x})^2 + (\frac{\partial\phi_{slm}}{\partial z})^2] \\ &+ p_{inc} - \rho g z \end{aligned} \tag{3.5}$$

Here p_{inc} is the pressure due to the incident regular waves, given as

$$p_{inc} = -\rho\frac{\partial\phi_I}{\partial t} - \rho U\frac{\partial\phi_I}{\partial x} - \frac{\rho}{2}[(\frac{\partial\phi_I}{\partial x})^2 + (\frac{\partial\phi_I}{\partial z})^2] \tag{3.6}$$

The two last terms in Eq. (3.5) are what give the nonlinear Froude-Krylov and hydrostatic restoring loads on the wetdeck. They can be further approximated at the wetdeck and expressed as $-\rho g(z-\zeta_{inc})$ for $z \leq \zeta_{inc}$ where ζ_{inc} is the incident wave elevation (Faltinsen (1990)). This means a pressure component that is hydrostatic relative to the incident wave elevation in the vicinity of the free surface. This pressure term contributes but is not dominant.

The terms associated with ϕ_{slm} in Eq. (3.5) have different order of magnitudes. The first term $-\rho\partial\phi_{slm}/\partial t$ which is associated with the fluid acceleration, has already implicitly from previous discussions been assumed to be large. The order of magnitude of the second term relative to the first term is UT_d/L where L is a measure of the wetted length and T_d is a measure of the slamming duration. If U is very large, this term should be considered. The other terms involving ϕ_{slm} in Eq. (3.5) are in general small relative to the first term. If the details of the jet flow at the intersection between the free surface and the body surface are studied, the pressure term $-\frac{1}{2}\rho|\nabla\phi_{slm}|^2$ should be included (Wagner (1932)). Since this is not focused on in this thesis, the quadratic velocity term associated with $\nabla\phi_{slm}$ is neglected.

Basically, two alternatives will be considered in our further analysis. The pressure due to slamming is approximated as $-\rho\partial\phi_{slm}/\partial t$ in the first case. This gives $\partial\phi_{slm}/\partial t = 0$ as a dynamic free surface condition. Since ϕ_{slm} is initially zero on the free surface, it implies that ϕ_{slm} remains zero on the free surface. This condition will by a Taylor expansion be transferred to a horizontal line $Z = 0$ where also the body boundary condition is transferred (See Fig. 3.1). Keeping the dominant term in the Taylor expansion implies that ϕ_{slm} is also zero on $Z = 0$, *i.e.*

$$\phi_{slm} = 0 \qquad \text{on } Z = 0 \text{ and } |x| > c(t) \tag{3.7}$$

Another case is that the first two terms in Eq. (3.5) have the same order of magnitude. This leads to a different dynamic free surface condition that has to be combined with a Kutta condition at the aft intersection point between the deck and the free surface. This will be dealt with later in Section 3.6.

The kinematic free surface condition expresses that free surface particles stay on the free surface. One approach is to use a Von Karman method. This means that the wetted surface follows simply from geometrical intersection between the incident waves and the wetted surface. Another approach is a Wagner method where the local uprise of the free surface due to the impact is accounted for. This gives only meaningful results when the wetted surface increases, *i.e.* during the water entry phase.

3.2.3 Body boundary condition

The body boundary condition expresses that there is no flow through the body surface. This means that the flow velocity normal to the body surface is equal to the component of the body velocity $\mathbf{V}$ normal to the body surface, *i.e.*

$$\frac{\partial\Phi}{\partial n} = \mathbf{V}\cdot\mathbf{n} \Longrightarrow \frac{\partial\phi_{slm}}{\partial n} = \mathbf{V}\cdot\mathbf{n} - \frac{\partial\phi_{add}}{\partial n} \qquad \text{on the body surface} \tag{3.8}$$

Here $\frac{\partial}{\partial n}$ denotes differentiation along the normal direction to the body surface. A geometrical consequence of the wetdeck is that the x-component n_1 of the surface normal vector is much smaller than the vertical component n_3. If positive normal direction is into the fluid domain, the vertical component n_3 can be approximated by -1.

We will allow for the possibility that U is large and is a dominant longitudinal fluid velocity. This means that even if n_1 is small, the normal velocity due to U must be considered. This can be expressed as $U(\eta_5 + \tau)$, where τ accounts for the local time averaged inclination of the wetdeck relative to the mean free surface. Positive τ and η_5 correspond to bow-up. The angle τ expresses then the local geometry as for instance due to the bow ramp. It includes also the trim due to hydrostatic and steady forward speed dependent hydrodynamic forces on the vessel in calm water. There is also a contribution due to time averaged nonlinear hydrodynamic loads caused by unsteady wave-body interaction. η_5 is the local time dependent angular motions of the vessel about the y-axis (See Fig. 2.3). It will in practice for the analyzed three-body model mean the pitch angle of the front body.

The vertical velocity of the body w_{body} can in the case of a rigid body in head sea be expressed as $d\eta_3/dt - xd\eta_5/dt$ where η_3 is the heave of the COG of the whole vessel. When the three-body model is considered, w_{body} is redefined in terms of the rigid body vertical velocity of the body where impact occurs.

The body boundary condition can be transferred to the horizontal line $Z = 0$ (See Fig. 3.1). Mathematically it is expressed as

$$\frac{\partial \phi}{\partial Z} = V_R(x,t) \qquad \text{on } Z = 0 \text{ and } a(t) < x < b(t) \tag{3.9}$$

where from now on ϕ means ϕ_{slm}. $V_R(x,t)$ is the relative impact velocity which in the case of impact on the front body of our three-body model can be expressed as

$$V_R(x,t) = \frac{\partial \eta_3^{(1)}}{\partial t} - x^{(1)} \frac{\partial \eta_5^{(1)}}{\partial t} - U(\eta_5 + \tau) - w \tag{3.10}$$

Here $x^{(1)}$ is a local longitudinal coordinate of the front body with $x^{(1)} = 0$ corresponding to the longitudinal position of the COG of the body. Further, $\eta_3^{(1)}$ and $\eta_5^{(1)}$ are the heave and pitch of the same body. w is the vertical velocity due to the incident waves which is here described by linear regular wave theory. It can be derived from Eq. (2.8) as

$$w = \Re\left\{ \frac{\partial \phi_I}{\partial z} \Big|_{z=0} \right\} = \omega_0 \zeta_a \cos(\omega_e t - kx) \tag{3.11}$$

Here ζ_a is the incident wave amplitude, ω_0 is the circular frequency of the waves, $k = \omega_0^2/g$ and $\omega_e = \omega_0 + kU$ is the circular frequency of encounter. $\Re$ means real part. This boundary condition is consistent with linear theory. The slope of the incident waves is accounted for indirectly when the wetted surface is found.

3.2.4 Boundary value problem

Figure 3.1 illustrates the boundary value problem in the case of the dynamic free surface condition $\phi = 0$. Since this condition is the same free surface condition used for a high-frequency oscillation problem, it is denoted as the high-frequency boundary value problem. We note from Fig. 3.1 that $2c(t)$ is the wetted length of the deck, X and Z are local coordinates with $X = x - l(t)$. Further, $b(t) - l(t) = l(t) - a(t) = c(t)$.

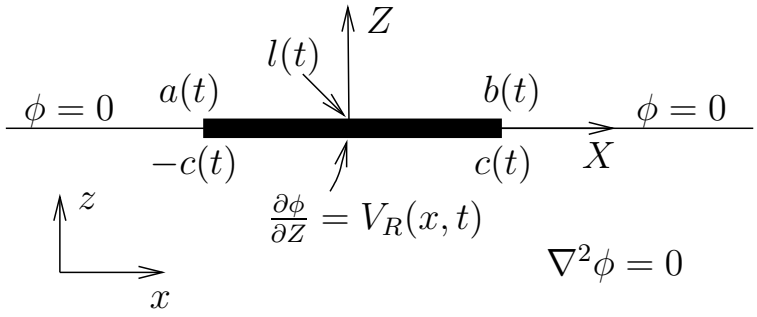

Figure 3.1 Two-dimensional high frequency boundary value problem for slamming. $a(t)$, $b(t)$ and $l(t)$ are ship fixed x-coordinates. X-Z is the local $2D$ coordinate system on the wetted part of the deck.

The boundary value problem described in Fig. 3.1 can be solved by using a vortex distribution from $X = -c$ to $X = c$. This requires additional conditions in order to get a unique solution. This follows by dividing V_R into one part which is symmetric about $X = 0$ and another part which is antisymmetric about $X = 0$. The velocity potentials associated with the symmetric and antisymmetric parts of V_R are required to be respectively symmetric and antisymmetric about $X = 0$. This leads to singular flow at $X = \pm c$, which expresses indirectly that spray occurs at $X = \pm c$. A local flow analysis like Wagner (1932) did is needed to describe the details of the jet flow associated with the spray. In Section 3.6 a different free surface condition will be considered. Uniqueness will then be imposed by requiring a Kutta condition at $X = c$ to get smooth water detachment from the wetdeck. This implies that spray occurs at $X = -c$, but not at $X = c$.

The following text describes different ways of determining $a(t)$ and $b(t)$, *i.e.* by a Von Karman based method and a Wagner based method. V_R will either be expressed in terms of a Fourier series or by using a linear approximation between $X = -c$ and $X = c$.

3.3 Von Karman based method

Here the wetted length during slamming is determined by finding the intersection points between the wetdeck and the undisturbed wave profile, *i.e.* a Von Karman (1929) type method. Expressed mathematically, slamming happens when relative vertical displacement

$$\eta_R = \eta_B(x,t) - \zeta + d(x) \tag{3.12}$$

is less than zero. Here $d(x)$ is the time independent wetdeck height above calm water. $\eta_B(x,t)$ is the vertical body motion, which is determined by the heave and pitch motion for a rigid body as

$$\eta_B = \eta_3 - x\eta_5 \tag{3.13}$$

Further, ζ is the wave elevation at t and x. This can consistently with linear theory be expressed as

$$\zeta = \zeta_a \sin(\omega_e t - kx) \tag{3.14}$$

Slamming will typically occur for our cases when the wave length is the order of the ship length. Based on that the wetted part is relatively short compared with the incident wave length, the impact velocity in Eq. (3.10) can be assumed to be spatially linear in the wetted area, *i.e.*

$$V_R(X,t) = V_1 + V_2 X \tag{3.15}$$

Here X is the local coordinate as in Fig. 3.1. If for instance the ship moves as a rigid body, then

$$\begin{aligned} V_1(x,t) &= \dot{\eta}_3 - l(t)\dot{\eta}_5 - U(\eta_5 + \tau) - \omega_0\zeta_a \cos(\omega_e t - kl(t)) \\ V_2(x,t) &= -\dot{\eta}_5 - \omega_0\zeta_a k \sin(\omega_e t - kl(t)) \end{aligned} \tag{3.16}$$

An exact expression for V_R will presented in Section 3.5. This is done by Fourier expanding V_R over the wetted length, as mentioned in Section 3.2.4.

The boundary value problem can, as already said in Section 3.2.4, be solved by using a vortex distribution along the wetted length and by requiring that the velocity potentials associated with V_1 and V_2 are respectively symmetric and anti-symmetric with respect to the Z-axis. Following the solution procedure of the lifting problem described in Newman (1977), we can determine the vortex density. This is related to the horizontal fluid velocity at the body surface. The velocity potential ϕ on the body surface follows by integrating the horizontal velocity and using that ϕ is zero on the free surface. This gives

$$\begin{aligned} \phi(X,t) = V_1\sqrt{c^2 - X^2} + \frac{1}{2}V_2 X\sqrt{c^2 - X^2} \\ \text{on } Z = 0 \text{ and } |X| < c(t) \end{aligned} \tag{3.17}$$

This formula has also been presented by *e.g.* Zhao and Faltinsen (1992) and Baarholm (2001). Section 3.5 applies a general representation of V_R, and will show that Eq. (3.17) is a special case.

The dynamic pressure p on the wetdeck associated with the slamming can be approximated as

$$\begin{aligned} p &= -\rho\frac{\partial\phi}{\partial t} \\ &= -\rho(V_1 + \frac{1}{2}V_2 X)\frac{1}{\sqrt{c^2 - X^2}}(c\frac{\partial c}{\partial t} - X\frac{\partial X}{\partial t}) \\ &\quad - \rho(\frac{\partial V_1}{\partial t} + \frac{1}{2}\frac{\partial V_2}{\partial t}X)\sqrt{c^2 - X^2} \\ &\quad - \frac{1}{2}\rho V_2\frac{\partial X}{\partial t}\sqrt{c^2 - X^2} \end{aligned} \tag{3.18}$$

Here $\frac{\partial X}{\partial t} = \frac{\partial}{\partial t}(x-l) = -\frac{\partial l}{\partial t}$. Further, by integrating Eq. (3.18) along the wetted part, we find the following instantaneous vertical impact force F_3 and pitch moment F_5 about $X = 0$:

$$\begin{aligned} F_3 &= B\int_{-c}^{c}(-pn_3)dX = B\int_{-c}^{c}pdX \\ &= -\rho\pi c\frac{\partial c}{\partial t}V_1 B - \rho\frac{\pi}{2}c^2\frac{\partial V_1}{\partial t}B \qquad (3.19) \\ &= -\frac{\partial}{\partial t}\Big(\frac{1}{2}\rho\pi c^2 V_1\Big)\,B \qquad (3.20) \end{aligned}$$

$$\begin{aligned} F_5 &= B\int_{-c}^{c}(-pn_5)dX = B\int_{-c}^{c}-p(-xn_3)dX \\ &= B\int_{-c}^{c}-p(X+l)dX \\ &= \frac{\partial}{\partial t}\Big(\frac{1}{2}\rho\pi c^2 V_1 l\Big)\,B + \frac{\partial}{\partial t}\Big(\frac{1}{16}\rho\pi c^4 V_2\Big)\,B \qquad (3.21) \end{aligned}$$

Here B is the width of the wetted part and ρ is the mass density of the water. Further, $n_3 = -1$, as described earlier. The first and second term in F_3 given by Eq. (3.19) will be referred to as the slamming and added mass term, respectively. The slamming term is set equal to zero during the water exit phase, as suggested by Kaplan (1987).

A buoyancy force can be found by integrating the pressure term that is hydrostatic relative to the instantaneous incident wave elevation, as discussed earlier in Section 3.2.2. The integration of the last two terms in Eq. (3.5) will give the nonlinear Froude-Krylov force and hydrostatic restoring force respectively on the wetdeck when slamming happens. The vertical force can be expressed as

$$F_{3,buoy} = \rho g\int_{a(t)}^{b(t)}(\zeta - \eta_B)dx \cdot B \qquad (3.22)$$

Here $a(t)$ and $b(t)$ are the x-coordinate of the two ends of the wetted part (See Fig. 3.1). $\zeta(x,t)$ and η_B are respectively the undisturbed wave elevation and the vertical wetdeck position at (x,t), and are given by Eq. (3.14) and Eq. (3.13). It follows that

$$\begin{aligned} F_{3,buoy} &= \int_{a(t)}^{b(t)}\Big(\zeta_a\sin(\omega_e t - kx) - \big(\eta_a + \frac{\eta_b - \eta_a}{b(t)-a(t)}(x-a(t)\big)dx\Big)\cdot B \\ &= \frac{\zeta_a}{k}\Big[\cos(\omega_e - kx)\Big]_{a(t)}^{b(t)}\cdot B - (\eta_a+\eta_b)\,c(t)\cdot B \qquad (3.23) \end{aligned}$$

Here η_a and η_b denote the vertical wetdeck positions at respectively $x = a$ and b.

The corresponding pitch moment about local COG of the foremost segment, where wetdeck slamming happens, is then simply expressed as

$$F_{5,buoy} = -X'_o F_{3,buoy} \qquad (3.24)$$

where X'_o means the X' value of the midpoint of the wetted length in the local COG system of the foremost segment. These expressions for $F_{3,buoy}$ and $F_{5,buoy}$ are also used in combination with the following methods.

3.4 Wagner based method

Wagner (1932) made an important progress in the analysis of slamming by accounting for the uprise of the water when determining the wetted length. We will generalize his approach to our case. V_R will be approximated by Eq. (3.15). Here we follow the same time stepping procedure as Zhao *et al.* (1996), *i.e.* the time steps are decided based on prescribed change in wetted length. The vertical velocity on the free surface due to ϕ is needed as part of this procedure. This can be expressed as

$$\begin{aligned}\frac{\partial\phi}{\partial Z} &= \frac{-V_1\,|X|}{\sqrt{X^2-c^2}} + V_1 + V_2 X \\ &\quad - \frac{1}{2}\mathrm{sign}(X)V_2(\sqrt{X^2-c^2} + \frac{X^2}{\sqrt{X^2-c^2}}) \\ &\quad \text{on } Z=0 \text{ and } |X| > c(t)\end{aligned} \tag{3.25}$$

Equation (3.25) has also been presented by *e.g.* Zhao and Faltinsen (1992) and Baarholm (2001). It will be shown in Section 3.5, where the exact expression of V_R is used, that Eq. (3.25) follows.

A Wagner based method can only be used during the water entry phase. This is connected with the dynamic free surface condition $\phi = 0$, which assumes the fluid acceleration is dominant relative to gravitational acceleration. This is only a good approximation in an initial stage. Instead a Von Karman method is used during the water exit phase. The formal expressions of F_3 and F_5 are the same as in Eqs. (3.20) and (3.21). Since the Von Karman method uses the dynamic free surface condition $\phi = 0$, one can also object against that method during the water exit phase. However, the Von Karman method will not lead to numerical difficulties in determining the intersection points as the Wagner method would do during the water exit phase. In Section 3.6 a different dynamic free surface condition appropriate for high speed is considered.

Briefly, in the Wagner based method, the time stepping is determined by a prescribed change in the wetted length Δc_{j+1} at time step j and the vertical distance ΔZ_{j+1} that a free surface particle should travel vertically during the time step Δt_{j+1} to hit the deck. The latter is given by (See Fig. 3.3 for illustration)

$$\Delta Z_{j+1} = \int_{\Delta t_{j+1}} (w + \frac{\partial\phi}{\partial Z} - V_{deck})dt \tag{3.26}$$

Here V_{deck} is the vertical velocity of the wetdeck at this moment. $\partial\phi/\partial Z$ and w are defined in Eq. (3.25) and (3.11), respectively. More details of this procedure will be described in the following text.

3.4.1 Local solution near intersection point

Equation (3.25) shows that $\partial\phi/\partial Z$ is singular at $|X| = c$. This can cause numerical problems in the time integration. To avoid this we will first approximate $\partial\phi/\partial Z$ at the two ends. This will enable us to analytically approximate the time integration in the vicinity of the two wetted deck

ends. A standard time integration procedure can be used outside these local areas. The nature of this local flow at the ends can be approximated by focusing only on the details at one end. The rest of the body appears in the small scale around the end as a semi-infinite body. Since the body has a vertical velocity and the free surface condition is $\phi = 0$, we can also say that this local flow would be the same as if we consider a double body in infinite fluid. By double body is meant the original body and the image body about the free surface. This is illustrated in Fig. 3.2 for a general case with interior angle α. The local corner flow will now be analyzed.

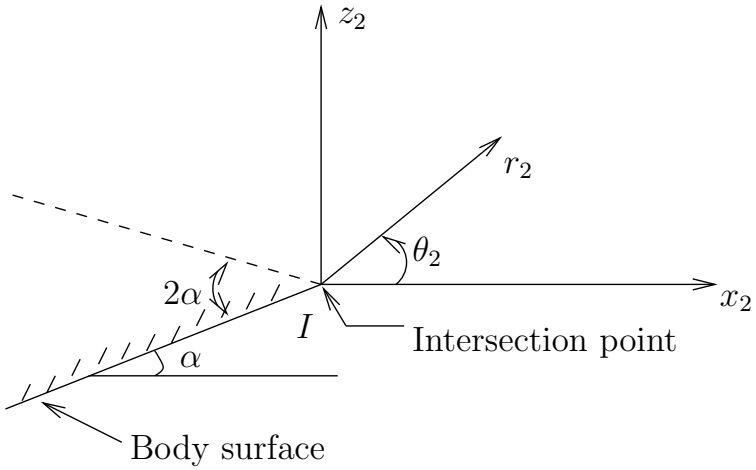

Figure 3.2 Local solution near the intersection point between body and free surface

In Figure 3.2, x_2 runs in the direction of the free surface profile from the intersection point I. α is the angle between the body and the free surface at I. For convenience a polar coordinate system r_2, θ_2 is introduced. We start with the general solution of the complex velocity potential W in the complex form (*e.g.* Art. 63 in Lamb (1932))

$$W = iAZ^n = \phi_{loc} + i\psi_{loc} \tag{3.27}$$

where A is a constant, Z is the complex variable with $Z = x_2 + iz_2 = r_2 e^{i\theta_2}$. Equation (3.27) gives

$$\text{Velocity potential:} \qquad \phi_{loc} = -Ar_2^n \sin(n\theta_2) \tag{3.28}$$

$$\text{Stream function:} \qquad \psi_{loc} = Ar_2^n \cos(n\theta_2) \tag{3.29}$$

By choosing n as $\frac{\pi}{2(\pi-\alpha)}$, one gets irrotational motion in which the boundary is composed of two rigid walls with an interior angle 2α between the walls, *i.e.* one gets the required solution for flow around the corner with angle 2α. This means

$$\phi_{loc} = -Ar_2^{\frac{\pi}{2(\pi-\alpha)}} \sin\Big(\frac{\pi}{2(\pi-\alpha)}\theta_2\Big) \tag{3.30}$$

Here it is easily seen that $\phi_{loc} = 0$ for $\theta_2 = 0$. This is consistent with the global free surface condition $\phi_{global} = 0$. Further, with $\theta_2 = -\pi + \alpha$, we then have the velocity potential

$$\phi_{loc} = Ar_2^{\frac{\pi}{2(\pi-\alpha)}} \qquad \text{on the body surface.} \tag{3.31}$$

From Eq. (3.30), velocities in r_2 and θ_2 directions can be derived as

$$u_{r_2} = \frac{\partial \phi_{loc}}{\partial r_2} = -A r_2^{\frac{\pi}{2(\pi-\alpha)}-1} \sin\Big(\frac{\pi}{2(\pi-\alpha)}\theta_2\Big) \frac{\pi}{2(\pi-\alpha)} \tag{3.32}$$

$$u_{\theta_2} = \frac{1}{r_2}\frac{\partial \phi_{loc}}{\partial_{\theta_2}} = -A r_2^{\frac{\pi}{2(\pi-\alpha)}-1} \cos\Big(\frac{\pi}{2(\pi-\alpha)}\theta_2\Big) \frac{\pi}{2(\pi-\alpha)} \tag{3.33}$$

The horizontal and vertical velocities can be found on the free surface by setting $\theta_2 = 0$, *i.e.*

$$u_{x_2} = u_{r_2}\Big|_{\theta_2=0} = 0 \qquad \text{zero flow along } x_2 \text{ axis,} \tag{3.34}$$

$$w_{loc} = u_{z_2} = u_{\theta_2}\Big|_{\theta_2=0} = -A\frac{\pi}{2(\pi-\alpha)} r_2^{\frac{\pi}{2(\pi-\alpha)}-1} \tag{3.35}$$

A is an unknown in Eq. (3.35). Further, α is zero in our case and A can be found by matching the local and global velocity potential, *i.e.*

$$\phi(X,t)\Big|_{X=\pm c} \text{(Eq. 3.17)} = \phi_{loc}\Big|_{\alpha=0} \text{(Eq. 3.31)} \tag{3.36}$$

This leads to $A = (V_1 \pm \frac{1}{2}V_2 c)\sqrt{2c}$ at $X = \pm c(t)$ respectively.

The following local solutions of vertical velocities on the free surface at the two ends are then obtained by Eq. (3.35).

$$w_{loc} = \begin{cases} -(V_1 + \frac{1}{2}V_2 c)\sqrt{\frac{c}{2(X-c)}} & X > c(t) \text{ and } X \to c(t), \\ -(V_1 - \frac{1}{2}V_2 c)\sqrt{\frac{c}{2(-c-X)}} & X < -c(t) \text{ and } X \to -c(t) \end{cases} \tag{3.37}$$

Here, the singularity of w_{loc} at $X = \pm c$ can be dealt with in the numerical time integration procedure by using the analytical local solution, as illustrated in the following section.

3.4.2 Time stepping procedure to find c(t)

By using Eq. (3.26) the corresponding vertical distance of free surface particles from time step j to $j+1$ near the intersection point can be expressed as

$$\begin{aligned} \Delta Z_{j+1} &= \int_{t_j}^{t_{j+1}} \big(w_{loc} + w - V_{deck}\big) dc \frac{dt}{dc} \\ &= -\left(\frac{dt}{dc}\right)_{m,j+1} A_{m,j+1}\sqrt{c_{j+1} - c_j} \\ &\quad + \left(\frac{dt}{dc}\right)_{m,j+1} (w - V_{deck})_{m,j+1} (c_{j+1} - c_j) \end{aligned} \tag{3.38}$$

Here subscript m means time averaged value. Since $c_{j+1} - c_j$ and ΔZ_{j+1} are known, $(dt/dc)_{m,j+1}$ can be determined from Eq. (3.38). This determines Δt_{j+1} as

$$\Delta t_{j+1} = \left(\frac{dt}{dc}\right)_{m,j+1} (c_{j+1} - c_j) \tag{3.39}$$

The flow at the two ends of the wetted part, *i.e.* at $x = a(t)$ and $b(t)$, are not the same. Further, the position $X = 0$ in the global coordinate system is changing with time due to the wetdeck motion and the incident wave. So for a prescribed $c_{j+1} - c_j$, the predicted Δt_{j+1} at $X = c$ and $X = -c$ will be different. Then some iteration steps are needed to match the right and left ends of the wetted length by requiring that the time duration in each time step for both ends should be the same. Numerically this relationship can be expressed as

$$\Delta t_{L,j+1} = \Delta t_{R,j+1} \Longrightarrow \left(\frac{dt}{dc}\right)_{m,j+1,L} (a_{j+1} - a_j) = \left(\frac{dt}{dc}\right)_{m,j+1,R} (b_{j+1} - b_j) \tag{3.40}$$

The indices L and R mean respectively the left and right hand side. Either side end can be used as the iteration base. Let us say we use the right hand side change as a base with setting the prescribed wetted length change as $c_{j+1} - c_j = b_{j+1} - b_j$. Equation (3.40) gives then the intermediate $a_{j+1,int}$ and consequently an updated $c_{j+1,int}$. Then iterations are carried out until the difference of $c_{j+1,int,N}$ from Nth iteration and $c_{j+1,int,N-1}$ from $(N-1)$th iteration is within required tolerance. Figure 3.3 briefly illustrates this stepping procedure, which is also presented in Zhao *et al.* (1996). But their iteration scheme is not the same. They first estimated the new leftside intersecting point a_{j+1} from its rate of the change with time in the previous time step. Additionally, the body had constant drop velocity in their studies.

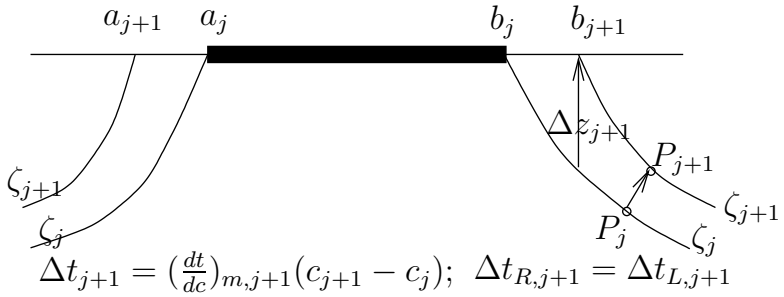

Figure 3.3 Time stepping of Wagner based method

When time step Δt_{j+1} is found, the free surface particles move with their local velocities, and the new free surface position ζ_{j+1} can be found. Since the slamming induced velocity potential ϕ yields zero horizontal velocity, the particles move horizontally with the horizontal velocity of the incident wave. If only the linear wave part is considered, the horizontal wave velocity can be expressed as

$$u = \Re\left\{ \frac{\partial \phi_I}{\partial x} \Big|_{z=0} \right\} = \omega_0 \zeta_a \sin(\omega_e t - kx) \tag{3.41}$$

The vertical velocity includes w from the wave particles as defined in Eq. (3.11) and the velocity $\partial\phi/\partial Z$ due to local pile-up effect as defined in Eq. (3.25). Here it is assumed that the vertical velocity is much higher than the horizontal velocity at the intersecting area. The reason is that vertical slamming induced velocity is singular at the intersecting points (See Eq. (3.25)) while the horizontal one is not.

The Wagner based solution procedure has been verified by comparing with the analytical solution presented in Zhao and Faltinsen (1992), for an incident wave crest hitting a horizontal fixed deck. Since the procedure requires that ΔZ_{j+1} in Eq. (3.38) is positive, *i.e.* that the wetted surface increases, the method works only during the water entry phase.

3.5 Exact representation of relative impact velocity V_R

3.5.1 Fourier expansion of V_R

In the earlier theories, V_R was assumed to be spatially linear in the wetted area. The exact expressions of V_R will now be accounted for. This is done by first expressing $V_R(x,t)$ as a Fourier series, *i.e.*

$$V_R = \sum_{n=0}^{\infty} A_n cos(n\theta) \tag{3.42}$$

where θ is defined by

$$X = c(t)\cos\theta \tag{3.43}$$

Here $\theta = 0$ and π correspond to respectively $X = c$ and $-c$. The derivation is still based on the high-frequency boundary value problem model illustrated in Fig. 3.1. The details will be shown for a ship with rigid body motions.

V_R in Eq. (3.10) can be rewritten as

$$V_R(X,t) = V_1(t) + V_2(t)X + V_3(t)\cos(kX) + V_4(t)\sin(kX) \tag{3.44}$$

with

$$\begin{aligned} V_1 &= \dot{\eta}_3 - l(t)\dot{\eta}_5 - U(\eta_5 + \tau) \\ V_2 &= -\dot{\eta}_5 \\ V_3 &= -\omega_0\zeta_a\cos(\omega_e t - kl(t)) \\ V_4 &= -\omega_0\zeta_a\sin(\omega_e t - kl(t)) \end{aligned} \tag{3.45}$$

Here it is noticed that V_1 and V_2 are not the same as V_1 and V_2 when V_R is expressed as $V_R = V_1 + V_2X$ (See Eqs. (3.16)).

The Fourier coefficients in Eq. (3.42) can be formally expressed as

$$\begin{aligned} A_0 &= \frac{1}{\pi}\int_0^{\pi} V_R\, d\theta \\ A_n &= \frac{2}{\pi}\int_0^{\pi} V_R\cos n\theta\, d\theta \end{aligned} \tag{3.46}$$

By using (See pp.402 in Gradshteyn and Ryzhik (1994))

$$\begin{aligned}\int_0^\pi \cos(kc\cos\theta)\cos n\theta\, d\theta &= \pi\cos\frac{n\pi}{2}J_n(kc)\\ \int_0^\pi \sin(kc\cos\theta)\cos n\theta\, d\theta &= \pi\sin\frac{n\pi}{2}J_n(kc)\end{aligned} \tag{3.47}$$

where J_n are Bessel functions of the first kind, and by noting that

$$\begin{aligned}\int_0^\pi \cos\theta\cos n\theta\, d\theta &= \begin{cases} 0 & \text{when } n\neq 1,\\ \frac{\pi}{2} & \text{when } n=1.\end{cases}\\ \int_0^\pi \cos n\theta\, d\theta &= \begin{cases} \pi & \text{when } n=0,\\ 0 & \text{when } n\neq 0.\end{cases}\end{aligned} \tag{3.48}$$

the Fourier coefficients of Eq. (3.42) can now be expressed as

$$\begin{aligned}A_0 &= V_1 + V_3J_0(kc)\\ A_1 &= V_2c + 2V_4J_1(kc)\\ A_{2n} &= 2(-1)^nV_3J_{2n}(kc),\ n=1,2,\ldots\\ A_{2n+1} &= 2(-1)^nV_4J_{2n+1}(kc),\ n=1,2,\ldots\end{aligned} \tag{3.49}$$

3.5.2 Derivation of the velocity potential

The solutions of the boundary value problem is found by using a vortex distribution from $X=-c$ to $X=c$ at $Z=0$. This is a similar solution technique as used for the steady linear lifting problem for a thin air foil in infinite fluid (Newman (1977)). We start with the following relationship between velocity components, vortex density γ and velocity potential ϕ on $Z=0_-$

$$u(x) = \frac{1}{2}\gamma(x) = \frac{\partial\phi}{\partial x} \tag{3.50}$$

$$v(x) = -\frac{1}{2\pi}\fint_{-c}^{c}\frac{\gamma(\xi)d\xi}{\xi - x} \tag{3.51}$$

Here u and v are respectively the horizontal and vertical velocity components. $\fint$ means principal value integration.

Similar assumptions can be made as done for the linear representation of V_R. This means that antisymmetric and symmetric velocity potential part can be implicitly associated with the antisymmetric and symmetric part of V_R respectively. This gives singularities at both leading and trailing edge, *i.e.* singularities at $\theta=0$ and $\theta=\pi$. This differs from the steady lifting problem in Newman (1977) where the Kutta condition at the trailing edge is introduced to get an unique solution. We start out by writing

$$\gamma = B_0\cot\theta + \sum_{n=1}^{\infty}B_n\sin n\theta \tag{3.52}$$

It will be shown in the following text that B_n can be related to A_n. Equation (3.52) is singular at $X = \pm c$, *i.e.* $\theta = 0$ and π. The following derivations will show that it is necessary to add a term in Eq. (3.52). When Newman (1977) represents γ for the steady lifting problem, he uses the term $B_0 \cot(\theta/2)$ instead of $B_0 \cot\theta$ in Eq. (3.52) in order to be consistent with the Kutta condition in his problem.

The relationship in Eq. (3.43) leads to $\xi = c\cos\theta_1$ and $d\xi = -c\sin\theta_1 d\theta_1$ with $\xi = \pm c$ referring to $\theta = 0,\ \pi$ respectively. Then the vertical velocity in Eq. (3.51) can be expressed as

$$v = -\frac{1}{2\pi} \fint_0^\pi \frac{\gamma(\theta_1)\sin\theta_1\, d\theta_1}{\cos\theta_1 - \cos\theta} \tag{3.53}$$

The Glauert integrals will be used and are defined as (See *e.g.* pp.186 of Newman (1977))

$$G_n(\chi) = \fint_0^\pi \frac{\cos n\theta\, d\theta}{\cos\theta - \cos\chi} \tag{3.54}$$

The first three terms are

$$G_0 = 0, \qquad G_1 = \pi, \qquad G_2 = 2\pi\cos\chi \tag{3.55}$$

G_n can more generally be expressed as

$$G_n = \pi\frac{\sin n\chi}{\sin\chi} \tag{3.56}$$

Using that

$$2\sin n\theta_1 \sin\theta_1 = \cos(n-1)\theta_1 - \cos(n+1)\theta_1 \tag{3.57}$$
$$-2\cos n\theta_1 \sin\theta_1 = \sin(n-1)\theta_1 - \sin(n+1)\theta_1 \tag{3.58}$$
$$\tag{3.59}$$

gives

$$\begin{aligned}\fint_0^\pi \frac{\sin n\theta_1 \sin\theta_1\, d\theta_1}{\cos\theta_1 - \cos\theta} &= \frac{1}{2}\left(G_{n-1}(\theta) - G_{n+1}(\theta)\right) \\ &= \frac{\pi}{2}\left[\frac{\sin(n-1)\theta - \sin(n+1)\theta}{\sin\theta}\right] \\ &= -\pi\cos n\theta \end{aligned} \tag{3.60}$$

Further, using that $\cot\theta = \cos\theta/\sin\theta$ gives

$$\fint_0^\pi \frac{\cos\theta_1}{\sin\theta_1}\frac{\sin\theta_1\, d\theta_1}{\cos\theta_1 - \cos\theta} = G_1(\theta) = \pi \tag{3.61}$$

Then it follows from Eq. (3.53) that

$$v = -\frac{1}{2}B_0 + \frac{1}{2}\sum_{n=1}^{\infty} B_n \cos n\theta \tag{3.62}$$

Since v must be equal to V_R given by Eq. (3.42), it gives $A_0 = -B_0/2$ and $A_n = B_n/2$. This leads to that Eq. (3.52) can be written as

$$\gamma = -2A_0 \cot\theta + 2\sum_{n=1}^{\infty} A_n \sin n\theta \tag{3.63}$$

By using the relationship between ϕ and γ in Eq. (3.50), ϕ can be found by integrating $\gamma/2$ along x. This gives by using that $\phi = 0$ at $x = -c$ that

$$\begin{aligned}
\phi &= \int_{-c}^{x} \frac{\partial \phi}{\partial x}\, d\xi \\
&= \int_{\pi}^{\theta} \Big(-A_0 \cot\theta_1 + \sum_{n=1}^{\infty} A_n \sin n\theta_1\Big)\,(-c\sin\theta_1)\; d\theta_1 \\
&= cA_0 \sin\theta - \frac{1}{2} cA_1 \Big(\theta - \pi - \frac{\sin 2\theta}{2}\Big) \\
&\quad - \frac{1}{2}\sum_{n=2}^{\infty} cA_n \Big(\frac{\sin(n-1)\theta}{n-1} - \frac{\sin(n+1)\theta}{n+1}\Big)
\end{aligned} \tag{3.64}$$

The free surface condition $\phi = 0$ should be satisfied at both the two ends of the wetted deck, *i.e.* at $\theta = 0$ and π. However, Eq. (3.64) gives $c\pi A_1/2$ at $\theta = 0$. It means that another term should be introduced into Eq. (3.64) to account for this. Since $1/\sqrt{c-x^2}$ is a homogenous solution of $\gamma(x)$ from Eq. (3.51), adding a term which is a constant times $1/\sin\theta$ to Eq. (3.63) will not destroy the above derivation. The vorticity γ can therefore be expressed as

$$\gamma = -2A_0 \cot\theta + 2\sum_{n=1}^{\infty} A_n \sin\theta + \frac{2K}{\sin\theta} \tag{3.65}$$

where K is a constant. Following the same procedure as used in deriving Eq. (3.64) yields the velocity potential ϕ as

$$\begin{aligned}
\phi = cA_0 \sin\theta &- \frac{1}{2} cA_1 \Big(\theta - \pi - \frac{\sin 2\theta}{2}\Big) - cK(\theta - \pi) \\
&- \frac{1}{2}\sum_{n=2}^{\infty} cA_n \Big(\frac{\sin(n-1)\theta}{n-1} - \frac{\sin(n+1)\theta}{n+1}\Big) \\
&\text{on} \quad Z = 0 \quad \text{and} \quad |X| \le c(t)
\end{aligned} \tag{3.66}$$

K can now be determined by requiring $\phi = 0$ at $\theta = 0$. This gives $K = -A_1/2$. Substituting K into Equation (3.66) gives

$$\begin{aligned}
\phi = &cA_0 \sin\theta + \frac{1}{4} cA_1 \sin 2\theta \\
&- \frac{1}{2}\sum_{n=2}^{\infty} cA_n \Big(\frac{\sin(n-1)\theta}{n-1} - \frac{\sin(n+1)\theta}{n+1}\Big) \\
&\text{on} \quad Z = 0 \quad \text{and} \quad |X| \le c(t)
\end{aligned} \tag{3.67}$$

where A_n are defined in Equation (3.49).

It can be shown that Eq. (3.67) is consistent with Eq. (3.17) which assumes $V_R = V_1 + V_2 X$. This means from Eq. (3.49) that $A_0 = V_1$, $A_1 = V_2 c$ and $A_n = 0$ for $n > 1$. By using Eq. (3.43), it follows that $c(t)\sin\theta = \sqrt{c^2 - X^2}$ and $c^2 \sin 2\theta = 2X\sqrt{c^2 - X^2}$. This leads to Eq. (3.17).

3.5.3 Slamming induced loads on the wetdeck

The slamming induced dynamic pressure can be approximated by

$$p = -\rho \frac{\partial \phi}{\partial t} \tag{3.68}$$

to be consistent with the dynamic surface condition in this boundary value problem, as discussed in Section 3.2.2.

It should be noted that besides c and A_n, θ is also a time dependent parameter. This means that

$$\frac{\partial \theta}{\partial t} = \frac{1}{c\sin\theta}\Big(\frac{\partial c}{\partial t}\cos\theta - \frac{\partial l}{\partial t}\Big) \tag{3.69}$$

Further, by integrating Eq. (3.68) along the wetted length, the following vertical impact force F_3 and pitch moment F_5 about $X = 0$ are obtained.

$$\begin{aligned} F_3 &= B\int_{-c}^{c} -\rho\frac{\partial\phi}{\partial t}dX = -\rho c\int_0^{\pi}\frac{\partial\phi}{\partial t}\sin\theta d\theta\, B \\ &= -\frac{\partial}{\partial t}\Big(\frac{1}{2}\rho\pi c^2\big(A_0 - \frac{A_2}{2}\big)\Big)\, B \end{aligned} \tag{3.70}$$

$$\begin{aligned} F_5 &= B\int_{-c}^{c} -pn_5 dX = -B\int_{-c}^{c}(l+X)p dX \\ &= -lF_3 - B\int_{-c}^{c} X\Big(-\rho\frac{\partial\phi}{\partial t}\Big)dX \\ &= -lF_3 + \rho c^2\int_0^{\pi}\frac{\partial\phi}{\partial t}\sin\theta\cos\theta d\theta\, B \\ &= \frac{\partial}{\partial t}\Big(l\frac{1}{2}\rho\pi c^2\big(A_0 - \frac{A_2}{2}\big)\Big)\, B + \frac{\partial}{\partial t}\Big(\frac{1}{16}\rho\pi c^3(A_1 - A_3)\Big)\, B \end{aligned} \tag{3.71}$$

This gives by using the relationship between A_n and V_n in Eq. (3.49) that

$$F_3 = -\frac{\partial}{\partial t}\Big\{\frac{1}{2}\rho\pi c^2\Big[V_1 + V_3\big(J_0(kc) + J_2(kc)\big)\Big]\Big\}\, B \tag{3.72}$$

$$\begin{aligned} F_5 =& \frac{\partial}{\partial t}\Big\{l\frac{1}{2}\rho\pi c^2\Big[V_1 + V_3\big(J_0(kc) + J_2(kc)\big)\Big]\Big\}\, B \\ &+ \frac{\partial}{\partial t}\Big\{\frac{1}{16}\rho\pi c^3\Big[V_2 c + 2V_4\big(J_1(kc) + J_3(kc)\big)\Big]\Big\}\, B \end{aligned} \tag{3.73}$$

It is easy to show in a similar way as was done for the velocity potential that Eqs. (3.70) and (3.71) are consistent with Eqs. (3.20) and (3.21) which assumes $V_R = V_1 + V_2 X$.

3.5.4 Wagner based method

When the wetted length $2c(t)$ is predicted by a Wagner based method, the vertical velocity due to ϕ on the mean free surface $Z = 0$ outside of the wetted length is needed. This expression is derived by starting with the following expression for the complex velocity given by Newman (1977).

$$u - iv = -\frac{1}{\pi}\frac{1}{(1-z^2)^{\frac{1}{2}}}\int_{-1}^{1}\frac{V_+(\xi)(1-\xi^2)^{\frac{1}{2}}}{\xi - z}d\xi \tag{3.74}$$

Here z represents the complex variable and length dimensions are non-dimensionalized by half of the wetted length.

We introduce length dimensions and note that care has to be taken in defining the branches of $\sqrt{c^2 - z^2}$. This has to be done consistently with how Newman (1977) derived Eq. (3.74). If the complex variable is defined as $X + iZ$, this implies for instance that

$$\sqrt{c^2 - z^2} = \begin{cases} -i\sqrt{X^2 - c^2} & \text{when } X > c(t),\ Z = 0 \\ +i\sqrt{X^2 - c^2} & \text{when } X < -c(t),\ Z = 0 \end{cases} \tag{3.75}$$

It now follows that the vertical velocity $\frac{\partial\phi}{\partial Z} = v$ on the free surface $Z = 0$ can be expressed as

$$\frac{\partial\phi}{\partial Z} = \frac{1}{\pi}\frac{\text{Sign}(X)}{\sqrt{X^2 - c^2}}\int_{-c}^{c}\frac{V_R\sqrt{c^2 - \xi^2}}{\xi - X}d\xi \tag{3.76}$$

Here $\text{Sign}(X)$ is 1 when $X > c(t)$ and -1 for $X < -c(t)$. Using the general Fourier expansion of V_R in Eq. (3.42) and that $\xi = c\cos\theta$ gives

$$\frac{\partial\phi}{\partial Z} = \frac{1}{2\pi}\frac{c\,\text{Sign}(X)}{\sqrt{X^2 - c^2}}\int_0^{\pi}\frac{\sum_{n=0}^{\infty}A_n\cos n\theta(1-\cos 2\theta)}{\cos\theta - X/c}d\theta \tag{3.77}$$

This will be rewritten by using the following formula (Eq.3.613.1 on page 366 in Gradshteyn and Ryzhik (1994))

$$\int_0^{\pi}\frac{\cos n\theta d\theta}{1 + a\cos\theta} = \frac{\pi}{\sqrt{1-a^2}}\left(\frac{\sqrt{1-a^2} - 1}{a}\right)^n \quad \text{for } a^2 < 1 \tag{3.78}$$

Substituting $a = -c/X$ which satisfies $a^2 < 1$ when $|X| > c$ gives

$$-\frac{X}{c}\int_0^{\pi}\frac{\cos n\theta d\theta}{\cos\theta - \frac{X}{c}} = \frac{\pi}{\sqrt{1 - \frac{c^2}{X^2}}}\left(\frac{\sqrt{1 - (\frac{c}{X})^2} - 1}{-\frac{c}{X}}\right)^n \tag{3.79}$$

i.e.

$$I_n = \int_0^{\pi}\frac{\cos n\theta d\theta}{\cos\theta - \frac{X}{c}} = \frac{-c\pi\,\text{Sign}(X)}{\sqrt{X^2 - c^2}}\left(\frac{\sqrt{X^2 - c^2} - |X|}{-c\,\text{Sign}(X)}\right)^n \tag{3.80}$$

We study now

$$H_n = \int_0^{\pi}\frac{\cos n\theta(1-\cos 2\theta)}{\cos\theta - \frac{X}{c}}d\theta \quad n = 0, 1, 2, \ldots \tag{3.81}$$

This is needed in evaluating Eq. (3.77). We start with $n = 0$, *i.e.*

$$H_0 = I_0 - I_2 = -\frac{2\pi\,\mathrm{Sign}(X)}{c}\big(|X| - \sqrt{X^2 - c^2}\big) \tag{3.82}$$

Further,

$$H_1 = \frac{1}{2}(I_1 - I_3) = \frac{1}{2}H_0\left(\frac{\sqrt{X^2 - c^2} - |X|}{-c\,\mathrm{Sign}(X)}\right) \tag{3.83}$$

Further, for $k \geq 2$

$$\begin{aligned} H_k &= \int_0^\pi \frac{\cos k\theta - \frac{1}{2}\big(\cos(k+2)\theta + \cos(k-2)\theta\big)}{\cos\theta - \frac{X}{c}}d\theta \\ &= I_k - \frac{1}{2}(I_{k+2} + I_{k-2}) = \cdots\cdots \\ &= 2\pi\,\mathrm{Sign}(X)\frac{\sqrt{X^2 - c^2}}{c}\left(\frac{\sqrt{X^2 - c^2} - |X|}{-c\,\mathrm{Sign}(X)}\right)^k \qquad \text{for } k \geq 2 \end{aligned} \tag{3.84}$$

Equation (3.77) can then be analytically expressed as

$$\begin{aligned} \frac{\partial\phi}{\partial Z} &= \frac{1}{2\pi}\frac{c\,\mathrm{Sign}(X)}{\sqrt{X^2 - c^2}}\big(A_0H_0 + A_1H_1 + \sum_{k=2}^{\infty} A_kH_k\big) \\ &= -A_0\frac{|X| - \sqrt{X^2 - c^2}}{\sqrt{X^2 - c^2}} \\ &\quad - A_1\frac{\big(|X| - \sqrt{X^2 - c^2}\big)^2}{2c\sqrt{X^2 - c^2}}\,\mathrm{Sign}(X) \\ &\quad + \sum_{k=2}^{\infty} A_k\left(\frac{\sqrt{X^2 - c^2} - |X|}{-c\,\mathrm{Sign}(X)}\right)^k \\ &\qquad\qquad \text{on} \quad Z = 0 \quad \text{and} \quad |X| > c(t) \end{aligned} \tag{3.85}$$

Here A_n can be found from Eq. (3.49).

It follows for large $|X|$ that

$$|X| - \sqrt{X^2 - c^2} = |X|\big(1 - \sqrt{1 - c^2/X^2}\big) \sim |X|\frac{1}{2}\frac{c^2}{X^2} = \frac{1}{2}\frac{c^2}{|X|} \tag{3.86}$$

This means that the velocity goes to zero when $|X| \to \infty$. Further, the term associated with A_n for odd number n is antisymmetric about $X = 0$, and the term associated with A_n for even number n is symmetric about $X = 0$.

Equation (3.85) can be controlled by checking with similar expressions derived by Kvålsvold (1994) where $A_n = 0$ for odd number n. Consistent results are obtained by neglecting the odd terms in our Eq. (3.85). It is noted that the expression Eq. (3.85) for $\partial\phi/\partial Z$ is consistent with our previous expression for $V_R = V_1 + V_2X$. This means from Eq. (3.49) that $A_0 = V_1$, $A_1 = V_2c$

and $A_n = 0$ for $n > 1$. Then only the first two terms in Eq. (3.85) are left. Further, expanding $(|X| - \sqrt{X^2 - c^2})^2$ in the second term and combining the second term with the first term lead to Eq. (3.25). The odd term with A_1 is therefore controlled. Since the other odd terms are of the same nature as A_{2k} with $k > 1$, we believe that Eq. (3.85) has been properly controlled.

In Eq. (3.85) it is only the A_0 and A_1 terms that have a square root singularity at $|X| = c$. An asymptotic expression of the vertical velocity near $X = \pm c$ is needed in the time integration of the free surface. This will enable us to properly account for the singularities in the time integration procedure. We concentrate first on $X = c$ and derive, based on Eq. (3.85), the following asymptotic expression $\partial\phi/\partial Z$ for small $|X - c|$ outside the body on $Z = 0$

$$\begin{aligned}\lim_{X>\to c(t)} \frac{\partial \phi}{\partial Z} &\simeq -A_0 \frac{c}{\sqrt{2c}\sqrt{X-c}} - A_1 \frac{c^2}{2c\sqrt{2c}\sqrt{X-c}} + \sum_{n=2}^{\infty} A_n \\ &= -\big(A_0 + \frac{1}{2}A_1\big)\frac{\sqrt{c}}{\sqrt{2(X-c)}} + \sum_{n=2}^{\infty} A_n \end{aligned} \tag{3.87}$$

Then with a prescribed wetted length change Δc_{j+1}, the vertical distance due to the local pile up of water at the right hand side of the wetted length is described by

$$\begin{aligned}\int_{t_j}^{t_{j+1}} \frac{\partial \phi}{\partial Z}\, dt &= \int_{t_j}^{t_{j+1}} \frac{\partial \phi}{\partial Z}\, dc \frac{dt}{dc} \\ &= \Big(\frac{dt}{dc}\Big)_{m,j+1} \Big\{ -\Big(\big(A_0 + \frac{1}{2}A_1\big)\sqrt{2c}\Big)_{m,j+1} \sqrt{\Delta c_{j+1}} + \sum_{n=2}^{\infty} \big(A_n\big)_{m,j+1} \Delta c_{j+1} \Big\} \end{aligned} \tag{3.88}$$

Here subscript $m, j+1$ means the time averaged value from t_j to t_{j+1}. Similar formulations at the left end of the wetted length can be derived. The time stepping procedure in Section 3.4.2 can then be followed.

3.6 Kutta condition model

Kutta condition is adopted from foil theory and is then a consequence of visual information of the flow. That shows a smooth detachment of the flow from the trailing edge of a lifting foil. If we apply this same concept to our slamming problem, it means that there is smooth detachment of water from the aft intersection point between the deck and the water. Baarholm (2001) introduced this model for wetdeck slamming on a stationary platform based on experimental observations. Figure 3.4 shows the flow details at the ends of the wetted deck for cases with and without Kutta condition. The upper figure shows that the local spray happens at both ends without applying Kutta condition. The lower one has a smooth detachment at the trailing edge by applying a Kutta condition, while spray is generated at the 'leading edge' $X = -c(t)$. Numerically it means that horizontal fluid velocity at the 'trailing edge' $X = c(t)$ is finite and continuous. 'Leading edge' and 'trailing edge' refer to nomenclature used in foil theory.

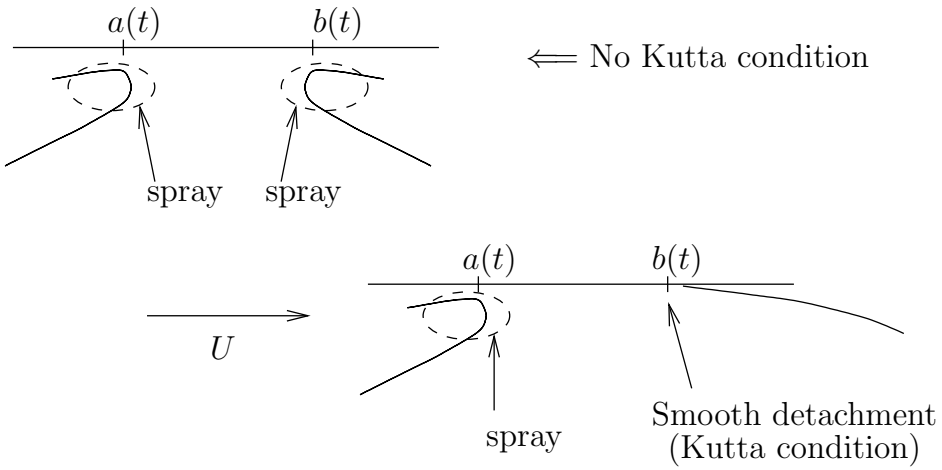

Figure 3.4 Flow details at the ends of the wetted deck

When the Kutta condition is applied in our case, it is assumed that U is much larger than the incident wave velocity and the fluid velocity caused by the impact. So a different dynamic free surface condition will be applied, leading to a new boundary value problem. This model is appropriate for wetdeck slamming on a high speed catamaran. Kvålsvold (1994) and Haugen (1999) did also consider wetdeck slamming on a high speed catamaran, but did not include a Kutta condition model. Faltinsen (1997) analyzed local slamming induced strains on a horizontal elastic plate of finite length that had a large forward speed relative to the drop velocity. An initial structural phase and a subsequent free vibration phase were considered. The problem during the free vibration phase was equivalent to steady state harmonic oscillations of an elastic thin lifting foil in infinite fluid. A Kutta condition was then needed at the 'trailing' edge. Here we approximate V_R by Eq. (3.15) as a spatially linear distribution on the wetted surface and uses a Von Karman method to determine the wetted length. The following text gives details of this Kutta condition method.

3.6.1 Boundary value problem

Different from Eq. (3.7), the more general dynamic free surface condition $\frac{\partial \phi}{\partial t} + U\frac{\partial \phi}{\partial x} = 0$ is now used, in combination with a Kutta condition at $X = c$. Since the initial condition is $\phi = 0$ on the free surface, this implies that ϕ remains zero on the upstream side ($X < -c$). However, for a free surface particle on the downstream side, it may have previously been at the wetted surface. This implies that there is a region $c < X < c+Ut$ where $\frac{\partial \phi}{\partial t}+U\frac{\partial \phi}{\partial x} = 0$ must be used (see Fig. 3.5).

The length Ut of this region follows by first considering a fluid particle on the free surface at the aft end at initial time $t = 0$ of slamming. Since the fluid particle velocity can be approximated as a horizontal velocity U, it follows that the fluid particle has travelled a horizontal distance Ut during time t. Fluid particles that start at $t = t_0$ at other free surface positions downstream of the aft end have an initial value $\phi = 0$. Since $\frac{\partial \phi}{\partial t} + U\frac{\partial \phi}{\partial x} = 0$, the ϕ-values for these fluid particles remain zero. The order of magnitude of the ratio between the two terms in this free

surface condition is UT_d/L where T_d is the time duration of the impact, and L is the maximum wetted length. It means implicitly that previous slamming models presented in details in this chapter assume UT_d/L to be small.

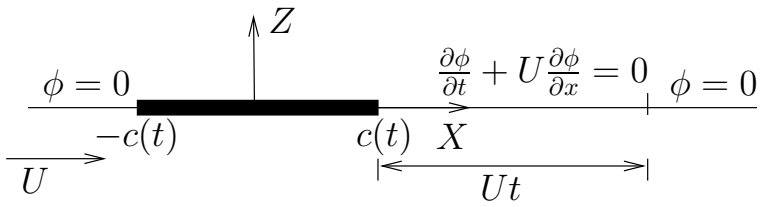

Figure 3.5 Boundary value problem accounting for Kutta condition at the aft intersection point ($X = c(t)$) between the deck and the free surface

The boundary value problem can be made equivalent to an unsteady linear lifting problem for a thin foil in an infinite fluid (See Appendix B). This means a vortex distribution with density $\gamma(X,t)$ along $-c < X < c + Ut$ is used, *i.e.* the vortex contribution from the 'wake' should also be accounted for. The word 'wake' has a physical meaning for the lifting problem but not in our case. The solution procedure in Newman (1977) for the unsteady lifting problem for a thin foil is followed. However, an accelerated local coordinate system is used here, while this is not done by Newman (1977). It means that $X = 0$ is changing with time. Further, the wetted length $2c(t)$, as well as the trailing edge position, are time dependent parameters. This influences the solution procedure and the results. Ulstein (1995) analyzed a similar impact problem, but he assumed that the aft body-water intersection was time independent and used a Wagner based method to find the forward body-water intersection. The water exit phase was neglected. We use a Von Karman based method which enables us to analyze both the water entry and exit phase.

Compared with Eq. (3.51), the vertical velocity component on the lower side the vortex sheet also includes the contribution from the 'wake', *i.e.*

$$\begin{aligned} v(x,t) &= -\frac{1}{2\pi}\fint_{-c}^{\infty}\frac{\gamma(\xi,t)}{\xi - x}d\xi \\ &= -\frac{1}{2\pi}\fint_{-c}^{c+Ut}\frac{\gamma(\xi,t)}{\xi - x}d\xi \end{aligned} \tag{3.89}$$

By using the equivalence between our problem and the unsteady lifting problem it follows that $\gamma(x,t) = \gamma(x - Ut)$ in the wake. Further, by accounting for the body boundary condition, applying Hilbert transforms and interchanging integrations, the solution of γ can be expressed as

$$\begin{aligned} \gamma(X,t) \;=\; & \frac{2}{\pi}\frac{1}{(c^2 - X^2)^{\frac{1}{2}}}\left\{\fint_{-c}^{c}\frac{(c-\xi)^{\frac{1}{2}}}{\xi - X}V_R(\xi,t)d\xi\right. \\ & \left. -\frac{1}{2}\int_{c}^{\infty}\frac{(\xi^2 - c^2)^{\frac{1}{2}}}{\xi - X}\gamma(\xi - Ut)d\xi\right\} \end{aligned} \tag{3.90}$$

This gives by inserting the linear expression of $V_R(\xi,t) = V_1 + V_2\xi$ into Eq. (3.90) in our $X-Z$ coordinate system that

$$\begin{aligned}\gamma(X,t) &= \frac{1}{(c^2-X^2)^{\frac{1}{2}}}\Bigg\{[-2V_1X + V_2(c^2-2X^2)] \\ &\quad - \frac{1}{\pi}\int_c^\infty \frac{(\xi^2-c^2)^{\frac{1}{2}}}{\xi - X}\gamma(\xi - Ut)d\xi\Bigg\} \end{aligned} \tag{3.91}$$

This follows by relating the first integral in Eq. (3.90) to Hilbert transforms as defined in Newman (1977).

Now by the relationship shown in Eq. (3.50), we integrate along the wetted length and find the velocity potential as

$$\begin{aligned}\phi(X,t) &= \int_{-c}^{X}\frac{1}{2}\gamma(X_1,t)dX_1 = \phi_1 + \phi_2 \\ &= V_1\sqrt{c^2-X^2} + \frac{1}{2}V_2X\sqrt{c^2-X^2} \\ &\quad - \frac{1}{2\pi}\int_c^{c+Ut}\gamma(\xi-Ut)\left[\pi - 2\arctan\Big(\sqrt{\frac{\xi+c}{\xi-c}}\tan\frac{\theta}{2}\Big)\right]d\xi \\ &\quad \text{for} \quad -c < X < c, \quad Z = 0_- \end{aligned} \tag{3.92}$$

Here $\theta = \arccos(\frac{X}{c(t)})$. The first two terms in Eq. (3.92) are referred to as ϕ_1, and is the solution when the Kutta condition is not applied (See Eq. (3.17)).

It should be noted that the spatial derivative term $-\rho U\frac{\partial\phi}{\partial x}$ must also be included when integrating pressure to get dynamic forces, *i.e.* $p = -\frac{\partial\phi}{\partial t} - \rho U\frac{\partial\phi}{\partial x}$. This results in the following vertical force F_3 and pitch moment F_5 about $X = 0$.

$$\begin{aligned}F_3 &= -\rho\pi c\frac{\partial c}{\partial t}V_1B - \frac{1}{2}\rho\pi c^2\frac{\partial V_1}{\partial t}B \\ &\quad - \frac{1}{2}\rho c\frac{\partial c}{\partial t}B\int_c^{c+Ut}\frac{\gamma(\xi-Ut)}{\sqrt{\xi^2-c^2}}d\xi \\ &\quad + \frac{1}{2}\rho UB\int_c^{c+Ut}\frac{\xi}{\sqrt{\xi^2-c^2}}\gamma(\xi-Ut)d\xi \end{aligned} \tag{3.93}$$

$$\begin{aligned}F_5 &= -lF_3 \\ &\quad + \frac{\partial}{\partial t}(l\frac{1}{2}\rho\pi c^2V_1)\,B + \frac{\partial}{\partial t}(\frac{1}{16}\rho\pi c^4V_2)\,B \\ &\quad + \frac{1}{4}\rho c\frac{\partial c}{\partial t}B\int_c^{c+Ut}\frac{\xi}{\sqrt{\xi^2-c^2}}\gamma(\xi-Ut)d\xi \\ &\quad - \frac{1}{4}\rho Uc^2B\int_c^{c+Ut}\frac{\gamma(\xi-Ut)}{\sqrt{\xi^2-c^2}}d\xi \\ &\quad - \frac{1}{2}\rho\pi Uc^2V_1B \end{aligned} \tag{3.94}$$

Here V_1 and V_2 are defined in Eq. (3.16). In Eq. (3.94), F_3 is expressed as in Eq. (3.93) and $l(t)$ is the mid x-position of the wetted length defined as before. The first two terms in Eq. (3.93) and the first three terms in Eq. (3.94) are exactly the same as Eqs. (3.19) and (3.21) in Section 3.3 when the Kutta condition at the aft end of the wetted surface is not considered. Detailed derivations of the above equations are given in Appendix B.

The two integrals extending over the wake in Eqs. (3.93) and (3.94), are evaluated numerically as:

$$\begin{aligned}\int_c^{c+Ut} \frac{\gamma(\xi - Ut)}{\sqrt{\xi^2 - c^2}} d\xi &= \sum_{i=1}^{N} \gamma_i \int_{\Delta\xi} \frac{d\xi}{\sqrt{\xi^2 - c^2}} \\ &= \sum_{i=1}^{N} \gamma_i \left[\ln(\xi + \sqrt{\xi^2 - c^2}) \right]_{\xi_{i-\frac{1}{2}}}^{\xi_{i+\frac{1}{2}}}\end{aligned} \tag{3.95}$$

$$\begin{aligned}\int_c^{c+Ut} \frac{\xi}{\sqrt{\xi^2 - c^2}} \gamma(\xi - Ut) d\xi &= \sum_{i=1}^{N} \gamma_i \int_{\Delta\xi} \frac{\xi d\xi}{\sqrt{\xi^2 - c^2}} \\ &= \sum_{i=1}^{N} \gamma_i \left[\sqrt{\xi^2 - c^2} \right]_{\xi_{i-\frac{1}{2}}}^{\xi_{i+\frac{1}{2}}}\end{aligned} \tag{3.96}$$

Here the domain from $\xi = c$ to $\xi = c + Ut$ is divided into N segments with length $\Delta\xi = U\Delta t$, as illustrated in Fig. 3.6. γ_i is the space averaged vortex density between $\xi_{i-\frac{1}{2}}$ and $\xi_{i+\frac{1}{2}}$. It should be noted that the trailing edge is changing with time, and that the ξ coordinate is based on the local $X - Z$ coordinate system.

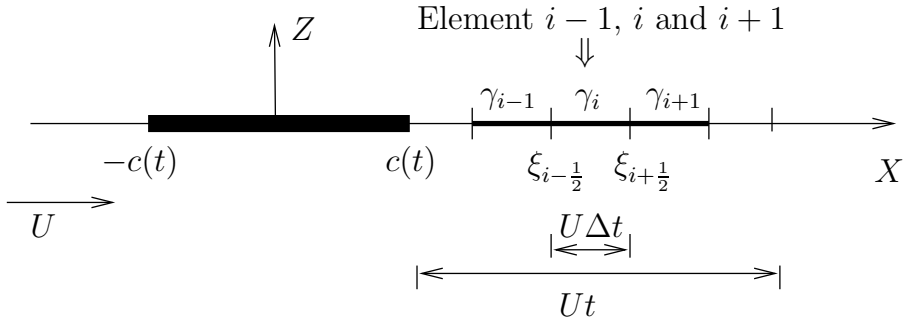

Figure 3.6 Numerical approximation of vortex distribution in the 'wake'

In order to determine $\gamma(\xi - Ut)$ in the previous equations, a Kutta condition has to be imposed at $X = c$. The Kutta condition implies that the fluid velocity must be finite at $X = c$. We note that the denominator in Eq. (3.91) expressing γ is zero for $X = c$. In order to get a finite answer for γ at $X = c$, it is necessary that the terms in the brackets in Eq. (3.91) are zero at $X = c$.

This gives the solution of γ at the trailing edge at time t in Eq. (3.97) by solving

$$\begin{aligned} -\pi(2V_1 + V_2 c)c &= \int_c^\infty \sqrt{\frac{\xi + c}{\xi - c}}\gamma(\xi - Ut)d\,\xi \\ &= \sum_{i=1}^{N} \gamma_i \left[\sqrt{\xi^2 - c^2} + c\ln(\xi + \sqrt{\xi^2 - c^2})\right]_{\xi_{i-\frac{1}{2}}}^{\xi_{i+\frac{1}{2}}} \end{aligned} \tag{3.97}$$

Here the newest generated vorticity γ_1 is the unknown. Other values γ_2 to γ_N are found in earlier time steps.

Application of the Kutta condition implies that U is much larger than the moving speed of the trailing edge. However, due to the initial quite large speed of the wetted area, the 'wake' vorticity created by earlier steps may be 'eaten up' in the following steps in an initial phase . By 'eaten up' is simply meant that a part of the free surface has become a part of the wetted surface in the new time step. This problem will be discussed in later chapters dealing with numerical results.

3.6.2 Verification

Extensive studies have been done previously for lifting surface problems where a Kutta condition is needed in a potential flow solution. Our numerical procedure was verified by comparing with classical analytical unsteady lifting solutions. One such case is the 'Wagner Function Problem'. It describes the transient lift problem due to a sudden change of vertical velocity for a flat plate. This means a foil accelerating instantaneously from rest at $t = 0$ to a constant velocity U with a constant angle of attack α. Figure 3.7 shows the numerical results, which is in perfect agreement with results presented in Newman (1977). The lift force is non-dimensionalized by the asymptotic lifting force $F_{t=\infty} = \pi\rho U^2 L\alpha$ for $t \to \infty$. Here L is chord length of the foil.

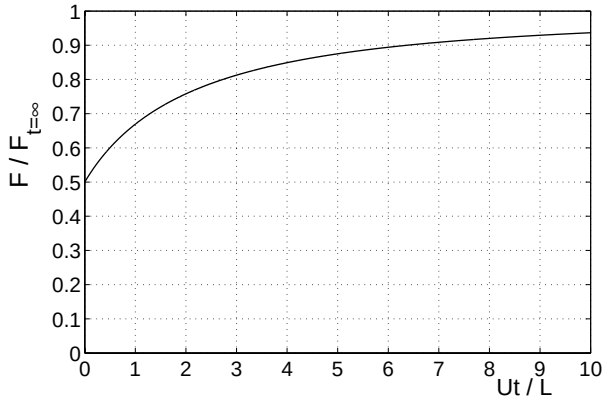

Figure 3.7 Transient two-dimensional linear lift force F on a flat plate of length L due to a sudden change in vertical velocity. Our theoretically predicted curves are consistent with results presented in Newman (1977).

3.7 Implementation of slamming models in global response model

Different theoretical slamming models, as well as their main derivative procedures, have been presented in this chapter. In the following Chapter 4, numerical calculations will be carried out accordingly to investigate the different factors in the slamming modelling, by comparing the calculated wetted length, slamming induced forces and global responses.

To improve the numerical stability in the global response, parts of the slamming induced vertical force and moment are expressed in terms proportional to accelerations, velocities and motions of the catamaran. The corresponding coefficients are moved to the left hand side of the equations motions. Details are given in Appendix B.

Chapter 4

Slamming Induced Response of a Rigid Catamaran

4.1 Introduction

The wetdeck of the test model was composed of four plates, notated in consecutive order as Deck1 to Deck4 from the bow (Fig. 2.1). Each deck was connected to the longitudinal aluminum frame by two transverse girders. Also each plate was stiffened by longitudinal stiffeners to minimize local flexibility. Deck2-4 are horizontal at a vertical distance of $0.34m$ from the base line of the hull. Deck1 has a small ramp angle at the bow with maximum height $0.39m$ relative to the base line. A more detailed description is given in Appendix A.

Chapter 3 introduced several slamming models. In this chapter, global response results based on the different slamming models are presented and discussed. For simplicity, the global flexibility is neglected in the calculations in this chapter, *i.e.* the catamaran is assumed to be a rigid body. Only heave and pitch responses are considered. The bow ramp angle of the wetdeck is neglected in the case studies in this chapter, *i.e.* a flat wetdeck is applied here. In Chapter 5, global hydroelastic response due to wetdeck slamming will be studied by accounting for the bow ramp angle.

As described in Chapter 3, there are four important factors influencing the slamming modelling: the determination of wetted length $2c(t)$, the approximation of the relative impact velocity V_R in the body boundary condition, the Kutta condition at the aft end of the wetted surface and the free surface condition. In the following sections, different effects will be investigated for the case of head sea regular incident waves with wave amplitude $\zeta_a = 0.05m$, wave period $T = 1.8s$ and ship forward speed $U = 1.9m/s$. Five slamming models are defined for later presentation of results in Table 4.1. A fourth order Runge-Kutta method is used with time step $0.0001s$ in the time integration. A build-up system from initial conditions to steady state conditions is used as described in Chapter 2. The steady state results are presented and discussed in the following sections.

Table 4.1 Definition of Model1 to Model5; 'FSC' means dynamic free surface condition between $X = c$ and $c + Ut$; the dynamic free surface condition at other X-values is $\phi = 0$. Here ϕ is velocity potential due to slamming. 'Kutta' means Kutta condition at aft end $X = c$.

Items	Model1	Model2	Model3	Model4	Model5
$2c(t)$	Von Karman	Wagner	Von Karman	Von Karman	Wagner
V_R	$V_1 + V_2 X$	$V_1 + V_2 X$	$\sum A_n \cos(n\theta)$	$V_1 + V_2 X$	$\sum A_n \cos(n\theta)$
FSC $(c : c + Ut)$	$\phi = 0$	$\phi = 0$	$\phi = 0$	$\frac{\partial \phi}{\partial t} + U\frac{\partial \phi}{\partial X} = 0$	$\phi = 0$
Kutta at $X = c$	No	No	No	Yes	No

4.2 Local rise-up effect

Chapter 3 described two different ways to calculate the wetted length. The Von Karman method is based on the undisturbed water-deck intersection points, while the Wagner type of method accounts for the vertical velocity from the local run-up of water due to the slamming induced flow during the water entry phase. Comparisons of wetted length, impact force, vertical motions, and vertical accelerations at the center of gravity of the whole catamaran are shown in Figs. 4.1 to 4.2. A spatially linear distribution of relative velocity in the wetted area (see Eq. (3.15)) is applied.

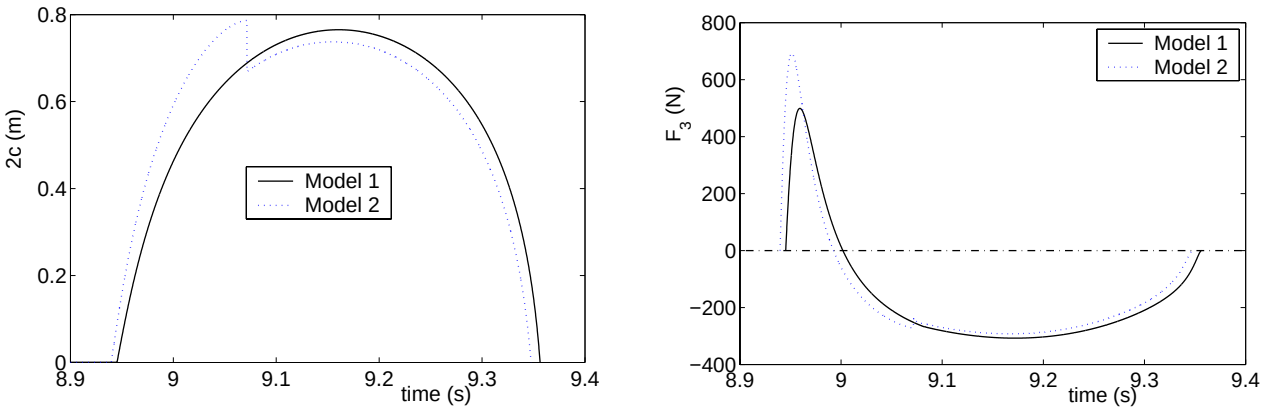

(a) Wetted length $2c(t)$ (b) Vertical impact force F_3

Figure 4.1 Comparison between Von Karman (Model1) and Wagner (Model2) based method for wetdeck slamming on a rigid catamaran (See Table 4.1); $T = 1.8s$, $\zeta_a = 0.05m$, $U = 1.9m/s$, head sea.

In the above two figures only the time interval of impact is shown. We see that the Wagner based method will influence the wetted length and then the forces on the wetted deck. Since the initial slamming occurs at the front end of the wetdeck and there is a finite angle initially between the free surface and the wetdeck, dc/dt is finite and the force is zero initially.

The Wagner method is basically more correct than the Von Karman method for the water entry phase. However, the Wagner method can not be applied during the water exit phase, as discussed in Section 3.4. The Von Karman method is therefore used in the water exit phase. The jump

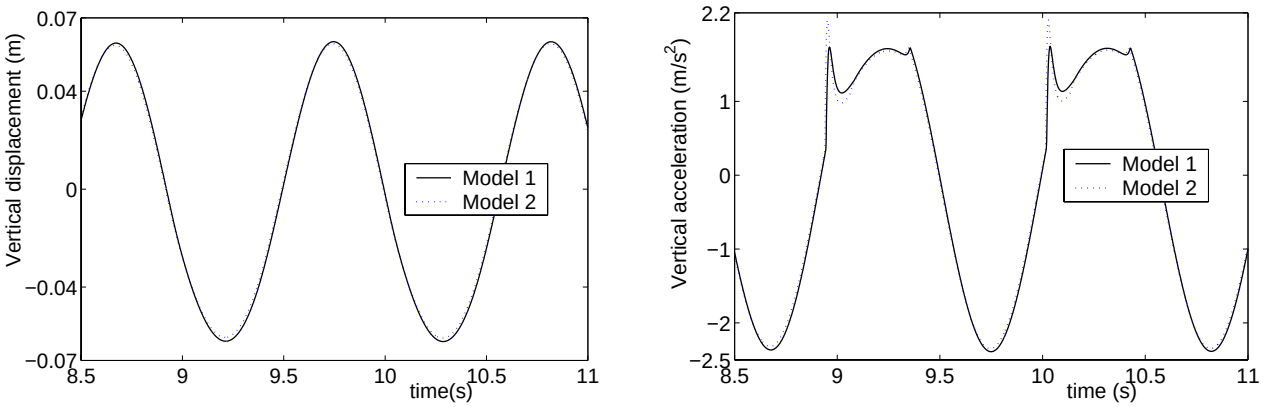

(a) Global response of η_3 at COG

(b) global response of $\ddot{\eta}_3$ at COG

Figure 4.2 Comparison between Von Karman (Model1) and Wagner (Model2) based method for wetdeck slamming on a rigid catamaran (See Table 4.1); $T = 1.8s$, $\zeta_a = 0.05m$, $U = 1.9m/s$, head sea.

occurring in the predicted wetted length by the Wagner approach (see Fig. 4.1(a)) corresponds to when a switch from the Wagner to the Von Karman method occurs. This switch causes a small jump in the predicted vertical impact force (Fig. 4.1(b)), while the jump is not noticeable in the results for heave motion and acceleration at COG (Fig. 4.2). The Wagner method influences the acceleration peaks, while the influence on global motions (Fig. 4.2(a)) is negligible.

Figure 4.3(a) and Fig. 4.3(b) illustrate the contributions from the linear incident wave loads and the slamming loads to the vertical motion and acceleration at COG of the rigid catamaran. Model1 is applied in this calculation. In the figures, '$\circ$' and '$\triangleleft$' represent the initial and ending times of the slamming. Figure 4.3(a) shows that slamming clearly influences the vertical motion response and the maximum values are changed from $0.0424m$ to $0.0603m$, an increase of 42.05%. This is case dependent and when global hydroelasticity is accounted for, the slamming induced motion is not so dominant (See Chapter 5). We consider the first slamming occurrence in Fig. 4.3, *i.e.* from $t = 8.9453s$ to $9.3564s$. When $t = 8.9625s$ the total acceleration response reaches a peak as shown in Fig. 4.3(b). The slamming induced part contributes then 45.15%. In the analysis accounting for global hydroelasticity effect presented in Chapter 5, large contributions from slamming induced acceleration are also shown.

Two-dimensional experimental and numerical studies by Baarholm (2001) for a fixed horizontal wetdeck showed the importance of accounting for the pile up effect during the water entry phase. Comparisons were made between the Von Karman and Wagner methods for a fixed horizontal wetdeck model with dimensions $L * B = 0.63m * 0.56m$ (Baarholm (2001)), where L is the length of the deck in the wave propagation direction of regular waves. The height of the deck above mean free surface was $0.04m$. Figures 4.4 show our calculations of the pile up effect on the wetted length and impacting forces as a function of time. Here a linear approximation of V_R is applied and the nonlinear Froude-Krylov force is included. Once more the Wagner method is only used during the water entry phase. Since the whole wetdeck becomes wetted, there is no jump in the wetted length like the one in Fig. 4.1(a). The third line denoted 'Wagner+Stokes'

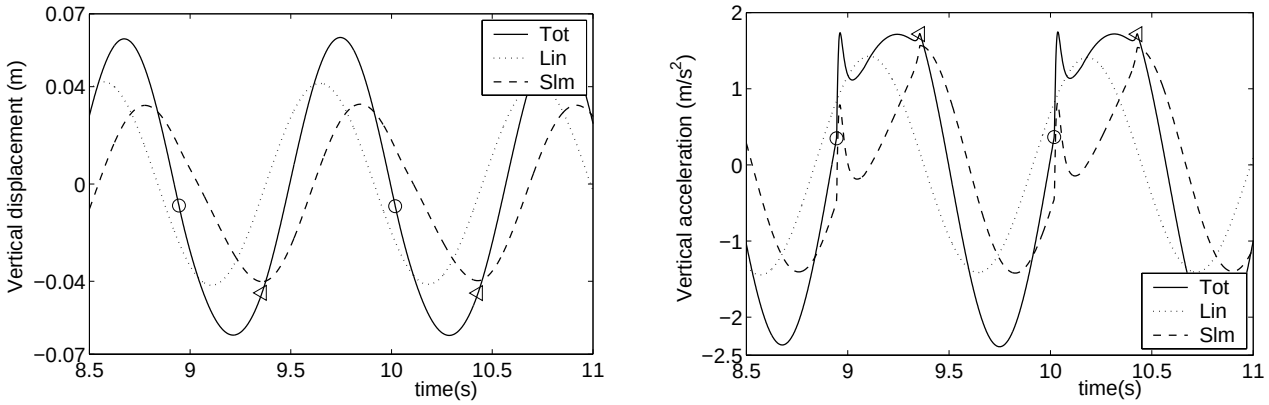

(a) η_3 at COG (Model1) (b) $\ddot{\eta}_3$ at COG (Model1)

Figure 4.3 Slamming influence on the global motion and acceleration by Model1 (See Table 4.1). 'Lin' and 'Slm' represent the response from the linear wave excitation loads and slamming loads respectively, 'Tot' is the total response; '$\circ$ and '$\triangleleft$' correspond to the starting and ending time of slamming. $T = 1.8s$, $\zeta_a = 0.05m$, $U = 1.9m/s$, head sea.

in Fig. 4.4 also accounts for second order incident wave effects. The results agree well with Baarholm's (2001) calculations based on using similar methods as ours. Additionally, the water entry phase agrees well with Baarholm's experiments. But this is not so for the water exit phase. In the water exit phase, the duration is 51.2% longer in the experiments and the minimum value in the experiment is 77.8% of what we predict. However, for the catamaran case studied here the Wagner based method has much less effect. Further, the duration of the slamming is well predicted by our method in the flexible catamaran cases to be considered (See Chapter 5). This may be due to that the platform deck is totally wetted and that the wetting lasts longer in Baarholm's case.

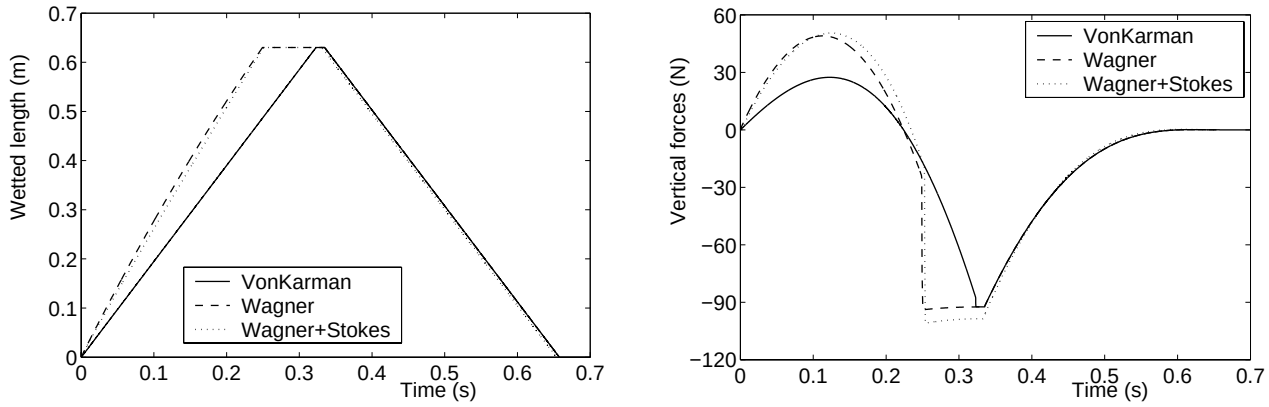

(a) wetted length (b) vertical impacting force

Figure 4.4 Water impact on a fixed rigid wetdeck with incident wave height $H = 0.12m$, wave period $T = 1.25s$ and air gap $\eta = 0.04m$ when no waves are present.

Figure 4.4 shows that the second order incident wave effects matter, but it is not dominant. The incident wave slope $k\zeta_a$ based on linear approximation of ζ_a is 0.107 in this case while it is at most 0.089 in our catamaran cases with wetdeck slamming. The ratio between maximum wave elevation based on second order wave theory and linear wave theory is $(1 + 0.5k\zeta_a)$ (*e.g.* Faltinsen (1990)). This is an indication that the second order incident wave effects are not dominant in the catamaran cases. It does also matter that the catamaran is free to move while the platform deck is restrained from oscillating. The catamaran motions play an important role in determining the wetted area when slamming occurs.

The agreement with experiments was improved in Baarholm's studies by incorporating a Kutta condition at the aft end of the wetted deck during water exit phase as well as nonlinear free surface conditions with gravity effects. Generally speaking, the longer the time duration of the wetting is relative to the wave period, the more important gravity becomes. This is associated with generated free surface waves during the impact. In the catamaran cases the wetting time is relatively smaller compared to the wave period in Baarholm's case and gravity will matter less. So it is more appropriate to neglect gravity in the free surface condition in our catamaran cases.

4.3 Effect of exact representation of V_R

The analysis in this section will examine if the linear approximation of V_R in the body boundary condition is satisfactory by comparing with Model3 where the exact expression of V_R is used. $V_R(x,t)$ is expanded into a Fourier series as shown in Eq. (3.44) in Chapter 3. The boundary value problem is solved as presented in Fig. 3.1. Figures 4.5 to 4.6 are for the case when $2c(t)$ is determined by the Von Karman method.

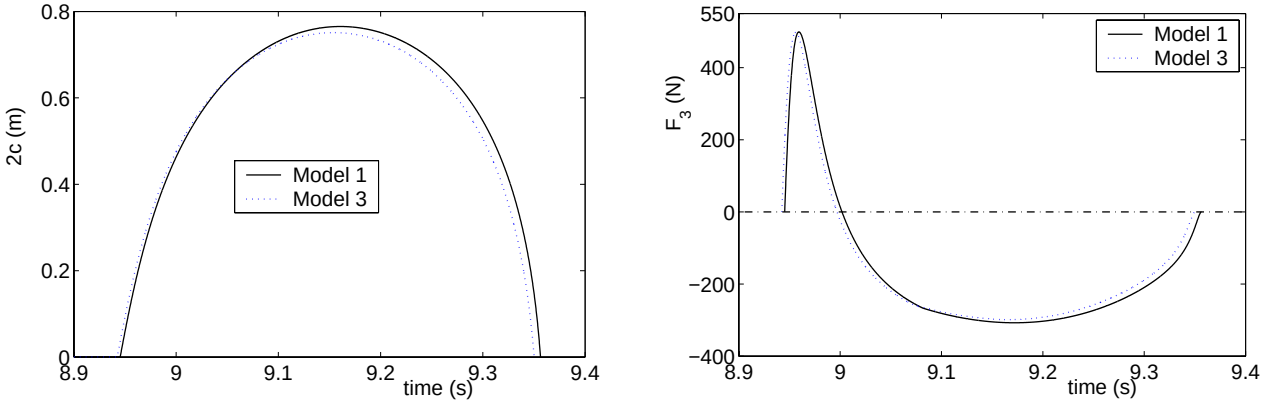

(a) Wetted length $2c(t)$ (b) Vertical impact force F_3

Figure 4.5 Comparison between linear (Model1) and exact representation of relative impact velocity V_R (Model3) for wetdeck slamming on a rigid catamaran (See Table 4.1); $T = 1.8s$, $\zeta_a = 0.05m$, $U = 1.9m/s$, head sea.

Figures 4.5 and 4.6 show that the Fourier expansion method does not influence the wetted length

and the force greatly, at least for this case. So the influence on the global responses is also quite small. The reason is that the incident wave length λ is large relative to $2c$. This means that the incident wave terms $\sin(kX)$ and $\cos(kX)$, where $k = 2\pi/\lambda$, can be approximated as respectively kX and 1 over the wetted area.

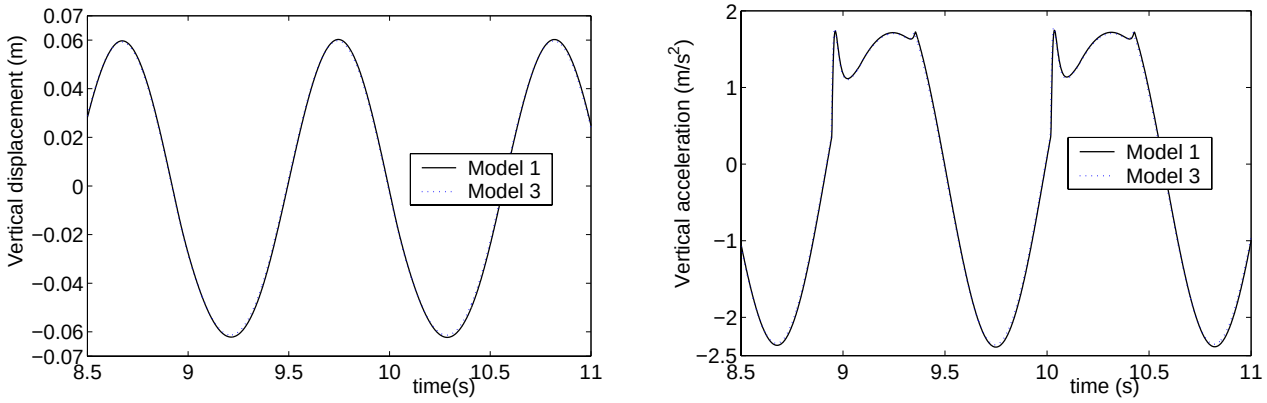

(a) Global response of η_3 at COG

(b) global response of $\ddot{\eta}_3$ at COG

Figure 4.6 Comparison between linear (Model1) and exact representation of relative impact velocity V_R (Model3) for wetdeck slamming on a rigid catamaran (See Table 4.1); $T = 1.8s$, $\zeta_a = 0.05m$, $U = 1.9m/s$, head sea.

Calculations and comparisons based on the Wagner method for $c(t)$ (see Section 3.5.4) were also done. This is illustrated in Figs. 4.7 and 4.8. Similar tendencies and results were found as in Figs. 4.5 and 4.6 for the Von Karman based case. The exact representation of V_R has a small influence on the wetted length, the wetdeck force and the vertical accelerations. However, the effect of using the Fourier expansion will depend on parameters like the deck height, wave amplitude and wave length. Obviously the longer the wetted length is relative to the incident wave length, the more appropriate it is to use the Fourier expansion method.

4.4 Kutta condition

Figures 4.9 to 4.10 present comparisons between cases with and without applying the Kutta condition at the aft end of the wetted length ($X = c(t)$). The formulas for the Kutta condition are presented in Section 3.6. The wetted length $2c(t)$ is in both cases based on the Von Karman method. The figures show that the Kutta condition has a larger influence than previously found by using a Wagner method instead of a Von Karman method or by not using Eq. (3.15) to approximate V_R in the body boundary condition. Figure 4.9 demonstrates that steady state slamming does not start at the same time in Model1 and Model4. This is a consequence of the transient phase of the numerical simulations.

Figure 4.11 illustrates the relative importance of the different force terms in Eq. (3.93) and compares it with corresponding terms in the case without a Kutta condition. The two first

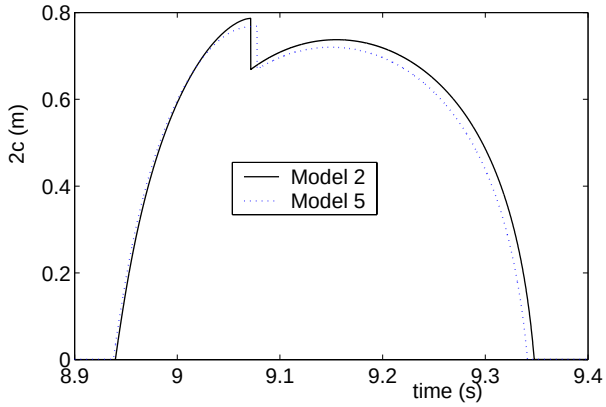

(a) Wetted length $2c(t)$

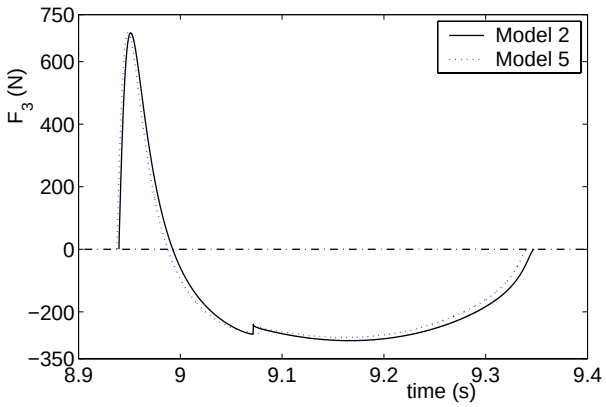

(b) Vertical impact force F_3

Figure 4.7 Comparison between linear (Model2) and exact representation of relative impact velocity V_R (Model5) for wetdeck slamming on a rigid catamaran (See Table 4.1); $T = 1.8s$, $\zeta_a = 0.05m$, $U = 1.9m/s$, head sea.

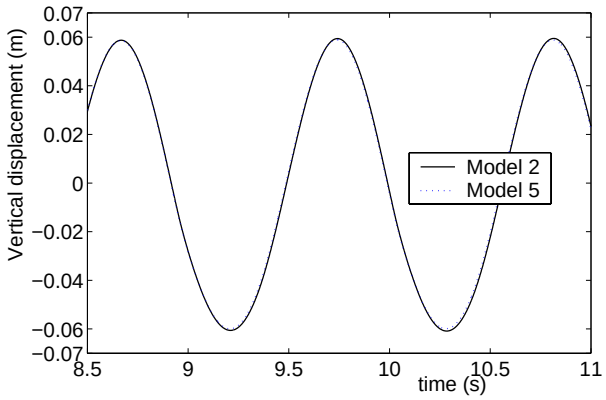

(a) Global response of η_3 at COG

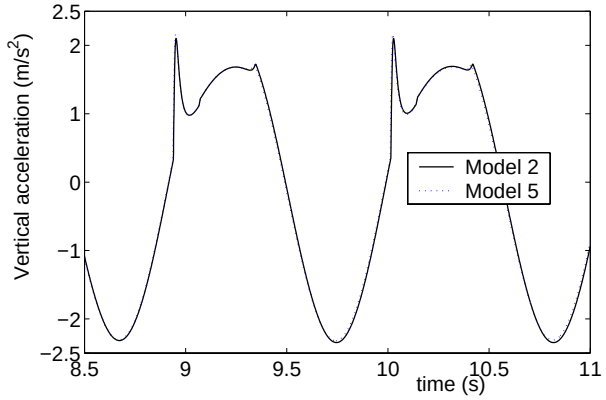

(b) global response of $\ddot{\eta}_3$ at COG

Figure 4.8 Comparison between linear (Model2) and exact representation of relative impact velocity V_R (Model5) for wetdeck slamming on a rigid catamaran (See Table 4.1); $T = 1.8s$, $\zeta_a = 0.05m$, $U = 1.9m/s$, head sea.

terms are previously called slamming and added mass terms, and are in Fig. 4.11 denoted as F_{31} and F_{32} respectively. The last terms in Eq. (3.93) are denoted $F_{3\gamma}$. Figure 4.11 shows that the slamming force term has a lower maximum value when the Kutta condition model is applied. The added mass terms are always negative and the no-Kutta-condition case gives a lower minimum than if Kutta condition is considered. The figures show clearly that the Kutta condition influences the force in the water exit phase. Studies by Baarholm (2001) (See also Baarholm and Faltinsen (2001)) for slamming loads on a horizontal fixed deck showed that the application of Kutta condition improves significantly the results in the water exit phase. However, their numerical model with Kutta condition is different from ours and is based on a boundary element method with exact nonlinear free surface conditions including the effect of gravity.

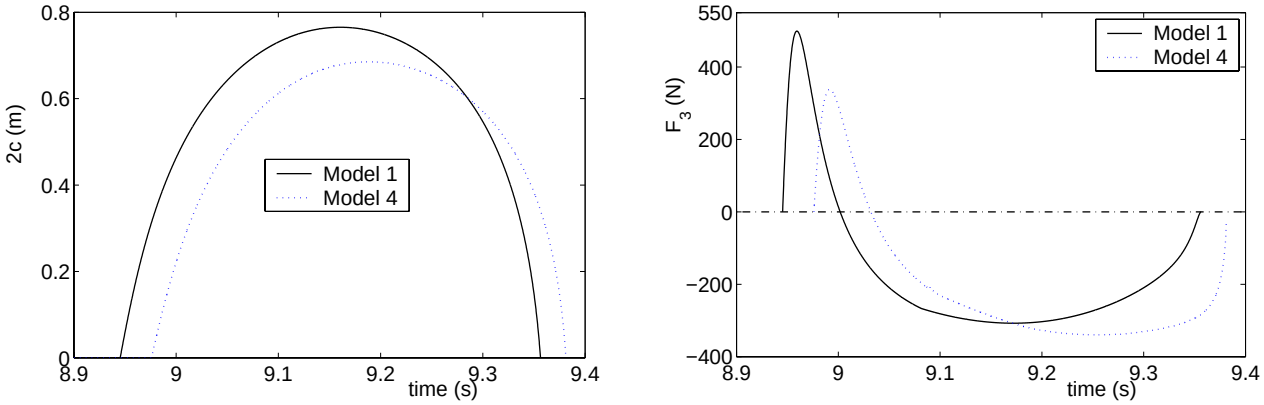

(a) Wetted length $2c(t)$ (b) Vertical impact force F_3

Figure 4.9 Comparison between without Kutta condition (Model1) and with Kutta condition at $X = c$ (Model4) for wetdeck slamming on a rigid catamaran (See Table 4.1); $T = 1.8s$, $\zeta_a = 0.05m$, $U = 1.9m/s$, head sea.

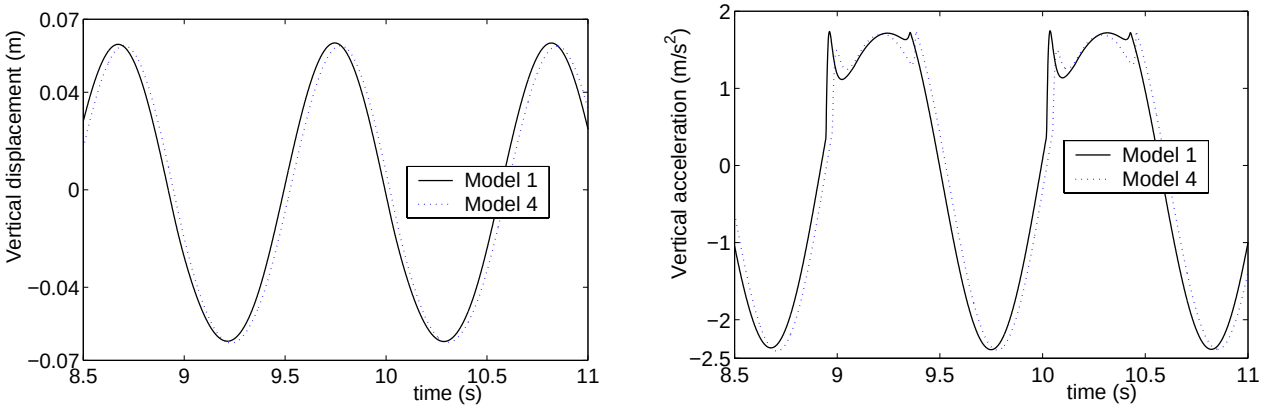

(a) Global response of η_3 at COG (b) global response of $\ddot{\eta}_3$ at COG

Figure 4.10 Comparison between without Kutta condition (Model1) and with Kutta condition at $X = c$ (Model4) for wetdeck slamming on a rigid catamaran (See Table 4.1); $T = 1.8s$, $\zeta_a = 0.05m$, $U = 1.9m/s$, head sea.

An implicit assumption in applying Kutta condition in Model4 is that the forward speed U is much larger than the horizontal fluid velocity. However, both da/dt and db/dt, the time rate of change of left and right ends of the wetted deck respectively, are in the initial impact phase much larger than U. This implies that a vortex sheet aft of the trailing edge can not be generated initially. By vortex sheet we are referring to the mathematical representation of the solution. It does not refer to physical vorticity. The consequence is that the Kutta condition can not be applied then. This occurs for this case during the first 0.0004 seconds. The application of the Kutta condition starts therefore after this small initial time. However, this is believed to have minor influence on the subsequent results.

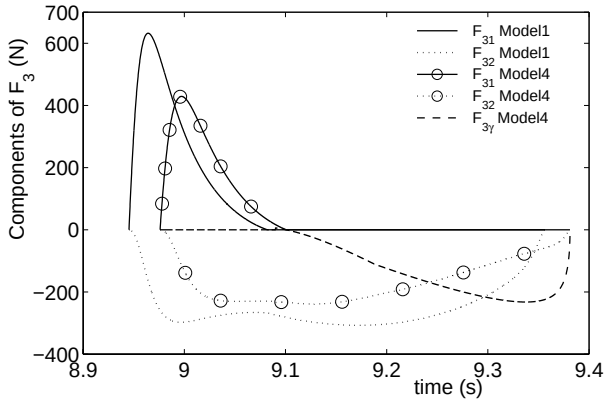

Figure 4.11 Comparison between slamming models without Kutta condition (Model1) and with Kutta condition at $X = c$ (Model4) for wetdeck slamming on a rigid catamaran (See Table 4.1); $T = 1.8s$, $\zeta_a = 0.05m$, $U = 1.9m/s$, head sea. Influence on the slamming force term F_{31}, the added mass term F_{32} and the additional force term $F_{3\gamma}$ when Kutta condition model is applied.

4.5 Discussion

Our five slamming models differ from the force and response model presented in Zhao and Faltinsen (1992). They used a Wagner based method and considered only the water entry phase. Further, they neglected the added mass term in the impact loads. There is an additional important difference in their case studies and ours. This is associated with that different ships and Froude numbers are used. Zhao and Faltinsen (1992) used the high-speed theory by Faltinsen and Zhao (1991) appropriate for Froude numbers larger than $0.4 \sim 0.5$. Since our Froude number is around 0.30, this high-speed theory is not applicable for cases here. In the case studied in this chapter the initial impact occurs at the front end of the deck. There is then finite angle between the free surface and the deck surface. This means that $\frac{dc}{dt}$ is finite. In Zhao and Faltinsen's case the initial impact does not occur at the deck end and the water free surface and the deck surface are initially tangential. When the impact occurs like this, $\frac{dc}{dt}$ is infinite initially. Since c is initially zero, the resulting vertical initial impact force is finite as illustrated by Eq. (1.1). The consequence is very large initial vertical accelerations of the ship. Even if there are also some peak values of acceleration initially in our numerical predictions, their values are far less than predicted by Zhao and Faltinsen (1992).

Figure 4.12 shows the influence on the response by including or not including the added mass term in the impact loads. Only the time history response of the vertical acceleration $\ddot{\eta}_3$ at the bow is shown. Linear response without accounting for slamming is also shown in the plot. The large influence of including the added mass term is demonstrated in the figure.

Figure 4.12, as well as the global responses presented in earlier sections, show two peaks in the time history of the acceleration, when the added mass term F_{32} is accounted for. The first peak occurring at the initial time of slammings is clearly the largest one. The following is another example to illustrate how the second peak is produced when the added mass term is

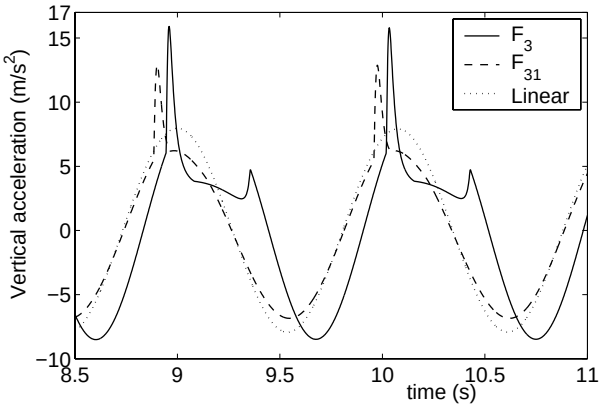

Figure 4.12 Wetdeck slamming induced vertical acceleration $\ddot{\eta}_3$ at the bow for case $T = 1.8s$, $\zeta_a = 0.05m$, $U = 1.9m/s$; by Model1 (See Table 4.1). F_3: both slamming force term and added mass term included; F_{31}: only slamming force term included; 'Linear': No wetdeck slamming included.

included. The studied case is for the same catamaran as before in head sea regular waves with $U = 1.8m/s$. The incident wave period is $1.9s$ and wave amplitude is $0.05m$. Linear expression of V_R in Eq. (3.15) and Von Karman method for $2c(t)$ are applied. Impact force components are shown in Fig. 4.13(a). The force history in Fig. 4.13(a) is used as input to an artificial dynamic system. This represents the uncoupled heave motions of the same catamaran. Another difference from the case in Fig. 4.12 is that linear wave induced motion response is not included.

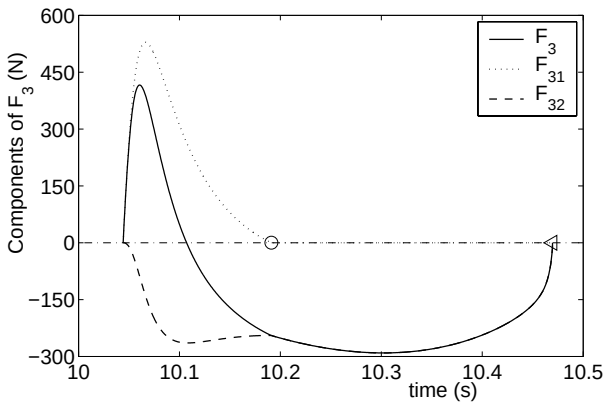

(a) Vertical force component

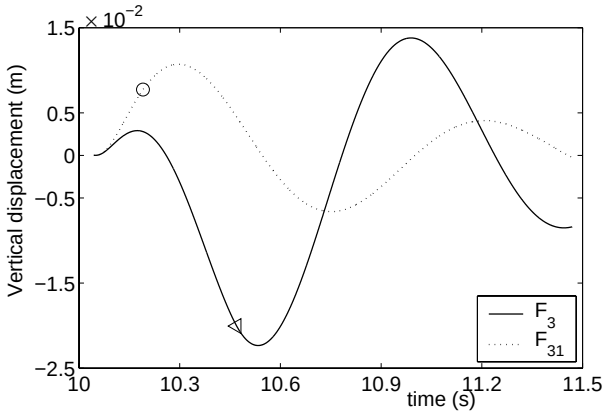

(b) Uncoupled η_3 response due to loading in Fig. 4.13(a)

Figure 4.13 Components of vertical impact loads for case $T = 1.8s$, $\zeta_a = 0.05m$, $U = 1.9m/s$ by Model1 (See Table 4.1), and the corresponding uncoupled vertical motion response on the same rigid catamaran. F_{31}: only slamming force term included, F_{32}: only added mass term included, $F_3 = F_{31} + F_{32}$: total response; '$\circ$' and '$\triangleleft$' are the ending time of loading due to respectively F_{31} and F_3.

Figures 4.13(b) to 4.14 are the corresponding time histories of vertical motion, velocity and acceleration. In the figure the impact loads start at $t = 10.0442s$. The sign '$\circ$' represents the ending time $t = 10.4697s$ of the slamming force term. Further, the sign '$\triangleleft$' means the ending

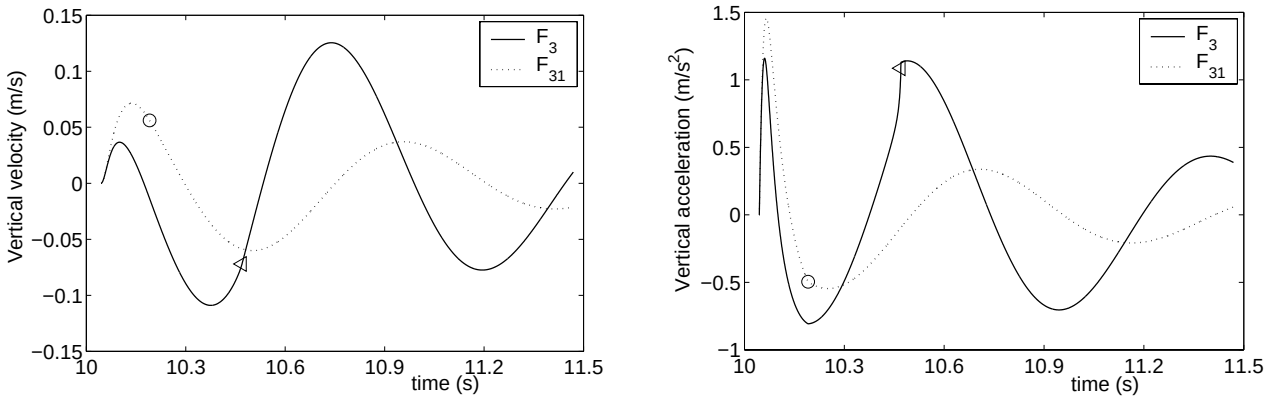

(a) Uncoupled $\dot{\eta}_3$ response due to loading in Fig. 4.13(a); (b) Uncoupled $\ddot{\eta}_3$ response due to loading in Fig. 4.13(a)

Figure 4.14 Uncoupled vertical velocity and acceleration for the rigid catamaran with $T = 1.8s$, $\zeta_a = 0.05m$, $U = 1.9m/s$ by the impact loading in Fig. 4.13(a). F_{31}: only slamming force term included, F_3: total response; '$\circ$' and '$\triangleleft$' are the ending time of loading due to respectively F_{31} and F_3.

time $t = 10.1919s$ of the total impact loading. So there is first a loading part and then after the loading there is a free vibration with initial conditions given by the velocity and motion after the loading time. The same catamaran is used to find the mass, damping and restoring terms in the dynamic system. Figures 4.13(b) to 4.14 show that the added mass term gives important contributions to the time history of the motions, velocities and accelerations. When the added mass term F_{32} is accounted for, the second peak in the response occurs. This is similar as in Fig. 4.12. This example illustrates also the importance of the water exit phase.

The previous examples have shown that the linear expression of V_R and Von Karman method for $2c(t)$ are good approximations for slamming induced response calculations. So such assumptions will be applied in the following chapters for hydroelastic analysis. The two-node bending will then dominate. Since the ratio between slamming duration and natural period for two-node bending is less than the ratio between slamming duration and heave and pitch natural periods, one should be careful in generalizing. In order to see what the influence of the time history of slamming loads is on global loads for the elastic model, we will examine the sensitivity by using the Kutta condition model in Section 7.2.3.

As mentioned in Chapter 2, to avoid that slamming happens right at the beginning of the time domain simulation, the linear wave excitation force is artificially built up during typically four wave periods to reach the steady state value. Examples in Chapter 7 will show that this kind of build up of the excitation loads will not influence the time domain properties of the steady state results. However, the transient phase causes different slamming starting moment when different slamming models are used. This means a time shift of the impact start moments as shown in figures in this chapter.

Chapter 5

Hydroelastic Response, Verification and Validation

5.1 Introduction

Based on the discussions in Chapters 2 and 3, further details of the three-body model, as well as the connecting beam modelling will be presented. A modal based method will be introduced to facilitate the solution of the equations of motions. Experimental validation and numerical verification will be made for this three-body dynamic system. Global hydroelastic responses with slamming will be analyzed numerically and experimentally. All the response cases will refer to steady state conditions in regular head sea waves. An artificial build-up phase of the wave excitation loads as described in Chapter 2 is used to reach steady state conditions in the numerical calculations. A transient phase is clearly seen in the experimental time records. However, what is judged as experimental steady state conditions does not show a perfectly periodic response. One reason is the change of the incident wave amplitude along the track of the model.

5.2 Structural data

5.2.1 Main data for the three rigid body parts

The catamaran is segmented into three rigid body parts and divided at $1.48m$ and $2.68m$ from the bow end. These two cuts are denoted as respectively Cut1 and Cut2 in Fig. 2.1. Based on the mass distribution of the catamaran (See Table A.2 in Appendix A), Table 5.1 lists the length (Lseg), mass, positions of the longitudinal centers of gravity and buoyancy, and pitch radius of gyration R_{55} about the local COG for each segment. Here 'Xcog' is the distance from the local center of gravity O_i (illustrated in Fig. 2.4) of the ship segment to the bow of the catamaran. Similarly 'Xcob' is the distance from the local center of buoyancy to the bow.

$R_{55}(1)$ is based on using the individual masses as listed in Table A.2 and assuming that the masses are concentrated at points corresponding to the coordinates shown in Table A.2. $R_{55}(2)$ accounts for a finite distribution of the mass, *i.e.* the local pitch radius of gyration of each mass element is accounted for. Values listed under 'Bouy.' multiplied with acceleration of gravity give the buoyancy force for each segment. Due to the large difference between buoyancy force and weight for each body, there is a large static vertical shear force at the connecting positions between the bodies. The static vertical shear forces and bending moments at zero forward speed are not included in the numerical and experimental results.

Table 5.1 Main data for ship segments

Component	Lseg	Mass	Buoy.	Xcog	Xcob	$R_{55}(1)$	$R_{55}(2)$
Unit	m	kg	kg	m	m	m	m
Fore(Body1)	1.48	57.83	35.80	0.869	1.090	0.275	0.477
Mid(Body2)	1.20	56.65	101.58	2.060	2.120	0.211	0.418
Aft(Body3)	1.42	131.52	108.62	3.348	3.316	0.393	0.475

5.2.2 Equivalent beam connections

The longitudinal connection between rigid body parts is composed of a steel spring and an aluminum transducer (See Fig. 2.1 and Fig. A.7). The lengths of the longitudinal spring and transducer are respectively $0.1m$ and $0.08m$. The total length is $0.21m$ by accounting for the connecting length of $0.03m$ between the transducer and spring. The effective stiffness of the longitudinal steel transducer and the aluminum spring are quite close. They were therefore modelled as one equivalent beam, with a bending stiffness of $(EI)_{eq} = 6.541 \cdot 10^3\, Nm^2$ and length of $L_{eq} = 0.21m$ in the three-body model. The detailed analysis is presented in Appendix A.6. The calculations in the following Section 5.3 will show that this approximation is reasonable and gives good results for mode shapes and eigenvalues.

The distances from the local center of gravity O_i of each body to the beam ends are also needed in the calculations (illustrated in Fig. 2.4). They are as follows $\overline{O_1A} = 0.431m$, $\overline{O_2B} = 0.550m$, $\overline{O_2C} = 0.490m$ and $\overline{O_3D} = 0.588m$.

5.3 Model validation without slamming

5.3.1 Eigenvalues and eigenvectors

It is important to control that the beam model represents the real longitudinal bending stiffness of the catamaran model. Experimental decay tests in calm water at zero ship speed with the same mass distributions as ours were analyzed in Økland (2002). Decay tests in air were also done but the results were less reliable (Økland (2002)). The test results of the wet and dry decay

tests will be compared with the numerical predictions by our three-body model.

The eigenvalue problem is obtained by first setting the excitation forces $\mathbf{F}_{gen}$ in Eq. (2.1) equal to zero. Here we make use of the first order differential equation system Eq. (2.44) introduced in Chapter 2. Equation (2.44) is a transformation of the second order differential equation system Eq. (2.1). This leads to the following eigenvalue problem

$$\widetilde{\mathbb{M}}\dot{\mathbb{X}} = \widetilde{\mathbb{K}}\mathbb{X} \tag{5.1}$$

where $\widetilde{\mathbb{K}}$ and $\widetilde{\mathbb{M}}$ are square matrices with dimensions 12×12 and defined in Eq. (2.45). Further, $\mathbb{X}$ is a column matrix with $\mathbb{X} = [X_1 \cdots X_i \cdots X_{12}]^T$, where X_{2i-1} with $i = 1, 2, 3$ are the heave velocities of body number i and X_{2i} with $i = 1, 2, 3$ are the pitch velocities of body number i. Further, X_{2i+5} with $i = 1, 2, 3$ are the heave motions of body number i and X_{2i+6} with $i = 1, 2, 3$ are the pitch motions of body number i. The eigenvalue problem is now formulated by assuming $\mathbb{X}$ has the time dependence $e^{\lambda t}$. This means that the eigenvalues λ are the solutions of

$$\widetilde{\mathbb{K}}\mathbb{X} = \lambda\widetilde{\mathbb{M}}\mathbb{X} \tag{5.2}$$

The eigenvalues λ are in general complex and the corresponding modes will also be complex. The system has 12 different eigenvalues where 6 of the values are complex conjugates of the other 6 values. The eigenvalues can be expressed as

$$\lambda = \omega_R + i\omega_I \tag{5.3}$$

where ω_I corresponds to the so-called damped frequency. This can be taken as an approximation of the natural frequency when the damping ratio is much less than 1.0. The damping ratio can then be approximated as ω_R/ω_I (See *e.g.* Bergan *et al.* (1986)).

So our system gives 6 sets of eigenvalues, damping ratios as well as the corresponding eigenvectors which have complex amplitudes. The two lowest modes represent coupled rigid body heave and pitch motions. The third mode is a two-node bending mode of the hull and the fourth mode is a three-node bending mode of the hull. The two highest modes correspond to shear displacements at the connecting beams, but these are not physical modes for a real catamaran.

Dry decay tests were done by lifting up the model from the ground by six relatively soft springs. Økland (2002) predicted experimentally the natural frequency for dry two-node bending as $36.53 rad/s$ with damping ratio 0.35%. The natural frequency was $88.50 rad/s$ for three-node bending with damping ratio 0.45%. However, Økland (2002) showed that data from dry decay tests are less reliable than those from wet decay tests. To calculate the dry natural frequencies of the three-body system, the static restoring forces are included in the dynamic system to avoid unphysical solutions and numerical problems. The static restoring terms provide spring effects for the rigid body motions. The soft spring system used in the experiments have a similar but not equal effect. Our three-body model predicts the natural period for two-node and three-node bending mode in rad/s as 34.03 and 74.65 respectively. However, structural damping ratios are not predicted by our three-body model.

Comparisons have also been made with the experimental results from the wet decay tests. An important consideration is that the hydrodynamic coefficients used in the eigenvalue calculations are frequency dependent. Since the natural periods of the heave and pitch of the test model is close to $1.0s$, the added mass and damping coefficients are in this case calculated for the period $1.0s$. This implies an error in the calculations of the higher natural frequencies. The ship speed U is zero. Table 5.2 then shows the experimental and numerical results for natural frequencies and damping ratios. The agreement is generally good. The two modes which are coupled rigid body heave and pitch motions are denoted as 'Heave & pitch' and 'Pitch & heave' respectively. There were no experimental results reported for the two highest modes.

Table 5.2 Theoretical and experimental values of natural frequencies and damping ratios. Experimental values are from wet decay tests in calm water and theoretical values are calculated from hydrodynamic coefficients for the catamaran with $T = 1.0s$ and $U = 0$.

	Natural frequencies (rad/s)		Damping ratio	
Mode	Exp.	Num.	Exp.	Num.
Heave & pitch	6.41	6.35	5.8 %	12.2 %
Pitch & heave	7.14	7.34	7.0 %	12.9 %
Two-node bending	27.56	29.84	2.0 %	2.1 %
Three-node bending	–	67.41	–	1.1 %

Table 5.2 shows that the agreement between experimental and theoretical results for wet two-node bending is good even if the structural damping has been neglected. It should be noted that for the two-node bending mode the structural damping ratio obtained from the dry decay tests is much smaller than the damping ratio in the wet decay tests. The agreement between experimental and theoretical damping ratios of heave and pitch coupled modes are less satisfactory. This damping is in our theory due to wave radiation. An important error source is the neglection of hull interaction, which influences the wave generation by the ship. We could in principle have included hull interaction in a strip theory but it is well known that this will amplify the hull interaction and that 3D effects matter. Further, our main concern is forward speed cases where the wave interaction is less pronounced. The wave interaction can for a high speed operating condition be negligible in resonant motion conditions (See Fig. 1.5 and corresponding discussion). This will be further discussed in the error analysis in Chapter 7 as well as in a comparative study with the experimental test case 1115 towards the end of this chapter.

One reason to the differences in experimentally and numerically predicted natural frequencies for two-node bending is the error caused by using a period of $1.0s$ in the calculations of hydrodynamic coefficients. Figure 5.1 shows the calculated added mass in heave when the catamaran is totally rigid. The kinks in the figure may be due to inaccuracies in the numerical solutions or the irregular frequencies (Hoff (2002)). The predicted value at frequency $45rad/s$ is used as the high-frequency asymptotic value. Figure 5.1 can be applied to give an indication of errors introduced when calculating the higher natural periods. Let us use the formula for natural period of a system with a single degree of freedom as a rough basis for doing that and then

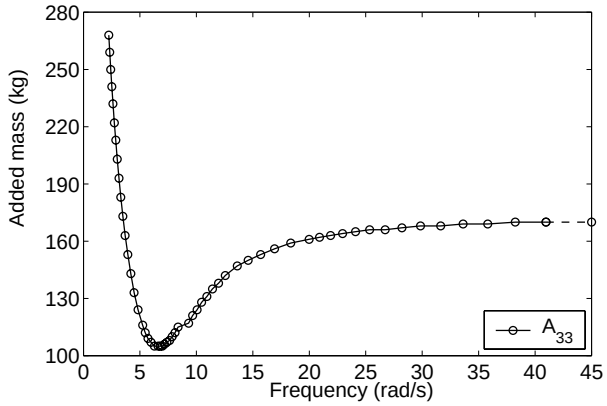

Figure 5.1 Calculated added mass A_{33} in heave at different circular frequencies of body oscillations for the rigid catamaran with $U = 0.0m/s$. No hull interaction. Strip theory.

multiply the calculated natural frequencies with the following ratio

$$\alpha = \sqrt{\frac{M + A_{33}\left(T = 1.0s\right)}{M + A_{33}\left(T = T_N\right)}} \tag{5.4}$$

Here M is the structural mass of the catamaran and T_N means the natural period of either two-node or three-node bending. Strictly speaking it would have been better to include the effect of the mode shapes and operate with generalized mass and added mass for each mode. Here is just a qualitative estimation to see the influence of the frequency dependency. The high frequency asymptotic added mass value is estimated as $170.0kg$, and the added mass for $T = 1.0s$ and $U = 0.0m/s$ is $105.0kg$. Accounting for $M = 246kg$ gives $\alpha = 0.92$. This leads to estimated natural frequencies of $27.45rad/s$ and $62.02rad/s$ for respectively the two-node and three-node bending modes. This gives actually very good agreement for the two-node bending. Økland (2002) did not present experimental natural frequency for three-node bending from the wet decay tests, but this was done by Økland *et al.* (1998). The value $63.20rad/s$ agrees reasonably with our estimate. Since our system is highly coupled, we have no better way to do this with a frequency domain model for hydrodynamic loads. A time domain model for the hydrodynamic loads is needed to more rationally deal with transient effects involving different natural frequencies (*e.g.* Ogilvie (1964)).

From the corresponding eigenvectors, we get the mode shapes. Eigenvectors show larger sensitivity relative to eigenvalues. This is due to the high stiffness terms from the connecting beams (See Eq. (2.37)). However, the relative small variation that this causes, will not destroy the model verification. Figure 5.2 are modes of the two-node and three-node longitudinal bending when the period $1.8s$ and a forward speed of $1.9m/s$ are used in the added mass and damping calculations. The mode shapes have similar patterns as the FEM results by Økland (2002), though they can not be completely the same due to differences in mass distribution. These complex eigenmodes are a consequence of the damping of the dynamic system, as well as the asymmetry of the added mass matrix due to forward speed effects. If these mode shapes are used to solve a free vibration problem, we would express the physical relative vertical motion of

the body as $\Re(\sum A_i \psi_i(x) e^{\lambda_i t})$. Here λ_i and $\psi_i(x)$ mean respectively ith eigenvalue and mode. A_i are complex constants to be determined by the initial conditions.

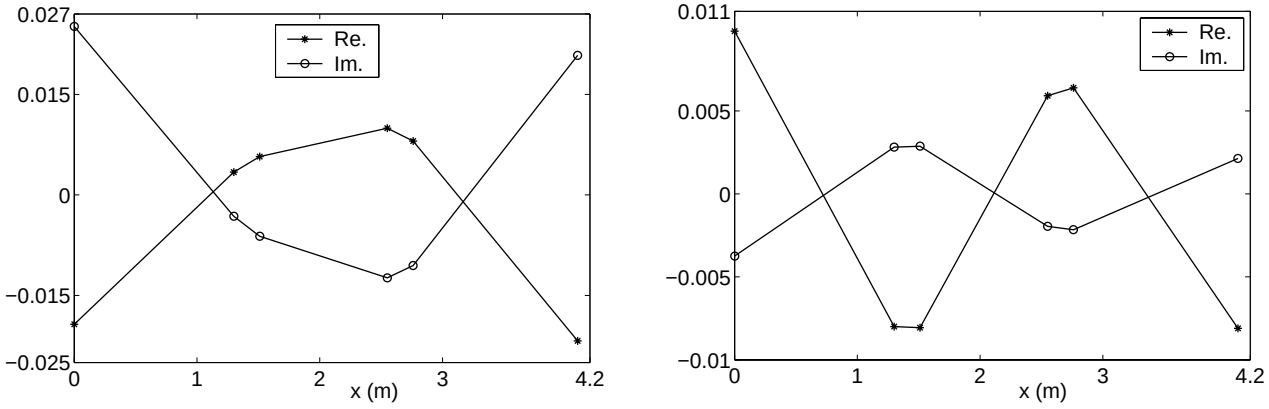

(a) Two-node longitudinal bending

(b) Three-node longitudinal bending

Figure 5.2 Calculated eigenmodes for two-node and three-node bending. X-axis is the longitudinal distance from the bow and 'Re.' and 'Im.' are the real and imaginary parts of the eigenmodes respectively. $U = 1.9m/s$, $T = 1.8s$

5.3.2 Linear global response comparisons

When the stiffness of the connecting beams increases, the wave induced response should converge towards the corresponding values for a rigid catamaran. This implies that the local vertical motion as a function of the longitudinal coordinate of the ship should approach straight lines. This is illustrated in Fig. 5.3. Head sea, a wave period of $1.8s$ and both zero speed and forward speed $1.9m/s$ were used in the calculations. The results agree well with the corresponding results based on the commercial computer program VERES (1999), which assumes a rigid catamaran and also uses the strip theory by Salvesen *et al.* (1970) without hull interaction in this case. Since VERES does not account for the pitch radius of gyration of mass points, the $R_{55}(1)$ data in Table 5.1 is used.

The following Fig. 5.4 shows a detail of the convergence study where the real and imaginary part of the complex pitch amplitude of the mid body of the three-body model is presented as a function of the inverse of the factor n. This means for a given n that a bending stiffness equal to n times the original bending stiffness has been used.

When the flexibility of the model is considered, satisfactory predictions of linear transfer functions or response amplitude operator (RAO) of relative vertical motion at the bow as well as vertical shear force (VSF) and vertical bending moment (VBM) at the connections between the ship segments have been obtained for head sea cases without wetdeck slamming. These are presented in the following figures.

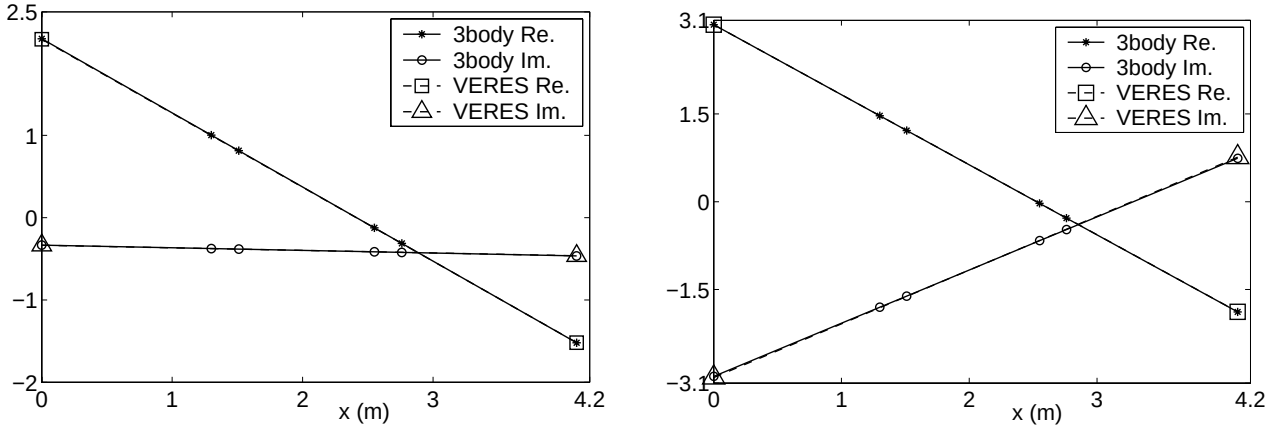

(a) $U = 0m/s$, $T = 1.8s$. Head sea

(b) $U = 1.9m/s$, $T = 1.8s$. Head sea

Figure 5.3 Comparisons of vertical motions predicted by VERES (1999) for the rigid catamaran and by the three-body model when $(EI)_{eq} \to \infty$. The stiffness is 1048576 times original $(EI)_{eq}$. X-axis is the longitudinal distance from the bow and 'Re.' and 'Im.' are the real and imaginary parts of the vertical motions divided by incident wave amplitude. No wetdeck slamming accounted for. Solid and dotted lines are overlapping.

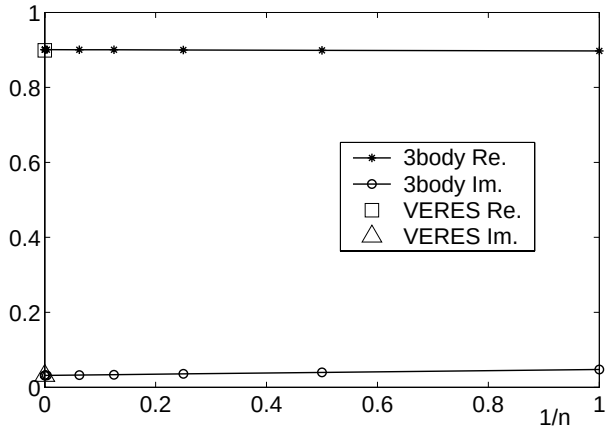

Figure 5.4 Convergence of real and imaginary parts of complex pitch amplitude of flexible body to rigid body results. Head sea, $T = 1.8s$ and $U = 0m/s$. X-axis is $1/n$, where n means that a bending stiffness of n times the original bending stiffness $(EI)_{eq}$ is used; 'Re.' and 'Im.' are the real and imaginary parts of the pitch amplitude in radians divided by incident wave amplitude in meters. No wetdeck slamming accounted for.

Figure 5.5 shows generally a good agreement of amplitudes of relative vertical motion at the bow when slamming does not occur. Data in the plot is non-dimensionalized by incident wave amplitude ζ_a, *i.e.* presented as Response Operator Amplitude (RAO).

Figures 5.6 to 5.7 present VSF and VBM comparisons at the two cuts for $U = 1.9m/s$ in head sea. No wetdeck slamming occurs here. The experimental values are obtained by adding the

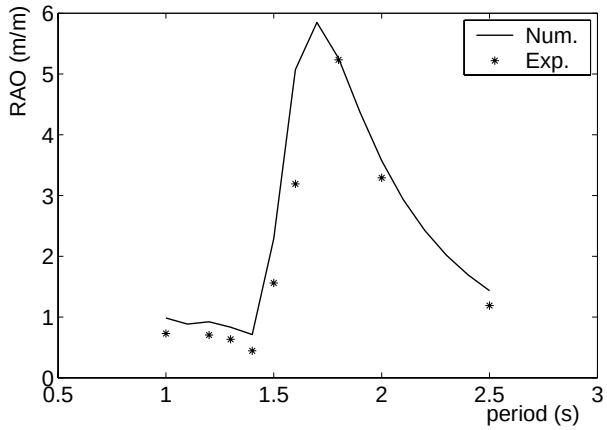

Figure 5.5 Comparison between experimental and numerical amplitudes of relative vertical motion at 0.045m from the bow; Results divided by incident wave amplitude. Head sea; $U = 1.9m/s$ in the calculations, U is close to $1.9m/s$ in the experiments (See Appendix A). No wetdeck slamming accounted for.

measured values for each side hull. The values for the two side hulls are not exactly the same, indicating that the free-running model was in a sea condition slightly different from head sea. The close results with VERES (1999) show that the influence of the flexibility on VSF and VBM is not large. However, this would not be the case with wetdeck slamming. There are some deviations with the experiments at some periods, especially noticeable for VBM at Cut1. A comprehensive discussion of experimental and theoretical error sources is given in Chapters 6 and 7. One relevant theoretical error source is hull interaction. Important experimental error sources are non-constant incident wave amplitude along the track of the model, trim angle and unintended mean roll angle. One should note that VERES does not account for the pitch radius of gyration of mass points. In order to be consistent with the VERES calculations, the $R_{55}(1)$ data in Table 5.1 is also used in '3body' results presented in Figs. 5.6 and 5.7. It will later be shown that accounting for the local pitch radius of gyration for each body as well as the experimental uncertainties improves the agreement between theory and experiments. However, the disagreement can not be completely explained.

The eigenvalue analysis showed that the system was dynamically unstable for wave periods $T = 2.0s$, $2.1s$, $2.2s$, and $2.3s$ when $U = 1.9m/s$. For instance for $T = 2.3s$ and $U = 1.9m/s$, the calculated complex eigenvalues λ (Eq. (5.3)) in rad/s are $-24.48 \pm i\,828.46$, $19.11 \pm i\,830.07$, $-0.51 \pm i63.76$, $-1.32 \pm i\,30.81$, $-0.52 \pm i\,7.05$ and $-2.07 \pm i\,5.81$. We see that the second set of the eigenvalues has a positive real part. This means that the response can not be damped out, leading to instability of the whole system. However, the positive real eigenvalue corresponds to the highest natural frequency and the ratio between the real and imaginary part of the eigenvalue is only 0.023. Positive real eigenvalues are also for the other cases related to one of the two highest eigenmodes. Later discussions will reveal that the two highest modes will in reality be strongly structurally damped. This means a dynamically stable system. There are no experimental data for the conditions where the eigenvalue analysis showed instability.

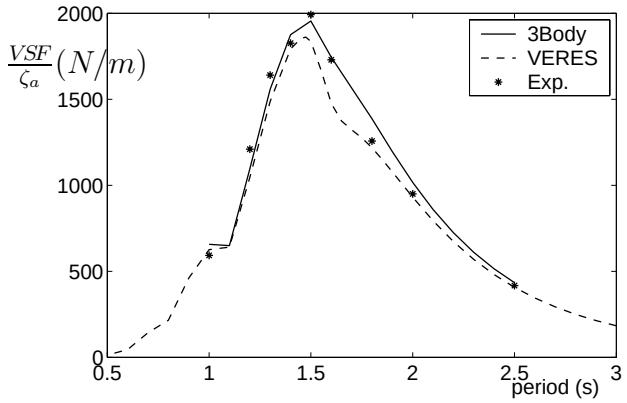

(a) VSF at Cut1

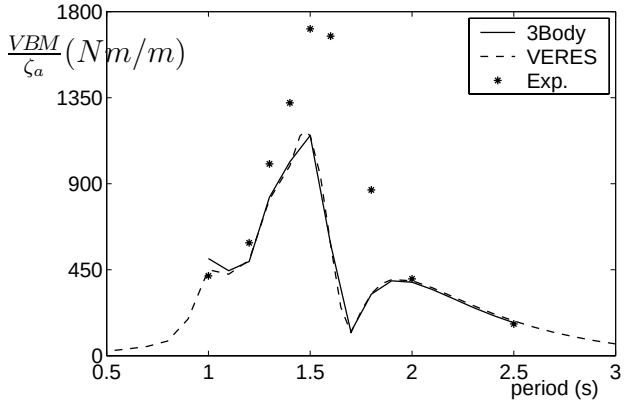

(b) VBM at Cut1

Figure 5.6 Comparisons between experimental and numerical amplitudes of vertical shear force (VSF) and vertical bending moment (VBM) at Cut1 as function of incident wave period. Head sea; $U = 1.9m/s$ in the calculations, U is close to $1.9m/s$ in the experiments (See Appendix A). No wetdeck slamming accounted for. Local pitch radius of gyration of mass elements excluded in calculations.

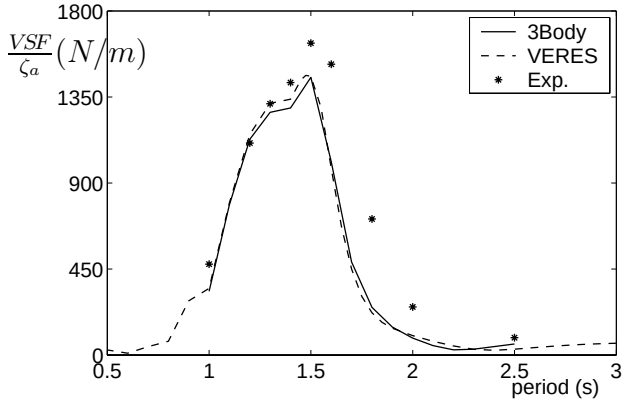

(a) VSF at Cut2

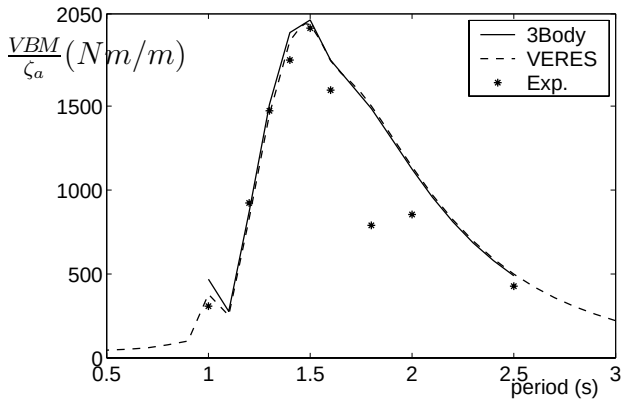

(b) VBM at Cut2

Figure 5.7 Comparisons between experimental and numerical amplitudes of vertical shear force (VSF) and vertical bending moment (VBM) at Cut2 as function of incident wave periods. Head sea; $U = 1.9m/s$ in the calculations, U is close to $1.9m/s$ in the experiments (See Appendix A). No wetdeck slamming accounted for. Local pitch radius of gyration of mass elements excluded in calculations.

The findings of positive real eigenvalues lead to a detailed examination of the hydrodynamic coefficients for the three rigid bodies. We worried about numerical errors and found that the heave (A_{33}) and pitch (A_{55}) added mass of the front body could be negative due to forward speed effects. This effect increases with increasing Froude number. For instance with $U = 1.9m/s$, $A_{33} = 1.031kg$ and $A_{55} = -1.274kgm^2$ for period of oscillations $T = 1.4s$, and $A_{33} = -2.394kg$ and $A_{55} = -3.232kgm^2$ for $T = 1.8s$. However, we then related these results to Gerritsma and Beukelman's (1964) experimental results for the longitudinal distribution of heave added mass and damping for a monohull at Froude numbers up to 0.3. Gerritsma and Beukelman's experimental results showed that the longitudinal distribution of added mass in heave could

have negative values in the bow region due to forward speed effects. Even if the ship hull used by Gerritsma and Beukelman (1964) differs in form from ours, their results could be used in a qualitative way to control our prediction of negative added mass values for the front body.

5.4 Dynamic response model with slamming

When wetdeck slamming occurs, the catamaran is excited by both steady state linear wave loading and transient slamming loads. The responses from those two load sources are linearly superimposed. The steady state response has a direct coupling effect to the wetdeck slamming induced response in terms of relative vertical motions and velocities that affect the slamming loads. The wetdeck slamming induced response depends on the added mass, damping and restoring coefficients associated with the side hulls.

5.4.1 Direct method

The six degree-of-freedom system of Eq. (2.1) defined in Chapter 2 can be directly solved by accounting for the linear wave loading and slamming loading and obtain steady state results as long as the system is dynamically stable (See corresponding discussions in Section 5.3.2). Since the results show that the two highest modes in the system for our test model correspond to very high natural frequencies ω_n, a small time step is needed to obtain numerical stability. These natural frequencies are for instance $849.85 rad/s$ and $689.91 rad/s$ when $U = 1.9 m/s$ and $T = 1.8 s$. However, the two highest modes are in reality strongly structurally damped. If this damping effect is not included, unrealistic large response due to the two highest modes occurs. In order to suppress this effect, the equation system of Eq. (2.1) was rewritten by a modal representation based on 'Rayleigh-Ritz-Condensation' method (*e.g.* Langen and Sigbjörnsson (1979)).

5.4.2 Modal based method

Generally speaking we can express the displacement vector $\mathbf{r}$ (dimension n) for the structure in terms of a reduced number of displacement parameters $\mathbf{q}$ (of dimension p) in the form of

$$\mathbf{r} = \mathbf{H}\mathbf{q} \qquad p \leq n \tag{5.5}$$

where the matrix $\mathbf{H}$ has dimensions $n \times p$ with columns constituting displacement patterns and $\mathbf{q}$ are corresponding weight factors, namely generalized coordinates. When the structure is subjected to a virtual displacement $\delta\mathbf{r}$, and by use of the general dynamic equation Eq. (2.1), the virtual work is

$$\delta\mathbf{r}^T\mathbf{F} = \delta\mathbf{r}^T\mathbf{M}\ddot{\mathbf{r}} + \delta\mathbf{r}^T\mathbf{B}\dot{\mathbf{r}} + \delta\mathbf{r}^T\mathbf{K}\mathbf{r} \tag{5.6}$$

Here the subscript *gen* is neglected from Eq. (2.1) to simplify the expressions.

Expressed by the generalized degrees-of-freedom $\mathbf{q}$, the virtual displacement $\delta\mathbf{r}$ becomes

$$\delta\mathbf{r} = \mathbf{H}\delta\mathbf{q} \tag{5.7}$$

Substituting Eqs. (5.5) and (5.7) into Eq. (5.6) gives

$$\delta\mathbf{q}^T\mathbf{H}^T\mathbf{F} = \delta\mathbf{q}^T(\mathbf{H}^T\mathbf{M}\mathbf{H}\ddot{\mathbf{q}} + \mathbf{H}^T\mathbf{B}\mathbf{H}\dot{\mathbf{q}} + \mathbf{H}^T\mathbf{K}\mathbf{H}\mathbf{q}) \tag{5.8}$$

This expression must be valid for an arbitrary displacement vector $\delta\mathbf{q}$, *i.e.*

$$\bar{\mathbf{M}}\ddot{\mathbf{q}} + \bar{\mathbf{B}}\dot{\mathbf{q}} + \bar{\mathbf{K}}\mathbf{q} = \bar{\mathbf{F}} \tag{5.9}$$

where $\bar{\mathbf{M}}$, $\bar{\mathbf{B}}$, $\bar{\mathbf{K}}$ and $\bar{\mathbf{F}}$ are generalized mass, damping, restoring and force matrices, with

$$\begin{aligned} \bar{\mathbf{M}} &= \mathbf{H}^T\mathbf{M}\mathbf{H} \\ \bar{\mathbf{B}} &= \mathbf{H}^T\mathbf{B}\mathbf{H} \\ \bar{\mathbf{K}} &= \mathbf{H}^T\mathbf{K}\mathbf{H} \\ \bar{\mathbf{F}} &= \mathbf{H}^T\mathbf{F} \end{aligned} \tag{5.10}$$

In our system $\mathbf{r}$ has dimension 6, referring to heave and pitch of each segment. $\mathbf{q}$ is the generalized coordinates, whose dimension is dependent on the selected number of modes. $\mathbf{H}$ can conventionally be established by a number of eigenmodes ϕ_i. Mathematically it can be expressed by

$$\mathbf{H} = [\phi_1 \ \phi_2 \ \cdots \ \phi_q] \tag{5.11}$$

where ϕ_i means the ith eigenvector with dimension 6, which is expressed by the heave and pitch displacement of each rigid body, *i.e.*

$$\phi_i = \left[u_i^1 \ \theta_i^1 \ u_i^2 \ \theta_i^2 \ u_i^3 \ \theta_i^3\right]^T \tag{5.12}$$

Here u and θ mean the heave and pitch motions respectively. Subscript i refers to the ith eigenmode and superscript $1, 2, 3$ refer to Body1, 2, 3 respectively. The eigenvalues and eigenvectors of the system are found from Eq. (2.1) by setting $\mathbf{F}_{gen}$ equal to zero, as described in Section 5.3.1. Noticing that for $U \neq 0$ cases, the eigenvectors are in complex forms, we here use instead the eigenmode results for $U = 0$ and zero damping to get real values. Then at each time step, $\mathbf{q}$ is calculated from Eq. (5.9) and $\mathbf{r}$ is then found from Eq. (5.5) for instantaneous slamming force calculations.

By this method, we can easily choose any number of modes we want. The modes are normally uncoupled in a normal mode method. This is not true in our case. In this Modal based method, the off-diagonal terms can be kept. Using this Modal based method and neglecting the two highest modes reduces the computing time significantly relative to the Direct method.

5.4.3 Comparisons between Direct method and Modal based method

In this section, we will compare the Direct method and Modal based method, showing that the Modal based method is efficient and accurate.

As discussed in Section 5.3.1, we get complex modeshapes in eigenvalue calculations for forward speed cases even with zero damping. This is the consequence of that the forward speed causes the elements m_{jk} in the matrix $\mathbf{M}_{gen}$ to differ from m_{kj} when $j \neq k$. For simplicity, the modes used in global response in the Modal based method are found by setting damping coefficients equal to zero and solving the linear equation system for the side hulls without excitation at zero speed.

The Direct method and the Modal based method will be compared for a case with wave period $T = 1.8s$, forward speed $U = 1.9m/s$ and incident wave amplitude $\zeta_a = 0.05m$. No bow ramp is included. The natural frequencies of this system in rad/s are 6.13, 7.14, 30.95, 68.52, 689.91 and 849.85. The natural frequencies for the corresponding undamped system with $U = 0m/s$ in rad/s are 5.70, 6.50, 28.01, 63.09, 555.53 and 778.69. Figure 5.8 shows the undamped dry modes of two-node and three-node longitudinal bending.

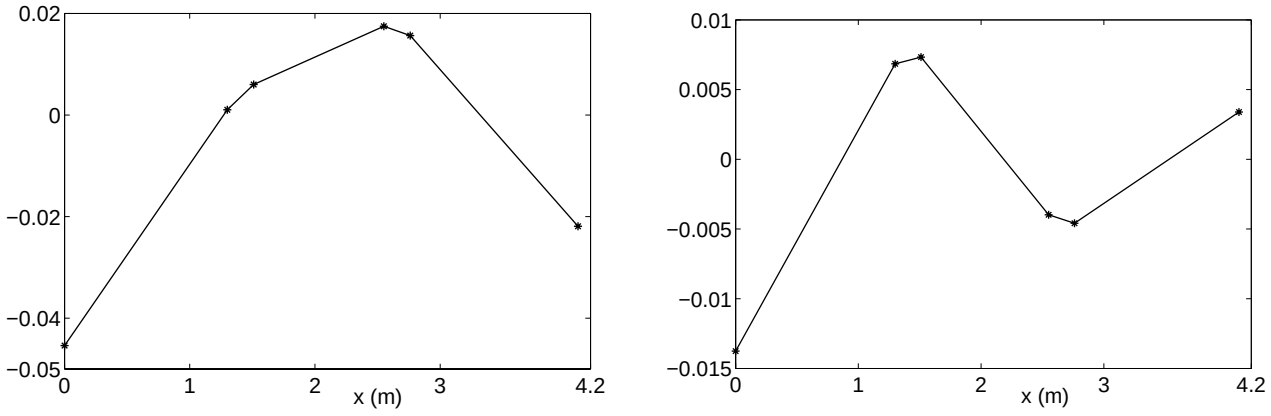

(a) Two-node longitudinal bending

(b) Three-node longitudinal bending

Figure 5.8 Flexible, undamped modes of catamaran model at zero forward speed; x-axis is the longitudinal distance from the bow.

The time history of vertical acceleration at the COG of Body2 by Direct method and Modal based method with the lowest four modes are shown in Figs. 5.9(a) and 5.10(a) respectively. Figure 5.9(b) presents spectral analysis of the time series in Fig. 5.9(a). Further, Fig. 5.10(b) shows the spectral analysis of the results in Fig. 5.10(a). The time domain from $8.556s$ to $15s$ is used for both cases in the Fast Fourier Transform (FFT) analysis. This corresponds to 6 wave encounter periods. We see that the Direct method gives large contributions from the highest two modes. In the experiments the time records have a sampling frequency of $100Hz$ for global force response and a sampling frequency of $1000Hz$ for slamming force. The experimental results for slamming force do not show the energy from these two highest modes. It means that they are highly structurally damped in reality.

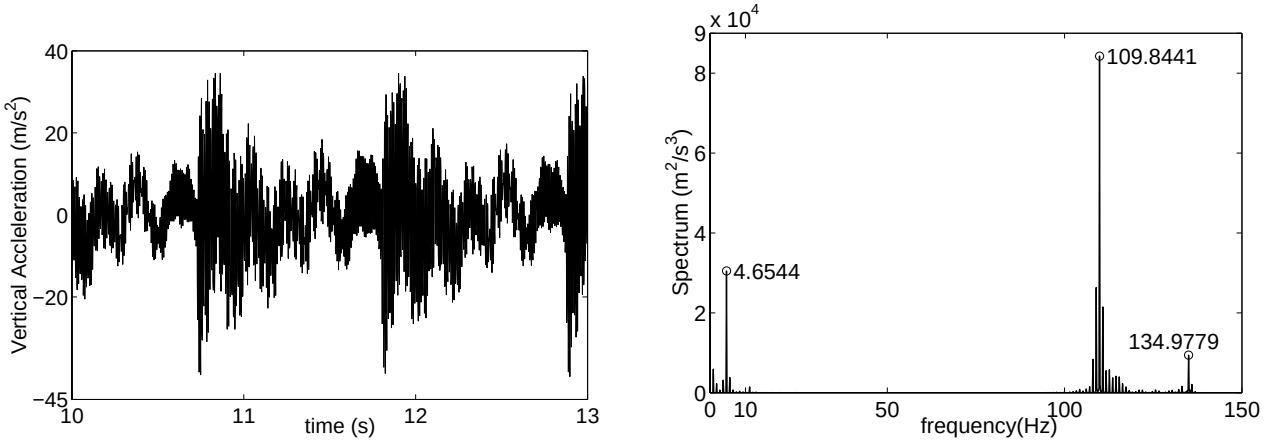

(a) $\ddot{\eta}_3$ (b) FFT analysis of Fig. 5.9(a)

Figure 5.9 Vertical acceleration $\ddot{\eta}_3$ at COG of Body2 by Direct method, $T = 1.8s$, $\zeta_a = 0.05m$, $U = 1.9m/s$, Head sea. In (b), numbers associated with the spectral peak values are the exact numbers for the corresponding frequencies.

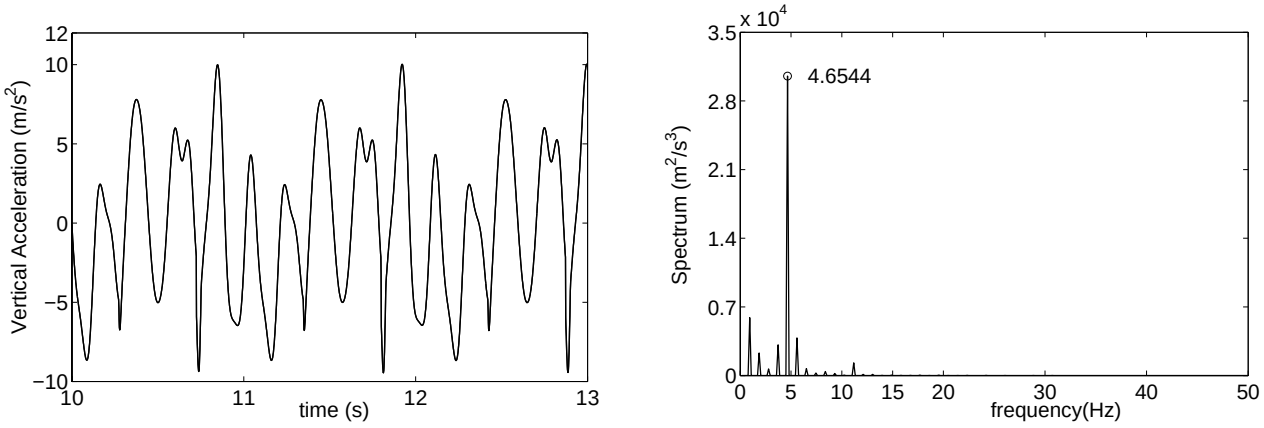

(a) $\ddot{\eta}_3$ (b) FFT analysis of Fig. 5.10(a)

Figure 5.10 Vertical acceleration $\ddot{\eta}_3$ at COG of Body2 by Modal based method; four lowest modes are included. $T = 1.8s$, $\zeta_a = 0.05m$, $U = 1.9m/s$, Head sea. In (b), numbers associated with the spectral peak values are the exact numbers for the corresponding frequencies.

Figure 5.11 shows that the spectral analysis of the time domain solution based on the Modal based method (Fig. 5.10(a)) gives nearly the same spectral distribution as shown in Fig. 5.9(b) for frequencies less than $15Hz$. After filtering out the spectral density for frequencies larger than $10Hz$ and performing an Inverse Fast Fourier Transform (IFFT), the two methods give practically the same time domain results (See Fig. 5.12).

The above analysis showed that the Modal based method can predict the same results as the Direct method but with less computer time. Further, the Modal based method is an efficient way to get rid of unphysical effects caused by higher modes. The following analysis will therefore

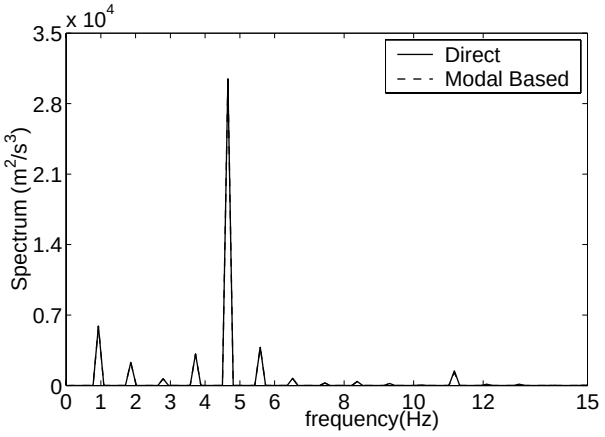

Figure 5.11 Comparison of energy distribution using Direct method and Modal based method for vertical accelerations at COG of Body2; Based on results in Figs. 5.9(b) and 5.10(b). Curves are overlapping.

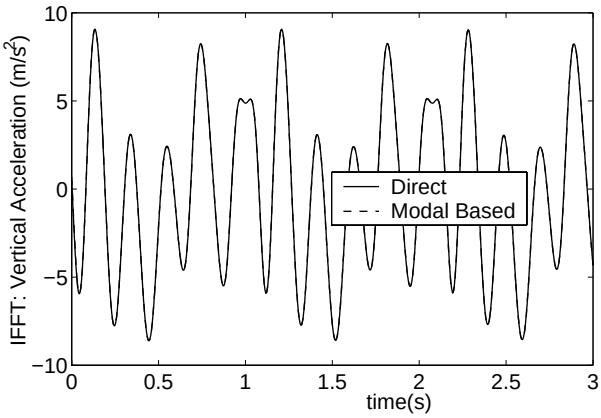

Figure 5.12 Vertical acceleration at COG of Body2. Comparison of Direct method and Modal based method by IFFT, frequencies $0 - 10Hz$ included. $T = 1.8s$, $\zeta_a = 0.05m$, $U = 1.9m/s$, Head sea. Curves are overlapping.

be based on the numerical results from the Modal based method. If the lowest four modes are used in the Modal based method for the previously studied cases, a time step $DT = 0.001s$ can be used in the Modal based method instead of $DT = 0.0001s$ in the Direct method. This will reduce the CPU time to 1/5 of what is required by the Direct method.

5.5 Global hydroelastic effects

To investigate how important the global hydroelasticity is when wetdeck slamming occurs and how much contributions come from the different modes, a case with head sea, wave period $T = 1.8s$, $U = 1.8m/s$ and $\zeta_a = 0.041m$ is studied. The bow ramp angle 3.72^0 of the wetdeck is accounted for in both the body boundary condition and in finding the deck-water intersection. The trim angle of the vessel is set equal to zero. The vertical shear forces and bending moments are calculated at the beam connecting positions at $1.48m$ and $2.68m$ from the bow, referred to as Cut1 and Cut2, respectively.

The notation 'noslam' in Figs. 5.13 to 5.16 means that slamming is not included. Furthermore, '$i$modes' implies that slamming is accounted for and that the lowest i modes are included. Figure 5.13 shows that the occurrence of slamming will have a small but noticeable influence on the motion response, while the number of modes has negligible influence on the motions. However, the influence of number of modes on velocity and acceleration is large, as shown in Fig. 5.14. The relative importance of slamming on motions and accelerations can be explained as follows.

Both the figures for global motion response (Fig. 5.14) and the figures for global force response (Figs. 5.15 and 5.16) show that a dominant effect is due to two-node bending. The vertical

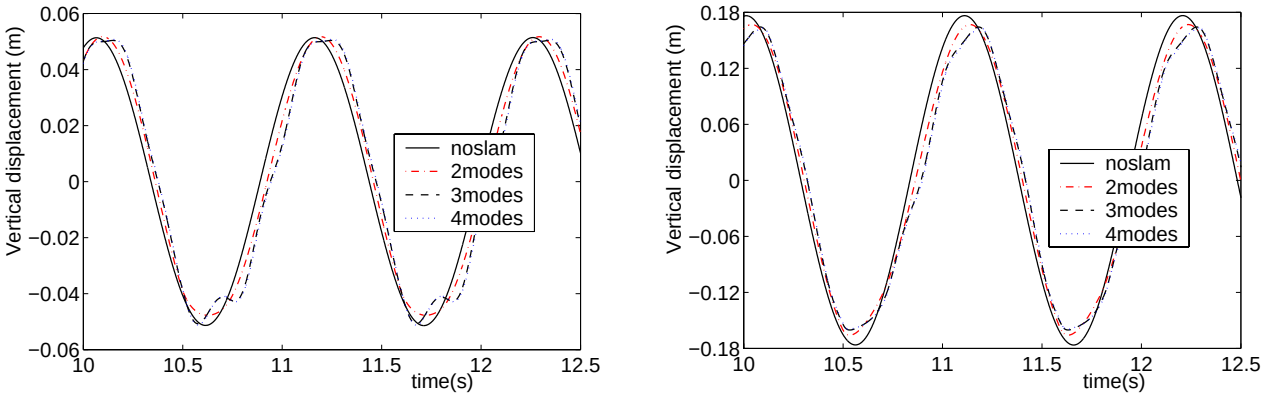

(a) η_3 at COG of Body2 (b) η_3 at bow of catamaran

Figure 5.13 Influence of slamming and number of modes on numerically predicted vertical motion (η_3); case 1114: Head sea, $U = 1.8m/s$, $T = 1.8s$, $\zeta_a = 0.041m$. '3modes' and '4modes' curves are almost overlapping.

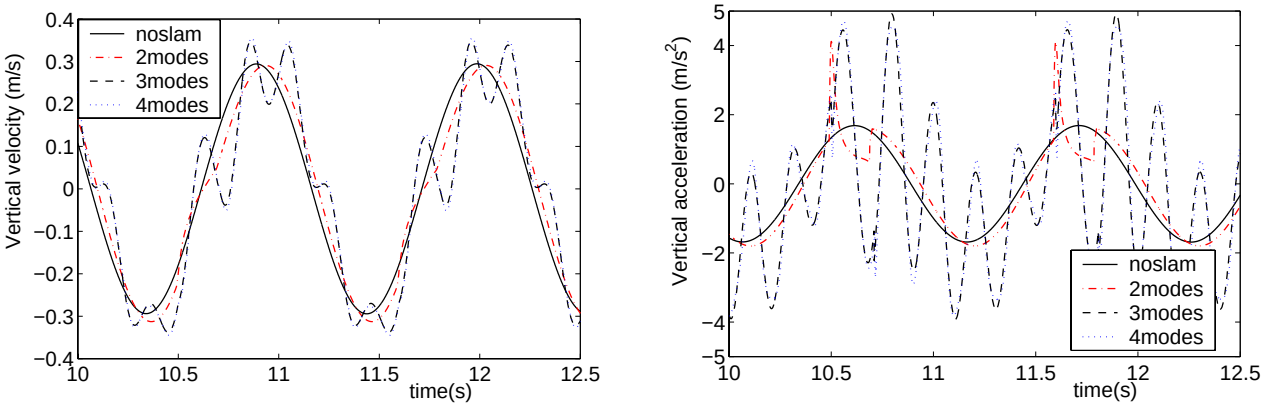

(a) $\dot{\eta_3}$ at COG of Body2 (b) $\ddot{\eta_3}$ at COG of Body2

Figure 5.14 Influence of slamming and number of modes on numerically predicted vertical velocity ($\dot{\eta_3}$) and acceleration at COG of Body2 ($\ddot{\eta_3}$); case 1114: Head sea, $U = 1.8m/s$, $T = 1.8s$, $\zeta_a = 0.041m$.

motion due to this mode can in the free vibration phase after the slamming loads be expressed as $A\psi(x)\cos(\omega_n t+\epsilon)$, where ψ is the mode shape, ω_n is the corresponding natural frequency and A is an amplitude which is assumed time independent due to negligible damping. The corresponding vertical accelerations can be expressed as $-\omega_n^2 A\psi(x)\cos(\omega_n t + \epsilon)$. Since ω_n is high, there is relatively speaking a larger influence on accelerations than on motions. We can see this by relating this to the vertical accelerations without accounting for impact. This amplitude can for a linear system in steady state conditions be expressed as $\omega_e^2 A_L$, where A_L is the corresponding motion amplitude. We then get the following ratio α between two-node and linear acceleration amplitudes

$$\alpha = \frac{\omega_n^2}{\omega_e^2}\frac{A_2}{A_L} \tag{5.13}$$

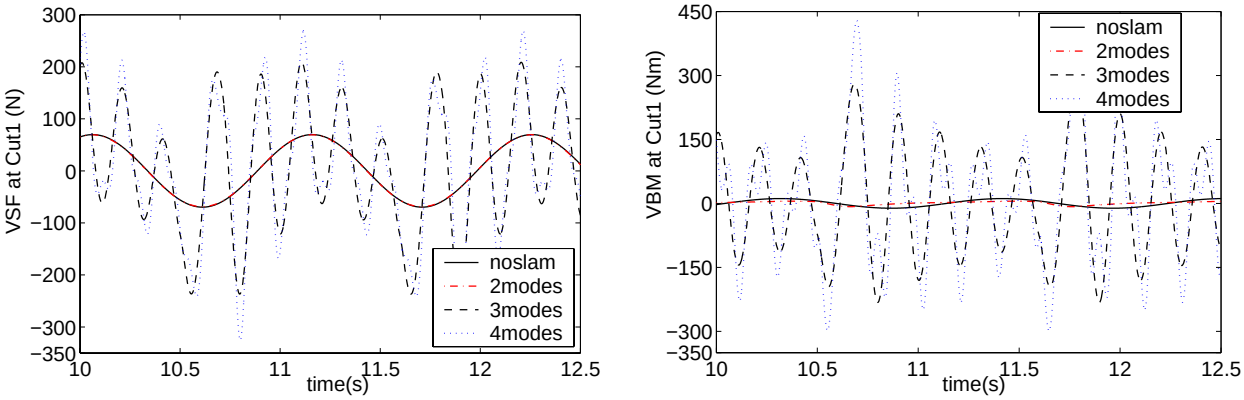

(a) VSF at Cut1 (b) VBM at Cut1

Figure 5.15 Influence of slamming and number of modes on numerically predicted vertical shear force (VSF) and vertical bending moment (VBM) at Cut1; case 1114: Head sea, $U = 1.8m/s$, $T = 1.8s$, $\zeta_a = 0.041m$. In (a), 'noslam' and '2modes' are almost overlapping.

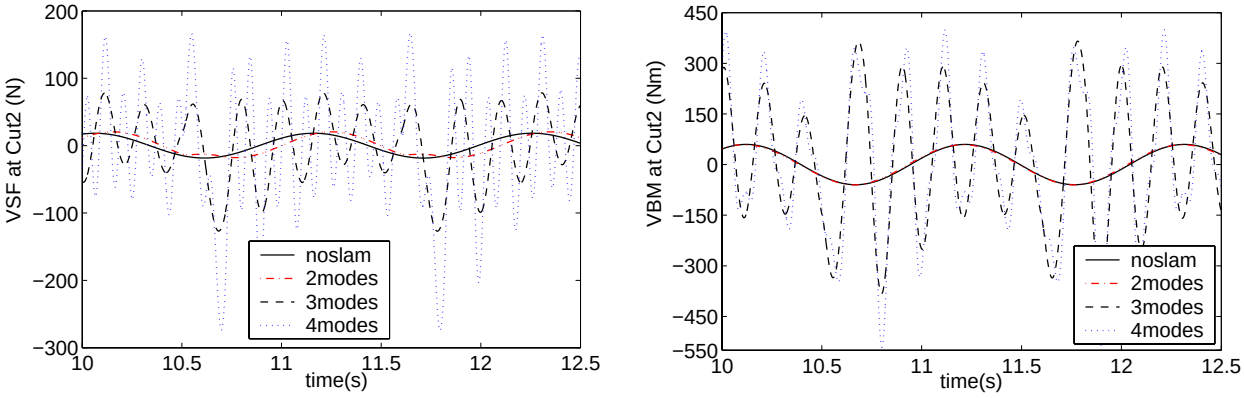

(a) VSF at Cut2 (b) VBM at Cut2

Figure 5.16 Influence of slamming and number of modes on numerically predicted vertical shear force (VSF) and vertical bending moment (VBM) at Cut2; case 1114: Head sea, $U = 1.8m/s$, $T = 1.8s$, $\zeta_a = 0.041m$. In (b), 'noslam' and '2modes' are almost overlapping.

Here A_2 means $A\psi(x)$ at the same x-value as A_L is evaluated. Since ω_n^2/ω_e^2 is very large, *i.e.* $30.92^2/5.73^2 = 29.12$ for this studied case, it demonstrates that two-node bending is relatively much more important for accelerations than for motions. If velocities are studied, then it is the ratio $\omega_n A_2/(\omega_e A_L)$ that is relevant. The ratio ω_n/ω_e is 5.40 for this studied case.

Plots in Fig. 5.15 show that the contribution from the different modes differ for vertical shear force (VSF) and vertical bending moment (VBM) at Cut1. When slamming is accounted for, VSF at Cut1 is dominated by two-node bending. The figure shows nearly no difference between the results with 'noslam' and '2modes'. This means small influence by slamming effects if only rigid body modes are considered. Further, there is a small contribution from three-node bending mode. However, VBM at Cut1 with slamming shows that rigid modes have a small influence,

two-node bending is dominant and three-node bending has a larger effect than VSF at Cut1. The results in Fig. 5.16 show that VSF at Cut1 and VBM at Cut2 share similar features of behaviour. The same is true for VSF at Cut2 and VBM at Cut1 except that two-node bending and three-node bending are equally important for VSF at Cut2. Generally speaking the three-node bending mode causes higher maximum and lower minimum values.

Ge *et al.* (2002a) showed calculations for the same vessel but where a flat wetdeck was used in finding the wetted length and a mean trim angle 0.85^0 of the vessel was considered. The wave conditions and the forward speed were the same as here. Similar tendencies and conclusions like here were found, but the exact relative contribution from each mode were not the same.

Since the response behavior depends on several factors like the flexibility properties of the ship and the time duration of slamming loads, the results in this section should not be generalized without further investigations.

5.6 Comparisons of numerical and experimental results with wetdeck slamming

Model tests were done by Økland and Aarsnes in the Ocean Basin at the Marine Technology Center in Trondheim in 1996. Regular incident waves were considered and the catamaran was self-propelled. An autopilot system with rudders on the two hulls was used to keep the heading. Global motions and loads were recorded. In the experiments, there are five cases with high wave amplitude as listed in Table A.5.

Table 5.3 presents general information about these five cases. Both the theoretical calculations and experimental results show that no slamming occurs for the short wave length case, *i.e.* case 1110. Cases 1114 and 1111 are slamming cases, in which the former is the most severe. For these two cases, theoretical predictions agree reasonably well with experimental records. For case 1112, the theoretical model predicts no slamming while experimental results show small slamming response with beating effects. For case 1115, both theory and experiments predicted slamming, but the theoretical results are much smaller.

Further, Table 5.4 presents maximum and minimum experimental values of vertical shear force and bending moments at Cut1 and Cut2 for the four cases where wetdeck slamming occurs. This is based on the time windows listed in Table A.7.

The relative vertical motions determine if wetdeck slamming happens, the time duration of the slamming and the time dependent wetted length. It matters where the water initially hits. The particular example presented in Fig. 1.1 shows that the longer the wave length is, the closer the initial impact is from the front end of the wetdeck. The wetdeck geometry plays a role in this context. If the wetdeck has a bow ramp and the tendency is that the water will hit at the front end of the wetdeck, a larger relative motion amplitude is needed for impact relative to a flat deck.

Table 5.3 Experimental high wave amplitude cases; 'Wave amplitude' refers to the mean recorded amplitude in the experiments at a fixed point in the middle of the tank.

Test case	1110	1111	1112	1114	1115
Speed (m/s)	1.90	1.84	1.86	1.80	2.00
Period (s)	1.3	1.5	1.8	1.8	2.0
Wave amplitude (m)	0.0475	0.0524	0.0259	0.0410	0.0483
Wave encounter period (s)	0.671	0.840	1.083	1.097	1.219
Exp. slamming	No	Moderate	Small	Most severe	Moderate
Num. slamming	No	Moderate	No	Most severe	Small

Table 5.4 Maximum and minimum values of experimental global loads for wetdeck slamming cases, based on the time windows listed in Table A.7. VSF: vertical shear force; VBM: vertical bending moment.

Case	VSF at Cut1 (N)	VBM at Cut1 (Nm)	VSF at Cut2 (N)	VBM at Cut2 (Nm)
1114	170/-260	280/-320	220/-190	250/-370
1111	170/-160	150/-150	110/-100	210/-190
1115	110/-160	150/-220	130/-60	170/-220
1112	60/-80	70/-90	60/-35	90/-90

Figure 5.17 shows numerically predicted time dependent wetted length $2c(t)$, as well as x-coordinates $a(t)$ and $b(t)$ corresponding to the front and aft intersection points between the free surface and the wetdeck. Cases 1111, 1114 and 1115 are presented. The initial impact occurs at the front end of the deck in the two longest wave length cases, *i.e.* for cases 1114 and 1115, while this is not so for case 1111. The impact duration and maximum wetted length are clearly largest for case 1114. This is consistent with the RAO of relative vertical motions at the bow presented in Fig. 5.5 and the wave amplitudes listed in Table 5.3.

Using only Fig. 5.5 and Table 5.3 suggests that the impact duration should be clearly larger for case 1115 than for case 1111. However, these two impact cases last nearly the same time in the numerical calculations. Further, case 1111 has clearly larger maximum wetted length than case 1115. A reason is that the water initially hits at the front end of the wetdeck in case 1115, while it initially hits at the junction between Deck1 and Deck2 in case 1111 (Deck1 and Deck2 are described in connection with Fig. 2.1 and Appendix A.3). This requires a higher relative vertical motion for case 1115 than for case 1111. The wetted area is in case 1111 nearly equally divided between Deck1 and Deck2. It is always within Deck1 in case 1115 while it is mainly within Deck1 in case 1114. The wetted area in case 1114 contains a small part of Deck2 from time $t = 11.7342s$ to $11.7833s$.

Both the relative vertical impact velocity and acceleration are important parameters for the magnitude of the slamming loads. Figure. 5.18(a) and Fig. 5.18(b) present the time history of

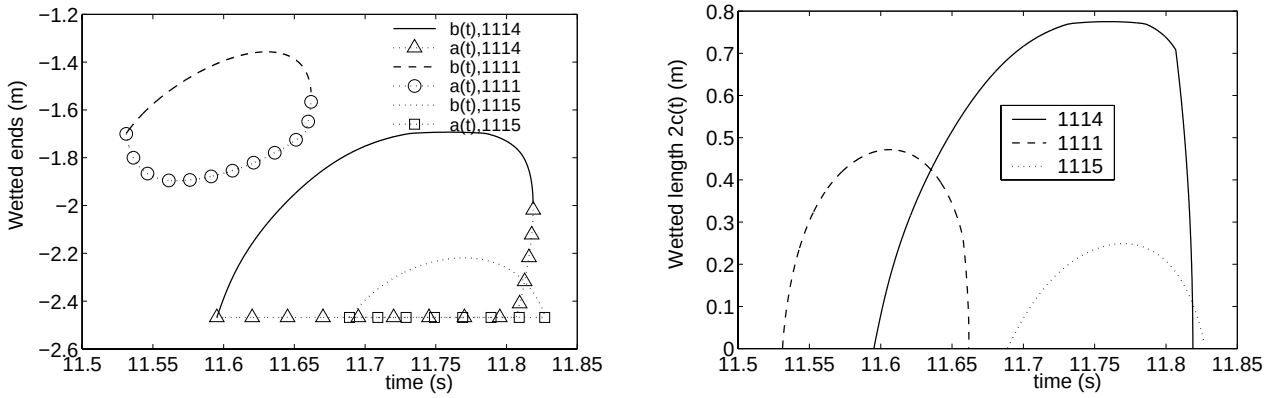

(a) Deck-water intersection coordinates (b) Wetted length

Figure 5.17 Calculated wetted length $2c(t)$ and x-coordinates $a(t)$ and $b(t)$ of intersection points between free surface and wetdeck for cases 1111, 1114 and 1115.

the relative impact velocity and acceleration for cases 1111, 1114 and 1115. We note that the maximum relative impact acceleration is nearly $2g$ for case 1114.

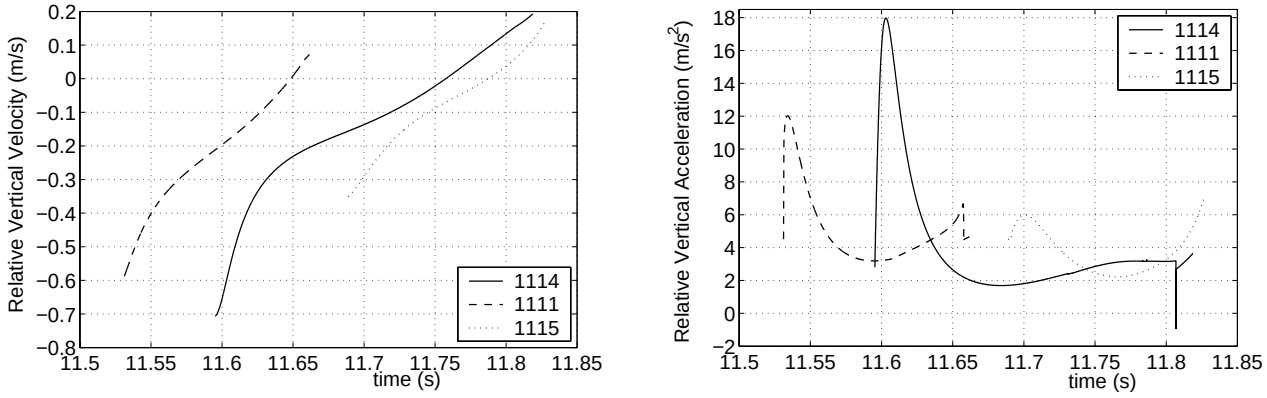

(a) Relative impact velocity (b) Relative impact acceleration

Figure 5.18 Calculated relative impact velocity and acceleration at the midpoint of the wetted length for cases 1111, 1114 and 1115.

The relative impact velocity V_R is clearly smallest for case 1115. This is partly associated with the fact that case 1115 has the largest wave length which means the smallest wave frequency and frequency of encounter. How this influences V_R can be seen from re-expressing the relative impact velocity given by Eq. (3.10) as

$$V_R = \omega_e \zeta_{Ra} \cos(\omega_e t + \alpha_R) + (\omega_e - \omega_0)\zeta_a \cos(\omega_e t + \alpha) - U(\eta_5 + \tau) \tag{5.14}$$

Here ζ_{Ra} and α_R are respectively amplitude and phase of relative vertical motion at the impact position. The second term contains the phasing α of the incident wave at the impact position. The factor $(\omega_e - \omega_0)$ can be expressed as $U\omega_0^2/g$ for head sea. If the impact is not too severe,

$\cos(\omega_e t + \alpha_R)$ should be close to zero at impact. The reasons are that relative vertical motions should be as large as possible and that velocity is 90 degrees out of phase with motion. We see that both the magnitude of the first and second term in Eq. (5.14) is increasing with frequency. The third term contains the pitch angle η_5. Figure 5.19 shows the pitch response for the forward ship segment. By referring to Fig. 5.19(a) we can see that the pitch angles at the initial impact time for cases 1111, 1114 are 1115 are respectively -0.0323, -0.0552 and -0.0605 in unit of radians. Further, considering the bow ramp angle $3.72^0 = 0.065rad$ and noting that the trim angle of the vessel is zero, the third term is relatively small, especially for case 1115. The relative impact acceleration is also clearly smallest for case 1115. This can be explained in a similar way as was done for the relative impact velocity.

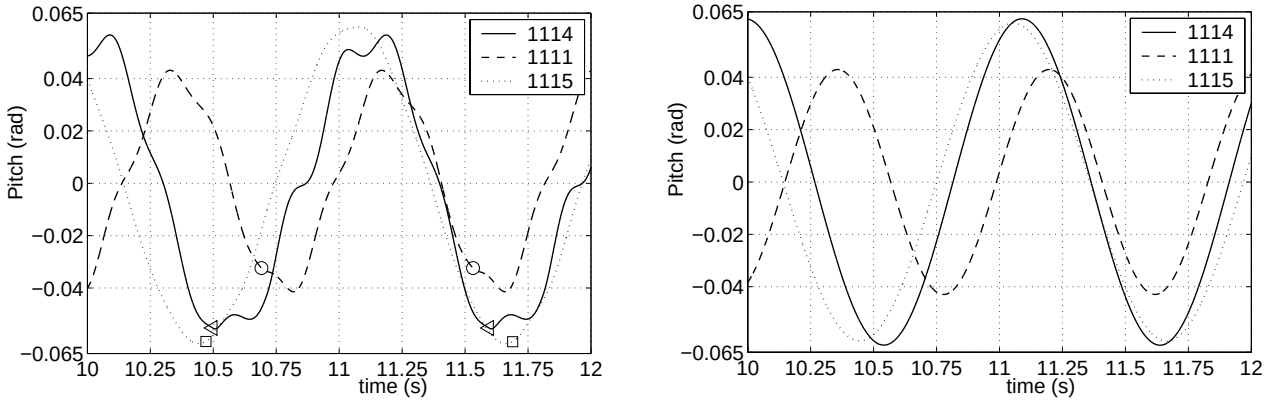

(a) Pitch response η_5 due to both wetdeck slamming and linear wave loads

(b) Linear response of η_5

Figure 5.19 Calculated pitch response η_5 of the forward segment of the three-body model for cases 1111, 1114 and 1115. In (a), triangles, circles and squares represent the initial impact moments for cases 1111, 1114 and 1115, respectively.

The following Figs. 5.20(a) to 5.20(c) show the time history of the impact loads, as well as the wetted length $2c(t)$ and the x-coordinates $a(t)$ and $b(t)$ of the intersection points between the free surface and the wetdeck. If Deck2 is wetted, an approximation is made in the body boundary condition on Deck2 by using the same local trim angle as for Deck1. The impact force starts in all three cases with zero. This is for cases 1114 and 1115 associated with that the water initially hits at the front end of the wetdeck and there is initially an angle between the free surface and wetdeck. This was earlier explained in Sections 1.2 and 4.5. The water hits initially at the junction between Deck1 and Deck2 in case 1111. Since there is an angle 3.72^0 between Deck1 and Deck2, the initial impact is similar as the water entry of a wedge. This means initially zero force. If the water had neither initially impacted at the junction between Deck1 and Deck2 nor at the front end of the wetdeck, the initial theoretical impact force would be a large finite value according to 2D theory. However, 3D effects occur in the initial phase of the impact. This is for instance due to local run-up at the side hulls. The three-dimensionality causes initially zero impact force (See also discussions in Section 1.2 and Section 4.5, as well as the example connected with Fig. 6.24).

There are three spikes in Fig. 5.20(a) occurring in the time history of impact loads for case

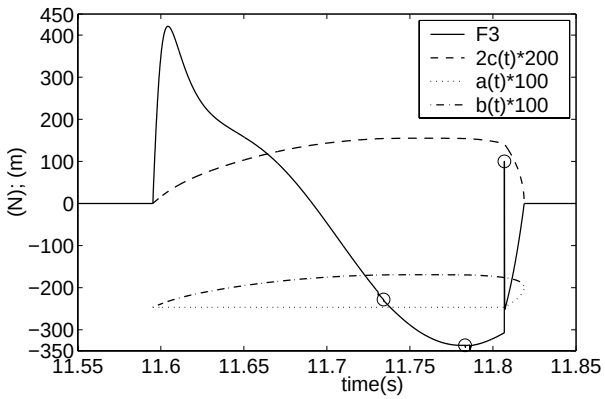

(a) Case 1114

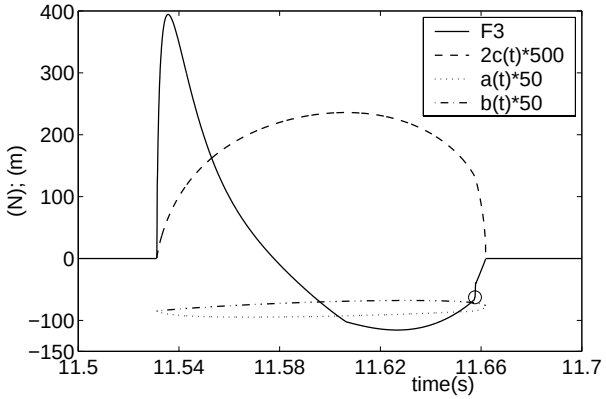

(b) Case 1111

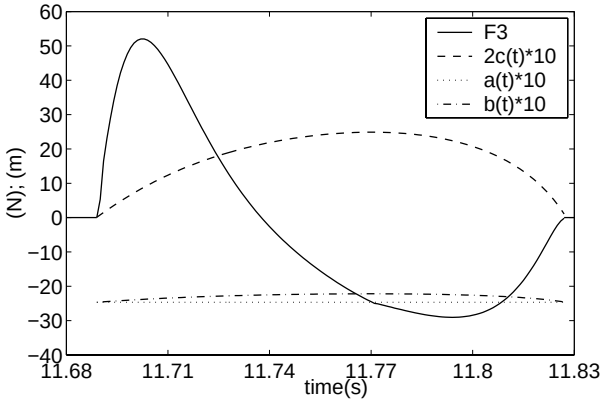

(c) Case 1115

Figure 5.20 Calculated impact force F_3, wetted length $2c(t)$, and wetted end x-coordinates $a(t)$ and $b(t)$ for cases 1114, 1111 and 1115. The circles $\circ$ in the impact force indicate spikes in case 1114 and discontinuity in case 1111.

1114. However, they are numerical errors. The first two are quite small and can not be shown in Fig. 5.20(a). They occur respectively when the wetted area starts and finishes to include a small part of Deck2. The large spike corresponds to when the forward deck-water intersection point starts moving from the front end of the wetdeck in the stern direction. The impact force in case 1111 is discontinuous at time $t = 11.6576s$. This corresponds to the time instant when the forward deck-water intersection point passes the junction between Deck1 and Deck2 during the water exit phase. The spikes in case 1114 and discontinuity in case 1111 have no noticeable influence on the wetdeck slamming induced global loads.

The slamming induced global response of the different modes depends on the duration of the loads relative to the natural period of the mode (*e.g.* Clough and Penzien (1993)). The ratios between slamming duration T_d and natural periods T_N for heave, pitch, two-node and three-node bending are for cases 1111, 1114 presented in Table 5.5.

For long-duration loadings, *i.e.* $T_d/T_N >\sim 1$, the dynamic magnification factor relative to static

Table 5.5 Ratios between slamming duration T_d and natural periods T_N for heave, pitch, two-node and three-node bending. $T_d = 0.1305s$, $0.2236s$ and $0.137s$ respectively for cases 1111, 1114 and 1115; based on calculated data.

	T_d/T_N [–]			
Case	heave & pitch	pitch & heave	two-node bending	three-node bending
1111	0.126	0.149	0.628	1.421
1114	0.218	0.253	1.100	2.435
1115	0.142	0.156	0.679	1.466

response depends according to Clough and Penzien (1993) strongly on the rate of increase of the load to its maximum value. This means by using the information in Table 5.5 that the initial impact phase matters in particular for three-node bending response for case 1114. This may be influenced by 3D flow effects for instance due to local run-up at the side hulls. It also turned out that the experimental results to be reported later contained influence of unwanted roll motions. This was due to non-head sea conditions caused by an unintended asymmetry of the structural mass distribution about the center plane of the vessel. The auto-pilot system used to keep the heading of the vessel will also contribute to rolling. The roll angle implies that the water does not simultaneously impact along the transverse cross-section of the wetdeck. This causes 3D flow effects.

For short-duration loads, *i.e.* $T_d/T_N <\sim 1/4$, the maximum response depends mainly on the force impulse. This is the case for heave and pitch response.

The typical impact load behaviour for all cases is a positive force during most of the water entry phase and a negative force during most of the exit phase. Since the absolute value of the minimum force and maximum force are of similar magnitude and the durations of the water exit and entry phase are of the same order, the contributions to the force impulse from the water entry and exit phase are strongly counteractive. Actually if the total impact load were expressed as $d(A_{33}V_R)/dt$, then the force impulse would be zero for the total impact. Since we include nonlinear Froude-Krylov and hydrostatic restoring loads on the wetdeck and the slamming term $V_R dA_{33}/dt$ is neglected during the water exit phase, the total force impulse will be non-zero. It will in the presented examples be evident that generally speaking the two-node bending mode response is the most important mode for global loads due to wetdeck slamming. Table 5.5 shows that two-node bending for cases 1111 and 1115 is neither a short-duration nor a long-duration load case.

The following text presents detailed comparisons between experimental and theoretical global wetdeck slamming induced loads. The trim angle of the vessel is set equal to zero in all the numerical calculations.

5.6.1 Case 1114

This is the most severe wetdeck slamming case in the experiments. Figures 5.21 to 5.24 show comparisons between experimentally and numerically predicted vertical shear force (VSF) and vertical bending moment (VBM) at Cut1 and Cut2. The case is numbered as $No.1114$ with head sea, incident wave period $T = 1.8s$, incident wave amplitude $\zeta_a = 0.041m$ and forward speed $U = 1.8m/s$. The wetdeck bow ramp angle 3.72^0 is included in finding the water-deck intersection and in the body boundary condition. The nonlinear Froude-Krylov and hydrostatic restoring forces on the wetdeck are included with maximum value around 1/10 of the maximum of total impact force. Only the results in steady state conditions are compared. Since the transient phase of the experiments is not clear, numerical results are time shifted to match the phase of experimental data. The experimental loads at the two cuts are the sum of the values from starboard and port side.

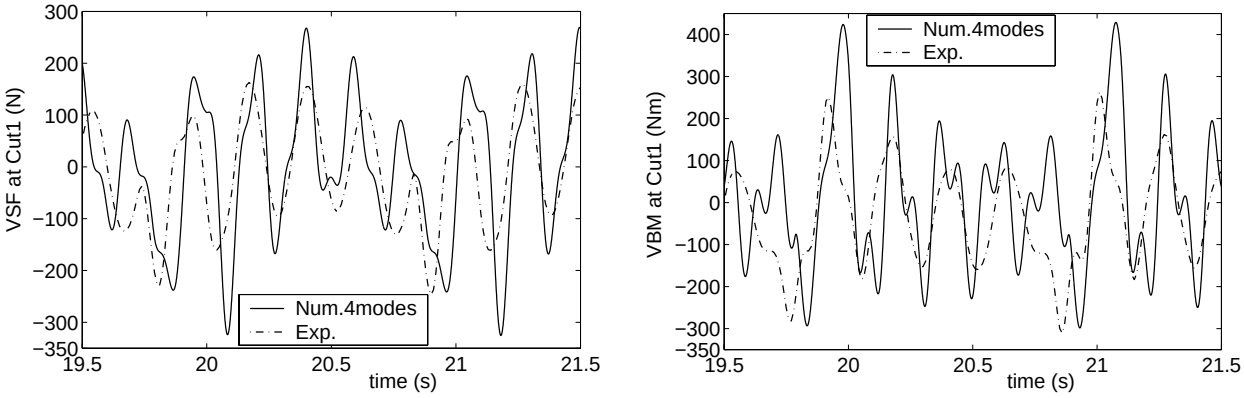

(a) VSF at Cut1

(b) VBM at Cut1

Figure 5.21 Theoretical and experimental predictions of vertical shear force (VSF) and vertical bending moment (VBM) at Cut1 for case 1114 with $U = 1.8m/s$, $T = 1.8s$ and $\zeta_a = 0.041m$. Four lowest modes are included in numerical results.

Generally speaking Figs. 5.21 to 5.22 show similar experimental and theoretical behaviour. However, the theoretical peak values are clearly larger than the experimental ones and numerical results of VSF at Cut2 show quite larger three-node bending contribution than the experimental results. Figures 5.23 to 5.24 are the comparisons when only accounting for the lowest three modes, *i.e.* accounting for the two-node bending but not the three-node bending mode. We note that the two-node bending mode is dominating in the experimental results. The three-node bending mode is much more damped in reality than in the theoretical model. Numerical simulations have also been done for the studied cases by adding structural damping for the three-node mode. However, there is not quantitative improvement by comparing with experimental results. So in later discussions the effect from the two-node bending mode will be focused on.

Figures 5.23 to 5.24 demonstrate a generally good agreement. However, there are some clear differences between theory and experiments. For instance this occurs for VBM at Cut1 and VSF at Cut2 around $t = 19.7s$ and $20.75s$ where theoretical and experimental results are out of phase.

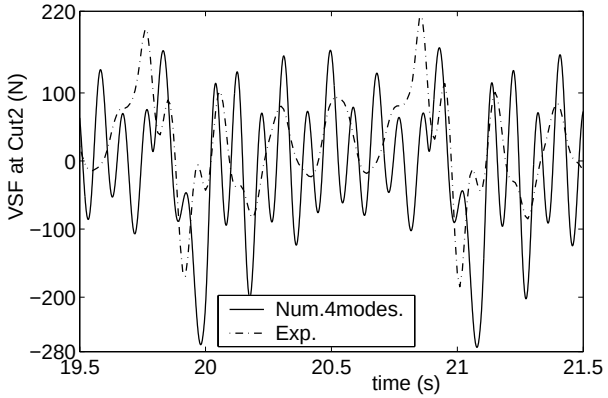

(a) VSF at Cut2

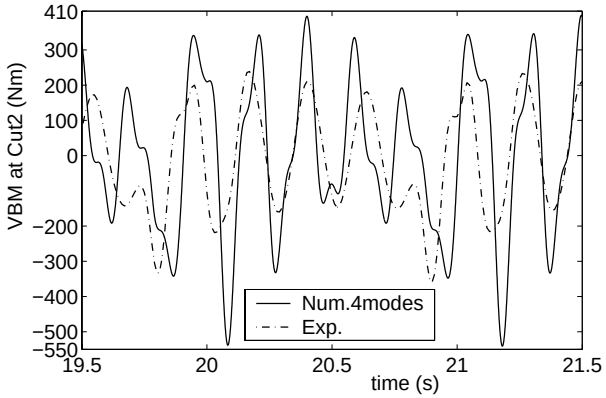

(b) VBM at Cut2

Figure 5.22 Theoretical and experimental predictions of vertical shear force (VSF) and vertical bending moment (VBM) at Cut2 for case 1114 with $U = 1.8m/s$, $T = 1.8s$ and $\zeta_a = 0.041m$. Four lowest modes are included in numerical results.

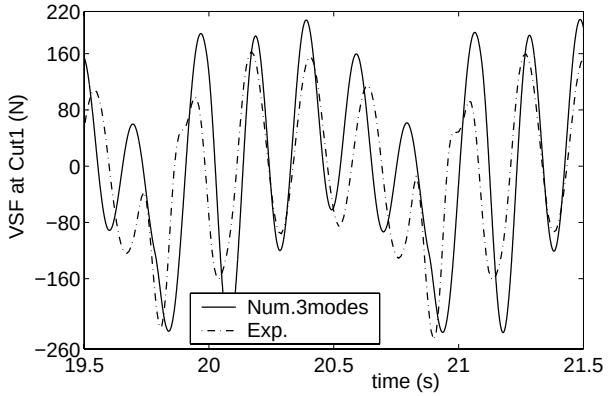

(a) VSF at Cut1

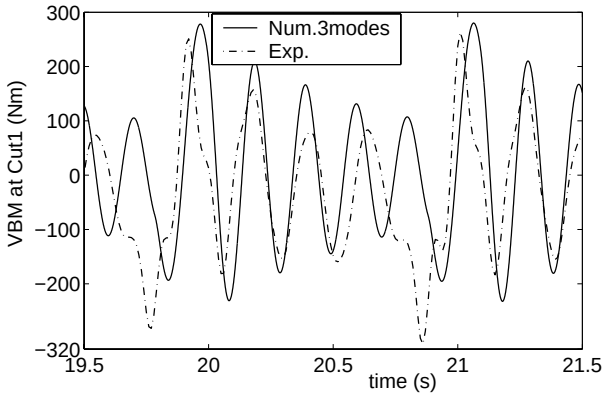

(b) VBM at Cut1

Figure 5.23 Theoretical and experimental predictions of vertical shear force (VSF) and vertical bending moment (VBM) at Cut1 for case 1114 with $U = 1.8m/s$, $T = 1.8s$ and $\zeta_a = 0.041m$. Three lowest modes included in numerical results.

If we study similar results with three-node bending included, we note that three-node bending has some influence on this behaviour. Some of the phase difference is also due to differences in the theoretical and experimental natural periods for two-node bending. This was earlier discussed in connection with the zero forward speed case presented in Table 5.2. An error source is that the encounter wave frequency is used to calculate the added mass associated with two-node bending. Similar estimates can be made as in Section 5.3.1 by using Eq. (5.4). The added mass in heave for $T = 1.8s$ and $U = 1.8m/s$ is $95.6kg$. It is noted here that the added mass in heave for cases with low oscillation frequency are dependent on the forward speed, while the high frequency asymptotic value is speed independent. So Fig. 5.1 still applies in this respect and gives the high frequency asymptotic added mass value as $170kg$. Accounting for $M = 246kg$ gives $\alpha = 0.906$. This means that the natural period for two-node bending will be 1.103 times the

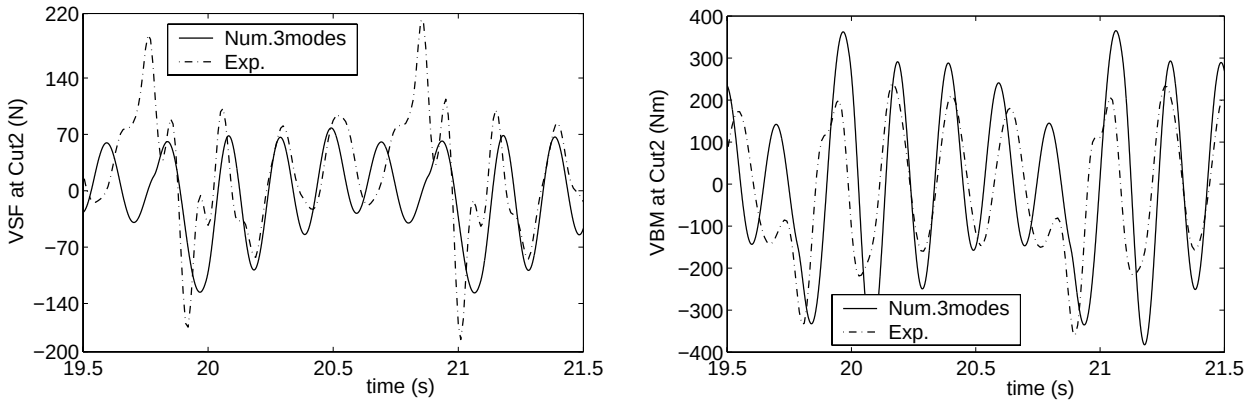

(a) VSF at Cut2 (b) VBM at Cut2

Figure 5.24 Theoretical and experimental predictions of vertical shear force (VSF) and vertical bending moment (VBM) at Cut2 for case 1114 with $U = 1.8m/s$, $T = 1.8s$ and $\zeta_a = 0.041m$. Three lowest modes included in numerical results.

numerically predicted value. By referring to Fig. 5.23(a), we see that results in the time domain $t = 20.0s$ to $20.8s$ covers four periods of 2node bending oscillation. The time durations for four exact periods are $0.62s$ and $0.72s$ respectively for theoretical and experimental results. Using the α-ratio improves the agreement. However, one should note that no coupling effects between modes are considered in this estimation, and that the oscillation periods of two-node bending in the experiments are not exactly the same from period to period due to wetdeck slamming. Since the maximum load is the most important, the small difference in the natural frequency is secondary.

Error sources both in experiments and theory will be discussed in Chapters 6 and 7. An error estimate of the experiments will be made. It shows that the most important error sources are trim angle, the changing incident wave amplitude along the track of the model, wave measurement inaccuracies as well as the asymmetric mass distribution about the center plane of the catamaran. One should also remember that Figs. 5.6 and 5.7 have shown that even for no slamming cases there are discrepancies between experimental and theoretical results for global load response. Figures 5.6 and 5.7 can be used as a reference even if the calculated values are based on a forward speed of $1.9m/s$. The figures show that for $T = 1.8s$, except for the vertical shear force at Cut1, that the relative differences between the experimentally and theoretically predicted values are not small. Considering the incident wave amplitude $0.041m$, it means that the deviation of vertical shear force at Cut2 is around $20N$, and the deviations of vertical bending moment at both the two cuts are about $30Nm$. However, these values are not so large compared with the contribution from the two-node bending.

As illustrated in Fig. 2.1, the wetdeck consists of four sections. They are notated as Deck1 to Deck4 from the bow to the stern. Slamming loads on the front deck, *i.e.* Deck1, will be studied theoretically and experimentally. There are four pin transducers for that deck. The positions and numbering of the transducers are illustrated in Appendix A.5. Adding the recordings from these four pin transducers should give the sum of the slamming force and the structural inertia

force of Deck1. However, it was detected that the force sign from Pin transducer $s5887$ should be changed. When slamming occurred, the theoretical model predicted slamming mainly within the surface area of Deck1. In order to compare with the experimental results theoretical structural inertia loads of Deck1 were added to the theoretical slamming loads. Details of the geometry of Deck1 are described in Appendix A.3. The mass of Deck1 is $9.1kg$ and the longitudinal center of the gravity of the deck is $0.34m$ from the front end of the deck.

Figure 5.25 presents the comparisons between the experimental and numerical slamming force with structural inertia force included. The lowest three modes are accounted for in the numerical results, *i.e.* three-node bending is excluded. In order to match the experimental slamming force peaks in Fig. 5.25, theoretical results in Fig. 5.25 are time shifted $0.07s$ to the left compared with the numerical global responses presented in Figs. 5.23 and 5.24. This illustrates uncertainties associated with the phasing of the impact relative to the ship motions as well as the physical description of the initial slamming phase. The numerically predicted start and end times of slamming are represented by circles ($\circ$) and triangles ($\triangleleft$) in Fig. 5.25. The first two impacts have in sequence the starting and ending instants at $t = 19.7103s$, $19.9339s$, $20.8079s$ and $21.0315s$.

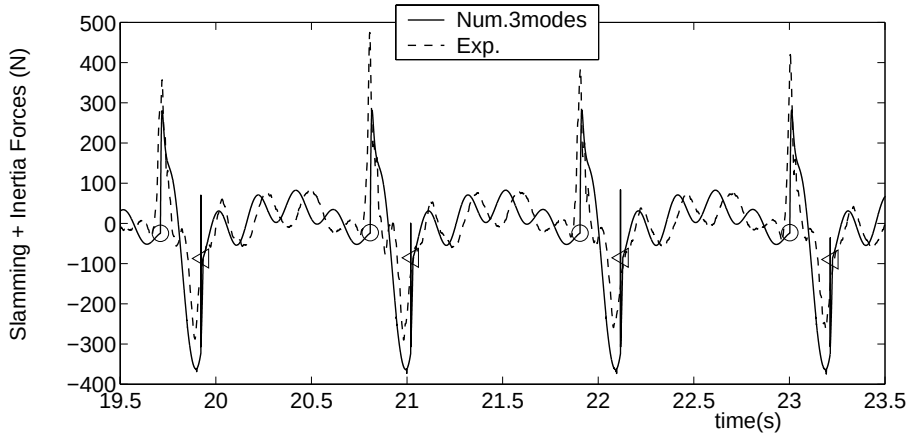

Figure 5.25 Theoretical and experimental predictions of slamming force on Deck1 for case 1114; structural inertia force of Deck1 included. Theoretical results are $0.07s$ shifted left compared with results in Figs. 5.23 and 5.24. The three lowest modes are included. The circles ($\circ$) and triangles ($\triangleleft$) represent the calculated initial and ending time instants of wetdeck slamming.

The theoretical slamming loads in Fig. 5.25, as well the results in Fig. 5.20(a), show the impact loading on the whole deck. It should be noted that the structural inertia force is included in Fig. 5.25 while not in Fig. 5.20(a). Previous discussions have mentioned that the wetted area includes Deck2 during a relatively short time period. The added mass term is then dominating. A correction can then be made by correcting the added mass term in the slamming loads. This is done in a simplified way by assuming the pressure loading is proportional to $\sqrt{c^2 - X^2}$. Here $X = 0$ corresponds to the midpoint of the wetted length and $2c(t)$ is the wetted length. One should note that X refers to a time-dependent coordinate system moving with the longitudinal

time varying velocity of the midpoint of the wetted length. This load distribution is exact according to our model if the relative impact velocity is spatially constant over the wetted length and only the added mass term is present. The total predicted slamming load on the wetdeck when slamming occurs on Deck2 is then multiplied with

$$\alpha = \frac{\int_{-c}^{d} \sqrt{c^2 - X^2} dX}{\int_{-c}^{c} \sqrt{c^2 - X^2} dX} \tag{5.15}$$

Here d is the X-coordinate of the aft end of Deck1. The minimum value of α is 0.9991, which occurs when $d = 0.3825m$ and $0.3875m$. This shows that the correctional effect is very small. When the wetted area includes the aft end of Deck1, it is possible that the flow will separate from Deck1. This is due to the different surface angles of Deck1 and Deck2 as seen from the data in Appendix A.3 or Fig. 6.20. This would require a Kutta condition model with fixed separation point. However, this has not been further pursued, but will have a minor effect in this case.

The force record in Fig. 5.25 between an end and subsequent start of an impact illustrates the non-dominant contribution of the structural inertia force. The time record of the structural inertia force during the time period without slamming shows main contributions from wave frequency and two-node bending induced vertical accelerations. The amplitudes of these acceleration components are well theoretically predicted. However, there is a natural period difference of two-node bending between experiments and theory in Fig. 5.25. This is as earlier discussed due to use of a frequency domain model where added mass is calculated at the wave encounter frequency (See discussion associated with Table 5.2 and Eq. (5.4)).

Figure 5.25 shows reasonable agreement for maximum slamming force and the duration of the impact. The characteristic behaviour that the impact loads are mainly positive during the water entry phase and negative during the water exit phase, is shown both in theory and experiments. The experimental minimum force value is about 75% of the theoretical minimum value in the time period presented in Fig. 5.25. These experiments show some influence of three-node bending during the impact phase but this is not present in the structural inertia force after the impact. However, theoretically predicted results do not show better agreement with experiments when three-node bending is included. The maximum slamming force changes clearly from one impact to the next impact. This initial peak value may be influenced by a small dynamic roll angle with non-zero mean value which was present during the experiments. The mean value was due to an unintended asymmetry in the mass distribution about the center plane of the catamaran. Except for this difference in slamming peak, the time history of the slamming force has similarities for different impacts. It appears from the resulting experimental global loads presented in Figs. 5.23 and 5.24, that the variations in peak value of the slamming force have a minor influence on the global loads. This is associated with the small changes in force impulse due to the variations in peak values.

Figures 5.26(a) to 5.26(b) show the different theoretical contributions to the vertical motion and acceleration at the bow for case 1114. In the figure, the circles and triangles correspond to the initial and ending time instants of wetdeck slamming. For this specific case, by investigating the first slamming in the figure, we can see that slamming starts at $t = 10.4979s$ and the slamming

induced response contributes 7.2% to the vertical motion. The acceleration is changed from $5.40m/s^2$ to $2.45m/s^2$ due to the slamming induced contribution of $-2.95m/s^2$. When the acceleration peak occurs at $t = 10.5062s$, the slamming induced response contributes respectively 6.8% and 70.5% to the vertical motion and acceleration. The minimum value of motion response was changed 9.0% from the linear response during the impact period.

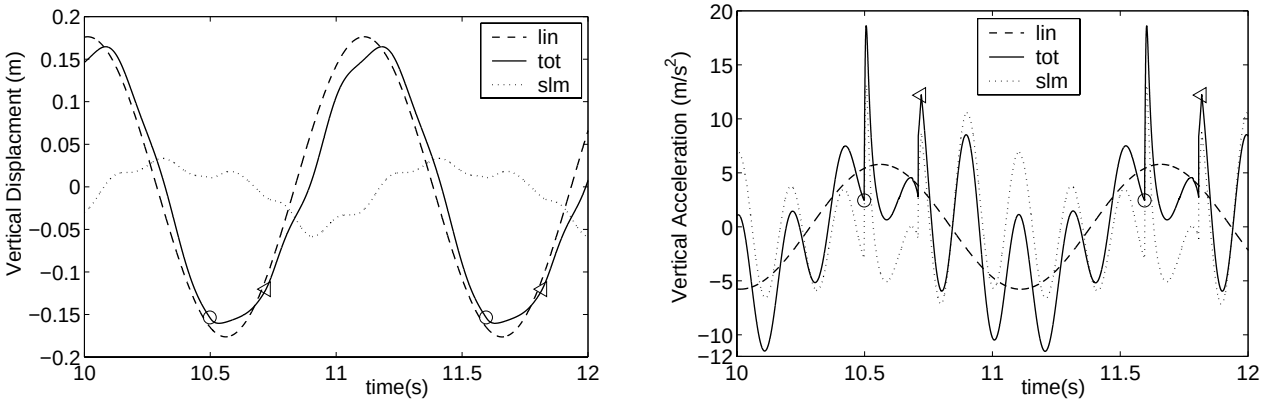

(a) η_3 at the bow

(b) $\ddot{\eta_3}$ at the bow

Figure 5.26 Theoretical predictions of vertical motion (η_3) and acceleration ($\ddot{\eta_3}$) at the bow of the catamaran; case 1114 with $U = 1.8m/s$, $T = 1.8s$ and $\zeta_a = 0.041m$, head sea. Three lowest modes included in numerical results. The circles ($\circ$) and triangles ($\triangleleft$) represent the calculated initial and ending moment of wetdeck slamming; 'lin' and 'slm' represent the response from linear wave frequency effects and slamming loads respectively, and 'tot' is the total response.

5.6.2 Case 1111

The following presentation shows another comparison between experimental and theoretical predictions of VSF and VBM when wetdeck slamming occurs. The conditions are head sea, $T = 1.5s$, $U = 1.84m/s$ and $\zeta_a = 0.0524m$, and is referred to as case 1111. The trim angle of the vessel is set equal to zero and the bow ramp angle is 3.72^0 in the calculations. Like in case 1114, the experimental loads at the two cuts are the sum of the values from starboard and port side. Further, only the steady state results are compared.

Figures 5.27 and 5.28 show the numerical predictions of global loads when considering either the lowest three or lowest four modes. Including four modes increases the peak values of the high vibratory response, but the three-node bending mode does not contribute as much as in case 1114. The experimental results show also some presence of the three-node bending mode. However, we do not achieve quantitative agreement of the three-node bending behavior. The experimental data show less contribution from three-node bending compared with numerical results, *i.e.* three-node bending mode is much more damped in reality than in our numerical model. It implies that the high-frequency oscillations are associated with the two-node bending mode of the hull.

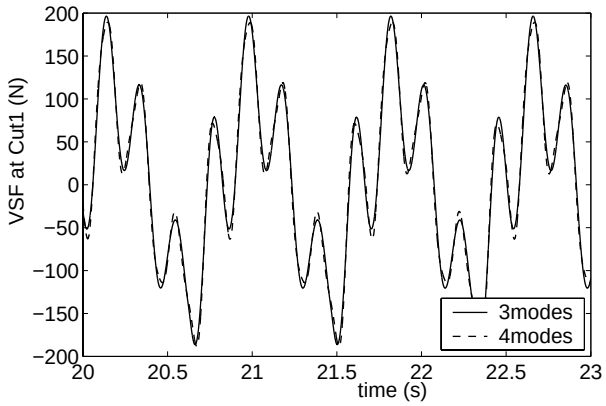

(a) VSF at Cut1

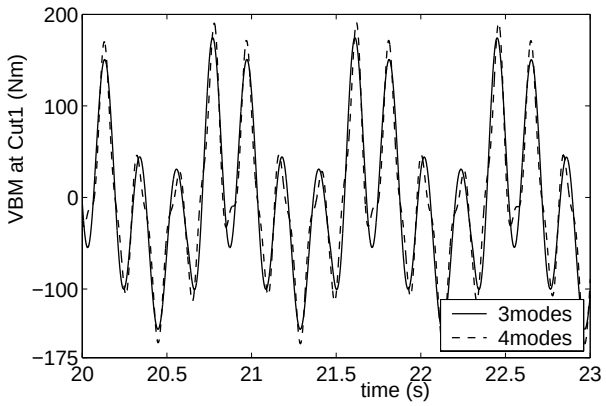

(b) VBM at Cut1

Figure 5.27 Theoretical predictions of vertical shear force (VSF) and vertical bending moment (VBM) at Cut1 for case 1111 with head sea, $U = 1.84m/s$, $T = 1.5s$ and $\zeta_a = 0.0524m$. '4modes': three-node bending mode included; '3modes': three-node bending mode not included.

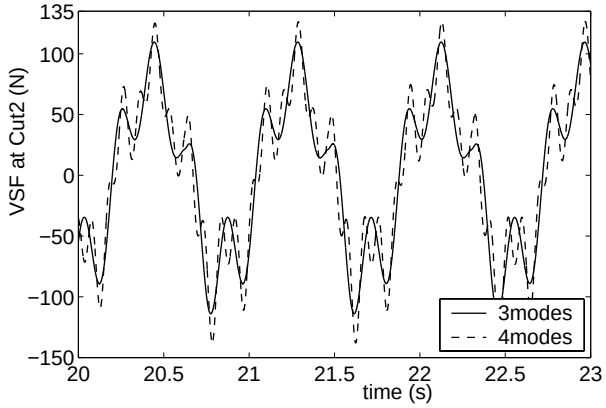

(a) VSF at Cut2

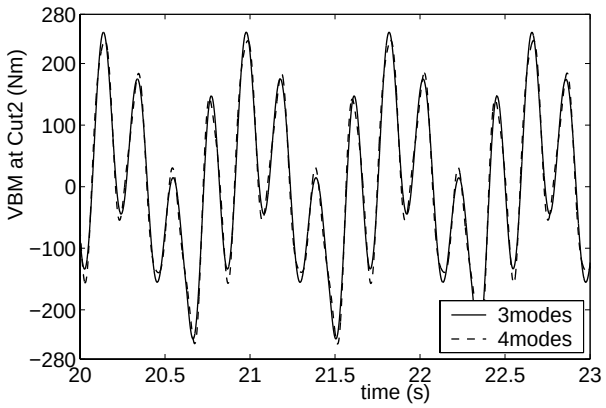

(b) VBM at Cut2

Figure 5.28 Theoretical predictions of vertical shear force (VSF) and vertical bending moment (VBM) at Cut2 for case 1111 with head sea, $U = 1.84m/s$, $T = 1.5s$ and $\zeta_a = 0.0524m$. '4modes': three-node bending mode included; '3modes': three-node bending mode not included.

Figures 5.29 and 5.30 show a reasonable agreement between theory and experiments. There is a relatively large influence from wetdeck slamming induced rigid body modes, which is as discussed in connection with Table 5.5 governed by the slamming force impulse. The previous case 1114 showed relatively less influence of wetdeck slamming induced rigid body modes. The theoretical and experimental error sources are similar as for case 1114. This will be further elaborated in Chapters 6 and 7. Further, even for cases without wetdeck slamming, theoretical and experimental predictions have some differences. Using Figs. 5.6 and 5.7 as a reference again, we see that for case $T = 1.5s$ the agreement is good except for vertical shear force at Cut2. It means in the latter case a deviation of around $35N$. Since there are relatively less contributions from the slamming part in this case, this deviation means more for the final results.

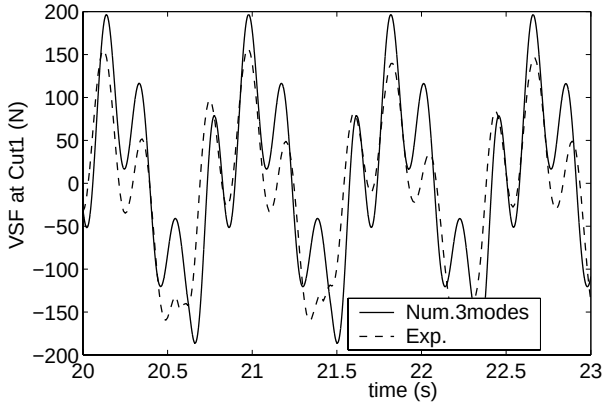

(a) VSF at Cut1

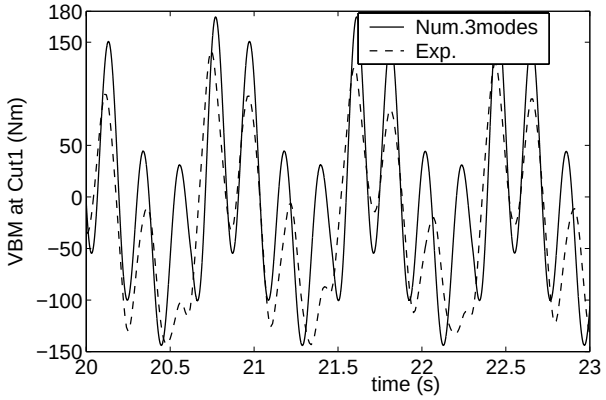

(b) VBM at Cut1

Figure 5.29 Theoretical and experimental predictions of vertical shear force (VSF) and vertical bending moment (VBM) at Cut1 for case 1111 with head sea, $U = 1.84m/s$, $T = 1.5s$ and $\zeta_a = 0.0524m$

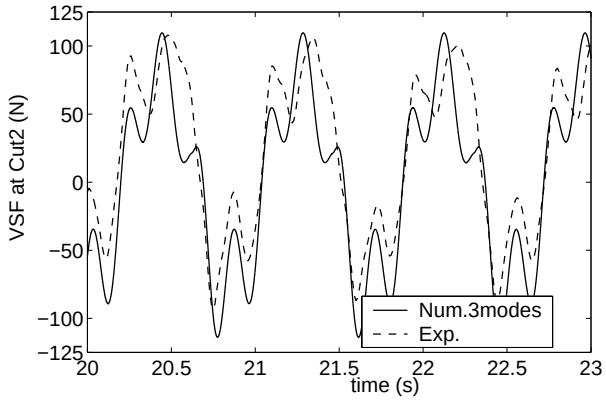

(a) VSF at Cut2

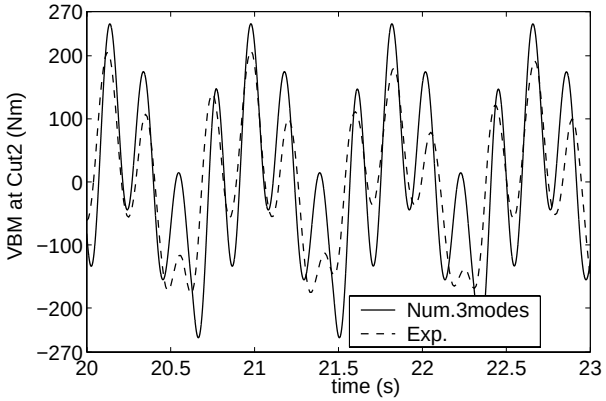

(b) VBM at Cut2

Figure 5.30 Theoretical and experimental predictions of vertical shear force (VSF) and vertical bending moment (VBM) at Cut2 for case 1111 with head sea, $U = 1.84m/s$, $T = 1.5s$ and $\zeta_a = 0.0524m$

Figure 5.31 shows the experimental and theoretical comparison of impact force on the deck. As discussed earlier the numerically predicted slamming covers Deck1 and Deck2 almost equally. The experimental results presented here are therefore the sum of the values from Deck1 and Deck2. However, the major impact force occurs on Deck1 in the experiments. There are high frequency vibrations in the experimental results, which are not predicted in our numerical model. This high frequency part is mainly from the force record on Deck2, which may be related to the local vibration of the deck or the instruments. The masses of Deck1 and Deck2 are respectively $9.1kg$ and $3.2kg$. The longitudinal centers of gravity of Deck1 and Deck2 are respectively $0.34m$ and $0.35m$ from the front end of Deck1 and Deck2.

Figures 5.32(a) to 5.32(b) show the components of the motion and acceleration at the bow. In the figures the circles and triangles represent respectively the initial and ending time instants of calculated wetdeck slamming. They are in sequence the time instants of $10.6912s$, $10.8218s$,

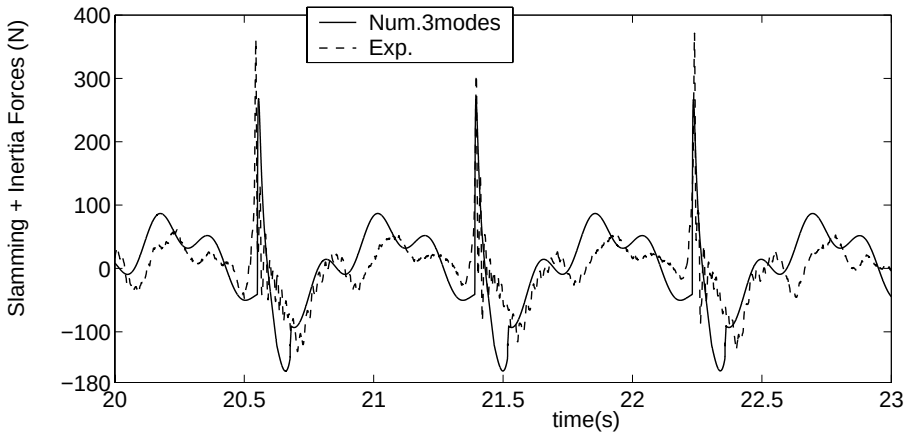

Figure 5.31 Theoretical and experimental predictions of slamming force on Deck1 for case 1111; structural inertia force on Deck1 and Deck2 included. Theoretical results are $0.07s$ shifted left compared with results in Figs. 5.29 and 5.30. The three lowest modes are included.

$11.5313s$ and $11.6618s$. When slamming happens at $t = 10.6912s$, the slamming induced response contributes 3.9% to the vertical motion. The acceleration is changed from $5.33m/s^2$ to $3.64m/s^2$ due to the slamming induced contribution of $-1.69m/s^2$. When the acceleration peak occurs at $t = 10.6954s$, the slamming induced response contributes 4.6% and 59.6% respectively to the vertical motion and acceleration. The minimum value of motion response was changed 9.8% from the linear response during the impact period.

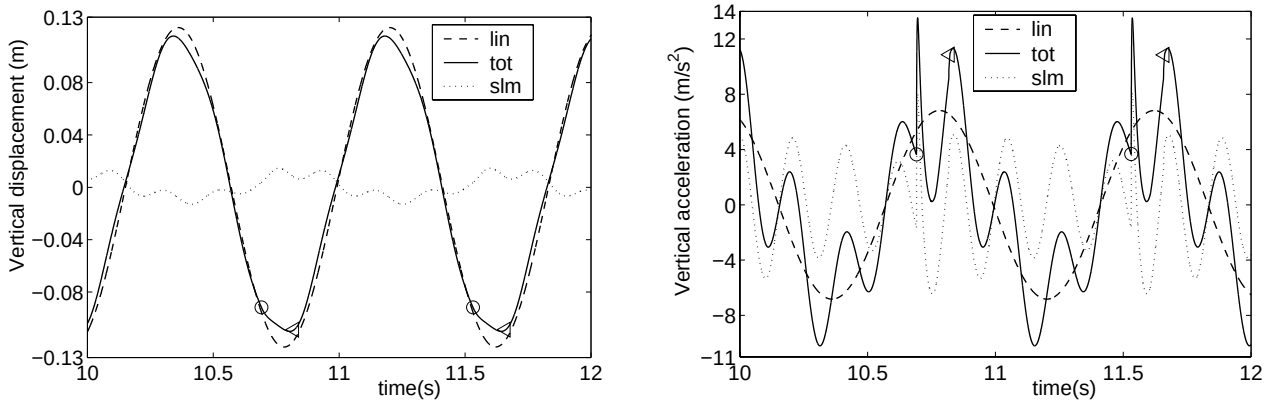

(a) η_3 at the bow (b) $\ddot{\eta_3}$ at the bow

Figure 5.32 Theoretical predictions of vertical motion (η_3) and acceleration ($\ddot{\eta_3}$) at the bow of the catamaran; case 1111: $U = 1.84m/s$, $T = 1.5s$ and $\zeta_a = 0.0524m$, head sea. Three lowest modes included in numerical results. The circles ($\circ$) and triangles ($\triangleleft$) represent the calculated initial and ending time instants of wetdeck slamming; 'lin' and 'slm' represent the response from linear wave frequency effects and slamming loads respectively, and 'tot' is the total response.

5.6.3 Case 1115

The conditions for case 1115 are head sea, $U = 2.00m/s$, $T = 2.0s$ and $\zeta_a = 0.0483m$. Both theory and experiments predict slamming. However, amplitudes of the numerically predicted slamming induced response are much smaller than the experimental values. Figures 5.33 and 5.34 present the experimental results for the global loads at the two transverse cuts. The values are obtained by adding the values from starboard and port side. The maximum numerical values by including two-node bending mode are only $87.6N$ and $59.09Nm$ for respectively vertical shear force at Cut1 and vertical bending moment at Cut1, $32.85N$ and $112.02Nm$ for vertical shear force at Cut2 and vertical bending moment at Cut2. The main reason is that the amplitude of two node bending is clearly under-predicted. The amplitude due to rigid body heave and pitch are well predicted (See Figs. 5.6 and 5.7).

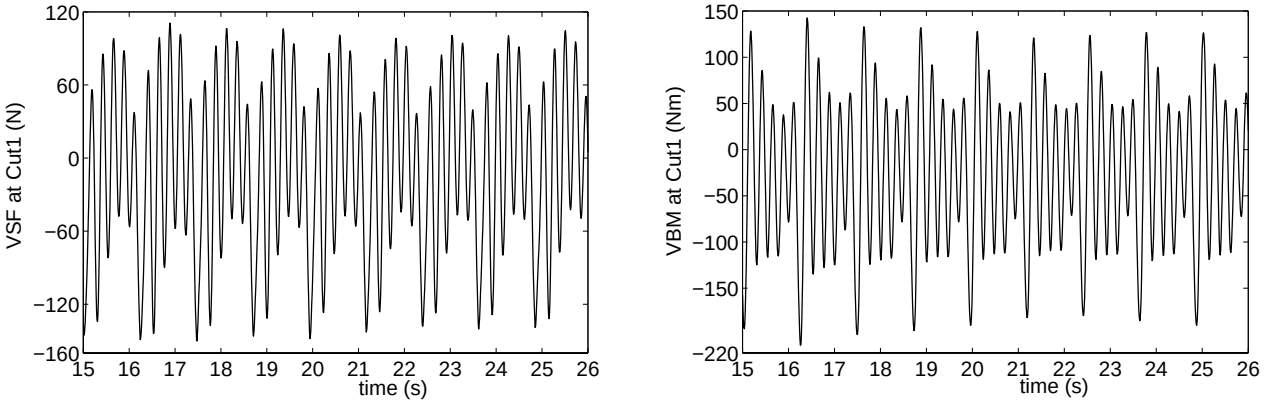

(a) VSF at Cut1 (b) VBM at Cut1

Figure 5.33 Experimental values of vertical shear force (VSF) and vertical bending moment (VBM) at Cut1 for case 1115 with head sea, $U = 2.00m/s$, $T = 2.0s$ and $\zeta_a = 0.0483m$

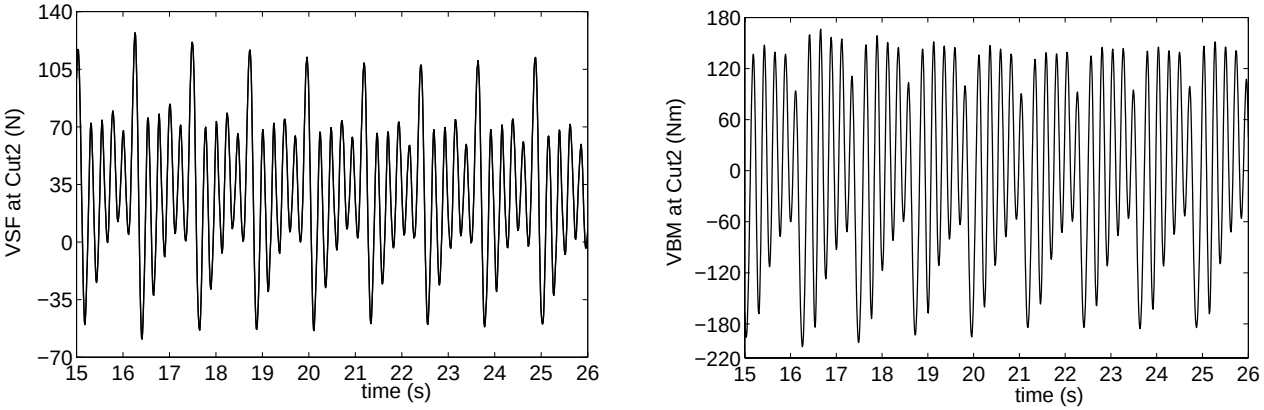

(a) VSF at Cut2 (b) VBM at Cut2

Figure 5.34 Experimental values of vertical shear force (VSF) and vertical bending moment (VBM) at Cut2 for case 1115 with head sea, $U = 2.00m/s$, $T = 2.0s$ and $\zeta_a = 0.0483m$

Figure 5.35 presents experimental slamming loads on Deck1. The structural inertia loads of Deck1 is included. By comparing this results with the theoretical slamming load in Fig. 5.20(c), we note that theory clearly underpredicts the slamming loads.

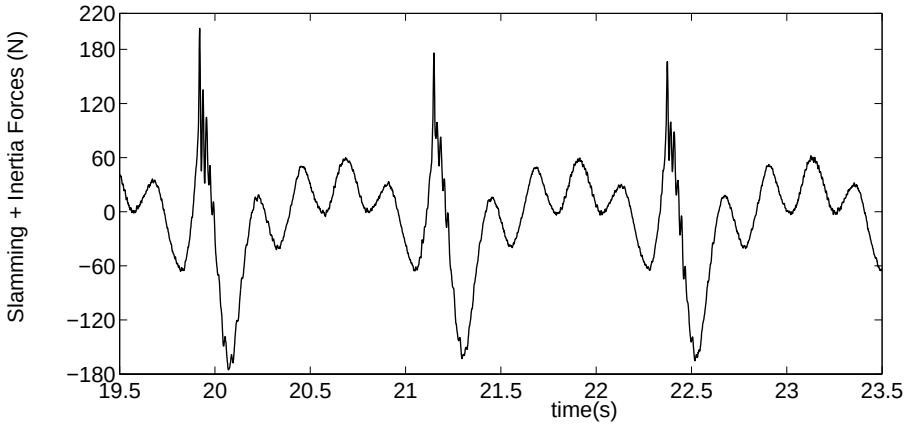

Figure 5.35 Experimental predictions of slamming force on Deck1 for case 1115 with head sea, $U = 2.00m/s$, $T = 2.0s$ and $\zeta_a = 0.0483m$; structural inertia force of Deck1 included.

One may wonder why this case shows clearly worse agreement between theory and experiments than cases 1111 and 1114. The previous detailed discussion of relative vertical motion, relative impact velocity and acceleration, as well as slamming loads gave plausible arguments why the theoretical slamming loads could be clearly smaller in case 1115 than in cases 1111 and 1114. This means also smaller wetdeck slamming induced global loads for this case. This is contrary to the experimental results which show that case 1115 is equally severe as case 1111. It is relevant in this context to question the sensitivity to parameters influencing slamming like incident wave amplitude, the sinkage and trim angle of the vessel. The discussion in Chapter 6 shows that these parameters are important experimental error sources. However, it is difficult based on the discussion in Chapter 6 to state that this will explain the relatively large differences between theory and experiments for this case.

Another error source is a small amplitude rolling in the experiments due to an unintended experimental asymmetry of the mass distribution about the center plane of the vessel that caused an incident wave direction slightly different from head sea. The rolling may also have been excited by the autopilot system. Økland (2002) predicted the natural period of roll is $1.16s$ based on wet decay tests. However, the energy analysis of roll data does not clearly show energy peak at such a period. Instead it has important energy consistent both at the frequency of encounter and energy in adjacent frequency area, as well as energy peaks at around $0.33Hz$ and $0.65Hz$. This is probably caused by the autopilot system (Martinussen (2002)). The energy analysis for the roll data for other cases share similar properties as said here. Since the maximum roll angle is only 0.8^0, roll will have a small effect on the relative vertical motion, relative impact velocity and acceleration. This means that the impact loads are only slightly influenced by roll.

One possible explanation of the difference between theory and experiments is the linear wave induced motion predictions based on strip theory and neglection of hydrodynamic hull interaction. Strip theory is a high frequency theory (Ogilvie and Tuck (1969)) and this case has lower frequency than cases 1111 and 1114. Moreover, hull interaction may matter. There are two important effects associated with hull interaction. One is the influence of waves generated from one side hull to the other one. Another is the piston resonance mode of the water between the two side hulls. The following text gives arguments that hull interaction matters most for case 1115 among the cases discussed previously.

The angle α between the outer part of the wave system generated by one independent hull and the center plane of the hull increases with decreasing frequency and forward speed (See discussions in Section 1.2 in connection with Fig. 1.5 and Section 7.2.2 in connection with Fig. 7.1). The calculations show that 65.56% of the length between perpendiculars of each hull from AP is affected by wave interaction for case 1115. The corresponding percentages for cases 1111 and 1114 are respectively 50.15% and 65.56% (See Section 7.2.2). This estimate shows that hull interaction due to the generated waves by side hulls are similarly important for the three cases.

Another effect is the piston mode of the water between the two hulls. Wave interaction is of special concern if natural modes for the fluid motion between the hulls are excited. The most relevant mode for heave and pitch motions is the piston mode. This means resonant fluid motion where the fluid particles between the two hulls move nearly vertically. Seen from a distance from the hull, it appears similar like a piston moving up and down between the two hulls. This is the same natural mode causing large amplitude fluid motions in a moonpool (Faltinsen (1990)). Ronæss (2002) showed that the calculated and experimental added mass and damping coefficients for heave and pitch of a catamaran were greatly affected in the vicinity of the natural period for the piston mode. Unified theory with hull interaction was the basis for the calculations. A simple formula by Molin (1999) for 2D flow conditions was used in the calculations of the natural period T_{piston} for the piston mode. Molin's expression is

$$T_{piston} = 2\pi\sqrt{\frac{h + \frac{d}{\pi}(\frac{3}{2} + \ln\frac{B_s}{2d})}{g}} \tag{5.16}$$

where B_s, d and h are defined in Fig. 5.36.

The hull shape shown in Fig. 5.36 was assumed in deriving Eq. (5.16). If midship values are used for the catamaran, it means that $h = 0.2225m$, $B_s = 1.02m$ and $d = 0.468m$. This gives $T_{piston} = 1.36s$. This is obviously an approximation both due to the difference in cross-sectional form from Fig. 5.36 and that the cross-sections change along the length of the ship. However, a similar approximation was made by Ronæss (2002) and it gave satisfactory results. The period of encounter for cases 1111, 1114 and 1115 are respectively $0.840s$, $1.097s$ and $1.219s$. It demonstrates that case 1115 will be most affected by the piston mode.

Ronæss (2002) examined the piston mode effect for a catamaran at $F_n = 0.15$ and head sea. The damping coefficients in heave and pitch around piston mode resonance were about twice as large as values predicted without hull interaction. The influence on coupled damping coef-

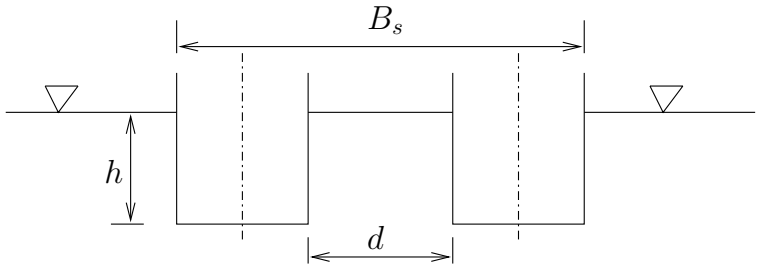

Figure 5.36 Notation used in Molin's (1999) formula (Eq. (5.16)) for natural period of piston mode resonance between the two hulls

ficients between heave and pitch was even larger. There was also a significant effect on added mass coefficients. For instance added mass in heave got close to zero and pitch added mass became negative. Ronæss' calculations were validated with good results by comparisons with experimental results by Kashiwagi (1993). If strip theory with hull interaction was applied, it would give clearly different results at piston mode resonance. Ohkusu's (1996) results are relevant in this context. Ohkusu (1996) presented both experimental and theoretical results for two-dimensional added mass and damping in heave for a cross-section of a catamaran. Each hull had a semi-circular cross section. Some of his results can be interpreted to be due to piston mode resonance. Ohkusu found both a large amplification of the damping and zero damping for frequencies near piston mode resonance. However, Ronæss did not predict small damping. Further, the added mass in heave in Ohkusu's results became negative with a minimum value close to minus three times the hull displacement. Ohkusu (1969) has presented results for different distances between the center planes of the two hulls. These results are similar as described in Ohkusu (1996). It is therefore hard to see that strip theory can quantitatively agree with Kashiwagi's (1993) experimental results for a catamaran at forward speed.

This piston mode resonance period corresponded to the wave length-ship length ratio $\lambda/L = 2.2$ in Ronæss' case. Here L means the length between the perpendiculars of the ship. Since the vertical motions for such long wave lengths are dominated by the influence of Froude-Krylov forces and hydrostatic forces, there was not a large effect of the piston mode on predicted heave and pitch. However, since our case 1115 corresponds to the lower $\lambda/L = 1.65$ and ω_e are closer to the resonant heave and pitch conditions, the effect of piston mode resonance can not be neglected a priori.

Even if we have argued that hull interaction matters in particular for case 1115, the previous comparison between theoretical and experimental values of relative vertical motion amplitude (See Fig. 5.5) does not show worse agreement for case 1115 than for cases 1111 and 1114. Actually the agreement is quite good. However, we have then left out possible experimental error sources. The relative motion measurement uses a similar technique as the wave measurements. The forward speed may cause additional inaccuracies (Greco (2001)), but according to Stansberg (2002) the inaccuracy is not larger than $1mm$. The measured incident wave amplitude for the relative motion, measurement at $T = 2.0s$ presented in Fig. 5.5 is $0.0145m$. This implies that the agreement between experimental and numerical predictions of relative vertical motion amplitude

can still be considered satisfactory. However, both amplitudes and phases of motions matter in predicting impact, but there is no experimental documentation of phases. An important effect of changes in motions and phases can be that the water does not initially hit at the front end of the wetdeck. This will cause longer slamming duration and will also change relative impact velocities and accelerations. Further, experimental and theoretical studies by for instance unified theory is therefore needed to fully explain case 1115. The unified theory has then to be modified to include the elastic properties of the catamaran.

5.6.4 Case 1112

The numerical model predicted no slamming in case 1112. The conditions are head sea, $U = 1.86m/s$, $T = 1.8s$ and $\zeta_a = 0.0259m$. The experiments recorded slamming for this case. However, the experimentally recorded global loads as shown in Figs. 5.37 to 5.38 are not large and have large beating effect. The experimental results are the sum of the values from starboard and port side.

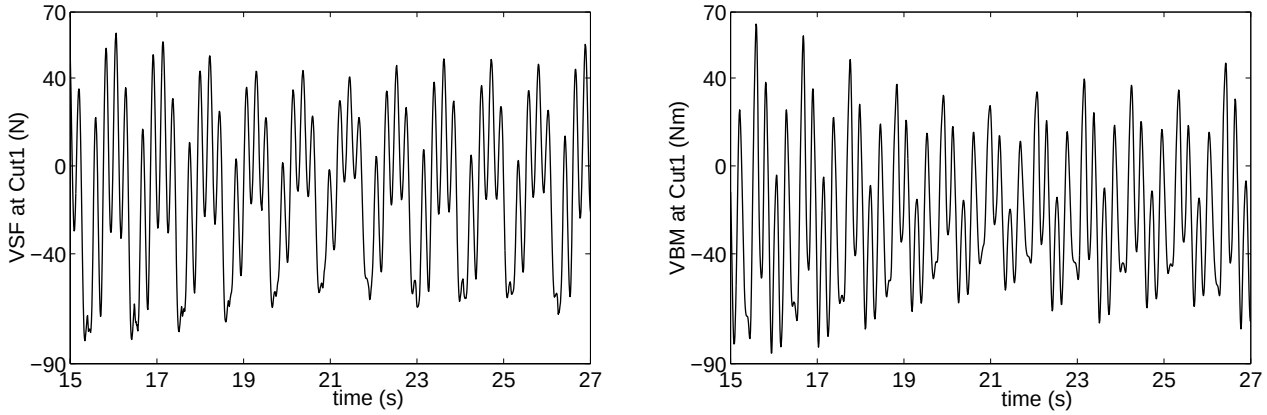

(a) VSF at Cut1

(b) VBM at Cut1

Figure 5.37 Experimental values of vertical shear force (VSF) and vertical bending moment (VBM) at Cut1 for case 1112 with head sea, $U = 1.86m/s$, $T = 1.8s$ and $\zeta_a = 0.0259m$

Since the experimental values are small, they may be sensitive to small changes in for instance incident wave amplitude. The numerical model was therefore used to study the sensitivity to incident wave amplitude. It was found that the lowest incident wave amplitude for impact to occur in the theoretical model is $0.032m$. This means a value about 20% larger than the experimental incident wave amplitude. It is possible that the small amplitude rolling present in the experiments can cause the beating effect in the experiments. The maximum roll angle was 0.6^0. Since the distance from the center plane of the catamaran to the inside of one side hull is $0.243m$, the maximum roll induced vertical motion is $0.0025m$. This corresponds to 9.8% of incident wave amplitude. Roll will also contribute to relative impact velocity and acceleration.

The discrepancy between experimental and theoretical results can be due to other sources. In Chapters 6 and 7 the error sources in the experiments and in the theoretical model will be

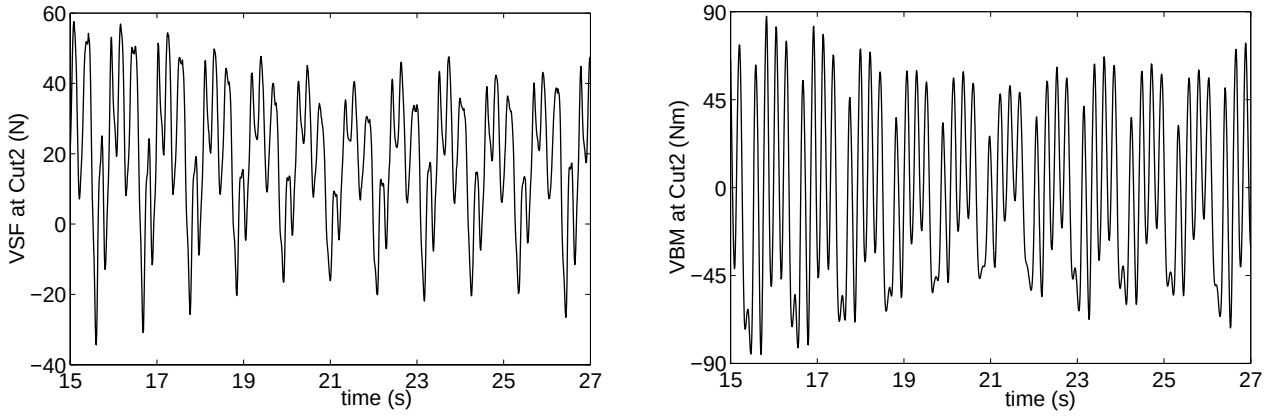

(a) VSF at Cut2

(b) VBM at Cut2

Figure 5.38 Experimental values of vertical shear force (VSF) and vertical bending moment (VBM) at Cut2 for case 1112 with head sea, $U = 1.86m/s$, $T = 1.8s$ and $\zeta_a = 0.0259m$

systematically investigated by using case 1114 as the base. Case 1112 has the same wave period as in case 1114 while case 1112 has a lower wave amplitude. The forward speed is nearly the same in the two cases. The discussion of the error sources for case 1114 is therefore relevant for case 1112.

5.7 Summary

The theoretical model has been verified and validated. Since it is necessary to account for large structural damping associated with the two highest modes of the three-body model, a modal based method is introduced and shown to give consistent results with solving the equations of motions directly. Since the added mass and damping coefficients for the side hulls are frequency dependent and chosen equal to the wave encounter frequency or close to the natural frequencies of heave and pitch in free decay tests, errors occur in natural frequencies for elastic modes. However, this has a secondary effect on maximum wetdeck slamming induced global loads. The theoretical model agrees reasonably well with experimental free decay tests and model tests in regular head sea waves without wetdeck slamming.

There are five cases with relatively large incident waves. The theory and the experiments agree that wetdeck slamming does not occur in one of these cases. The most severe slamming case show reasonable agreement between theory and experiments both for global loads and slamming force. There are two moderate slamming cases. One of the cases agrees well. The disagreement for the second case is thoroughly investigated. The most plausible reason is found to be hull interaction in the vicinity of a piston mode resonance between the two hulls. However, this needs further investigations where a theoretical method that properly accounts for hull interaction is used. In the fifth high amplitude wave case, minor wetdeck slamming with beating occurs in the experiments. The beating may be caused by roll. The wave amplitude has to be increased with about 20% in the theoretical model to predict slamming. The wetdeck slamming cases show

that two-node longitudinal bending gives in general the most important contribution to vertical shear forces and bending moments at the two transverse cuts studied in the experiments.

Chapter 6

Error Analysis in the Experiments

6.1 Introduction

6.1.1 Overview

Error sources in the experiments and theoretical model will be identified respectively in Chapter 6 and Chapter 7, and the resulting uncertainties in predicted wetdeck slamming induced response will be discussed. However, it should be noted that there can be other error sources besides items discussed in these two chapters. The focus in the error analysis is on case 1114 (See Table A.7 in Appendix A), *i.e.* a case with the specified (intended) test wave amplitude $\zeta_a = 0.05m$, wave period $T = 1.8s$ and head sea. The measured wave amplitude was $0.041m$. This is the most severe slamming case in the experiments.

The report of the panel on validation procedures of the 19th ITTC (International Towing Tank Conference) (Aláez *et al.* (1990)) gives a broad description of validation procedures. Examples are given for resistance and maneuvering tests, speed and power trials, strip theory and three-dimensional diffraction/radiation program. It is still not state of the art with error analysis in the marine hydrodynamics field. This is true even in research. An important reason is that it is a difficult task. However, this should not prevent that attempts are made to judge the reliability of experimental and theoretical results.

The experimental errors can be divided into random (repeatability) errors and systematic (bias) errors. Since the experiments were not repeated, we can not assess explicitly random errors. The focus is therefore on systematic errors. Further, it is difficult for us to evaluate errors associated with instrumentation, data acquisition and data analysis. However, there is a long experience with processing of the experimental data and most of the instrumentation. The systematic experimental error sources to our knowledge will be investigated and the relative errors will to a large extent be predicted by using our computer code.

6.1.2 Measurement systems in the experiments

Model tests were done in the Ocean Basin at the Marine Technology Center in Trondheim in 1996 by Aarsnes and Økland. Økland and Moan (1998), Økland *et al.* (1998) and Økland (2002) reported results for zero forward speed. However, the experimental results were never properly reported for our cases with forward speed. This caused problems in trying to interpret the results long time after they were done. Both Økland and Aarsnes have been helpful in that respect.

The tested cases for forward speed are listed in Table A.7 in Appendix A. Regular incident waves were considered and the catamaran model was self propelled. An autopilot system was used to keep the heading. The experiments were planned so that the ship model should encounter regular incident head waves with constant amplitude along the track of the model. It is shown later that this is not exactly so. Both cases with and without slamming were tested. Standard equipment and procedures were to a large extent employed. However, using an elastic model was for instance not standard.

Three different systems were used for motion measurements, *i.e.* MRU (Motion Response Unit) system, Optical system and Three-Accelerometer System. The measurement positions are illustrated in Fig. A.5 in Appendix A. All the three measurement systems were installed on the mid segment of the catamaran.

The MRU system was installed on the inside hull on the starboard side. It uses a gyro system for rotational displacements and accelerometers combined with time integration to find translatory displacements. All the translatory displacements are referring to the point where the MRU system is installed.

The Optical instruments measured displacements in three orthogonal directions at three points, from which the translatory and rotational displacements at the $L_{PP}/2$ position of the center plane of the catamaran was predicted.

The Three-Accelerometer system uses accelerometers at three points as illustrated in Fig. A.5 in Appendix A. Translatory displacements at the points are found by integrating twice the time history of the accelerations. By assuming a rigid body and using that the displacement at any point P can be expressed as $\vec{\eta}_o + \vec{\omega} \times \vec{r}$, where $\vec{\eta}_o$ is translatory displacement of a given point O, $\vec{\omega}$ is the rotational vector of the body, and $\vec{r}$ is the position vector between points O and P, we can by measurements at three different points find rotational displacements of the rigid body.

All these three different systems should in principle give data that overlap each other in the time domain. However, different computers were used to log the data. Since the three systems have different starting time and the relations between these starting times were not recorded, phases of corresponding curves differ. There are some particular drawbacks for two of the systems. The Three-Accelerometer system predicted unreliable angular rotations. A reason may be due to the double integration of acceleration and that the accuracy in predicted translatory displacements at the three points is not sufficient to further derive angular rotations. It should also be noted that there is considerable less experience with the Three-Accelerometer system than with the

other two measurement systems. The Optical system will be influenced by objects that block the infrared light going between a transmitter and the diodes on the model. The consequence is spikes occurring in some records. The sampling frequency for the Optical system was only $9Hz$. The final results were then linearly interpolated into data corresponding to $100Hz$ sampling frequency. This causes discontinuities in the derivative of the time record. There are also some uncertainties in the base reference value of vertical displacement.

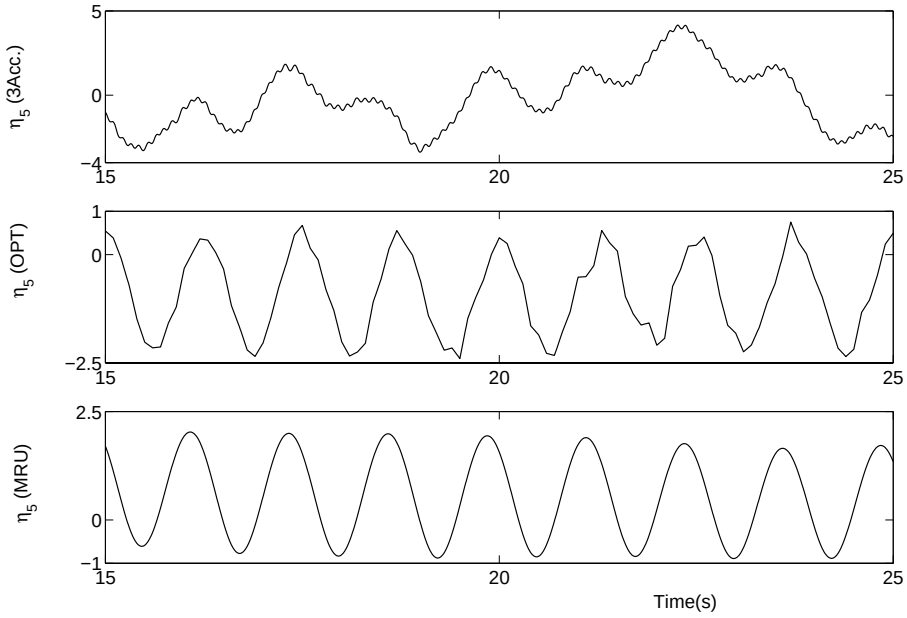

Figure 6.1 Pitch time record for case 1108 with intended wave amplitude $\zeta_a = 0.015m$ and wave period $T = 2.0s$; Measured wave amplitude is $0.0145m$. No wetdeck slamming. Pitch angle unit is degree.

For instance Fig. 6.1 is part of the recorded results for pitch angle for case 1108. This shows the drawbacks for the different systems mentioned above. Obviously the record from the Three-Accelerometer system is not reliable. Records from the Optical and MRU system predict opposite values of mean pitch angle. The values are respectively -0.94^0 and 0.60^0. The corresponding first harmonic values are 1.301^0 and 1.357^0, respectively, which means 4.1% relative deviation based on the MRU data. The uncertainties in the mean values lead to important experimental uncertainties in global load predictions. This will be further presented and discussed later. Both the Optical and MRU system data will be investigated and discussed when data from both of these two systems are available.

Since the catamaran model is flexible, we can only approximately estimate the experimental motions at the other parts of the model by assuming one rigid body. However, the errors will be small if no wetdeck slamming occurs. This was earlier documented in Figs. 5.6 and 5.7. If severe wetdeck slamming occurs, the two-node bending gives a significant influence on the vertical accelerations. This is illustrated in Figs. 5.26(b) and 5.32(b). However, the contribution from the flexibility on the wetdeck slamming induced motions is less pronounced. The

computer calculations for the cases reported in this thesis indicate a relative error up to 10% in predicting the vertical motions at FP by assuming a rigid body (See Figs. 5.26(a) and 5.32(a)).

Global response forces are measured at the connecting transducers of the different segments in each hull. The slamming forces on the wetdeck were also recorded by pin transducers on the deck. Section A.5 gives the detailed positions and the numbering system of the transducers in the experiments.

6.1.3 Experimental error sources

In the following error analysis, wetdeck slamming induced global loads will be focused on. We will study case 1114, which had the most severe slamming induced responses in the experiments. What we will do is to assess the uncertainties in the experiments and examine the consequences of those for vertical shear force (VSF) and vertical bending moment (VBM) at two transverse cuts of the catamaran model. This will to a large extent be done by using our computer code. This procedure can of course also be applied to other test cases. The error sources that will be concentrated on, are related to

- forward speed
- ambient waves: wave frequency effect, seiching, measurement inaccuracy
- Roll, yaw and sway
- sinkage
- trim
- mass distribution
- model geometry

Here steady state conditions are considered. The error analysis provides an insight into the sensitivity of the global wetdeck slamming induced loads to the above-mentioned various parameters.

6.2 Forward speed

6.2.1 Speed loss in the experiments

The intended forward speed was $3.0m/s$. However, the experimental data showed that there was a significantly smaller speed in the experiments. This happened both for the cases with the low incident expected wave amplitude of $\zeta_a = 0.015m$ without wetdeck impact and cases with the higher incident expected wave amplitude of $\zeta_a = 0.05m$. We have here used the words 'expected wave amplitude' to emphasize that this was the intended wave amplitude. It will later be clear that the measured wave amplitude differs. Some of the higher amplitude cases had wetdeck

slamming, which have been presented and discussed in Chapter 5.

There are two ways to investigate the forward speed in the experiments. One way is by examining the surge motion record from the Optical system. Another way is by spectral analysis of the time domain series of the global responses. Figure 6.2 shows the surge record based on the Optical system for case 1107 with incident wave period $T = 1.8s$ and intended wave height $H = 0.03m$. A steady forward speed means that the time derivative of surge is constant when the wave induced oscillatory surge motions are filtered out. Based on the experimental log, the good time window in this case is approximately from $t = 14.0s$ to $t = 26.0s$. A least square method was used in this time range to estimate the time derivative of surge. This gave a forward speed of $U = 1.90m/s$ in this case.

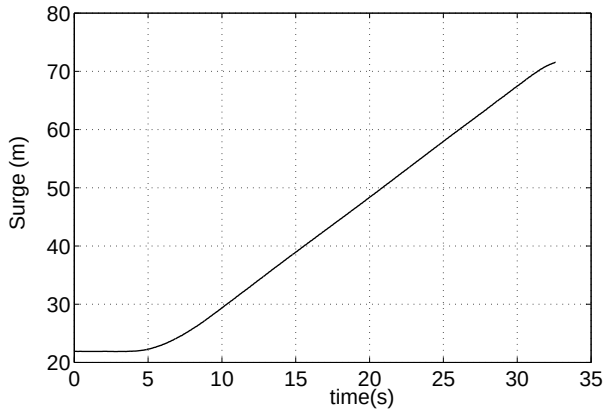

Figure 6.2 Surge data for case 1107 by Optical measurement system; Incident head sea regular waves with $T = 1.8s$ and measured $\zeta_a = 0.0142m$

Table A.5 in Appendix A presents the estimated forward speed based on the surge motion record for the other examined cases. We have also used spectral analysis to estimate in an indirect way the forward speed. Figure 6.3(a) presents the time domain record of the vertical shear force at the longitudinal transducer-5891, *i.e.* the front connection of the starboard side of the catamaran (See Fig. A.4). The corresponding spectrum based on analyzing the time record from $t = 14.0s$ to $t = 25.81s$ when the forward speed is steady is presented in Fig. 6.3(b). No impact occurred in this case. This means that the steady-state dynamic response was approximately linearly dependent on incident wave amplitude and oscillating with the frequency of encounter.

Figure 6.3(b) gives an encounter frequency of $0.9306Hz$. There is the relationship $f_e = f_0 + 2\pi U/g * f_0^2 \cos\beta$ between incident wave frequency f_0 and encounter wave frequency f_e. Here U is the forward speed and g is the gravitational acceleration, and β is the angle between the incident wave and ship heading with $\beta = 0$ expected here. This gives with $f_0 = 1/T = 0.5556Hz$ an estimated velocity of $U' = 1.90m/s$. It matches the estimated data from the surge curve. Actually the model had a small unintended mean yaw angle of 0.4^0 in this case. However, this has a negligible influence on our estimate.

Table A.5 in Appendix A shows that the forward speed in the experiments for different cases are within a range from $1.8m/s$ to $2.0m/s$. In cases 1111, 1112, 1114 and 1115, the forward speed

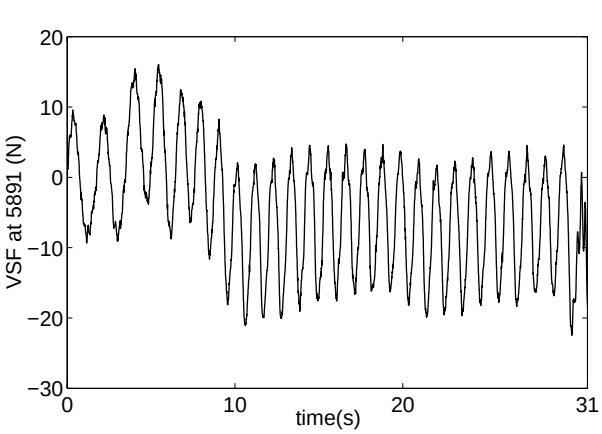

(a) Time record of VSF at Transducer-5891

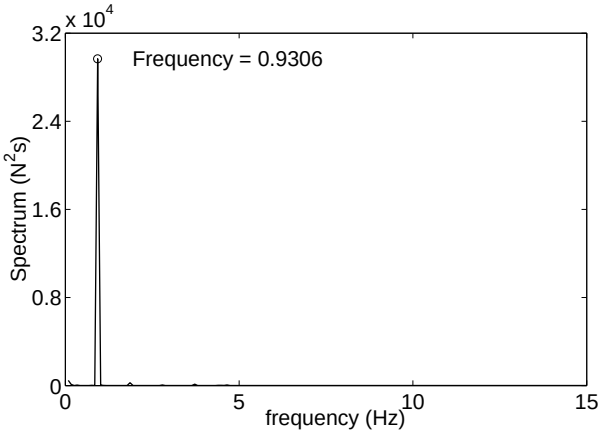

(b) Spectral analysis of time record from $t = 14s$ to $25.81s$ in Fig. 6.3(a)

Figure 6.3 Measured vertical shear force (VSF) at Longitudinal transducer-5891 (at Cut1), for case 1107 with wave period of $1.8s$ and measured wave amplitude $0.0142m$ in head sea. No wetdeck slamming.

is respectively $1.84m/s$, $1.86m/s$, $1.80m/s$ and $2.00m/s$. These are the cases when wetdeck slamming happens.

One point that needs to be noticed, is that the predicted peak frequency value of the spectrum depends on the length of the analyzed time record. Theoretically the energy analysis based on Fast Fourier Transformation (FFT) should give fixed energy distribution when the time record is long enough. However, in our case, the number of oscillations with steady-state conditions are not sufficiently high for a reliable FFT analysis. This means that different lengths of the time record will give different peak frequencies. For instance if the time record from $14s$ to $26s$ Fig. 6.3(a) is used, this gives $f_e = 0.9151Hz$. The result shown in Fig. 6.3(b) is based on using the time record from $14s$ to $25.81s$. This covers approximately 11 periods in Fig. 6.3(a). Though the difference is not so large, it leads to some uncertainty. Marintek has a standard procedure which automatically analyzes the time record from the measurements. This includes the first harmonic frequency of the time record. It has been controlled that forward speeds predicted based on f_e from Marintek's analysis in the different cases are almost the same as the ones predicted by the surge curves. These different ways of analyzing what the forward speed is, gives a maximum variation of $\pm 0.01m/s$.

6.2.2 Speed influence on slamming induced response

Forward speed is an important parameter for slamming. In practice, reducing forward speed can often be an effective way to avoid severe slamming. As indicated above, the speed in the experiments is determined with a small uncertainty. To illustrate the sensitivity between wetdeck slamming induced global loads and forward speed, we have used our computer code for $U = 1.8m/s$ and $1.9m/s$. Figures 6.4 and 6.5 show the speed influence on VSF and VBM at

the two cuts. Table 6.1 shows that the peak values differ by approximately 30% based on the $U = 1.8m/s$ case.

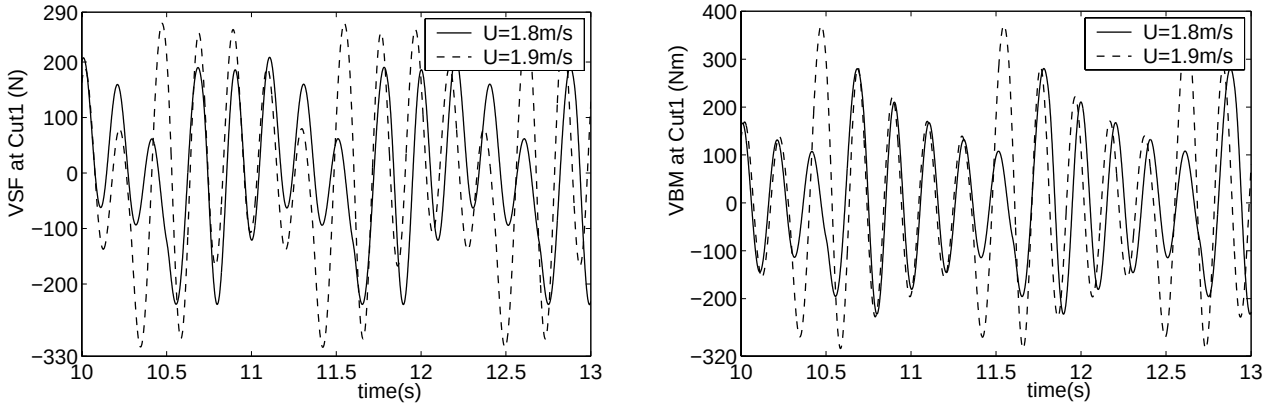

(a) VSF at Cut1 (b) VBM at Cut1

Figure 6.4 Speed influence on vertical shear force (VSF) and vertical bending moment (VBM) at Cut1 for case 1114, $T = 1.8s$, $\zeta_a = 0.041m$, head sea; Calculated values.

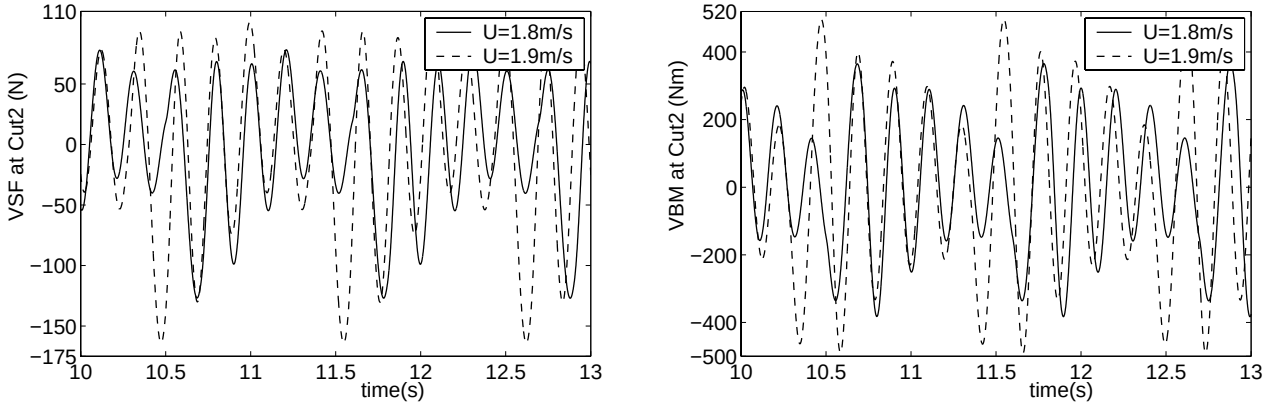

(a) VSF at Cut2 (b) VBM at Cut2

Figure 6.5 Speed influence on vertical shear force (VSF) and vertical bending moment (VBM) at Cut2 for case 1114, $T = 1.8s$, $\zeta_a = 0.041m$, head sea; Calculated values.

Table 6.1 Speed influence on maximum values of global loads for case 1114; $U = 1.8m/s$ is the basis of the ratio calculations.

Speed(m/s)	VSF Cut1(N)	VBM Cut1(Nm)	VSF Cut2(N)	VBM Cut2(Nm)
U=1.8	237.2	280.7	127.1	383.2
U=1.9	314.4	371.3	164.3	498.2
Increase Ratio [-]	32.5 %	32.3 %	29.3 %	30.0 %

These data will be used as a basis to quantify the uncertainty in the global loads due to uncertainty in the forward speed. We assume the uncertainty in the forward speed is at most $0.01m/s$. This means a relative error in the experimental measured global loads of approximately 3.0% as illustrated in Table 6.1.

Table 6.2 Relative errors in global loads due to error in speed; Case 1114 with wetdeck slamming

	VSF Cut1(N)	VBM Cut1(Nm)	VSF Cut2(N)	VBM Cut2(Nm)
Relative Error	0.033	0.032	0.029	0.030

6.3 Ambient waves

Figure 6.6 gives the geometrical dimensions of the Ocean Basin that was used during the tests. The tank has both a longcrested wave maker and a wave maker that can create short-crested waves. There are beaches on the opposite sides of both the longcrested and short-crested wave makers. The longcrested wave maker which is situated along one of the two short sides of the tank, was used in the experiments that we are now analyzing. The ship model had a straight course in the longitudinal direction of the tank. Figures 6.6(a) and 6.6(b) give the sketch of the Ocean Basin used in the experiments from both the top view and the longitudinal side view. The tank has dimensions of $L \times B \times D = 80m \times 50m \times 10m$. The tank bottom is adjustable but the water depth of $10m$ was used in these tests. This means that the studied incident waves are not influenced by the water depth. The beach length L_{beach} is $16m$. The catamaran (illustrated as point P_0 in the figures) was running along a mid track of the basin. Further, the starting point was around $L_0 = 20m$ from the beach end.

The instantaneous position of the catamaran model for case 1107 as a function of time is presented in Fig. 6.2. It starts at rest $21.889m$ from the end of the beach and achieves a constant speed at $t = 11.0s$, when it is $31.313m$ from the beach end. The constant speed range where the measurements are analyzed, ends at $t = 26s$ when the model is $L_E = 20.119m$ from the longcrested wave maker. The distance $B/2$, from the long side with the short-crested wave maker is $25m$.

Regular waves were generated by the longcrested wave maker. Waves were measured $34.6m$ from the longcrested wave maker and $25m$ from the shortcrested wave maker without the catamaran model present. It is expected based on Marintek's experience that the incident wave amplitudes will not be uniform in space. However, since only one wave gauge was used, we can not quantify this effect directly. Further, there is no published documentation on how this varies for different specified wave conditions. For regular waves we can divide the spatial variation to be either a wave frequency effect or due to low frequency seiching, *i.e.* sloshing, in the tank. Since the ship will react very differently to seiching and wave frequency effects, we have to consider them as two separate error sources.

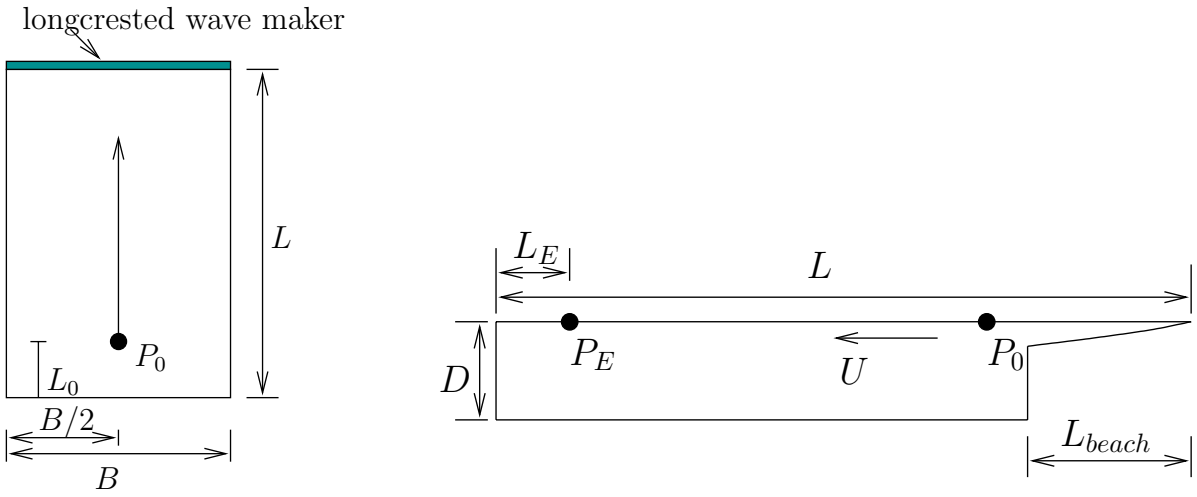

(a) Top view

(b) Longitudinal side view

Figure 6.6 Top and side view of the Ocean Basin used in the experiments. P_0 and P_E refer respectively to the starting and ending positions of the tested catamaran.

6.3.1 Wave frequency effects

Carl T. Stansberg, who is responsible for the wave generation systems at Marintek, says that the wave amplitude can vary as much as 10% along the track of the vessel due to wave frequency effects. Possible physical reasons are

1. *Local effects at the wave maker.* This occurs typically in a $5m$ distance from the wave maker and is therefore not important in our case.

2. *Dissipation of the waves.* Since the wave length is not very small relative to the track length of our model, this is believed to be unimportant.

3. *Diffraction effects of the tank.* If the tank was shaped exactly rectangular and the longcrested wave maker covered the whole tank breadth, there would not be such an effect. However, this is not the case. For instance diffraction may occur due to the parabolic beach opposite to the shortcrested wave maker, *i.e.* along one of the longitudinal side walls.

4. *Reflection from the wave beach.* The wave beach opposite to the longcrested wave maker will reflect some waves during the tests. This depends on the wave period. The reflection ought to be less than 5% according to Stansberg (2002), but exact information is not available.

5. *Ship generated waves* will be reflected from the tank walls. Due to the forward speed and the frequency of encounter in the examined cases, these reflected waves will not be incident to the ship model. This can be seen by using the studies by Ronæss and Faltinsen (2000).

6. *Nonlinear effects* may cause instabilities and modulation of the waves. However, the examined incident wave slopes are small, which means that the nonlinear effects should not be a major concern.

7. *Waves present in the basin from earlier tests.* Since we did not do the tests and such information is not documented, we can not outrule this possibility. However, using standard practice with waiting sufficient time between each test should minimize this effect.

Since we can not quantify the error sources mentioned above, we have to use Stansberg's (2002) estimate based on other tests for the upper bounds in variation in the wave frequency amplitude along the track of our ship model. We concentrate on case 1114 where significant wetdeck slamming occurred, and case 1107 without slamming. The tested wave period for cases 1107 and 1114 were both $T = 1.8s$ with expected wave amplitude of $0.015m$ and $0.05m$ respectively. Figures 6.7 and 6.8 show the time record at center of the basin for cases 1107 and 1114, when test model was not present.

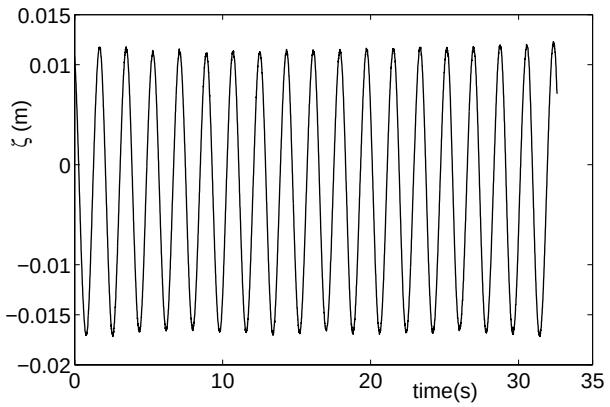

Figure 6.7 Time record of measured incident waves in case 1107

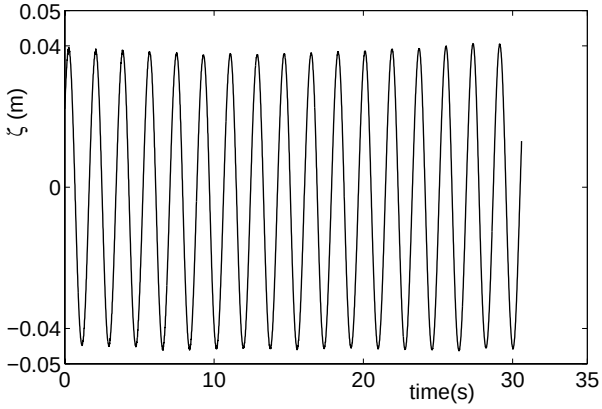

Figure 6.8 Time record of measured incident waves in case 1114

The records show different time scales. One is associated with the wave period and the others are due to longer periods. The reason to the long period oscillations is believed to be seiching. However, from the spectral analysis, we can not figure out the typical low frequency oscillations and the corresponding wave height.

We will use our computer code to see what the consequence on global loads due to errors in the incident wave amplitude is. Figure 6.9 and Table 6.3 show that changing the incident wave amplitude ζ_a from $0.041m$ to $0.039m$ decreases the peak values of VSF and VBM with approximately 10%.

Table 6.3 The influence of incident wave amplitude on global loads for case 1114

Wave Amplitude	VSF Cut1(N)	VBM Cut1(Nm)	VSF Cut2(N)	VBM Cut2(Nm)
0.041m	237.2	280.7	127.1	383.2
0.039m	211.1	223.7	104.9	339.3
Increase Ratio [-]	-11.0 %	-20.3%	-17.4 %	-11.5 %

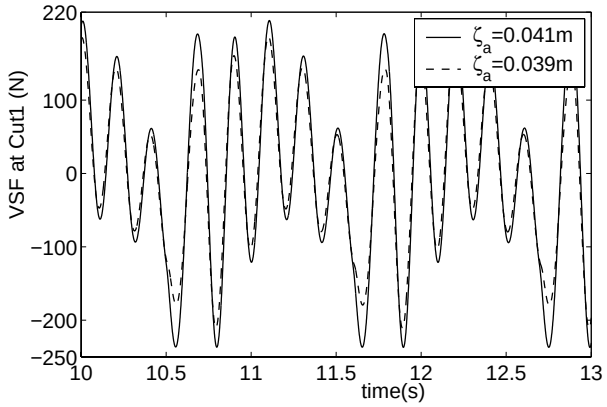

(a) VSF at Cut1

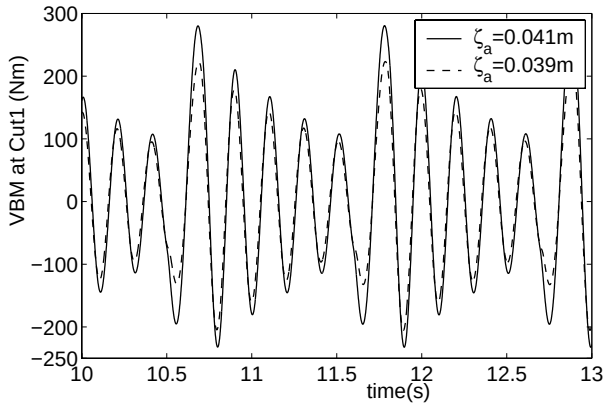

(b) VBM at Cut1

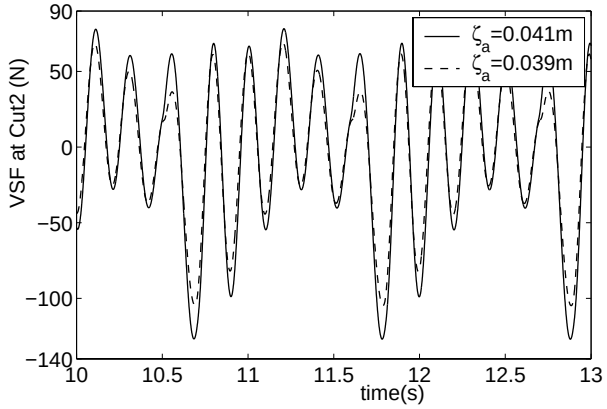

(c) VSF at Cut2

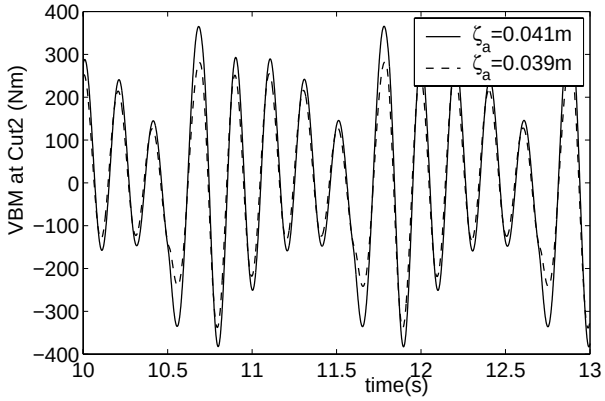

(d) VBM at Cut2

Figure 6.9 The influence of incident wave amplitude on vertical shear force (VSF) and vertical bending moment (VBM) at Cut1 and Cut2; Case1114 with $T = 1.8s$, $U = 1.8m/s$, head sea; Calculated values.

Based on Stansberg's (2002) experience, the spatial variation along the basin is about 10% from $10m$ from the wave maker over a distance of $50m$. By examining the time domain when we compare between theory and experiments in Figs. 5.23 to 5.24, relating that to a position in the tank relative to the wave probe and assuming that the spatial variation of incident wave is linear, it is found that the variation in incident wave amplitude within the time domain that we do comparisons would be less then $\pm 2.5\%$. Assuming an uncertainty in the incident wave amplitude of $\pm 2.5\%$ of mean value, gives an uncertainty in the wave amplitude of $\pm 0.041 * 2.5\% = \pm 0.001m$. This means that the resulting experimental global loads have a maximum relative error of about 10% as shown in Table 6.4.

Table 6.4 Relative errors in global loads due to error in incident wave amplitude; Case 1114 with wetdeck slamming

	VSF Cut1(N)	VBM Cut1(Nm)	VSF Cut2(N)	VBM Cut2(Nm)
Relative Error	0.055	0.102	0.087	0.057

6.3.2 Seiching in the model basin

There is theoretically an infinite number of sloshing modes with different natural periods in the tank. It is the lowest modes with the highest natural periods that are normally dominant. Our concern is natural modes causing free surface variations along the track of the vessel, that is in the longitudinal direction of the tank. We will approximate the modes by assuming a rectangular tank and 2D flow. The natural period of the lowest mode with a rectangular cross-section is

$$T_N \approx \frac{2L}{\sqrt{gD}}. \tag{6.1}$$

where L is the tank length and D is the tank depth (Faltinsen (1990)). This is based on linear shallow water theory, *i.e.* $L \gg D$. The free surface elevation associated with this lowest mode can be expressed as

$$\zeta = A\sin(\frac{\pi}{L}X)\cos(\frac{2\pi}{T_N}t + \xi_1) \tag{6.2}$$

where A and ξ_1 are unknown constants. Further, $X = 0$ is in the middle of the tank and $X = \pm L/2$ corresponds to the tank ends.

Due to the presence of the beach the longitudinal cross-section of the Ocean Basin is not rectangular. It can be shown (Morand and Ohayon (1995)) that the natural period will be between the natural period for a rectangular tank with $L = 80m$ and a rectangular tank with $L = 64m$. The difference between the length of these tanks is the length of the wave beach. Using L equal to $80m$ and $64m$ gives respectively T_N equal to $16.2s$ and $12.9s$. We can in principle by spectral analysis of the time record of the waves find the energy in the vicinity of the seiching frequency and then determine the seiching amplitude at the wave measurement position X. By using Eq. (6.2) we can then determine A by considering both $L = 80m$ and $L = 64m$. This gives then an indication of A during the tests. We will later return to this matter.

We will now study the vessel's response due to seiching and assume that there is only one mode present like expressed by Eq. (6.2). Since the wave length associated with this mode is much longer than the ship length, the ship behaves like a cork. This means that the seiching induced heave is equal to the wave elevation given by Eq. (6.2) at the position of COG of the ship. The seiching induced pitch is equal to the free surface slope which can be expressed as

$$\frac{d\zeta}{dX} = \frac{\pi}{L}A\cos(\frac{\pi}{L}X)\cos(\frac{2\pi}{T_N}t + \xi_1) \tag{6.3}$$

Both ζ and $d\zeta/dX$ must be evaluated at the instantaneous longitudinal position of the vessel's COG. However, it is unnecessary to account for the effect of the incident regular waves in this context. This means that the time dependence of the seiching induced pitch can be expressed as

$$\eta_{5S} = \frac{\pi}{L}A\cos(\frac{\pi}{L}U(t - t_0))\cos(\frac{2\pi}{T_N}t + \xi_1) \tag{6.4}$$

where we must require that the ship is at $X = 0$ at $t = t_0$. This determines the time t_0. By simple trigonometric rules, Equation (6.4) can also be expressed as

$$\eta_{5S} = 0.5\frac{\pi}{L}A\{\cos((\frac{2\pi}{T_N} + \frac{\pi}{L}U)t + \xi_1 - \frac{\pi}{L}Ut_0) + \cos((\frac{2\pi}{T_N} - \frac{\pi}{L}U)t + \xi_1 + \frac{\pi}{L}Ut_0)\} \tag{6.5}$$

This gives that the seiching induced pitch oscillates with the frequencies $1/T_N \pm U/2L$, which means $0.062 \pm 0.012\ Hz$ when $L = 80m$ and $0.077 \pm 0.015\ Hz$ when $L = 64m$, for $U = 1.9m/s$.

This slowly varying trim angle will influence the wetdeck slamming induced global loads. One effect is that slamming loads are influenced through the body boundary conditions on the wetdeck (See Eq. (3.9)). Another effect is that the trim angle influences directly the hydrodynamic loads on the side hulls. This can be explained by using Fig. 6.3(a) that presents VSF of Cut2 at starboard side when no wetdeck slamming occurs. The spectral analysis of the time record from $14s$ to $25.81s$ presented in Fig. 6.3(b) shows energy peaks at the wave frequency and at a small frequency.

This low frequency effect is associated with both the seiching induced pitch and the spatially changing incident wave amplitude. We concentrate now on seiching. This can be explained by considering the mean VSF in Fig. 6.3(a) over one slowly varying oscillation period. This gives a slowly varying time record of VSF that can be explained by a quasi-steady analysis. When t is small, the mean value of VSF in Fig. 6.3(a) is close to zero. The reason is simply that the recordings do not include the shear forces due to differences in weight and buoyancy. As t increases the ship speed increases and the ship speed influences the steady hydrodynamic loads on the side hulls. We see this if we express the steady pressure by Bernoulli's equation as

$$p = p_a - \rho g z + \frac{\rho}{2}(U^2 - U_{loc}^2) \tag{6.6}$$

Here p_a is atmospheric pressure, which does not contribute to the global loads. z is a vertical coordinate with z positive upwards and $z = 0$ in the mean free surface. This means that the second term is the hydrostatic pressure causing buoyancy forces on the hull at zero forward speed. U_{loc} is the local fluid velocity if we use a reference frame moving with the ship's forward speed U. U_{loc} will for instance be influenced by the steady wave making due to the ship. The trim angle will directly influence the magnitude of U_{loc}. The consequence is that the trim angle influences the global loads. When the trim angle is small, we may decompose the global loads into one term independent of trim angle and one term proportional to the trim angle. If we look at the time record in Fig. 6.3(a) for $t > 11s$, constant speed U has been obtained and the slowly varying VSF can as a possibility be related to the seiching induced pitch angle. However, there are also other contributions to the slowly varying VSF. This is associated with the mean wave induced loads on the side hulls. Since the incident waves vary along the track of the vessel, we get a slowly varying effect like previously described by the steady hydrodynamic loads.

The spectral analysis of the wave record in Figs. 6.7 and 6.8 gives one peak frequency of incident wave frequency $f_0 = 0.556Hz$ as well as a small energy area for frequencies less than $0.1Hz$. However, the energy analysis of different wave records can not predict the seiching period as expected. One reason is that the time record is not sufficiently long for a seiching analysis. Further, the wave measurement point is close to a standing wave node, so we can not get reliable data from the measurements to estimate seiching period and amplitude. If we base our estimate on Marintek's experience from other tests where many more wave probes were used, we should according to Stansberg (2002) not have a seiching amplitude larger than $2mm$. By using Eq. (6.3) with $L = 64m$, this gives a pitch angle of 0.0056^0 due to seiching.

Since it is not only seiching induced pitch that causes an error in trim, we will in Section 6.5.2 on trim further discuss the error in wetdeck slamming induced global loads due to trim by combining other effects. However, due to this very low estimate of seiching induced pitch angle, there is negligible influence on the global induced load response.

The seiching induced heave causes negligible errors in wetdeck slamming induced global loads. Since the heave is equal to the local seiching amplitude, the relative distance to the wetdeck does not change and hence the slamming loads are not effected. Further, the submerged volume of the vessel is not changed due to this effect. This means hydrodynamic loads on the side hulls are not effected.

6.3.3 Wave measurement inaccuracies

The measurement accuracy by the wave probes is not exactly known. The free surface tension at the wave probe causes meniscus effects and is an error source in the measurements. If the ambient velocity at the wave probe is high, the local water elevation due to the probe may matter. Ventilation may occur due to suction on the downstream side of the probe as an extreme case of high velocity. These error sources were discussed by Greco (2001) and related to the diameter of the wave probe. The meniscus effect is most relevant in our case. Stansberg (2002) suggests that the measurement accuracy could be $\pm 0.001m$. We should consider this as an error source that is independent of the wave frequency effects. The analysis presented in Fig. 6.9 can serve as basis for estimating the corresponding error. This gives Table 6.5.

Table 6.5 Relative errors in global loads due to error in wave measurements; Case 1114 with wetdeck slamming

	VSF Cut1(N)	VBM Cut1(Nm)	VSF Cut2(N)	VBM Cut2(Nm)
Relative Error	0.055	0.102	0.087	0.057

6.4 Roll, yaw and sway

Head sea was intended but a small deviation from head sea occurred in the experiments, causing small amplitude roll, yaw and sway. In addition there was a constant small roll angle due to an unintended asymmetric mass distribution about the center plane. An autopilot system was used to keep the heading of the vessel. This may also cause rolling. These effects can not be simulated by our numerical model.

The different experimental cases gave different mean yaw angles. Furthermore, the MRU and the Optical measurement systems predicted different mean values for the same case. However, the mean heading relative to head sea was not large and less than 1^0. Experimental data showed

that the ship also had an unintended mean roll angle of less than 1^0, which means that the deck plate will not be wetted at the same moment transversely as assumed in the 2D analysis. This kind of 3D effect influences in particular the initial impact force. The 3D effect is particular large if the initial impact occurs at flat part of the deck away from the front end of the wetdeck. The initial 2D slamming force is then finite while the initial 3D slamming force is always zero. Since the numerically predicted slamming occurs initially at the front end of the wetdeck, the initial 2D slamming load is zero in case 1114 (See Fig. 5.20(a)).

The consequence of the roll, yaw and sway is that the measured VSF and VBM on the two hulls were not identical. Figure 6.10 illustrates the difference of measured VSF and VBM data at Cut1 and Cut2 between the starboard and port hulls for case 1114.

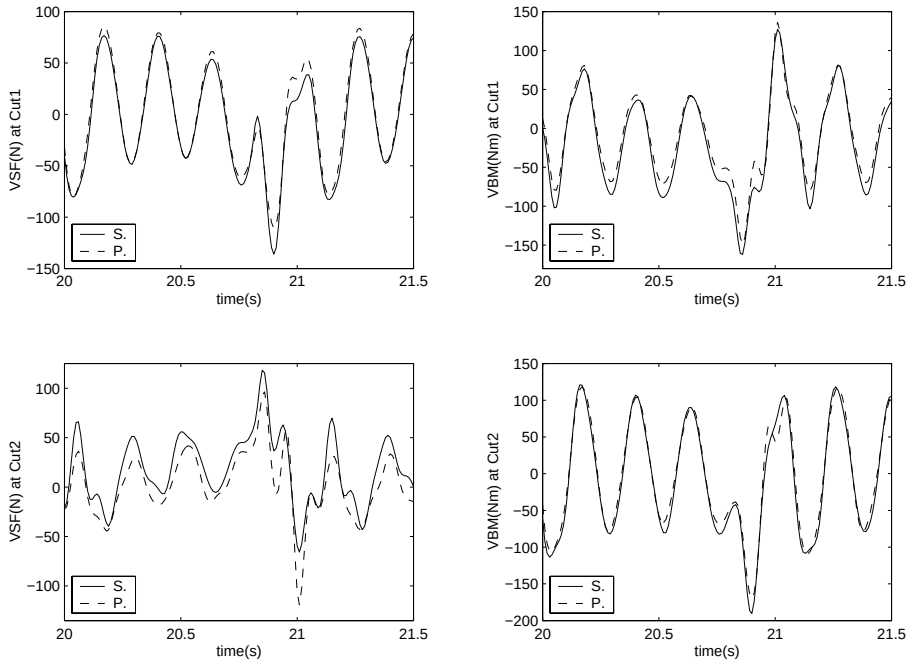

Figure 6.10 Experimental vertical shear force (VSF) and vertical bending moment (VBM) for case 1114 at starboard (S.) and port (P.) side hulls of the vessel

Further, Figs. 6.11 to 6.12 show the local maximum and minimum values of the time record for case 1114. We note that the difference between measured VSF and VBM at starboard and port side hull at the two cuts is largest for VSF at Cut2. From the maximum and minimum values in these figures, relative error between the starboard and port side can be estimated. For example for the maximum peaks of vertical shear forces at Cut1, there are 10 pairs of data shown in Fig. 6.11(a). The two values in each pair are respectively from starboard and port side. Standard deviation and mean values can be calculated by this pair of data. Further, the ratio between the standard and mean value gives the relative error between two side hulls. The mean value of the ratios from the 10 pairs data is then taken as the representative relative deviation of the maximum peak of vertical shear forces at Cut1. Similar estimation is done for the minimum values in Fig. 6.11(a). The same procedure can be applied for other load data in Figs. 6.11(b)

to 6.12. This gives Table 6.6.

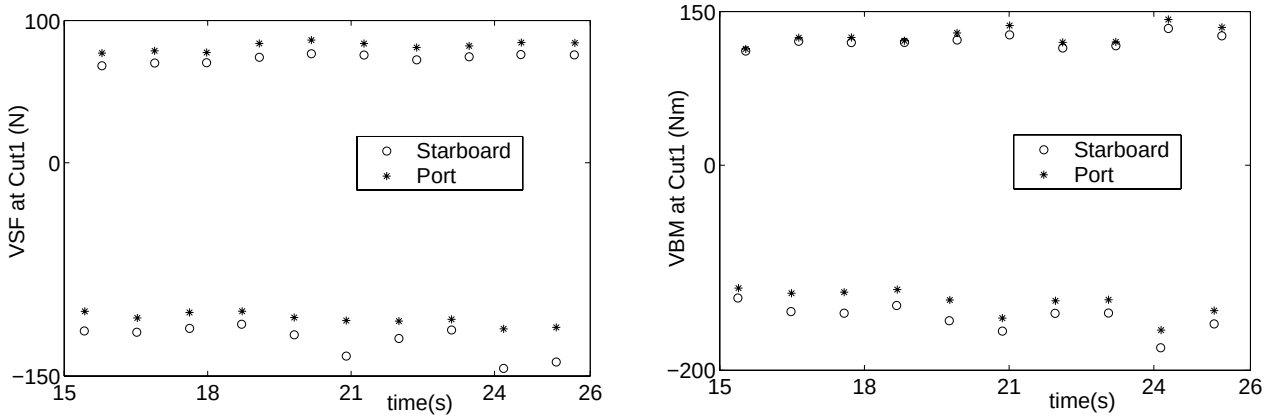

(a) VSF at Cut1 (b) VBM at Cut1

Figure 6.11 Local maximum and minimum values of vertical shear force (VSF) and vertical bending moment (VBM) at longitudinal transducers at Cut1 at starboard and port side hulls, case 1114

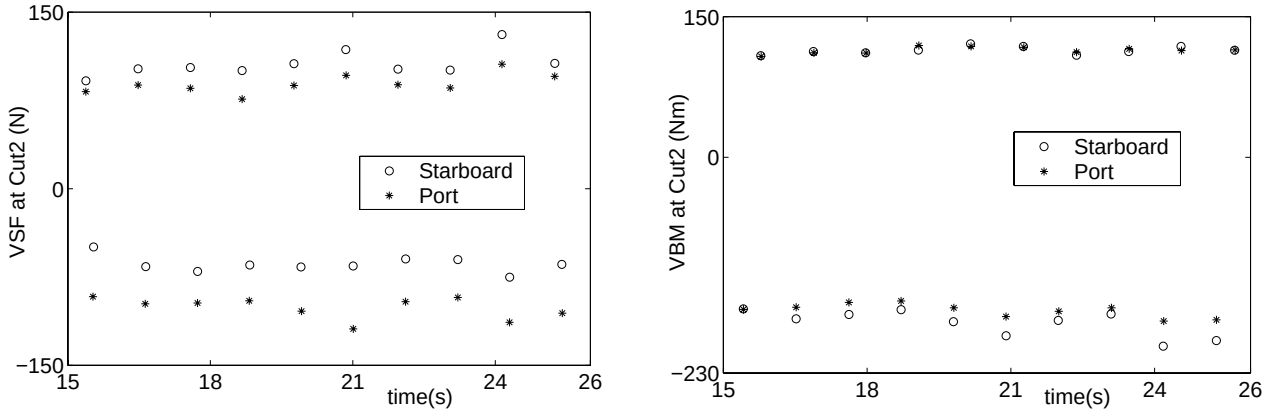

(a) VSF at Cut2 (b) VBM at Cut2

Figure 6.12 Local maximum and minimum values of vertical shear force (VSF) and vertical bending moment (VBM) at longitudinal transducers at Cut2 at starboard and port side hulls, case 1114

It is seen that the largest starboard and port side deviation occurs at VSF at Cut2. Here the absolute maximum values of the vertical shear forces and vertical bending moments are of concern. It means that minimum VSF at Cut1, minimum VBM at Cut1, maximum VSF at Cut2 and minimum VBM at Cut2 will be listed to represent the relative error. Table 6.7 then presents the resulting relative error of the global forces at Cut1 and Cut2 due to the asymmetry of measured values on starboard and port sides.

Table 6.6 Relative deviation of peak values of vertical shear force (VSF) and vertical bending moment (VBM) in Figs. 6.11(a) to 6.12(b). 'Max.' and 'Min.' refer to maximum and minimum of the corresponding load data.

VSF	Max. at Cut1	Min. at Cut1	Max. at Cut2	Min. at Cut2
Relative deviation [–]	0.078	-0.091	0.123	-0.317
VBM	Max. at Cut1	Min. at Cut1	Max. at Cut2	Min. at Cut2
Relative deviation [–]	0.030	-0.076	0.013	-0.055

Table 6.7 Relative errors in global loads due to roll, yaw and sway. Case 1114 with wetdeck slamming

	VSF Cut1(N)	VBM Cut1(Nm)	VSF Cut2(N)	VBM Cut2(Nm)
Relative Error	0.091	0.076	0.123	0.055

6.5 Sinkage and trim angle

The steady trim angle and sinkage of the vessel would effect the slamming occurrence. The experimental trim angle is -0.074^0 at zero forward speed and calm water. The negative value means bow down. However, the trim angle will change with forward speed for a ship moving in calm water. Further, the presence of incident waves interacting with the ship causes a mean second order trim moment. This means a contribution to the trim angle that is proportional to the incident wave amplitude square. The physical explanation is similar as for mean wave drift forces (Faltinsen (1990)). Our numerical method can not estimate this effect and we must rely on experimental recordings. However, the recordings based on the MRU and the Optical measurement system as well as the measurements of the relative vertical motions by a wave probe at the bow did not show consistent results.

The cases that we studied here have Froude number (Fn) between 0.30 and 0.33. Molland *et al.* (1995) presented experimental mean sinkage and trim angles for different types of catamaran hulls at different Froude numbers. However, there were no incident waves during the experiments. The model shapes presented in their paper do not completely match ours, but the general tendency of the influence of mean sinkage and trim angles on Fn is clear. The results show that the mean trim angle starts to have a large influence from forward speed when Fn is larger than 0.35. The value was less than 0.25 degree when $Fn < 0.35$ for all the tested vessels. The mean sinkage value depends on Fn but it is not larger than 5% of the ship draft when $Fn \leq 0.35$. It corresponds to that the mean sinkage is less than $0.05 \times 0.22 = 0.01m$ in our case. The analysis in Section 6.5.1 will show the mean heave value is only $-0.002m$ based on the experimental results. The mean sinkage due to seiching has been discussed in Section 6.3, and is believed to have negligible effects on slamming induced global loads.

6.5.1 Sinkage effect

The influence of sinkage on global loads can partly be seen from the previous studies of the wave elevation influence in Section 6.3. The reason is that both wave elevation and sinkage will affect the relative vertical motion at the slamming position in a similar way. This means that there is a similar influence on the wetted length of the wetdeck. However, the waves contribute directly to the relative impact velocity, while the sinkage does not. We therefore has to investigate separately the influence of wetdeck height.

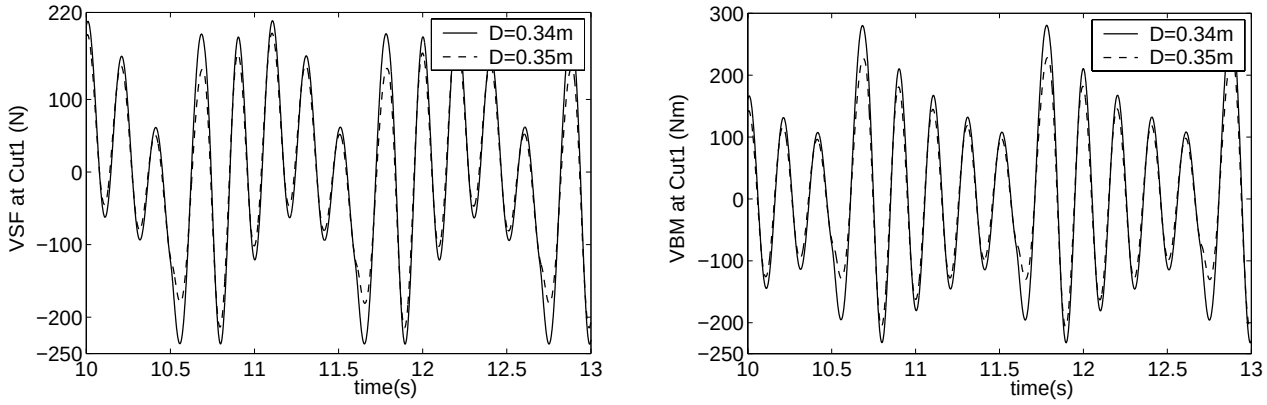

(a) VSF at Cut1

(b) VBM at Cut1

Figure 6.13 The influence of wetdeck height measured from base line on vertical shear force (VSF) and vertical bending moment (VBM) at Cut1 for case 1114, deck height D is at COG and is measured relative to base line; Calculated values.

Table 6.8 The influence of wetdeck height on global loads for case 1114

Deck Height	VSF Cut1(N)	VBM Cut1(Nm)	VSF Cut2(N)	VBM Cut2(Nm)
0.34m	237.2	280.7	127.1	383.2
0.35m	214.8	229.0	108.9	345.0
Increase Ratio [-]	-9.4 %	-18.4%	-14.3 %	-10.0 %

Figure 6.13 and Table 6.8 show that when deck height is changed from $0.34m$ to $0.35m$ referring to the base line and COG, peak values of VSF and VBM will be decreased at most by 18%. It is noted that we have not changed the draft accordingly in the calculations of hydrodynamic loads on the side hulls. Since vertical loads are considered, the draft has a minor influence relative to length and breadth. In the experiments, the different measurement systems for motions gave inconsistent results for mean values of motions. The vertical reference value for the optical system can not be trusted. In order to make estimates, we have relied on the MRU system. In case 1107, the MRU system gave $-0.00069m$ sinkage at the point where the MRU system was installed. Sinkage is defined as positive downwards. It is noted that the MRU system is installed $2.08m$ from the stern, and that the global COG in our system is $1.632m$ from the stern.

This means that the MRU position has the x-coordinate $-0.448m$ in our global COG system. Further, the MRU system gives the mean trim angle 0.630^0 with positive value corresponding to bow up. Based on the relationship between heave and pitch $\eta_3 - x\eta_5$ in our coordinate system, a mean heave value of $-0.002m$ is found. Based on this value and the previous deck height analysis, we can estimate the error in global loads due to mean sinkage is around 3.0%, as shown in Table 6.9. However, we here have in the estimate of sinkage assumed that the trim has no uncertainty. This is not correct as will be clear in the next section on trim.

Table 6.9 Relative errors in global loads due to error in sinkage; Case 1114 with wetdeck slamming

	VSF Cut1(N)	VBM Cut1(Nm)	VSF Cut2(N)	VBM Cut2(Nm)
Relative Error	0.019	0.037	0.029	0.020

6.5.2 Trim effect

Figures 6.14 to 6.15 and Table 6.10 show that the inclusion of a small mean trim angle of 0.3^0 for case 1114 can greatly decrease the peak values. The increase of mean trim angle by 0.3^0 will decrease the peak values of vertical shear force and bending moment at two cuts approximately 20%. Further, the maximum double amplitude values will be influenced at the similar rates.

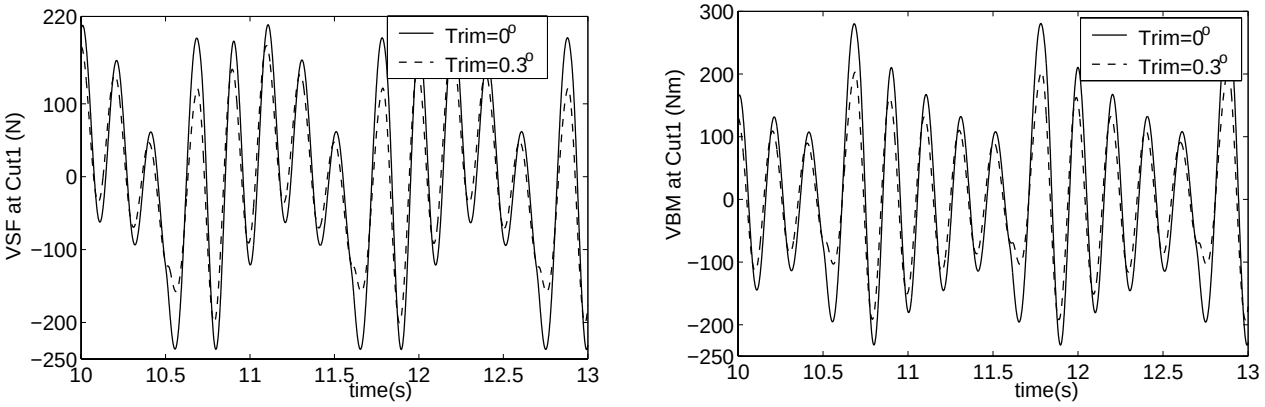

(a) VSF at Cut1

(b) VBM at Cut1

Figure 6.14 The influence of trim on vertical shear force (VSF) and vertical bending moment (VBM) at Cut1 for case 1114. Calculated values.

The MRU and Optical system predicted for case 1107 mean trim angles of 0.630^0 and -0.854^0 respectively. This causes uncertainty in estimating the mean trim angle. The error due to slowly varying seiching induced angle was discussed in Section 6.3 and gave negligible amplitude. This is therefore unnecessary to consider in this context. Since the measurements for our case indicate uncertainties, the experimental results presented Molland *et al.* (1995) are used as a basis for the estimate. Molland *et al.* (1995) shows that the change in mean trim angles due to forward speed are not larger than 0.25^0 in all the experiments done for $F_n < 0.35$. The mean trim angle

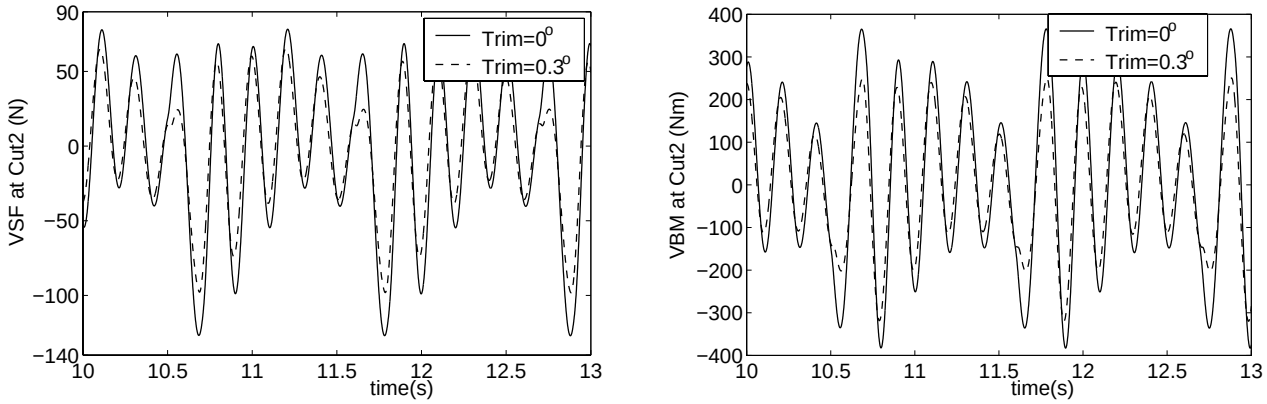

(a) VSF at Cut2

(b) VBM at Cut2

Figure 6.15 The influence of trim on vertical shear force (VSF) and vertical bending moment (VBM) at Cut2 for case 1114. Calculated values.

Table 6.10 Trim influence for case 1114. 'Max.' means the maximum value in the global response and 'Range' means the value between maximum and minimum. Calculated values.

Trim (deg.)	VSF Cut1(N)	VBM Cut1(Nm)	VSF Cut2(N)	VBM Cut2(Nm)
0.0^0 (Max.)	237.2	280.7	127.1	383.2
0.3^0 (Max.)	200.8	204.0	98.3	320.1
Increase Ratio [-]	-15.3 %	-27.3 %	-22.6 %	-16.5 %
0.0^0 (Range)	446.0	513.4	205.5	749.2
0.3^0 (Range)	381.2	396.2	164.1	570.9
Increase Ratio [-]	-14.5 %	-22.8 %	-20.2 %	-23.8 %

at zero speed is in our case -0.074^0. If 0.25^0 is taken as the mean trim angle, the relative error for the slamming induced global loads is at most 0.23, as in Table 6.11.

Table 6.11 Relative errors in global loads due to error in trim; Case 1114 with wetdeck slamming

	VSF Cut1(N)	VBM Cut1(Nm)	VSF Cut2(N)	VBM Cut2(Nm)
Relative Error	0.128	0.228	0.189	0.137

6.6 Mass distribution

Since the mass distribution of the catamaran was reported in terms of rather few mass points together with an estimated local pitch radius of gyration (See Appendix A.4), there is an uncertainty related to the experimental mass distribution. Figures 6.16 to 6.17 show the effect on

global loads by setting the local pitch radius of gyration of mass points equal to zero when no wetdeck slamming occurs. This indicates that the effect of errors in mass distribution is not dominant except for VSF at Cut2.

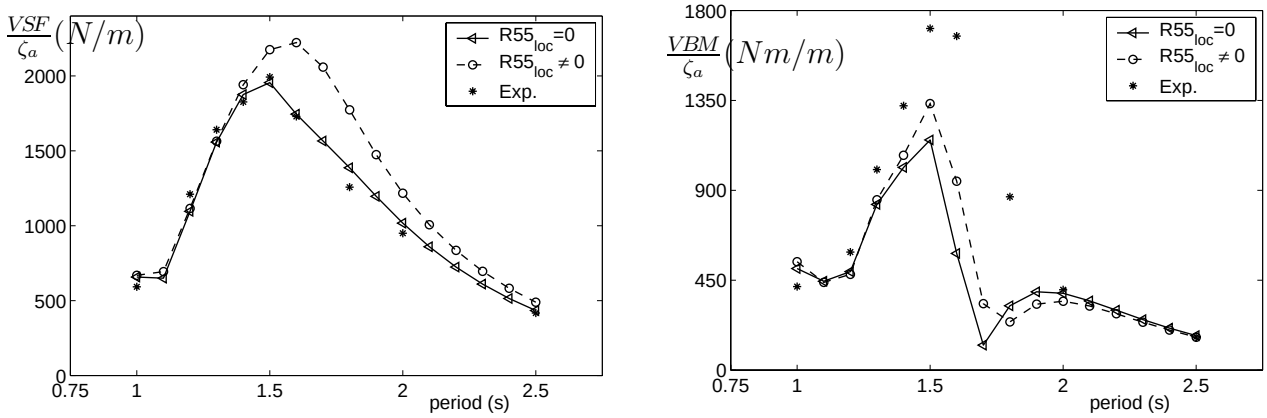

(a) VSF at Cut1 (b) VBM at Cut1

Figure 6.16 Influence of local pitch radius of mass distribution on linear transfer function of vertical shear force (VSF) and vertical bending moment (VBM) at Cut1 with $U = 1.9m/s$; No wetdeck slamming

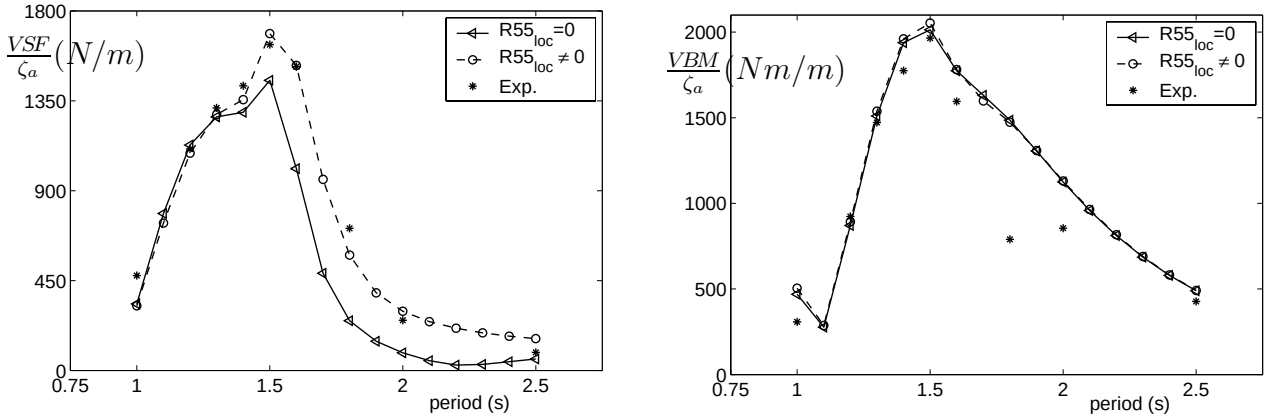

(a) VSF at Cut2 (b) VBM at Cut2

Figure 6.17 Influence of local pitch radius of mass distribution on linear transfer function of vertical shear force (VSF) and vertical bending moment (VBM) at Cut2 with $U = 1.9m/s$; No wetdeck slamming

Figures 6.18 to 6.19 and Table 6.12 show the mass distribution effect on the global VSF and VBM effect when wetdeck slamming happens for case 1114. It shows that the deviation can be around 25%. We note from the figures that the different mass distribution will change the eigenfrequencies of higher modes.

In reality the effect of error in mass distribution is far as extreme as shown in Figs. 6.18 to 6.19 and Table 6.12. However, we have no possibility to control this in more detail. Therefore this

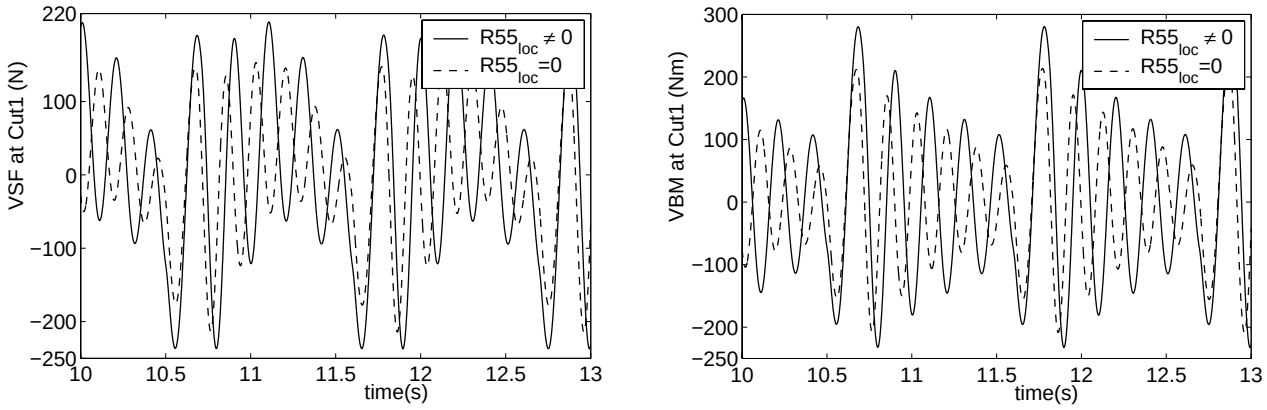

(a) VSF at Cut1 (b) VBM at Cut1

Figure 6.18 The influence of mass distribution on vertical shear force (VSF) and vertical bending moment (VBM) at Cut1 for case 1114. Calculated values.

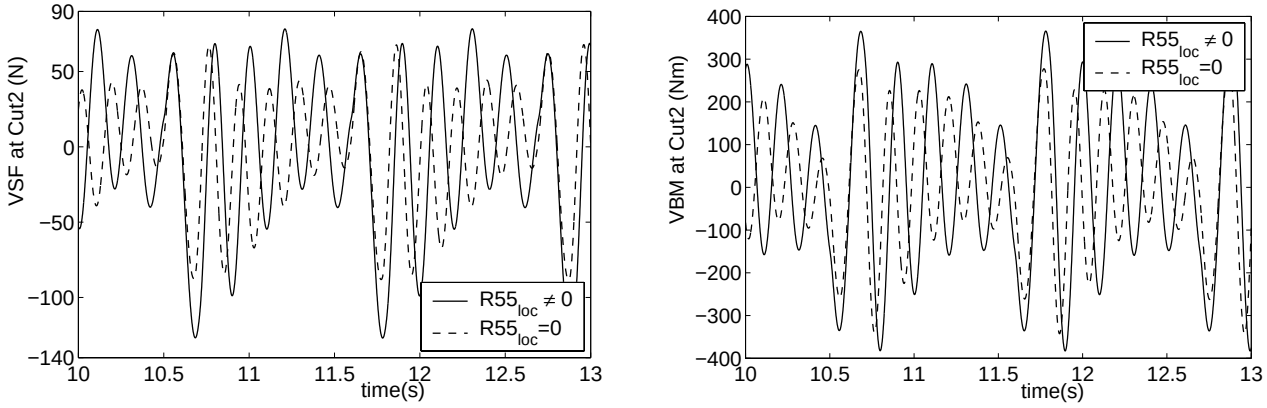

(a) VSF at Cut2 (b) VBM at Cut2

Figure 6.19 The influence of mass distribution on vertical shear force (VSF) and vertical bending moment (VBM) at Cut2 for case 1114. Calculated values.

Table 6.12 The influence of mass distribution on maximum values of global loads for case 1114

$R55_{loc}$	VSF Cut1(N)	VBM Cut1(Nm)	VSF Cut2(N)	VBM Cut2(Nm)
$\neq 0$	237.2	280.7	127.1	383.2
$= 0$	214.9	214.5	88.6	343.9
Increase Ratio [-]	-9.4 %	-23.6 %	-30.3 %	-10.3 %

source of uncertainty will not be included in the following combined error estimation.

We should also recall that we already have reported on a consequence of the error in the mass distribution. This was associated with that mass distribution was not completely symmetric with

respect to the center plane of the catamaran and caused an unintended small mean roll angle. This contributed to that the ship heading was slightly different from head sea. The consequence of this was also oscillatory roll, yaw and sway motions. This effect has been investigated in Section 6.4.

6.7 Model geometry

Uncertainties occur due to manufacturing accuracy of the model. However, this is hard to quantify. It can also occur due to wrong information. For instance we had for a long time been informed to have a body plan that gives the bow ramp angle 6.35^0. Then it turned out that it was 3.72^0 (See Fig. 6.20). We will illustrate the sensitivity of global wetdeck induced loads to the bow ramp angle.

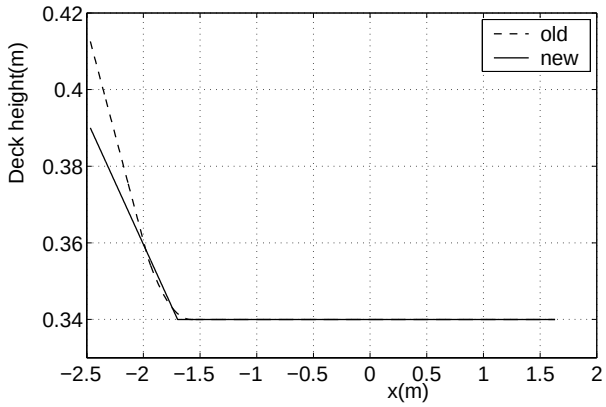

Figure 6.20 Longitudinal cross-section of wetdeck surface illustrating bow ramp angles 3.72^0 and 6.35^0. $x = 0$ refers to the longitudinal COG of the catamaran.

Figures 6.21 to 6.22 compare the results for a bow ramp angle of 3.72^0, of 6.35^0 and flat wetdeck case. Table 6.13 shows that the relative deviation can be around 50% between the two finite angle cases. Figures 6.21 to 6.22 and Table 6.13 present also the data for theoretical results when the wetdeck is flat. Then the relative deviation of global forces for the flat deck and the 3.72^0 bow ramp case is around 15%.

Figure 6.23 shows the time history of the vertical impact load in the two bow ramp cases. It should be noted that the water hits initially at the front deck end for the 3.72^0 bow ramp case while it hits initially at a distance from the front deck end and in a flat part of Deck1 for the 6.35^0 bow ramp case. This gives larger initial impact force for the 6.35^0 bow ramp case as discussed in Section 1.2. This is also shown in Fig. 6.23. The peak value for case 6.35^0 reaches $12000N$. However, the 3.72^0 bow ramp case give much larger global loads than the 6.35^0 bow ramp case. The force magnitude except for the initial phase is generally much larger for the 3.72^0 bow ramp case. Furthermore, the slamming load lasts much longer for the 3.72^0 bow ramp case. This is a simple consequence of that the higher bow ramp angle cause a larger vertical distance to the

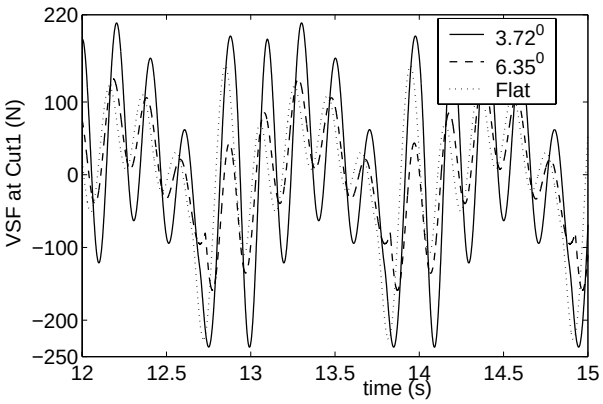

(a) VSF at Cut1

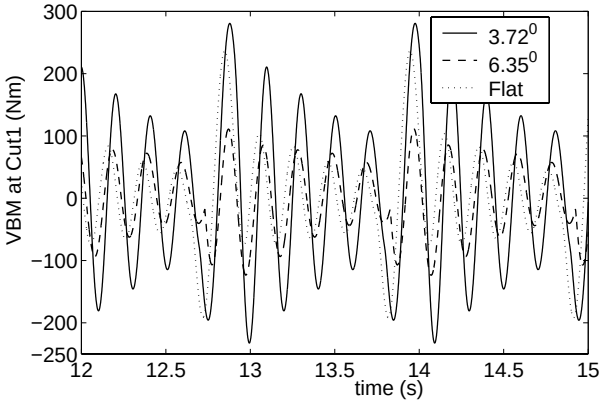

(b) VBM at Cut1

Figure 6.21 Influence of bow ramp angle on vertical shear force (VSF) and vertical bending moment (VBM) at Cut1 for case 1114; Calculated values

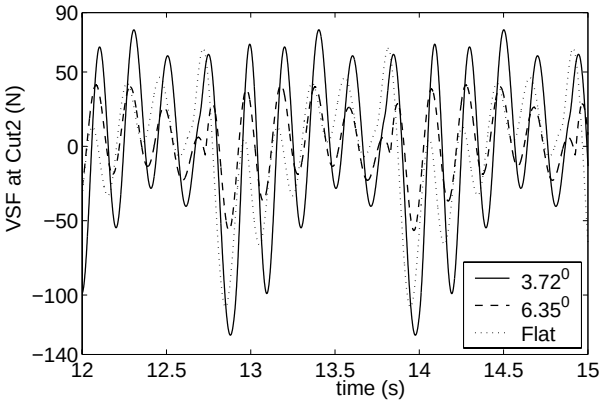

(a) VSF at Cut2

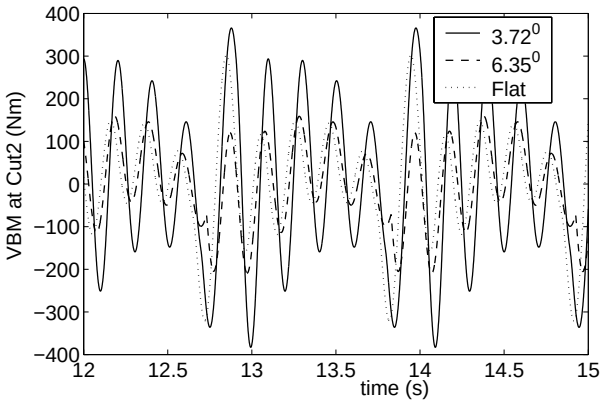

(b) VBM at Cut2

Figure 6.22 Influence of bow ramp angle on vertical shear force (VSF) and vertical bending moment (VBM) at Cut2 for case 1114; Calculated values.

Table 6.13 Influence of bow ramp angle on maximum values of global loads for case 1114; the 'increase ratio' is calculated by comparing bow ramp angles 6.35^0 and 3.72^0 cases, and the 'flat' and 3.72^0 cases; 3.72^0 is the base case in both calculations.

Wetdeck	VSF Cut1(N)	VBM Cut1(Nm)	VSF Cut2(N)	VBM Cut2(Nm)
Bow ramp 3.72^0	237.2	280.7	127.1	383.2
Bow ramp 6.35^0	170.1	142.8	66.1	238.7
Increase Ratio [-]	-28.3 %	-49.1 %	-48.0 %	-37.7 %
Flat	231.7	242.8	110.5	329.5
Increase Ratio [-]	-2.1 %	-13.5 %	-13.0 %	-14.0 %

mean free surface. This explains the higher global loads for the 3.72^0 bow ramp case and shows the sensitivity of slamming.

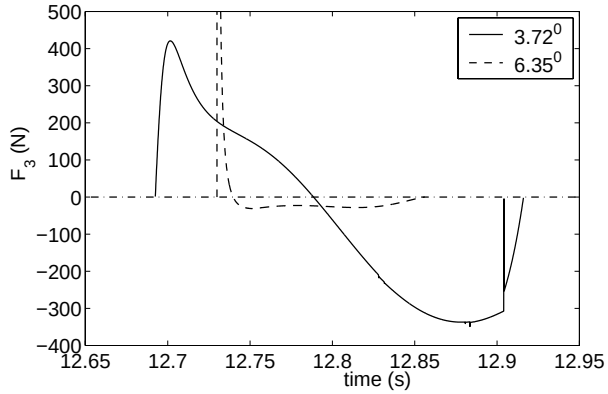

Figure 6.23 Vertical impact force comparison for bow ramp angles 3.72^0 and 6.35^0, case 1114; Calculated values.

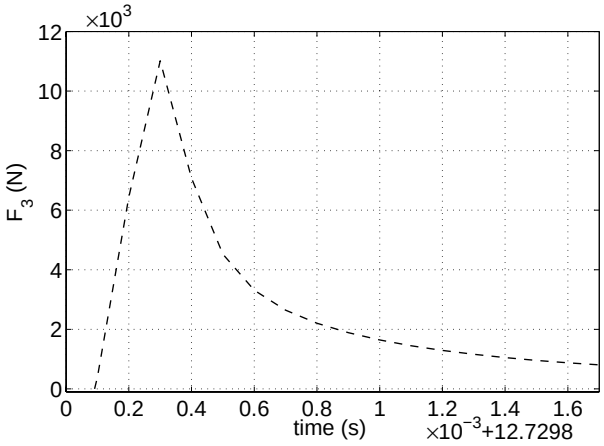

Figure 6.24 Vertical impact force during initial slamming phase; Bow ramp angle 6.35^0, case 1114; Calculated values.

The above analysis shows the influence of the angle between water and ramp to the global response. Further studies are needed to find out the sensitivity to the other geometric shapes of the wetdeck in the bow area. This example also illustrates consequences of possible human errors in the experimental results. We certainly hope that we have got the information about the bow ramp angle right, but there could be other undetected errors like wrong distance between the base line and the wetdeck.

6.8 Summary

Assuming that all the error sources discussed above are stochastically independent, we can combine the effect of the elementary error sources by $\Delta = \sqrt{\sum_i \Delta_i^2}$. Here Δ_i is the relative error associated with error source number i and Δ is the combined relative error. This gives the results presented in Table 6.14.

It is seen from Table 6.14 that the largest contribution is from the trim angle. The errors due to the spatially changing incident waves and in the wave measurement are equally the second most important for VBM. The errors associated with roll, yaw and sway is the second most important for VSF. We can now relate the error estimates to the comparisons between experiments and theory presented in Figs. 5.23 to 5.24 for case 1114. The agreement will be improved if experimental relative error is accounted for, as shown in the following Figs. 6.25 and 6.26.

Figures 6.25 and 6.26 show that numerical values are almost located within the experimental band. However, the values at the Cut2 have still visible differences. Obviously there are also

Table 6.14 Relative error in global loads due to individual error sources as well as combined experimental relative error due to these error sources; case 1114

Error source	VSF Cut1(N)	VBM Cut1(Nm)	VSF Cut2(N)	VBM Cut2(Nm)
speed	0.033	0.032	0.029	0.030
Wave amplitude	0.055	0.102	0.087	0.057
Seiching	~ 0.0	~ 0.0	~ 0.0	~ 0.0
Wave measurement	0.055	0.102	0.087	0.057
Roll, yaw and sway	0.091	0.076	0.123	0.055
Sinkage	0.019	0.037	0.029	0.020
Trim	0.128	0.228	0.189	0.137
COMBINED	0.179	0.285	0.260	0.172

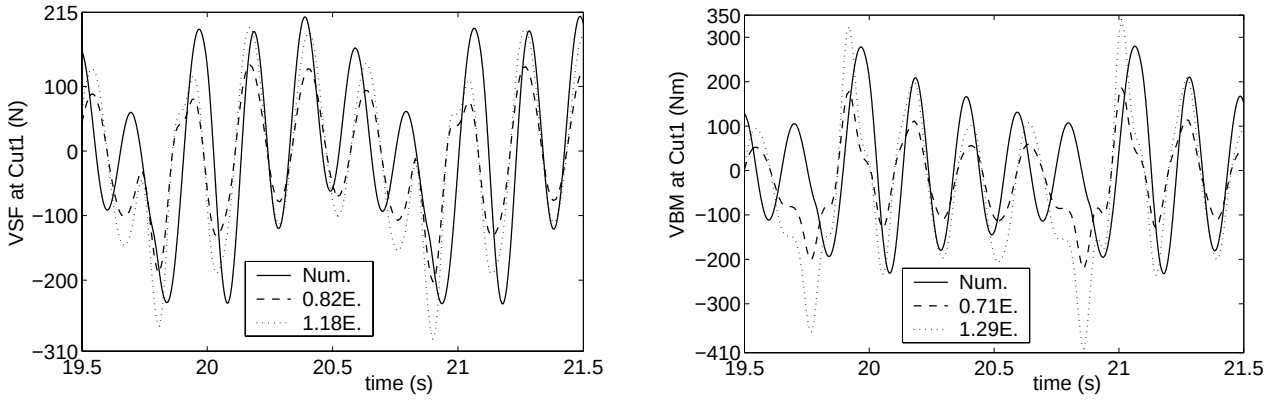

(a) VSF at Cut1

(b) VBM at Cut1

Figure 6.25 Comparisons between Experimental and Numerical values of vertical shear force (VSF) and vertical bending moment (VBM) at Cut1 for case 1114; Experimental data band based on the relative error in Table 6.14, 'E.' means that the experimental data are obtained by adding the values of the starboard and port sides.

theoretical error sources, which will be discussed in the following chapter. It will be shown that hull interaction can be an important theoretical error source. The nonlinear forces on the side hull may also contribute to the deviation. It is noted here that due to the difficulty in making reasonable error estimates associated with mass distribution and model geometry, they are not included in Table 6.14. Furthermore, no random errors are accounted for in Table 6.14. Since the experiments were not repeated, this is impossible to do. This means that only systematic errors are considered. However, there may be other systematic errors associated with instrumentation, data acquisition and data analysis. Since we did not do the experiments, and there is a long experience with the equipment and data procedure, we chose in this context not to consider these error sources.

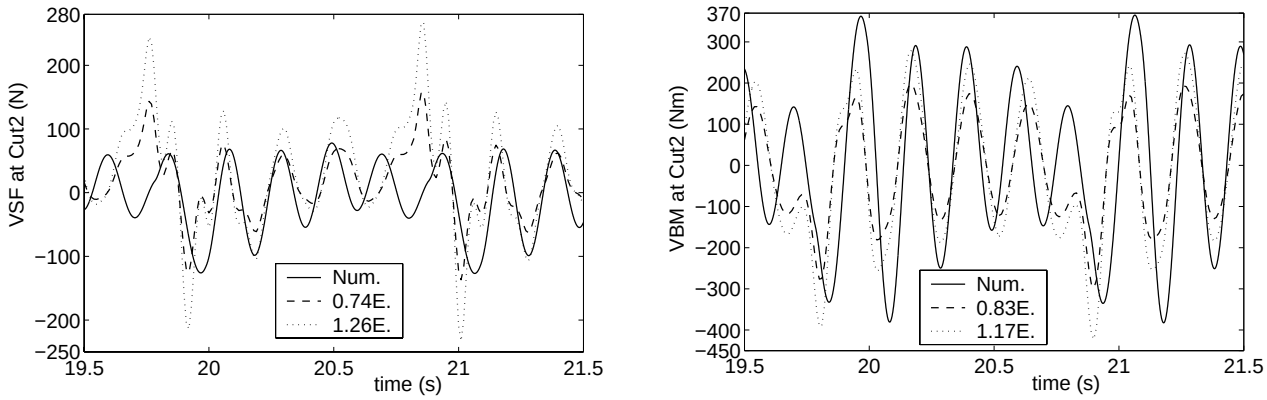

(a) VSF at Cut2

(b) VBM at Cut2

Figure 6.26 Comparisons between Experimental and Numerical values of vertical shear force (VSF) and vertical bending moment (VBM) at Cut2 for case 1114; Experimental data band based on the relative error in Table 6.14, 'E.' means that the experimental data are obtained by adding the values of the starboard and port sides.

Chapter 7

Error Analysis in the Theory

7.1 Introduction

Theoretical errors can be classified as physical, human and numerical errors (See Faltinsen and Svensen (1990), The report of the 19th ITTC panel on validation (Aláez *et al.* (1990))). Moan *et al.* (1991) in the report of the committee IV.1 on design philosophy of the 11th ISSC illustrated how the analysis procedure can be divided into different stages: physical reality, conceptual model, continuous mathematical model, discrete numerical model, computer code, and results presentation by available input data. Each step involves some specific error sources and needs validation or verification.

Herein, physical errors are associated with that we have made a conceptual model of physical reality and represented this by a continuous model based on some assumptions or simplifications of the physical effects. The model needs then to be validated. That means for instance comparisons with model tests with properly controlled experimental errors. Benchmark numerical codes can also be used as part of the validation process. Since no analytical solutions exist of the total continuous mathematical model, the model has to be discretized and numerical errors would obviously arise. Convergence studies and comparisons with analytical solutions for specific cases and/or with benchmark numerical results based on the same continuous mathematical model are means to verify that the discretized mathematical model is consistent with the continuous mathematical model.

Human errors can be involved at different stages of the process. Human errors in implementing a numerical method are due to programming errors, use of wrong input data or interpretation errors of results. Presence of no programming errors can never be guaranteed, but will obviously be decreased by increasing number of verification and validation tests. Since the main program is self made except for the part that calculates hydrodynamic coefficients on the side hulls, the danger of wrong input data and interpretation errors is minimized. Another way of detecting human errors is by comparative studies by independent users and computer programs based on

the same theory. This has for instance been done by ITTC, ISSC and Nielsen and Herfjord (1992) for wave induced motion and loads on ships and marine structures. Since the total theoretical model for global wetdeck slamming induced response is new and developed as a part of this thesis, this is obviously impossible in our case. So we focus on the physical and numerical errors. It should be noted that systematic verification and validation of our theoretical model have been done in Chapter 5 for both with slamming and without slamming cases. Verification studies for the slamming model were presented in Chapters 3 and 4. The error source investigations in this chapter will make the numerically and physically theoretical error analysis more complete. However, many effects can only be qualitatively discussed.

The tested cases 1111, 1112,1114, 1115 with wetdeck slamming (See Table A.7) will be discussed for physical error effects. The most severe slamming case, *i.e.* case 1114 with $T = 1.8s$, $U = 1.8m/s$ and $\zeta_a = 0.041$ in head sea, is still used in the quantitative error analysis.

7.2 Physical errors

In this section, the physical errors associated with

- incident waves
- side hull hydrodynamics: linear hydrodynamic effects, nonlinear side hull forces
- slamming modelling: 3D slamming, Kutta condition, other slamming model errors
- structural modelling: transverse bending
- transient phase

will be discussed.

7.2.1 Incident waves

Linear incident waves are assumed in calculating the global loads. Second order wave theory was used in calculating the impact forces on a fixed horizontal platform deck in Fig. 4.4. This showed that second order wave effects have a small influence on the impact loads for the incident wave conditions that we consider for the catamaran cases. The consequence is also a small influence on the global response. This indicates that the linear wave assumption for the cases studied, is appropriate.

7.2.2 Side hull hydrodynamics

Important theoretical error sources are associated with the hydrodynamic loads on the side hulls, when using a linear frequency domain strip theory solution where the frequency corresponds to the frequency of encounter and no hydrodynamic interaction between the side hulls are considered. The error sources are related both to linear and nonlinear hydrodynamic loads.

Linear Hydrodynamic effects

There are two main subjects to be considered. One is associated with using a frequency domain solution instead of a time domain solution. The other subject is related to the errors in the frequency domain solution.

Since the impact on the wetdeck causes transient hydrodynamic loads on the side hulls, a time domain solution should ideally have been used instead of a frequency domain solution for the linear hydrodynamic loads on the side hulls. A time domain solution for hydrodynamic effects means that the hydrodynamic loads due to body motion can not be expressed explicitly in terms of added mass and damping terms. Instead convolution integrals are used (Ogilvie (1964)). It is straightforward theoretically to transform a linear frequency domain solution to a time domain solution (Ogilvie (1964)), but the numerical implementation is troublesome. It needs very accurate estimates of either added mass or damping coefficients for all frequencies. The numerical inaccuracies using a time domain solution as outlined by Ogilvie (1964) have for instance been pointed out by Adegeest (1995) and Rognebakke and Faltinsen (2002).

Only the encounter frequency is considered in this thesis when calculating added mass and damping coefficients. However, the frequencies associated with transient wetdeck slamming induced global two-node and three-node bending differ clearly from the frequency of encounter. It has in Chapter 5 been pointed out that this causes some differences between experimental and theoretical natural frequencies for two-node and three-node bending. But this effect has small influence on maximum wetdeck slamming induced global loads. The error sources due to the presence of many frequencies will therefore not be pursued further. Instead the following discussions on the error sources of the linear side hull hydrodynamics will be based on a frequency domain solution.

The strip theory assumes implicitly small or moderate Froude number. It does not account for all the wave systems generated by the ship hull. It neglects the interaction between the local steady and unsteady flow. It is basically a high-frequency theory derived for monohulls (Ogilvie and Tuck (1969)). The high-frequency assumption implies that the resulting waves have a wave length of the order of cross-sectional length dimension. When we apply the strip theory to the catamaran, hydrodynamic interaction between the side hulls is neglected. The error caused by this will be further discussed in the following text.

The $2\frac{1}{2}D$ high speed theory by Faltinsen and Zhao (1991) has a better theoretical basis than the strip theory, when Froude number is larger than $0.4 \sim 0.5$. It accounts for the divergent wave systems and neglect the transverse wave systems. Froude number in cases 1111, 1114, 1115 with the length $3.78m$ between perpendiculars are 0.302, 0.296 and 0.328 respectively. However, if only Body1 is considered, then the Froude number is respectively 0.483, 0.472 and 0.525 based on using the length $1.48m$ of the forward segment as a characteristic length. Since there is no rational way to combine the $2\frac{1}{2}D$ theory and the strip theory, strip theory is applied here.

The strip theory predicts only wave system which has wave crests parallel to the ship's longitudinal axis and extending over the ship length. This is inconsistent with the theoretical far-field wave picture. If interaction between the ship hulls is considered by strip theory, it will cause

unrealistic wave interaction between the two hulls at certain frequencies. This can cause large errors in motion and load predictions (Hadler *et al.* (1974)), and is the reason why hydrodynamic hull interaction is neglected in this study.

If the unified theory by Newman (1977) was applied to a catamaran by assuming that the two hulls are hydrodynamically in each others far-field, a more realistic hull interaction can be predicted (Ronæss and Faltinsen (2000)). The unified theory assumes implicitly small and moderate Froude number (Ronæss (2002)) and neglects the interaction between unsteady and local steady flow. The results of wave predictions by a single hull presented by Ronæss and Faltinsen (2000) can be used to qualitatively judge the importance of wave interactions between the two hulls. The interior angle α between the outer part of the wave system and the ship's longitudinal axis can be expressed as

$$\tan\alpha = \frac{g}{2\omega_e U} \tag{7.1}$$

This implies that the waves caused by one of the hulls will be incident to the other hull at a distance of 65.56% of the length between perpendiculars from AP for case 1114. The corresponding numbers for cases 1111, 1112, 1115 are respectively 50.15%, 63.95% and 65.56%. These values show that the length along the ship side hulls of wave interaction is similar for the cases studied.

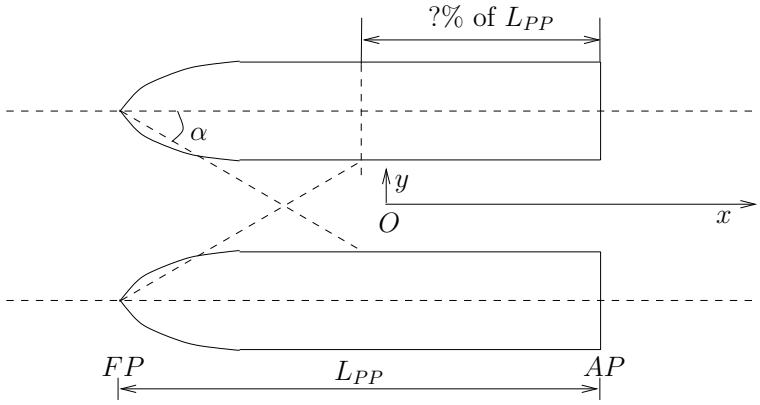

Figure 7.1 Illustration of hull interaction due to wave generation; α is the angle between center line of one hull and the outer part of the wave system generated by one hull without the presence of the other hull.

Wave interaction is of special concern if natural modes for the fluid motion between the hulls are excited. The most relevant mode for heave and pitch motions is the piston mode similar to what happens in a moonpool. This was extensively discussed in Section 5.6.3, where it was found to be of concern for case 1115. This discussion shows that hull interaction should be examined.

We will also illustrate by the model tests that hull interaction must be present. Figure 7.2 shows calculated and experimental relative vertical motion amplitudes at the midpoint of the catamaran, *i.e.* $1.96m$ from AP along the mid longitudinal section. No wetdeck slamming

occurs. The calculations assume that the wave elevation is the incident wave elevation. This is a good approximation at the bow as shown by Fig. 5.5. However, this is not the case at the midpoint. If we use the simple wave angle formula in Eq. (7.1), it shows also that there will be waves caused by the hull at the midpoint of the catamaran. Further, since the formula as described above implies that waves generated by one hull affect the other one, it shows that hull interaction must be considered.

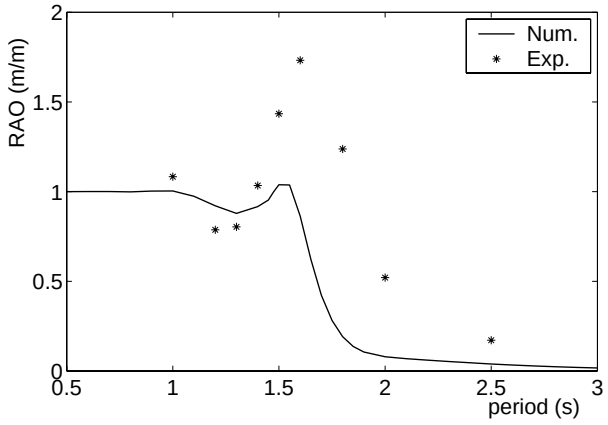

Figure 7.2 Experimentally and theoretically predicted transfer function (RAO) of relative vertical motions at $1.96m$ from AP. Cases without wetdeck impact. $U = 1.9m/s$ in the calculations; Experimental forward speed slightly different (See Table A.7 in Appendix A). Head sea.

An alternative theoretical way to calculate the hydrodynamic loads on the side hulls would for instance be to use a 3D Boundary Element Method with Rankine singularities and account for the proper free surface conditions. This would be a more numerically oriented method than the unified theory. It will require significantly longer simulation time and computer storage. This may imply practical limitations if time domain solution is needed to obtain statistical design values. Care must be shown in minimizing numerical errors for instance due to the panel size, implementation of a far-field condition and numerical differentiation in the free surface conditions. Since potential flow is then assumed, viscous effects must be included by empirical formula. However, since the considered hull has no sharp corner at transverse cross-sections along the ship, no significant vortex shedding in transverse cross-sectional planes of the ship is expected. This minimizes viscous effects. Using a model based on Navier-Stokes equation to rationally include viscous effects is still in its infancy relative to a potential flow method.

We should ideally have estimated the errors associated with all the above-mentioned error sources and analyzed the consequence for the response variables of interest. This may have been possible if a benchmark numerical method was available. We are aware of numerical methods which are theoretically more sophisticated than ours (See for instance the state-of-the-art review by Jensen *et al.* (2000)). However, if a more sophisticated code was applied, we had to properly control numerical errors when applying this method. Further, this method may also have physical errors. For instance not all methods account properly for the interaction between local steady and unsteady flow. Bertram (1995) has discussed the importance of this effect. Flow

separation from a transom stern is another difficulty occurring typically for Froude numbers larger than 0.3. Another matter which is relevant but does not strictly speaking belong in a section on linear effects, is the ability to handle nonlinear effects. This is needed in order to have a consistent rational method to predict wetdeck slamming induced global loads. However, this is still associated with difficulties for instance in how to handle breaking waves, body-water intersection and flow separation. Therefore rational linear methods are extended to nonlinear flow simulations by for instance including nonlinear Froude-Krylov and restoring loads and to find body-water intersection by a Von Karman type method.

Instead we will first use the linear strip theory in the frequency domain, *i.e.* for cases with no slamming, and compare with experiments. Some of this has already been presented in Chapter 5. For instance Fig. 5.5 shows reasonable agreement of the amplitude of relative motion at the bow. Since phases also play an important role in slamming predictions, phases should ideally also be compared. However, the recordings of different response variables were not synchronized relative to the incident wave measurements. An attempt was then made to estimate phases by using measured relative vertical motions at the bow, in combination with heave and pitch records. This was done by systematically varying the phasing between the recordings and by assuming the wave at the bow was unaffected by the ship and equal to regular waves with a given amplitude. However, the procedure was not completely satisfactory. One possible reason is that the incident wave amplitude was varying along the track of the vessel. This variation may cause a 10% change in wave amplitude as discussed in Section 6.3. In the following the detailed procedure for case 1114 is described.

As mentioned earlier, cases 1114 and 1107 had the same incident wave period $T = 1.8s$ but the expected (or intended) wave amplitudes were respectively $0.05m$ and $0.015m$. There is severe wetdeck slamming in case 1114 while no slamming happens in case 1107. The phases will be estimated from the data from case 1107 in order to minimize nonlinear effects . Since our linear theory is also part of the model for wetdeck slamming induced response, we will then later use the experience from case 1107 to see the consequences for wetdeck slamming induced global loads in case 1114.

It has been shown implicitly in Figs. 5.6 and 5.7 that the pitch motion at the mid segment could represent the pitch in the forward segment well for cases without slamming. So in this investigation a rigid catamaran is assumed to find phases by matching the numerical and experimental undisturbed incident waves at the bow point.

The velocity potential Φ_I of the incident waves is in our numerical model expressed as

$$\Phi_I = \frac{g\zeta_a}{\omega_0} e^{kz} e^{i(\omega_e t - kx)} \tag{7.2}$$

where ζ_a is the incident wave amplitude. x and z are defined by the global coordinate system in Fig. 2.3. ω_0 and ω_e are respectively circular frequencies of waves and encounter. k is the wave number and i is the complex unit. By using the linear dynamic free surface condition, we can

express the incident wave elevation ζ as

$$\begin{aligned}\zeta &= -\frac{1}{g}(\frac{\partial \Phi_I}{\partial t} + U\frac{\partial \Phi_I}{\partial x}) \qquad \text{on } z=0 \\ &= -i\zeta_a e^{i(\omega_e t - kx)} = \zeta_a e^{i(\omega_e t - kx - \frac{\pi}{2})} \\ &= \zeta_a e^{i(\omega_e t + \alpha_\zeta)} \qquad \text{with} \qquad \alpha_\zeta = -kx - \frac{\pi}{2}\end{aligned} \tag{7.3}$$

The relative vertical motion at the bow can be expressed as the relative displacement between the vertical deck motion and the incident waves at the bow. Then the incident wave elevation at the bow can be written as

$$\begin{aligned}\zeta_{aN} e^{i(\omega_e t + \alpha_{\zeta N})} =& \eta_{3aN} e^{i(\omega_e t + \alpha_{3N})} - x_N \eta_{5aN} e^{i(\omega_e t + \alpha_{5N})} \\ &- \eta_{raN} e^{i(\omega_e t + \alpha_{rN})}\end{aligned} \tag{7.4}$$

Here the subscript N refers to the 'Numerical' system. x_N is the x-coordinate of the bow point in the global COG system, corresponding to $x_N = -2.433m$. η_{raN} and α_{rN} are the amplitude and phase of relative displacement at the bow point. Similarly η_{iaN} and α_{iN} are amplitude and phase respectively, for heave ($i = 3$) and pitch ($i = 5$). Further, $\alpha_{\zeta N} = -kx_N - \frac{\pi}{2}$ as defined in Eq. (7.3). Here all the phases are relative to $e^{i\omega_e t}$.

There is a similar relationship as in Eq. (7.4) for the experimental system. Experimental data by the MRU system are used in our estimates. Heave and relative vertical displacement are in the experiments positive downwards into the water, *i.e.* opposite to our numerical system. However, the numerical and experimental systems have the same definition of positive pitch. This means positive pitch corresponds to bow up. The incident waves at the bow can then be expressed as

$$\begin{aligned}\zeta_{aE} e^{i(\omega_e t + \alpha_{\zeta E})} =& -\eta_{3aE} e^{i(\omega_e t + \alpha_{3E})} - x'_E \eta_{5aE} e^{i(\omega_e t + \alpha_{5E})} \\ &- (-\eta_{raE} e^{i(\omega_e t + \alpha_{rE})})\end{aligned} \tag{7.5}$$

where subscript E refers to experimental data. The symbols have otherwise the same physical definition as in Eq. (7.4). $\zeta_{aE} e^{i(\omega_e t + \alpha_{\zeta E})}$ is unknown and will be calculated by the right hand side of Eq. (7.5) with $\alpha_{\zeta E} = \alpha_{\zeta N}$. The measured bow point is here referred to the MRU measurement position with x' positive pointing towards the stern. This gives $x'_E = -1.985m$.

Figure 7.3 presents the experimental time records of heave and pitch from the MRU system for case 1107. It covers a steady-state time window with 9 encounter periods from $t = 15.74s$ to $25.74s$. Based on the data in Fig. 7.3, the vertical deck motion at the bow can be found from $\eta_{3E} + x'_E \eta_{5E}$ as shown in Fig. 7.4. Both the calculated and measured relative vertical displacement curves at the bow in Fig. 7.4 follow the experimental direction definition, *i.e.* positive downwards. We can see that the two curves in Fig. 7.4 are almost 180^0 out of phase. Since the MRU and the wave-probe measurements at the bow were not synchronized, these two curves should be phase shifted. It means that both curves in Fig. 7.4 should be phase shifted, such that a reasonable incident wave is obtained. Here $\eta_{3E} + x'_E \eta_{5E}$ curve was for instance time shifted to the right with $\delta t = 0.34s$. Then the incident wave at the bow is found as in Fig. 7.5, by subtracting the shifted curve of '$\eta_{3E} + x'_E \eta_{5E}$' from the curve 'Rel.Disp.Exp.'. This means

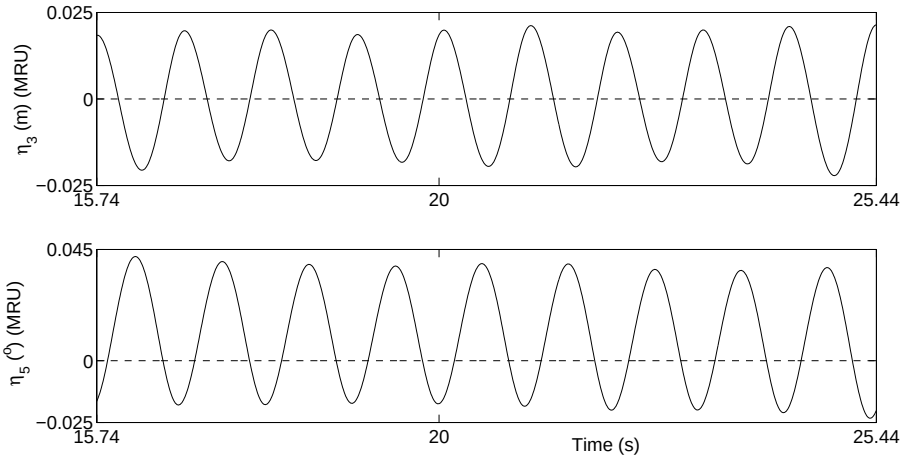

Figure 7.3 Time record of heave and pitch measured by the MRU system for case 1107.

that there is a phase shift of $\alpha_s = -\omega_e \delta t = -1.98 rad$ with $\omega_e = 0.93 rad$ in this case 1107. A mean value of $0.0265 m$ was deducted to get Fig. 7.5.

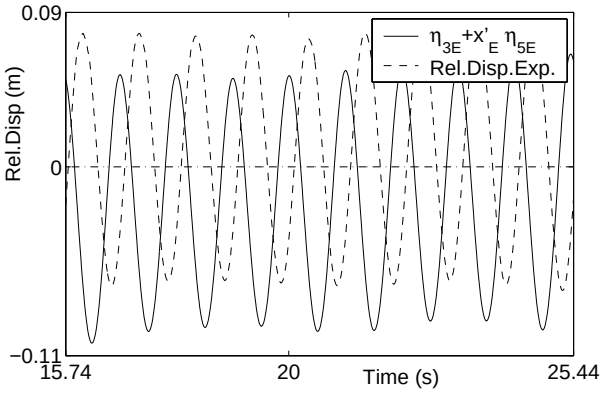

Figure 7.4 Calculated vertical deck position and experimental relative vertical motion at the bow for case1107; Subscript 'E' means experiment

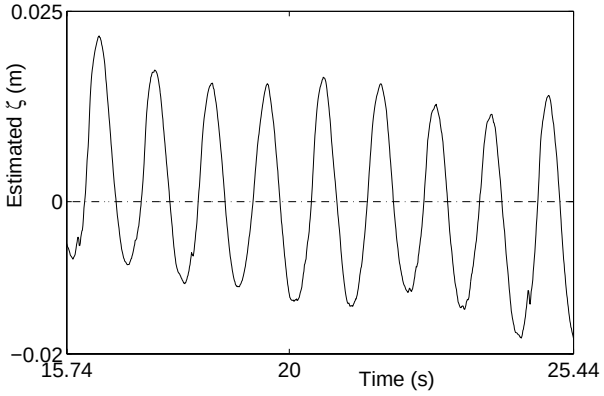

Figure 7.5 Estimated incident waves at the bow based on experimental data for case 1107

The incident wave at the bow given by Eq. (7.5) should then be expressed as

$$\begin{aligned}\zeta_{aE} e^{i(\omega_e t + \alpha_{\zeta E})} =& \eta_{3aE} e^{i(\omega_e t + \alpha_{3E} + \pi + \alpha_s)} - x'_E \eta_{5aE} e^{i(\omega_e t + \alpha_{5E} + \alpha_s)} \\ & - \eta_{raE} e^{i(\omega_e t + \alpha_{rE} + \pi)}\end{aligned} \tag{7.6}$$

Before we can match Eq. (7.6) with Eq. (7.4), one should notice that x'_E refers to the MRU measurement point while x_N is relative to the global COG. So a coordinate transformation is needed. This leads to a phase difference for heave. This is expressed as in Eq. (7.7), with positive

direction downwards.

$$\begin{aligned}\eta_{3E\_COG} &= \eta_{3aE}e^{i(\omega_e t+\alpha_{3E})} + (x'_E - x_N)\eta_{5aE}e^{i(\omega_e t+\alpha_{5E})} \\ &= \eta_{3aE\_COG}e^{i(\omega_e t+\alpha_{3E\_COG})}\end{aligned} \tag{7.7}$$

This will give a new curve, in which phase (α_{3E_COG}) relative to the incident waves at the bow can be expressed as

$$\alpha_{3E\_COG} - \alpha_{\zeta E} = \underbrace{\alpha_{3E\_COG} - \alpha_{3E}}_{\delta_{33\_COG}} + \underbrace{\alpha_{3E} - \alpha_{\zeta E}}_{\delta_{\zeta 3\_mru}} \tag{7.8}$$

Here δ_{33_COG} is calculated from the two heave curves at the MRU measurement point and COG of catamaran. Further, $\delta_{\zeta 3\_mru}$ is calculated from the heave curve in Fig. 7.3 and the estimated incident wave at the bow in Fig. 7.5.

Then Eq. (7.6) can be expressed by referring to the global COG system, as

$$\begin{aligned}\zeta_{aE}e^{i(\omega_e t+\alpha_{\zeta E})} =& \eta_{3aE\_COG}e^{i(\omega_e t+\overbrace{\alpha_{3E\_COG}+\pi+\alpha_s}^{\alpha'_{3E}})} - x_N\eta_{5aE}e^{i(\omega_e t+\overbrace{\alpha_{5E}+\alpha_s}^{\alpha'_{5E}})} \\ &- \eta_{raE}e^{i(\omega_e t+\alpha_{rE}+\pi)}\end{aligned} \tag{7.9}$$

Further, the phase difference can be expressed as

$$\delta_{12} = \alpha_2 - \alpha_1 = -\omega_e(t_2 - t_1) \tag{7.10}$$

for two sinusoidal curves defined as

$$\begin{aligned}y_1 &= \cos(\omega_e t + \alpha_1) = \cos(\omega_e(t + t_1)) \\ y_2 &= \cos(\omega_e t + \alpha_2) = \cos(\omega_e(t + t_2))\end{aligned} \tag{7.11}$$

Based on the relationship in Eqs. (7.11) and (7.10), and by comparing the curves in Figs. (7.3) to (7.5), we can get the phase differences as follows

$$\begin{aligned}\delta_{\zeta 3\_mru} &= \alpha_{3E} - \alpha_{\zeta E} = 3.420\,rad \\ \delta_{\zeta 5\_mru} &= \alpha_{5E} - \alpha_{\zeta E} = 0.845\,rad \\ \delta_{\zeta r\_mru} &= \alpha_{rE} - \alpha_{\zeta E} = 1.665\,rad \\ \delta_{33\_COG} &= \alpha_{3E\_COG} - \alpha_{3E} = -0.551\,rad\end{aligned} \tag{7.12}$$

By using Eqs. (7.10), (7.8) and (7.12), we can now find the phase difference between motions relative to incident waves at the bow based on experimental data, *i.e.*

$$\begin{aligned}\delta_{3\zeta\_E} &= \alpha'_{3E} - \alpha_{\zeta E} \\ &= \alpha_{3E\_COG} + \pi + \alpha_s - \alpha_{\zeta E} \\ &= \delta_{33\_COG} + \delta_{\zeta 3\_mru} + \pi + \alpha_s\end{aligned} \tag{7.13}$$

$$\begin{aligned}\delta_{5\zeta\_E} &= \alpha'_{5E} - \alpha_{\zeta E} \\ &= \alpha_{5E} + \alpha_s - \alpha_{\zeta E} \\ &= \delta_{\zeta 5\_mru} + \alpha_s\end{aligned} \tag{7.14}$$

The phases of the motions relative to the incident waves at the same point should numerically and experimentally be the same, *i.e.*

$$\underbrace{\alpha_{iN} - \alpha_{\zeta N}}_{\delta_{i\zeta\_N}} = \underbrace{\alpha'_{iE} - \alpha_{\zeta E}}_{\delta_{i\zeta\_E}} \tag{7.15}$$

with $i = 3, 5$ for heave and pitch, respectively.

Together with Eq. (7.13) and using that $\alpha_{\zeta N} = \alpha_{\zeta E} = -kx_N - \frac{\pi}{2}$, we get

$$\alpha_{3N} = \delta_{3\zeta\_E} - (\frac{\pi}{2} + kx_N) \tag{7.16}$$

$$\alpha_{5N} = \delta_{5\zeta\_E} - (\frac{\pi}{2} + kx_N) \tag{7.17}$$

Finally the experimentally based phase as well as the RAO values are derived as presented in Table 7.1. The table also gives the corresponding theoretical data based on the rigid catamaran for the no slamming case. It shows that the difference between theory and experiments is much larger for phases than for the RAO values.

Table 7.1 Predictions of phases and amplitudes based on experimental data for heave and pitch for case 1107. 'Deg.' refers to the unit of degree.

	heave		pitch	
Mode	RAO (m/m)	Phase (Deg.)	RAO (Deg./m)	Phase (Deg.)
Num.	0.85	8.0	1.29	48.0
Exp.	0.65	-46.1	1.35	18.0

The experimentally based data in Table 7.1 are used instead of those from the strip theory based predictions in the numerical calculations of wetdeck slamming induced global loads. This means that they are used in the contribution from linear theory to relative vertical motions, relative impact velocity and acceleration. The following Figs. 7.6 and 7.7 show that the relative vertical motions by strip theory based and the experiment based estimation give phase differences in global response. However, the maximum values are not greatly influenced. The oscillations following the initial oscillation after impact show large differences in amplitude. The estimated data is somehow not so reliable, but it demonstrates that the phases matter. The reason why the experimentally obtained phases are not under full control, is that the incident regular waves with constant amplitude is assumed. The results in Fig. 7.5 do not show this. It has already been mentioned that the incident wave amplitudes may in reality have a 10% variation along the track of the vessel.

We will use the results as an indicator of physical errors associated with our model for linear hydrodynamic loads on the side hulls. The maximum values will be concentrated on. By taking the experimentally based values as the 'truth', the relative errors are as presented in Table 7.2.

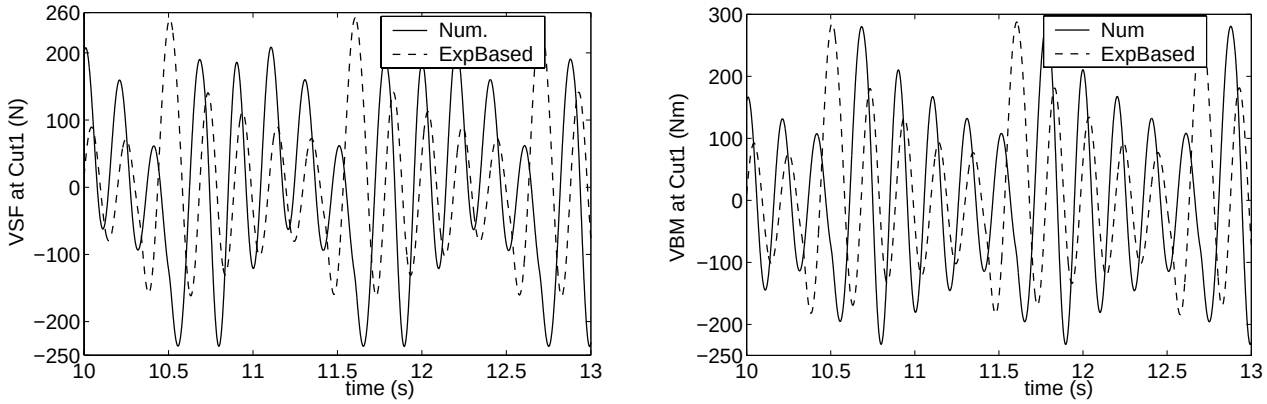

(a) VSF at Cut1 (b) VBM at Cut1

Figure 7.6 Comparison of numerical results with experimentally based (Exp.Based) motions and without experimentally based corrections; Vertical Shear Force (VSF) and Vertical Bending Moment (VBM) at Cut1 for case 1114.

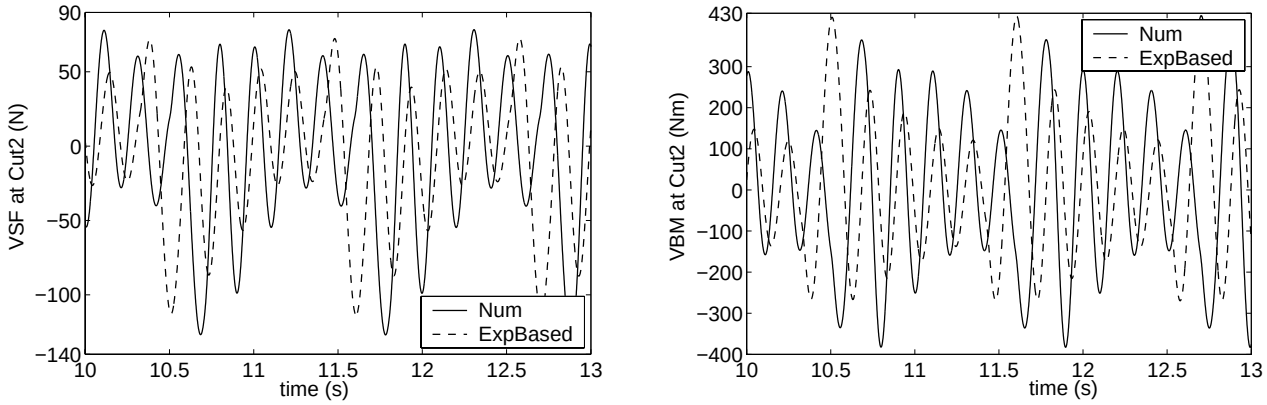

(a) VSF at Cut2 (b) VBM at Cut2

Figure 7.7 Comparison of numerical results with experimentally based (Exp.Based) motions and without experimentally based corrections; Vertical Shear Force (VSF) and Vertical Bending Moment (VBM) at Cut2 for case 1114.

Table 7.2 Relative theoretical errors in describing maximum values of wetdeck slamming induced global loads due to physical errors in describing linear hydrodynamic loads on the side hulls; case 1114. VSF: vertical shear force; VBM: vertical bending moment.

Exp.Based	VSF Cut1(N)	VBM Cut1(Nm)	VSF Cut2(N)	VBM Cut2(Nm)
No	237.1639	280.7300	127.0879	383.2460
Yes	253.2223	288.8660	114.3323	425.0285
Relative error	0.0634	0.0282	0.1116	0.0983

Nonlinear side hull forces

Nonlinear side hull forces will matter for cases with or without wetdeck slamming. This is traditionally done by including nonlinear hydrostatic restoring and Froude-Krylov forces and adding water entry forces by a Von Karman approach (*e.g.* Wu and Moan (1996)). A comparative study presented by Jensen *et al.* (2000) for the S175 monohull ship showed that this in combination with strip theory could explain the nonlinear trends in the experiments. However, this nonlinear effect was small relative to linear side hull effects. Further, since the studied side hulls do not have large flare, we should not expect dominant contribution to the global loads from the nonlinear hydrodynamic loads on the side hulls.

However, including nonlinear side hull forces will affect relative vertical motions and impact velocities. This alters the slamming loads and therefore the global loads. We can therefore not conclude based on the S175 hull investigations. Since the different nonlinear terms may cause cancelling effects (Sagli *et al.* (1997)), care should be shown when using different methods to calculate the nonlinear forces. Wu *et al.* (1996) investigated the nonlinear side hull effects on the global hydroelastic response for a catamaran. Their catamaran had similar body geometry as ours. The connecting parts are much more soft and therefore more elastic than ours. No wetdeck slamming was accounted for. They showed that including the nonlinear side hull terms could improve the agreement between the theoretical and experimental results. However, in wetdeck slamming cases studied here, connections are much more rigid. This may mean that global hydroelastic effect due to including the nonlinear side hull effects could be less influential. Further, as shown in experimental and theoretical results in Chapter 5, the force response when wetdeck slamming occurs is dominated by the wetdeck slamming induced part, rather than the response part from wave excitation forces on the side hulls. Further studies are needed to get a complete assessment.

7.2.3 Slamming

3D slamming

Ge *et al.* (2002a) studied theoretically initial 3D wetdeck slamming effects associated with roll. It requires that the water initially hit at a flat part of the deck away from the front end. A semi-elliptic approximation of the wetted surface was made. The semi-axis of the ellipse was determined by finding the geometrical intersection between the incident wave and the deck. The impact loading F_3 was expressed in terms of the time derivative of infinite frequency heave added mass A_{33} times relative impact velocity based on Scolan and Korobkin's (2001) formula. A_{33} is given analytically in terms of the complete Elliptic function which depends in a simple way on the semiaxis of the semi-elliptic approximation of the wetted surface. The formulas are as follows

$$F_3 = \frac{d}{dt}(A_{33}V) \qquad \text{with} \quad A_{33} = \frac{2\pi}{3}\frac{\rho a^2 b}{E(e)} \tag{7.18}$$

Here $e = \sqrt{1-(a/b)^2}$ with $b > a$, and $E(e)$ is the complete elliptic function. a and b are the semi-axis of the elliptic approximation of the wetted area. In this qualitative estimate, V is

approximated as the relative impact velocity at the initial instant of slamming.

Ge *et al.* (2002a) showed that using this approach in an initial phase until the whole cross-section of the deck was wetted gave small differences in global loads relative to using a 2D slamming model. However, this was a case study and the conclusions should not be generalized without further investigations. Since the water in case 1114 hits initially at the front end of the wetdeck in the numerical model, this 3D slamming model can not be applied. Further, in the theoretical error analysis, we should assume head sea with no effect of roll, yaw and sway.

Since a catamaran at high-forward speed is considered and the wave impact occurs in forward part of the deck, the free surface elevation can to a large extent be approximated by the incident waves. Further, the horizontal cross-section of the deck has a flat surface. The slamming induced flow can therefore be approximated by 2D flow in longitudinal cross-sectional planes.

However, there is in reality local run-up at the side-hulls. This causes 3D slamming effects. A measure of the thickness of the run-up can be seen from the theoretical water entry analysis by Zhao and Faltinsen (1993). The studies are for water entry of wedges with constant impact velocity. The deadrise angle varied between 4^0 and 81^0. The forward speed causes the local run-up to initially hit aft of what a strip theory predicts. This may be explained by a $2\frac{1}{2}D$ nonlinear theory by considering earth-fixed transverse cross planes and let the ship move with forward speed through the cross-sectional planes. One can then conceptually understand that any flow disturbance created in a ship-fixed cross-sectional plane will move downstream with the forward speed. A strip theory does not account for this. A further analysis is needed to quantify the local run-up effect on the wetdeck slamming.

Kutta condition

In Chapter 4, calculations for the rigid catamaran case showed that Kutta condition at the aft intersection point between deck and free surface changes the force history and corresponding global responses, especially during the water exit phase. However, in the cases studied in Chapter 5 with the flexible model, the influence from Kutta condition is negligible. One reason for this difference may be the shorter time duration here (about 0.28s) relative to the rigid catamaran case presented in Chapter 4 (around 0.4s). Figure 7.8 shows that applying Kutta condition has a small influence on the time history of the vertical impact force on the wetdeck. This is based on case 1114 with 3.72^0 bow ramp angle. Higher modes than the two-node bending mode are neglected. We should note that the impact occurs initially at the bow end of the wetdeck. This means initially zero slamming force. The visible spike in the numerical results corresponds to when forward end of the wetted length leaves the bow end during the water exit phase . It must be a numerical error and has no influence on global wetdeck slamming induced loads, as discussed in Section 5.6.

Other slamming model errors

The slamming model comparisons for a rigid body in Chapter 4 have shown that the additional effects of using Wagner method during the water entry phase and Fourier expansion of relative

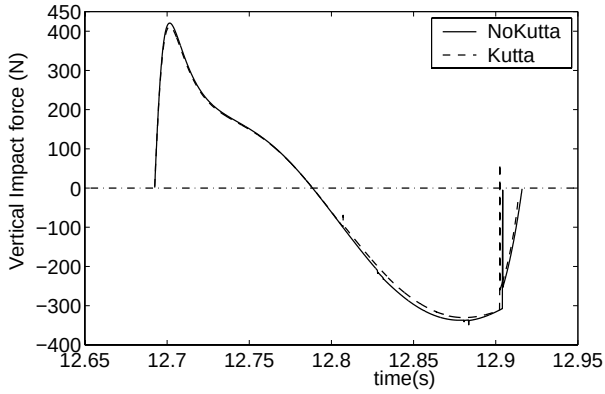

Figure 7.8 The influence on the vertical impact force by using the slamming model with Kutta condition; case 1114

velocity of V_R have a negligible influence on global response for our studied rigid body cases. The above analysis indicates that the global hydroelastic response is not strongly sensitive to the theoretical slamming model as long as 2D flow conditions are assumed.

The wetdeck slamming model assumes two-dimensional flow in longitudinal cross-sectional planes. This is based on that the wetdeck has a horizontal cross-sectional shape and that wetdeck impact due to local run up at the side hulls have minor global effect. However, wetdecks may have wedge shaped cross-sections. This implies that a three-dimensional slamming model should be considered. The studies by Scolan and Korobkin (2001) and Chezhian (2002) are useful in this context. They both use a Wagner type method to find body-water intersection. This has to be modified to a Von Karman method to describe the water exit phase. Scolan and Korobkin's method is most appropriate for small angles β between undisturbed free surface and body surface. Corresponding two-dimensional studies by Faltinsen (2002) show that it is more correct to satisfy the exact body boundary condition like Chezhian does for $\beta >\sim 10^o$. 3D flow will also matter for our wetdeck shape in oblique sea.

7.2.4 Structural modelling

Transverse bending

Ideally transverse bending modes should be included in the theoretical model for head sea conditions. The transverse bending mode can be important in oblique sea or beam sea cases. However, in head sea or close to head sea cases, the transverse bending moment has much less influence than the longitudinal ones (*e.g.* Faltinsen *et al.* (1992)). In this section it is shown that the transverse bending has a small effect on the longitudinal response of concern herein.

The experimental results from transverse transducers 5888, 5889 and 5890 (See Fig. A.4) can be used to investigate transverse bending, pitch connecting moment and vertical shear force in a longitudinal cut of the wetdeck. By adding the results from these transducers, we find the vertical shear force and transverse bending moment in a longitudinal cut of the deck at the center

plane of the catamaran. The transducers are not exactly at the center plane (See Table A.3), but the small differences in positions from the center plane are believed to cause negligible errors.

Figures 7.9 to 7.12 show the results for cases 1107 and 1114. The two cases have the same wave period $T = 1.8s$. The forward speed is $1.9m/s$ and $1.8m/s$ respectively for cases 1107 and 1114. However, the incident wave amplitude is sufficiently small in case 1107 for no wetdeck slamming to occur like it does in case 1114.

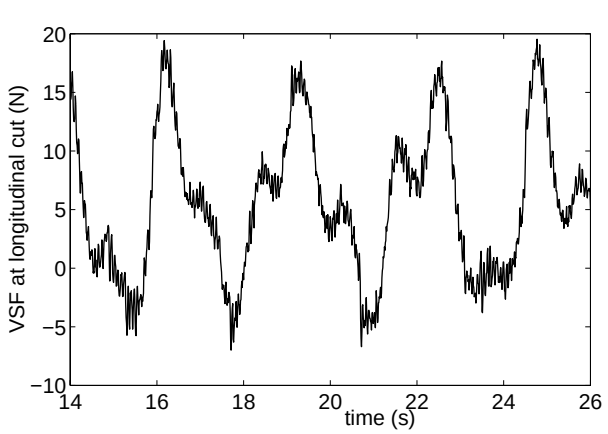

(a) VSF at the longitudinal center plane cut

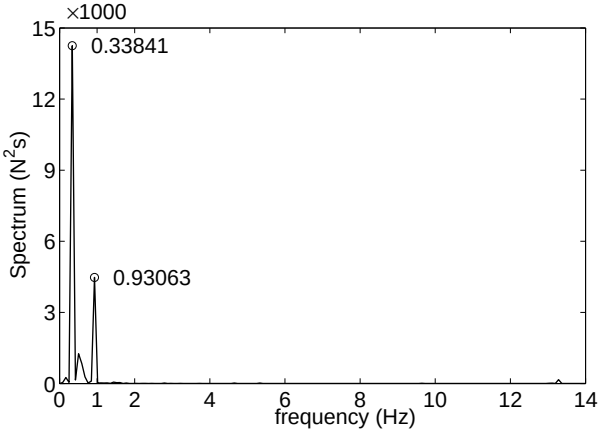

(b) FFT analysis of time record from $t = 14s$ to $25.81s$ in Fig. 7.9(a)

Figure 7.9 Time record and energy analysis of measured vertical shear force (VSF) at the longitudinal center plane cut of the catamaran; Case 1107. In (b), numbers associated with the spectral peak values are the exact numbers for the corresponding frequencies.

Figures 7.9 to 7.12 present both the time history and spectral analysis of vertical shear force and transverse bending moment in the longitudinal center plane cut of the catamaran. In order to explain the results, it is useful to refer to the theoretical formulas presented by Faltinsen *et al.* (1992) for a rigid catamaran. Hydrodynamic hull interaction was neglected. Linear steady state conditions, *i.e.* without wetdeck slamming, were considered. The formulas are as follows for vertical shear force V_3^{cp} and transverse bending moment V_4^{cp} in the longitudinal center plane cut. By using the notations of the hydrodynamic coefficients in this thesis, they are

$$V_3^{cp} = 0.5\Big\{(My_A + A_{33}y_B)\ddot{\eta}_4 + B_{33}y_B\dot{\eta}_4 + K_{33}y_B\eta_4 + F_3 i\sin(ky_B\sin\beta)e^{i\omega_e t}\Big\} \tag{7.19}$$

$$V_4^{cp} = 0.5\Big\{F_4^L i\sin(ky_B\sin\beta)e^{i\omega_e t} + M(y_A - y_B)\ddot{\eta}_3 - 2\Big[\int_A xydM\Big]\ddot{\eta}_5\Big\} \tag{7.20}$$

F_3 and F_4^L relate respectively to the total vertical wave excitation load on the catamaran and the wave excitation roll moment on a side hull. y_A is the y-coordinate in the global coordinate system of the center of the gravity of one half part ($y > 0$) of the catamaran obtained by intersecting along the center plane of the catamaran. y_B means the y-coordinate of the center plane of the side hull with positive y-value. $-\int_A xydM$ is the coupled structural inertia moment in

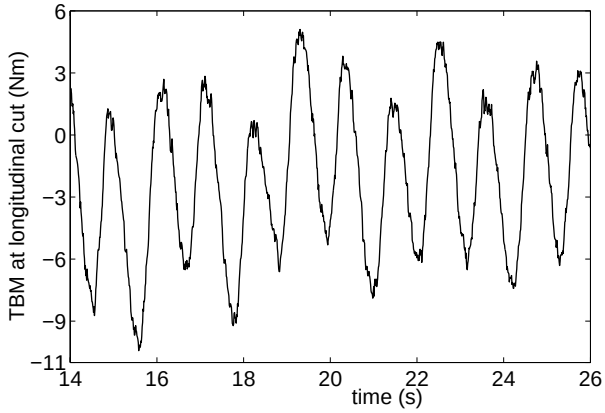

(a) TBM at the longitudinal center plane cut

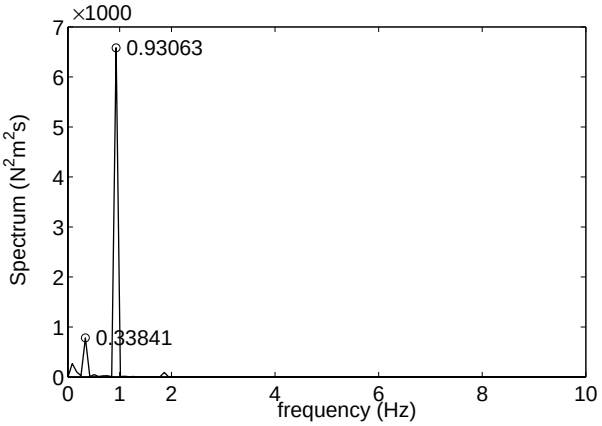

(b) FFT analysis of time record from $t = 14s$ to $25.81s$ in Fig. 7.10(a)

Figure 7.10 Time record and energy analysis of measured transverse bending moment (TBM) at the longitudinal center plane cut of the catamaran; Case 1107. In (b), numbers associated with the spectral peak values are the exact numbers for the corresponding frequencies.

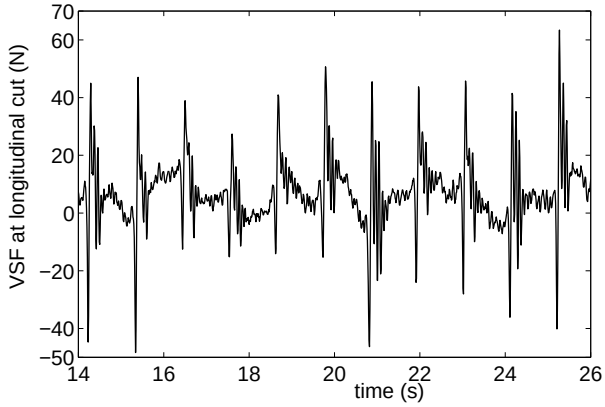

(a) VSF at the longitudinal center plane cut

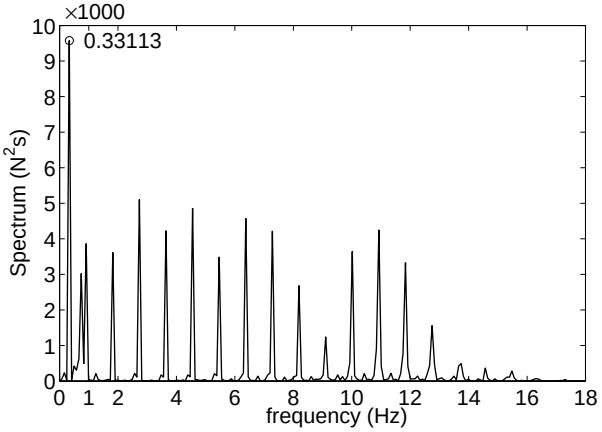

(b) FFT analysis of time record from $t = 14s$ to $25.81s$ in Fig. 7.11(a)

Figure 7.11 Time record and energy analysis of measured vertical shear force (VSF) at the longitudinal center plane cut of the catamaran; Case 1114. In (b), numbers associated with the spectral peak value are the exact numbers for the corresponding frequency.

roll-pitch of the above-mentioned half part of the catamaran.

If head sea is considered, V_3^{cp} is zero, and V_4^{cp} is non-zero and depends on the heave and pitch accelerations of the vessel. Head sea was intended in the experiments but the unintended asymmetry of mass distribution about the center plane of the catamaran contributed small amplitude roll, yaw and sway. Figure 7.13 shows the steady state time history and spectral analysis of roll during case 1107. There are two dominant frequencies. One is associated with the frequency of encounter $f_e = 0.931Hz$ and the other one is $0.338Hz$. There is also some visible energy contri-

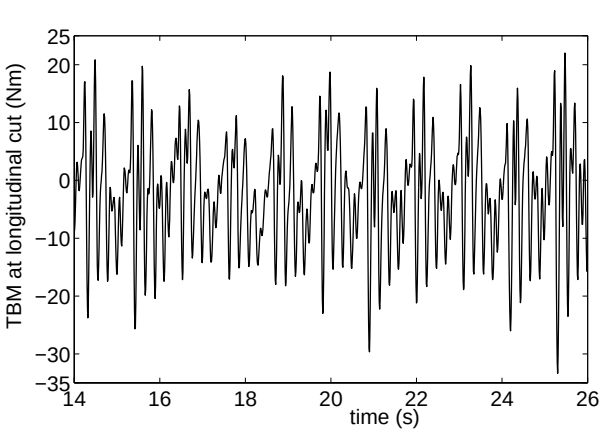

(a) TBM at the longitudinal center plane cut

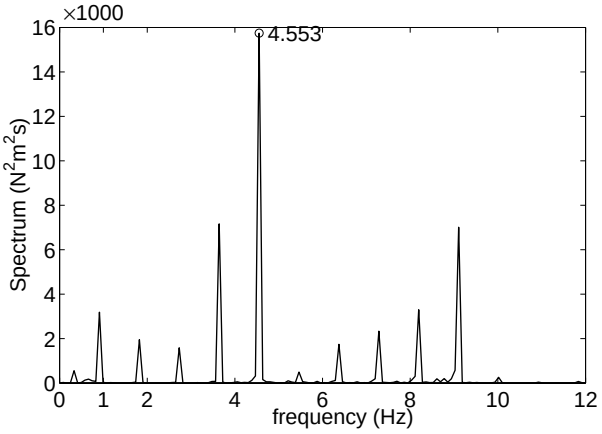

(b) FFT analysis of time record from $t = 14s$ to $25.81s$ in Fig. 7.12(a)

Figure 7.12 Time record and energy analysis of measured transverse bending moment (TBM) at the longitudinal center plane cut of the catamaran; Case 1114. In (b), numbers associated with the spectral peak value are the exact numbers for the corresponding frequency.

bution around the natural period of roll mode, which is $0.862Hz$ according to Økland (2002). The reason for the relatively large energy around $0.338Hz$ is likely to be due to the autopilot system (Martinussen (2002)).

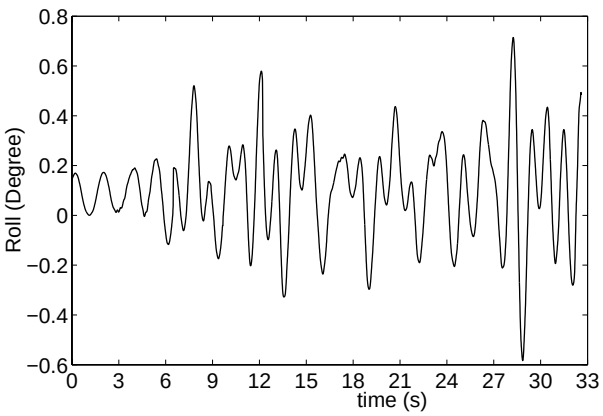

(a) Measured roll data by MRU measurement system

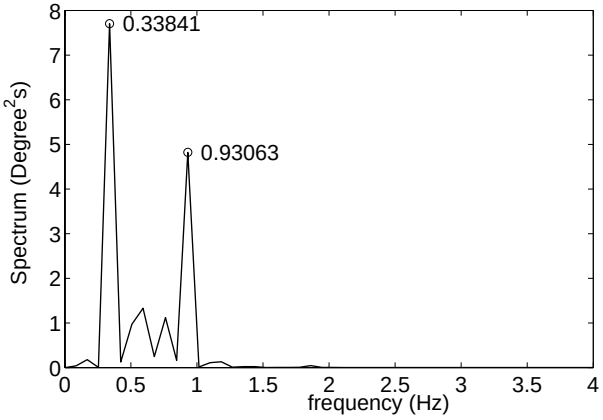

(b) FFT analysis of time record from $t = 14s$ to $25.81s$ in Fig. 7.13(a)

Figure 7.13 Time record and energy analysis of measured roll of the catamaran; MRU measurement system; Case 1107. In (b), numbers associated with the spectral peak values are the exact numbers for the corresponding frequencies.

The spectral analysis of the vertical shear force for case 1107 presented in Fig. 7.9(b) shows clearly the presence of the dominant frequencies in the roll data. This is consistent with Eq. (7.19). The natural frequency for transverse bending according to Økland (2002) is $5.88Hz$ from wet decay tests. There are no noticeable effect of the transverse bending mode. The transverse

bending moment for case 1107 presented in Fig. 7.10(b) show dominant energy content at the frequency of encounter. This is as explained by Eq. (7.20) strongly influenced by the heave and pitch acceleration of the catamaran. The values of both vertical shear forces and transverse moments for case 1107 are small. When wetdeck slamming occurs, *i.e.* case 1114, the values of vertical shear forces and transverse bending moments in a longitudinal cut of the catamaran are clearly increased, but they are still small relative to vertical shear forces and bending moments at the transverse cuts. Table 7.3 gives for both cases 1107 and 1114 the range of the VSF and TBM of the longitudinal cut at the center plane, as well as the VSF and VBM values at the two transverse cuts.

Table 7.3 Vertical shear force (VSF) and transverse bending moment (TBM) at the longitudinal center plane cut of the catamaran, and VSF and vertical bending moment (VBM) at the transverse cuts (Cut1 and Cut2); time domain from $14s$ to $26s$; cases 1107 and 1114. The values at the longitudinal cut are found by adding results from the transverse transducer-5888, 5889 and 5890 (See Fig. A.4 for location). The values at Cut1 and Cut2 are the summation of the data from starboard and port side. Both maximum and minimum values are presented.

	Case 1107	Case 1114
VSF at longitudinal cut (N)	20/-8	70/-50
TBM at longitudinal cut (Nm)	6/-11	25/-35
VSF at Cut1 (N)	8/-38	170/-260
VBM at Cut1 (Nm)	-5/-35	280/-320
VSF at Cut2 (N)	36/7	220/-190
VBM at Cut2 (Nm)	16/-17	250/-370

The spectral analysis for vertical shear forces and transverse bending moments at the longitudinal cut for case 1114 show the presence of energy at many frequencies. However, there are no dominant energy at the natural frequencies for instance for bending and pitch connecting/torsional modes which according to Økland (2002) are the same.

The experimental results of global wetdeck slamming induced global loads at Cut1 and Cut2 in case 1114 can be used to quantify the relative theoretical errors in neglecting the transverse bending mode in our theoretical model. This is done by a spectral analysis of the time records during steady state conditions and by noting that the natural frequencies for transverse bending and pitch connecting/torsional modes have the same value $5.88Hz$ according to Økland (2002). The energy between $5.71Hz$ and $6.04Hz$ have been calculated for each global load components. A relative theoretical error is then estimated by taking the square root of this energy part and dividing by the square root of the total energy. The results are presented in Table 7.4 showing a maximum relative error of 2.8%.

Table 7.4 Relative theoretical errors in describing wetdeck slamming induced global loads at transverse cuts (Cut1 and Cut2) due to physical errors in neglecting dynamic hydroelastic effects due to the transverse bending mode; Case 1114. VSF: vertical shear force; VBM: vertical bending moment.

	VSF Cut1(N)	VBM Cut1(Nm)	VSF Cut2(N)	VBM Cut2(Nm)
Relative error	0.0099	0.0042	0.0151	0.0279

7.2.5 Effect of transient phase

In the experiments there is a transient phase for ship motions to reach steady state conditions. This is artificially done in the numerical method as described by Eq. (2.41) and the accompanying text. In most calculations a period of four wave periods is used to build up the full wave excitation loads. The steady state numerical results must be independent of this artificial transient phase. Figure 7.14 shows for case 1114 the effect of using either four or three wave periods to build up the wave excitation load. Figs. 7.14(a) and 7.14(b) show respectively the transient and steady state phase for wetdeck slamming induced vertical shear force at Cut1. The difference in response is negligible during the steady state phase. Vertical bending moment at Cut1, as well as the global loads at Cut2 show the same property. A longer transient phase with five wave period has also been studied. Results show that there is no effect on the global response.

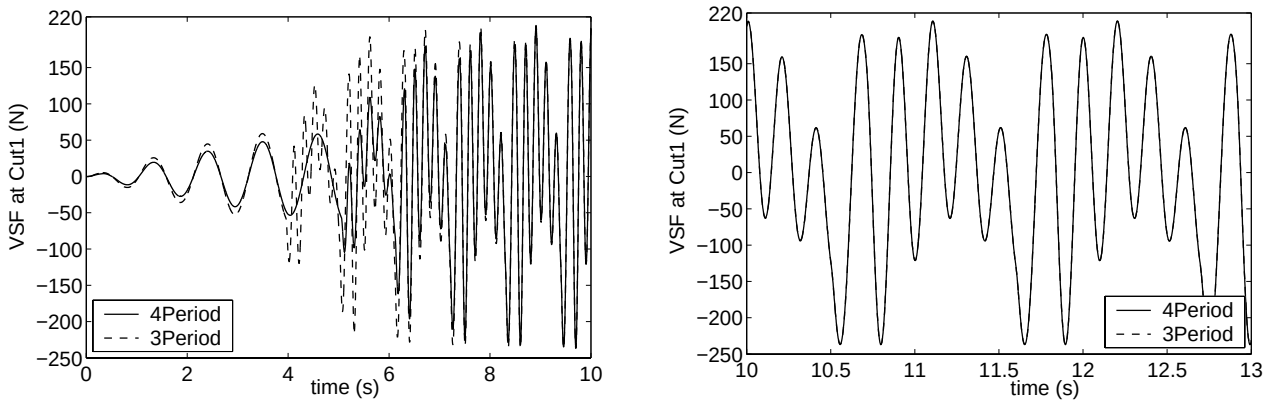

(a) Transient phase

(b) Steady state phase

Figure 7.14 The influence on the vertical shear force (VSF) at Cut1 due to different time durations (4 and 3 wave periods) of the build up phase of the calculated wave excitation loads; Case 1114.

7.3 Numerical errors

Numerical errors associated with the strip theory for the linear hydrodynamic loads on the side hulls will be first discussed. A convergence study of the time integration of the equations of motions of wetdeck slamming induced response will also be presented.

7.3.1 Strip theory

Numerical error sources when using strip theory are associated with for instance the number of strips and number of offset points. Resulting errors have been studied by convergence analysis by Faltinsen and Svensen (1990). In our calculations 40 strips along the ship are used and there are 40 offset points on each cross section of one hull to describe the mean submerged hull surface. Both Marintek's (Hoff (2001)) experience and Faltinsen and Svensen showed that this will cause negligible errors in predicted strip theory response.

7.3.2 Time integration of equations of motions

It has been controlled that the fourth order Runge-Kutta method for time integration of the equations of motions gives converged results by decreasing the time step DT. We will exemplify this by showing the results obtained when the Kutta condition model is used to find the impact loads on the wetdeck for case 1114.

The solution procedure for the slamming loads with Kutta condition involves to a large extent analytical expressions, which are not believed to cause numerical errors. However, the influence of the vorticity distribution aft of the trailing edge (or aft deck-water intersection point), is numerically approximated. Equations (3.95) and (3.96) in Chapter 3 show that the vorticity distribution is assumed constant over each element aft of the trailing edge. The element length is determined by the travelling length of the vorticity during each time step. This means that the element size is dependent on the time step DT. By decreasing the time step, we can check the convergence. Maximum absolute load values at the two cuts are used in this analysis. Figures 7.15 to 7.16 show either minimum or maximum values of vertical shear force (VSF) and vertical bending moment (VBM) at Cut1 and Cut2 by using different time steps. The smallest DT used in the numerical calculations is $0.1 \cdot 10^{-3}$ second.

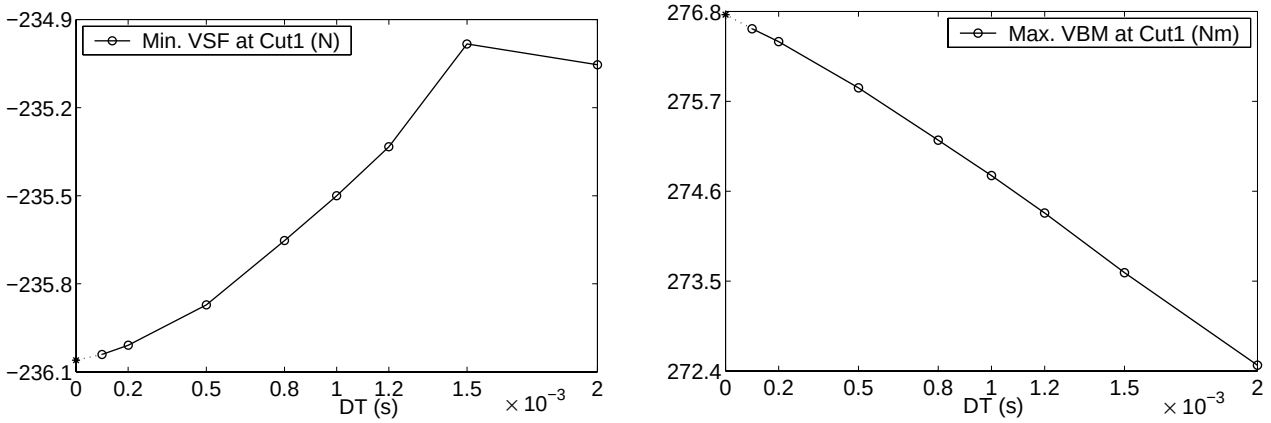

(a) Minimum VSF at Cut1

(b) Maximum VBM at Cut1

Figure 7.15 Convergence study by using slamming model with Kutta condition; Minimum vertical shear force (VSF) and maximum vertical bending moment (VBM) at Cut1 versus different time step values DT; case 1114.

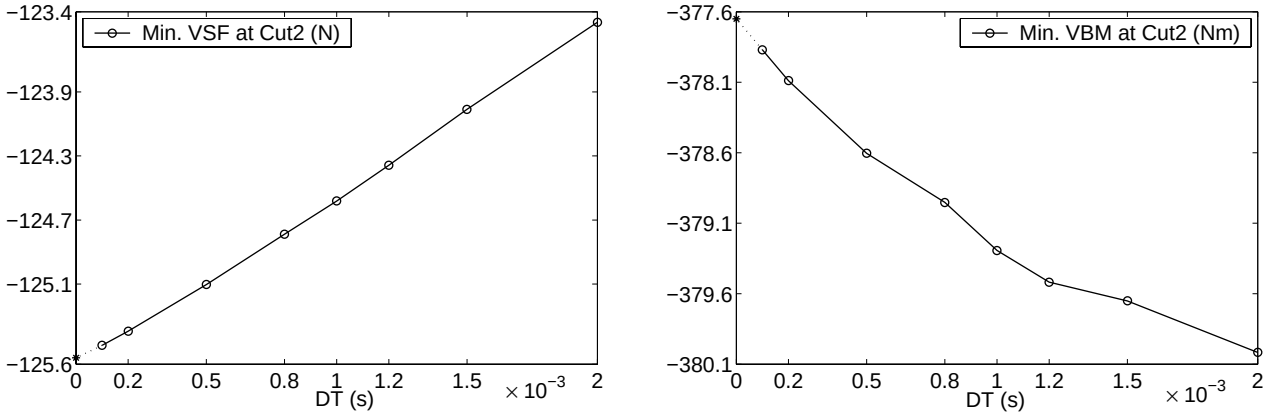

(a) Minimum VSF at Cut2

(b) Minimum VBM at Cut1

Figure 7.16 Convergence study by using slamming model with Kutta condition; Minimum vertical shear force (VSF) and minimum vertical bending moment (VBM) at Cut2 versus different time step values DT; case 1114.

Based on the calculated values for different DT values, we have extrapolated to $DT = 0$. This is then considered as the converged value. Table 7.5 gives the converged value and the value at $DT = 0.001s$ for VSF and VBM at Cut1 and Cut2. $DT = 0.001s$ is the time step used in most of our numerical calculations. It shows that the relative error by using $DT = 0.001s$ is $O(10^{-3})$, which means that our data based on a time step of $0.001s$ are reliable. For this specific case, the CPU time used for simulating 15 seconds when $DT = 0.0001s$ can be six times the time used when $DT = 0.001s$.

Table 7.5 Relative theoretical errors in describing wetdeck slamming induced global loads due to numerical errors in the time integration. Based on converged maximum or minimum global load values ($DT = 0$) (See Figs. 7.15(a)-7.16(b)) and the values calculated at $DT = 0.001s$. Slamming model with Kutta condition is used for the slamming loads, case 1114. VSF: vertical shear force; VBM: vertical bending moment.

DT(s)	VSF Cut1(N)	VBM Cut1(Nm)	VSF Cut2(N)	VBM Cut2(Nm)
0.001	-235.5001	274.7909	-124.5815	-379.2930
0.000	-236.0600	276.7600	-125.5600	-377.6500
Relative Error [-]	0.0024	0.0071	0.0078	0.0044

Numerical errors occur initially when the water hits within a flat area. The free surface has then to be initially tangential to the wetdeck surface. This means that the time rate of change of the wetted length is initially infinite. This would require a special time integration procedure which utilizes an analytical solution of the initial impact phase. This is not done and we follow our normal time integration procedure. This implies large errors in the initial impact loads. However, the error in wetdeck slamming induced global loads are small. The initial slamming occurs at

the front end of the wetdeck for cases 1111, 1112, 1114 and 1115 where experimental wetdeck slamming results are available. So there is not such an error source for the cases presented here.

7.4 Summary

Case 1114 in the model tests are focused on in the theoretical error analysis. Theoretical errors are divided into physical and numerical errors. It is shown by convergence studies that numerical errors associated with time integration and strip theory discretization cause a relative error in wetdeck slamming induced global response of $O(10^{-3})$ if our standard numerical approximations are made.

It is difficult to do a physical error analysis of our theoretical model. This could for instance partly be done by using a benchmark numerical method that includes properly the 3D flow effects and flow nonlinearities. Even if more sophisticated numerical methods exist for the linear flow problem associated with the side hulls, they would in practical use require a proper numerical error analysis. This has not been done. There exists no rational numerical method that can completely deal with the nonlinear flow problem. Instead model tests results were analyzed to indicate that hull interaction ought to be considered. It is also suggested that nonlinear side hull forces and 3D initial slamming effects due to run-up at the side hulls ought to be studied. Relative theoretical errors in the wetdeck slamming induced global loads due to physical errors in linear hydrodynamic loads on the side hulls (See Table 7.2) and due to neglection of transverse bending modes (See Table 7.4) are estimated.

It is noted that these error estimates are smaller than the corresponding experimental error estimates presented in Table 6.14, and can not completely explain the differences between theory and experiments. Also the experimental error sources for instance due to mass distribution and bow ramp geometry are neglected due to the difficulty in assessing these errors in an objective manner. Even if this will increase the experimental error estimates, it is felt that more effort should be in the future done in improving the theory.

Chapter 8

Conclusions and Future Perspectives

8.1 Conclusions

Global hydroelastic effects due to wetdeck slamming on a high-speed catamaran in regular head waves are studied theoretically and experimentally. The Froude numbers are between 0.30 and 0.33. The wetdeck has a bow ramp with a horizontal transverse cross-section. The important elastic properties of the test model are theoretically accounted for by using small elastic beam elements connecting three rigid bodies.

The hydrodynamic loads on the side hulls are based on the linear frequency domain strip theory by Salvesen *et al.* (1970). No hull interaction is considered. By formulating forces on each hull separately, an important modification of the strip theory is needed due to the forward speed effect on the second and third body counted from FP. This implies end terms at the forward ends of these two bodies. Stokes theorem is used to derive those terms. The details of the restoring terms due to the beam elements between the three rigid bodies are presented.

The three-body model without wetdeck slamming is validated by comparing with experimental eigenvalues for coupled heave and pitch rigid-body types of modes as well as for two-node and three-node vertical bending. Mode shapes are verified by comparing with FEM results by Økland (2002). It is also documented by comparing with model tests that the model gives satisfactory predictions of relative vertical motion amplitude at the bow as well as amplitudes of vertical shear forces and bending moments when no wetdeck slamming occurs.

Five wetdeck slamming load models are presented. They all assume that the structure is locally rigid and that the flow due to slamming is two-dimensional in a longitudinal cross-sectional plane. Both a Wagner and a Von Karman type of approach are used to find the wetted length. However, the Wagner based method can not be used to describe the water exit phase, *i.e.* when the wetted length decreases. The relative impact velocity is either represented exactly or approximated by a linear function over the wetted length. The exact method uses a Fourier series

representation of the relative impact velocity. A high-frequency dynamic free surface condition is used. Detailed derivations are given by representing the flow as a vortex distribution over the wetted length and solving the corresponding boundary value problem analytically. Since the wave length of the incident waves is long relative to the wetted length in the studied cases, it is shown that the linear approximation of the relative impact velocity is sufficient.

The effect of high forward speed on the slamming loads is investigated by modifying the dynamic free surface condition and including a Kutta condition at the aft end of the wetted deck. The Kutta condition implies smooth detachment of the flow. However, spray will occur at the front end of the wetted length. This flow can be made mathematically equivalent to the linear unsteady lifting problem of a thin foil in infinite fluid. An important difference is that the wetted length and hence the aft end in our problem is time dependent. This influences the slamming loads. It is shown in one case with a rigid catamaran that this Kutta condition model matters in describing the global wetdeck slamming induced response. However, in the cases where experiments and theory for the elastic model are compared, the effect is not significant. It is in general shown that the water exit phase is important in describing global wetdeck slamming induced response.

The model for wetdeck slamming induced global elastic response includes 6 modes. The two highest modes are unrealistic for the catamaran model considered. A reason is that the very high structural damping associated with these two modes is not accounted for. In order to eliminate these high modes, the modal based method outlined by *e.g.* Langen and Sigbjörnsson (1979) is used. The method is verified to give consistent results with solving the original equations of motions directly in the time domain.

Comparisons are made with experimental results for wetdeck slamming induced vertical shear forces and bending moments at the cuts between the three rigid bodies, that the catamaran is composed of. There are five cases with high incident wave amplitude. The theory and the experiments agree that wetdeck slamming does not occur in one of these cases. There is a reasonable agreement between theory and experiment in the most severe slamming case and in one case with moderate slamming. However, the agreement is unsatisfactory for another moderate slamming case. The theoretical predictions are too low. This is thoroughly investigated by comparing details like theoretical predictions of relative vertical motions, impact positions, wetted length, relative impact velocity and accelerations as well as slamming loads for the different slamming cases. Since the case which does not agree with experiments correspond to the longest wave length, *i.e.* smallest wave frequency and frequency of encounter and the water initially hit at the front end of the deck, it is found plausible that both the slamming duration and the relative impact velocity and acceleration should be smaller than in other cases even if the relative vertical motion is comparable with the other moderate slamming case. This causes both smaller slamming loads and global wetdeck slamming induced loads. A plausible explanation of the failure of the theory is believed to be a piston mode resonance of the fluid motion between the hulls. Even if hull interaction had been included in the strip theory, the piston mode resonance effect can not be adequately described. The fifth case shows small slamming effects with beating, *i.e.* that the response is slowly varying relative to the frequency of encounter. The wave amplitude

has to be increased by 20% in the theoretical calculations relative to the experimental incident wave amplitude, in order to predict slamming. It is also found that the unintended roll motions in the experiments matter for the relative vertical motions and can be the source of beating effect.

Both theory and experiments show a strong influence of two-node bending. There are also some influence of three-node bending, which is not so satisfactorily predicted. Since the three-node bending has a lower natural period than the two-node bending, it is believed that more details in the time history of the slamming loads matter. An example could be the initial uprise of the slamming loads, which in the experiments are likely to be influenced by 3D flow effects due to roll and run-up along the side hulls. Since a linear frequency domain solution with the frequency of encounter is used to calculate the added mass coefficients of the side hull, there are errors in the predictions of the natural frequencies for two-node and three-node bending. However, this has a secondary effect on the predictions of wetdeck slamming induced global loads. The agreement between theoretical and experimental slamming loads is reasonable for cases where experiments and theory show a reasonable agreement in global force response. Both the time duration and maximum and minimum values of slamming load are satisfactorily predicted. Both theory and experiments document that the force is in general positive during the water entry phase and negative during the water exit phase. The absolute values of the maximum and minimum of the slamming load are of the same order of magnitude.

An estimate of experimental errors is made. Since the experiments were not done as part of this thesis, we are limited in the experimental error analysis. Further, random errors can not be identified due to that each experiment was done once. Systematic errors in experiments due to

- Forward speed
- Changing incident wave amplitudes along the track of the model
- Wave measurements
- Seiching (sloshing) in the model basin
- Roll, sway and yaw
- Sinkage
- Trim
- Mass distribution
- Model geometry

are discussed and error estimates of experimentally predicted vertical shear forces and bending moments are made for the most severe slamming case. This is done by first estimating errors associated with each item mentioned above and then the theoretical model is to a large extent used to find the corresponding errors in global responses. It is shown that the trim angle is the most important error source. The changing incident wave amplitudes along the track of the model and the wave measurement inaccuracies are equally the second most important error

source for vertical bending moment at the two transverse cuts studied in the experiments. The errors associated with roll, yaw and sway is the second most important for vertical shear force at the two cuts. This roll, yaw and yaw effect is partly due to an unintended mass distribution causing a small mean roll angle. However, the autopilot system may also matter. The other error sources are negligible. The estimated combined relative errors in experimentally predicted vertical shear forces and bending moments are between 0.17 and 0.29. Accounting for this error further improves the agreement between theory and experiments.

The errors in the theoretical model is investigated partly quantitatively and partly qualitatively. Since there is not a benchmark theoretical model that properly includes all physical effects, we have to some extent rely on experimental results. The discussion is divided into

- incident wave nonlinearities,
- side hull hydrodynamics,
- slamming modelling,
- structural modelling,
- transient phase.

It is suggested that hydrodynamic hull interaction matters. This would require that a 3D hydrodynamic model that properly accounts for the forward speed on the hull generated waves, is used instead of a strip theory. Since the slamming induced global response is a transient phenomena, a time domain solution for the hydrodynamic side hull loads may matter. It is demonstrated by experimental results that the neglection of dynamic transverse bending in the theoretical model is appropriate for head sea cases.

8.2 Future perspectives

The model for the hydrodynamic loads on the side hulls should be improved. It is felt that in particular linear hydrodynamic interaction between the side hulls is important and should be given priority. This could for Froude numbers lower than 0.4 be done by generalizing the unified theory by Newman (1978) and accounting for the global flexibility of the ship hulls. The studies by Ronæss (2002) on hydrodynamic interaction between rigid hulls are useful in this context. She assumes that the two hulls are hydrodynamically in each others far-field. That means that the disturbance on one hull from the other hull is in terms of longitudinal line distributions of sources and transverse dipoles along the center plane of the hull. The global dry modes of the hull can be calculated by standard FEM computer programs and coupled with the hydrodynamic calculations. When the Froude number is larger than 0.4, the high speed theory by Faltinsen and Zhao (1991) can be used in a similar way as Hermundstad (1996) did for a flexible hull. He also considered hull interaction.

The next step is to include nonlinear hydrodynamic loads on the side hulls. It can be done in a similar way as is standard for nonlinear strip theory calculations (Jensen *et al.* (2000)). This

means that nonlinear Froude-Krylov and hydrostatic restoring loads have to be incorporated together with water entry loads based on a Von Karman approach. Wu *et al.* (1996) shows that for no slamming cases including the nonlinear hydrodynamic loads on side hulls can improve the agreement between the theoretical and experimental results. The theoretical and experimental results in this thesis have shown that when wetdeck slamming occurs, the global response is dominated by the wetdeck slamming induced part rather than the response part from wave excitation forces on side hulls. This implies that further studies are needed to state the importance of nonlinear hydrodynamic loads on the side hulls for wetdeck slamming cases.

Our studies have concentrated on regular incident waves. However, design conditions are based on irregular waves. The theoretical model needs to be generalized to this case. This may increase the importance of using a time domain model for the linear hydrodynamic loads on the side hulls. A frequency domain model has been used in this study.

The wetdeck slamming model assumes two-dimensional flow in longitudinal cross-sectional planes. This is based on that the wetdeck has a horizontal cross-sectional shape and that wetdeck impact due to local run up at the side hulls have minor global effect. However, wetdecks may have wedge shaped cross-sections. This implies that a three-dimensional slamming model should be considered. 3D flow will also matter for our wetdeck shape in oblique sea.

A final objective is to develop a numerical method that can predict wetdeck slamming induced global response of multihull vessels in any sea state and at any forward speed. This involves long term statistical description of combined load effects due to both transient slamming induced whipping and steady state linear and nonlinear wave loads.

References

Aarsnes, J. V. (1994). An experimental investigation of the effect of structural elasticity on slamming loads and structural response. Technical Report MT60 A95-0053,602119.00.01, MARINTEK, Trondheim, Norway.

Aarsnes, J. V. and J. R. Hoff (1998). Full scale test with Ulstein test vessel. Technical report, Marintek, Trondheim, Norway.

Adegeest, L. J. M. (1995). *Nonlinear hull girder loads*. Ph. D. thesis, Faculty of Mechanical Engineering and Marine Technology, Delft University of Technology, Netherlands.

Aláez *et al.*, J. A. (1990). Report of the panel on validation procedures. 19th International Towing Tank Conference, Volume 1, Madrid, Spain.

Baarholm, R. (2001). *Theoretical and experimental studies of wave impact underneath decks of offshore platforms*. Ph. D. thesis, Department of Marine Hydrodynamics, Norwegian University of Science and Technology, Trondheim.

Baarholm, R. and O. M. Faltinsen (2001). A boundary element method for solving water impact on a platform deck. In *In Proc. of 20th Offshore Mechanics and Arctic Engineering Conference*, Rio De Janeiro, Brazil.

Baarholm, R., O. M. Faltinsen, and K. Herfjord (2001). Water impact on decks of floating platforms. In *In Proc. of 8th Int. Symp. on Practical Design of Ships and Other Floating Structures*, Shanghai, China. Elsevier Science Ltd.

Bergan, P. G., P. K. Larsen, and E. Mollestad (1986). *Svingning av konstruksjoner*. Trondheim, Norway: Tapir Forlag.

Bertram, V. (1995). Numerical investigation of steady flow effects in three-dimentional seakeeping computation. In *22th Symp. on Naval Hydrodyanmics*, Washington D.C., pp. 417–431. National Academy Press.

Bishop, R. E. D. and W. G. Price (1979). *Hydroelasticity of ships*. Cambridge: Cambridge University Press.

Blagovenschensky, S. N. (1962). *Theory of ship motion*. New York, USA: Dover.

Cheney, W. and D. Kincaid (1999). *Numerical mathematics and computing*. USA: The University of Texas at Austin, Brooks/Cole Publishing Company.

Chezhian, M. (2002). *Three dimensional analysis of slamming (to be published)*. Ph. D. thesis, Department of Marine Technology, Norwegian University of Science and Technology, Trondheim.

Clough, R. W. and J. Penzien (1993). *Dynamics of structures, 2nd ed.* McGraw-Hill, Inc.

Dobrovol'skaya, Z. N. (1969). On some problems of similarity flow of fluid with a free surface. *Journal of Fluid Mechanics 36*, 805–829.

Faltinsen, O. M. (1990). *Sea loads on ships and offshore structures*. Cambridge: Cambridge University Press.

Faltinsen, O. M. (1997). The effect of hydroelasticity on ship slamming. *Phil. Trans. Royal Society of London A355*, 575–591.

Faltinsen, O. M. (1999). Water entry of a wedge by hydroelastic orthotropic plate theory. *J. Ship Research 43*(3), 180–193.

Faltinsen, O. M. (2000). Hydroelastic slamming. *J. Mar. Sci. Technol. 5*(2), 49–65.

Faltinsen, O. M. (2002, March). Water entry of a wedge with finite deadrise angle. *J. Ship Research 46*(1), 1–13.

Faltinsen, O. M., C. Ge, and T. Moan (2002). Slamming on wetdeck - local and global analysis. In *Proceedings of High Speed Marine Vehicles*, Naples, Italy.

Faltinsen, O. M., J. R. Hoff, J. Kvålsvold, and R. Zhao (1992). Global loads on high-speed catamarans. In *PRADS*, Newcastle, England, pp. 360–373.

Faltinsen, O. M. and T. Svensen (1990). Incorporation of seakeeping theories in CAD. In G. van Oortmerssen (Ed.), *Proceedings of the international symposium on CFD and CAD in ship design*, Wageningen, the Netherlands, pp. 147–164. Elsevier.

Faltinsen, O. M. and R. Zhao (1991). Numerical prediction of ship motion at high forward speed. *Phil. Trans. Royal Society A.334*, 241–252.

Ge, C., O. M. Faltinsen, and T. Moan (2002a). Global flexible response due to wetdeck slamming for a catamaran accounting for forward speed. In *21th Int. Conference on Offshore Mechanics and Arctic Engineering*, Oslo, Norway.

Ge, C., O. M. Faltinsen, and T. Moan (2002b). Modeling of wetdeck slamming for a catamaran at forward speed. In *Int. Maritime Assoc. of the Mediterranean*, Crete, Greece.

Gerritsma, J. and W. Beukelman (1964). The distribution of the hydrodynamic forces on a heaving and pitching ship model in still water. In *5th ONR symposium*, Bergen, pp. 219–251.

Gradshteyn, I. S. and I. M. Ryzhik (1994). *Tables of Integrals, Series and Products, 5th edition*. New York: Academic Press.

Greco, M. (2001). *A two-dimensional study of Green-water loading*. Ph. D. thesis, Department of Marine Hydrodynamics, Norwegian University of Science and Technology, Trondheim.

Hadler, J. B., C. M. Lee, J. T. Birmingham, and H. D. Jones (1974). Ocean catamaran seakeeping design, based on the experiences of USNS Hayes. Annual meeting, The Society of Naval Architects and Marine Engineerings.

Haugen, E. M. (1999). *Hydroelastic analysis of slamming on stiffened plated with application to catamaran wetdeck*. Ph. D. thesis, Department of Marine Hydrodynamics, Norwegian University of Science and Technology, Trondheim.

Haugen, E. M., O. M. Faltinsen, and J. V. Aarsnes (1997). Application of theoretical and experimental studies of wave impact to wetdeck slamming. In *4th International Conference on Fast Sea Transportation*, Sydney, Australia, pp. 423–430. Baird Publications.

Hermundstad, O. A. (1996). *Theoretical and experimental hydroelastic analysis of high speed vessles*. Ph. D. thesis, Department of Marine Structures, Norwegian University of Science and Technology, Trondheim.

Hermundstad, O. A., J. V. Aarsnes, and T. Moan (1999, March). Linear hydroelastic analysis of high-speed catamarans and monohulls. *J. Ship Research 43*(1), 48–62.

Hoff, J. R. (2001). Private communications.

Hoff, J. R. (2002). Private communications.

Jensen *et al.*, J. (2000). Report of special task Committee VI.1 on extreme hull girder loading. In H. Ohtsubo and Y. Sumi (Eds.), *Proc. 14th Int. Ship and Offshore Structures Congress*, Amsterdam, pp. 263–320. Elsevier.

Kaplan, P. (1987). Analysis and prediction of flat bottom slamming impact of advanced marine vehicles in waves. In *Int. Shipbuilding Progress*, pp. 44–53.

Kaplan, P. (1991). Structural loads on advanced marine vehicles, including effects of slamming. In *FAST'91, Volume II*, Trondheim, Norway, pp. 781–795.

Kashiwagi, M. (1993). Heave and pitch motions of a catamaran advancing in waves. In *2nd Inter. Conf. on Fast Sea Transportation*, Yokohama, Japan. Dec.

Korobkin, A. (1996). Water impact problems in ship hydrodynamics. In M. Okkusu (Ed.), *Ch. 7 in Advances in marine hydrodynamics*. Computational Mechanics Publications, Southampton, Boston.

Kvålsvold, J. (1994). *Hydrolastic modelling of wetdeck slamming on multihull vessles*. Ph. D. thesis, Department of Marine Hydrodynamics, Norwegian University of Science and Technology, Trondheim.

Kvålsvold, J., O. M. Faltinsen, and J. V. Aarsnes (1995). Effect of structural elasticity on slamming again wetdeck of multihull vessels. In *Proc. PRADS'95*, Korea, pp. 1.684–1.699. The Society of Naval Architects of Korea.

Lamb, H. (1932). *Hydrodynamics*. Reprinted by Dover, New York: Cambridge, England 6th ed. Cambridge University Press.

Langen, I. and R. Sigbjörnsson (1979). Dynamisk analyse av konstruksjoner, tapir, trondheim, norway. Relevant material translated to English lecture notes by Leira, B.J. et al., 1999, Dept. of Marine Structures, NTNU, Trondheim.

Martinussen, K. (2002). Private communications.

Meyerhoff, W. K. (1965). Die berechnung hydroelasticher stösse. *Schiffstecknik 12 60*, 18.

Moan *et al.*, T. (1991). Report of Committee IV.1: Design philosophy. In P. H. Hsu and Y. S. Wu (Eds.), *Proceedings of the 11th Int. Ship and Offshore Structures conference*, China, pp. 575–661. Elsevier applied science.

Molin, B. (1999). On the piston mode in moonpools. In *14th Int. Workshop on Water Waves and FLoating Bodies*, Michigan, USA. Port Huron.

Molland, A. F., J. F. Wellicome, and P. R. Couser (1995). Resistance experiments on a systematic series of high speed displacement catamaran forms: variation of length-displacement ratio and breadth-draught ratio. The Royal Institution of Naval Architects, Southampton.

Morand, H. S. and R. Ohayon (1995). *Fluid structrure interaction*. Wiley.

Newman, J. N. (1977). *Marine hydrodynamics*. Cambridge, USA: MIT Press.

Newman, J. N. (1978). The theory of ship motions. *Advances in Applied Mathematics 18*, 221–282.

Nielsen, F. G. and K. Herfjord (1992). Fps 2000 project 1.1. comparative study. evaluation of results and discussion of practical methods. Technical report, E&P Research Center, Norsk Hydro, Bergen, Norway.

NORDFORSK (1987). The nordic cooperative project. seakeeping performace of ships, assessment of a ship performace in a seaway. Technical report, MARINTEK, Trondheim, Norway.

Ochi, M. K. (1964). Prediction of occurrence and severity of ship slamming at sea. In *Fifth symposium on naval hydrodynamics*, Washington DC: Office of naval research - Department of the Navy, pp. 545–596.

Ogilvie, F. T. (1964). Recent progress toward the understanding and prediction of ship motions. In *Proc. 5th Symp. on Naval Hydrodynamics*, Bergen, Norway, pp. 3–128.

Ogilvie, T. F. and E. O. Tuck (1969). A rational strip-theory of ship motion: Part I. Technical Report Report No. 013, Department of Naval Architecture and Marine Engineering, The University of Michigan.

Ohkusu, M. (1969). On the heaving motion of two circular cylinders on the surface of a fluid. *Reports of Research Institute for Applied Mechnics 17*(58), 167–185.

Ohkusu, M. (1996). Hydrodynamics of ships in waves. In M. Ohkusu (Ed.), *In Advances in Marine Hydrodynamics'*, Boston, pp. 77–131. Computational Mechanics Publications.

Økland, O. D. (2002). *Theoretical and experimental analysis of wetdeck slamming*. Ph. D. thesis, Department of Marine Technology, Norwegian University of Science and Technology, Trondheim.

Økland, O. D. and T. Moan (1998). Prediction of slamming loads and extreme structural response for large twin hull vessels. In *ISOPE'98, Vol. IV*, pp. 229–236.

Økland, O. D., T. Moan, and J. V. Aarsnes (1998). Structural response in large twin hull vessels exposed to severe wetdeck slamming. In *PRADS'98*, Haad, The Netherlands.

Rognebakke, O. F. and O. M. Faltinsen (2002). Coupling of sloshing and ship motions. To be published in J. Ship Research.

Ronæss, M. (2002). *Wave induced motions of two ships advancing on parallel course*. Ph. D. thesis, Department of Marine Hydrodynamics, Norwegian University of Science and Technology, Trondheim.

Ronæss, M. and O. M. Faltinsen (2000). Hydrodynamic forces and motions of two ships advancing on parallel course in waves. In *4th Osaka Colloquium on seakeeping performance of ships*, Japan.

Sagli, G., M. Wu, and T. Moan (1997). Nonlinear wave load effects for design of slender monohull. In *NAV'97*, Sorrento, Italy, pp. 8.3–8.16.

Salvesen, N., E. O. Tuch, and O. M. Faltinsen (1970). Ship motions and sea loads. *Trans. Soc. Nav. Arch. and Marine Engineers 78*(10), 250–287.

Scolan, Y. M. and A. A. Korobkin (2001). Three-dimensional theory of water impact (Part 1. Inverse Wagner Problem). *J. Fluid Mech. 440*, 293–326.

Skjørdal, S. O. (1978). *Wave induced oscillations of ship hulls*. Ph. D. thesis, Department of Marine Hydrodynamics, Norwegian University of Science and Technology, Trondheim.

Spiegel, M. R. (1959). *Theory and problems of vector analysis and an introduction to tensor analysis*. New York: Schaum Publishing Co.

Spiegel, M. R. (1962). *Theory and problems of advanced calculus*. New York: Schaum Publishing Co.

Stansberg, C. T. (2002). Private communications.

Ulstein, T. (1995). *Nonlinear effects of a flexible stern seal bag on cobblestone oscillations of an SES*. Ph. D. thesis, Department of Marine Hydrodynamics, Norwegian University of Science and Technology, Trondheim.

VERES (1999). *VERES program by 2D strip theory for catamaran* (Version 3.23.5 ed.). Trondheim: MARINTEK. User's Manual; Theoretical Manual.

Verhagen, J. H. G. (1967). The impact of a flat plate on a water surface. *J. Ship Research 11*(4), 211–223.

Von Karman, T. (1929). The impact on seaplane floats during landing. In *Technical Note No. 321*, pp. 309–313. National Advisory Committee for Aeronautics.

Wagner, H. (1932). Uber stoss- und gleitvorgange an der oberflache von flussigkeiten. *Zeitschr. Fur Angew. Math. und Mech. 12*(4), 193–235.

Wu, M., J. V. Aarsnes, O. A. Hermundstad, and T. Moan (1996). A practical prediction of wave-induced structural reponse in ships with large wamplitude motion. In P. Hsu and Y. Wu (Eds.), *21st Symp. on Naval Hydrodynamics*, Washington DC, pp. 148–161. Office of Naval Research.

Wu, M. and T. Moan (1996, 2). Linear and nonlinear hydroelastic analysis of high speed vessels. *J. Ship Research 40*(2), 149–163.

Zhao, R. and O. M. Faltinsen (1992). Slamming loads on high-speed vessels. In *19th Symposium on Naval Hydrodynamics*, Korea.

Zhao, R. and O. M. Faltinsen (1993). Water entry of two-dimensional bodies. *J. Fluid Mech. 246*, 593–612.

Zhao, R., O. M. Faltinsen, and J. V. Aarsnes (1996). Water entry of arbitrary two-dimensional sections with and without flow separation. In *21st Symposium on Naval Hydrodynamics*, Trondheim, Norway, pp. 118–133.

Zhao, R., O. M. Faltinsen, and H. Haslum (1997). A simplified non-linear analysis of a high-speed planning craft in calm water. In *Proc. FAST'97*, Sydney, Australia.

Appendix A

Model test information

Some model test information will be given in this Appendix A. The items that are needed in this thesis are presented here and in the main text. More details of the experimental setting can be found in Økland (2002).

A.1 Main particulars of the model

Table A.1 Main particulars of the catamaran model

Overall length	L_{OA}	4.10m
Length between perpendiculars	L_{PP}	3.78m
Beam of the catamaran amidships at waterline	B_{WL}	1.02m
Beam of one hull amidships at waterline	b_{WL}	0.267m
Displacement	∇	246.0kg
Draft at AP	D_{AP}	0.220m
Draft at FP	D_{FP}	0.225m
Wetdeck height above calm water at COG	$d(x)$	0.115m
Vertical COG from base line	VCG	0.335m
Longitudinal COG from bow	LCG	2.468m
Roll radius of gyration about COG	R_{44}	0.372m
Pitch radius of gyration about COG	R_{55}	1.128m
Yaw radius of gyration about COG	R_{66}	1.179m

A.2 Body plan

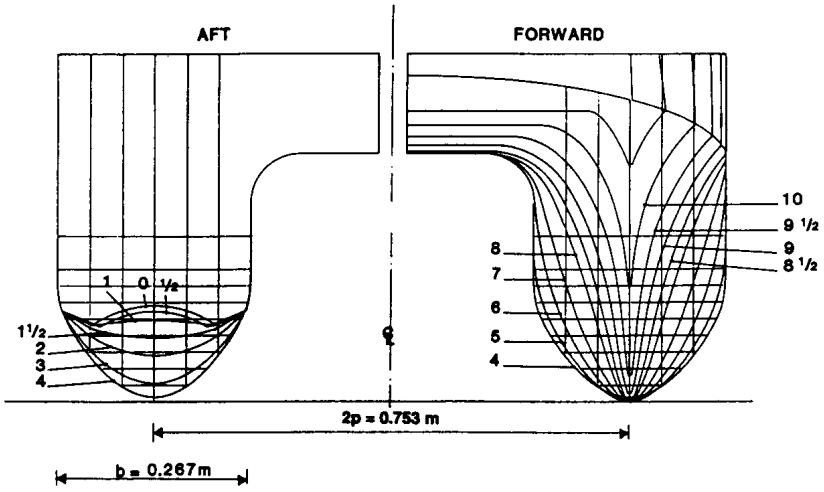

Figure A.1 Body plan of the catamaran model

A.3 Deck geometry

The wetdeck consists of four decks, notated as Deck1, Deck2, Deck3 and Deck4 from bow to stern, as shown in Fig. 2.1. Deck2,3,4 are flat plates $0.34m$ above the base line. Deck1 is flat with forward end $0.39m$ above the base line and aft end $0.34m$ above the base line. The geometrical dimensions of the different plates are shown in Fig. A.2.

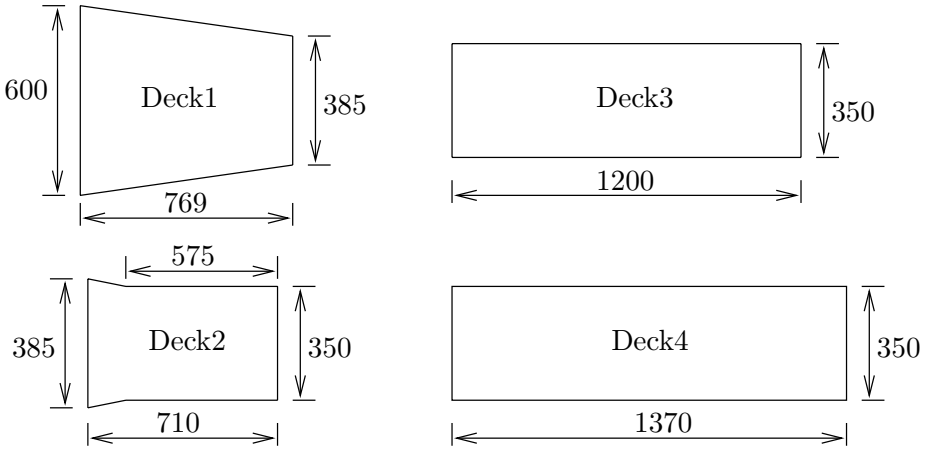

Figure A.2 Geometry of wetdeck parts, Deck1 to Deck4 are the four wetdeck plates from the bow to stern (Fig. 2.1). The length unit is mm.

A.4 Mass distribution of the catamaran model

Table A.2 presents the mass distribution of the catamaran. Some key terms in the table are explained in the following text. Figure A.3 shows the longitudinal distribution of the mass points listed in Table A.2.

Name	Comments
LCG	longitudinal distance of center of gravity from the bow of the catamaran
TCG	y coordinate of center of gravity with $y = 0$ at the center plane of the catamaran
VCG	vertical distance of center of gravity from the base line of the catamaran
SB	Starboard side of the catamaran
PB	Port side of the catamaran
fore	Forward section of the segmented model
mid	Mid section of the segmented model
aft	Aft section of the segmented model
TR+SPR	Connecting transducer and spring between segments
PR	propeller
Suspension	Suspension for wetdeck plates
r_{44}, r_{55}, r_{66}	Except for the bottom line: Local radius of gyration in respectively roll, pitch and yaw for each mass element. Bottom line: Total radii of gyration with respect to COG of the catamaran

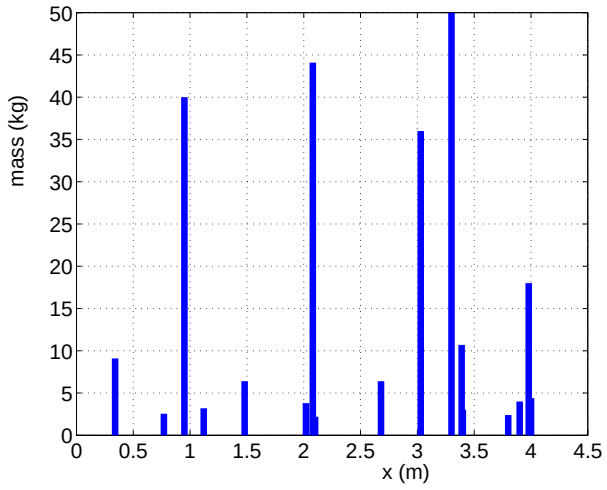

Figure A.3 Mass distribution in the longitudinal direction based on data in Table A.2 with $x = 0$ at the bow.

Table A.2 Mass distribution of the catamaran. The coordinate axes here are parallel with the coordinate system in Fig. 2.3. $x = 0$ refers to the bow of the catamaran.

Component	Mass	LCG	TCG	VCG	r_{44}	r_{55}	r_{66}
Unit	Kg	m	m	m	m	m	m
Hull SB fore	20.000	0.950	0.330	0.250	0.100	0.450	0.550
Hull SB mid	17.000	2.080	0.330	0.250	0.100	0.350	0.450
Hull SB aft	25.000	3.300	0.330	0.250	0.100	0.400	0.500
Hull PS fore	20.000	0.950	-0.330	0.250	0.100	0.450	0.550
Hull PS mid	17.000	2.080	-0.330	0.250	0.100	0.350	0.450
Hull PS aft	25.000	3.300	-0.330	0.250	0.100	0.400	0.500
TR+SPR, SB aft	3.200	2.680	0.335	0.310	0.000	0.000	0.100
TR+SPR, SB fore	3.200	1.480	0.335	0.310	0.000	0.000	0.100
TR+SPR, PS aft	3.200	2.680	-0.335	0.310	0.000	0.000	0.100
TR+SPR, PS fore	3.200	1.480	-0.335	0.310	0.000	0.000	0.100
TR+SPR, deck fore	2.300	0.770	0.000	0.440	0.000	0.000	0.000
TR+SPR, deck mid	2.300	2.080	0.000	0.440	0.000	0.000	0.000
TR+SPR, deck aft	2.300	3.390	0.000	0.440	0.000	0.000	0.000
deck plate fore	9.100	0.340	0.000	0.350	0.100	0.230	0.200
deck plate fore second	3.200	1.120	0.000	0.350	0.100	0.270	0.200
deck plate center	4.800	2.080	0.000	0.350	0.100	0.300	0.300
deck plate aft	5.400	3.390	0.000	0.350	0.100	0.400	0.400
Suspension mid	3.000	2.080	0.000	0.420	0.200	0.400	0.400
Suspension aft	3.000	3.390	0.000	0.420	0.200	0.400	0.400
Motor SB	18.000	3.030	0.450	0.650	0.100	0.000	0.000
Motor PS	18.000	3.030	0.865	0.650	0.100	0.000	0.000
PR+shaft SB	2.000	3.900	0.350	0.000	0.000	0.000	0.000
PR+shaft PS	2.000	3.900	-0.350	0.000	0.000	0.000	0.000
RudderContr.SB	1.200	3.800	0.350	0.400	0.000	0.000	0.000
RudderContr.PS	1.200	3.800	-0.350	0.400	0.000	0.000	0.000
RudderMachine, SB	2.200	4.000	0.350	0.400	0.000	0.000	0.000
RudderMachine, PS	2.200	4.000	-0.350	0.400	0.000	0.000	0.000
MRU	3.800	2.020	-0.210	0.310	0.000	0.000	0.000
Rudder/plastic, SB	0.100	2.100	0.350	0.400	0.000	1.200	1.200
Rudder/plastic, PS	0.100	2.100	-0.350	0.400	0.000	1.200	1.200
Pulsetrigger	3.000	3.400	0.350	0.400	0.000	0.000	0.000
Cables etc.	2.000	2.100	-0.150	0.400	0.300	1.000	1.000
Ballast, SB	9.000	3.980	0.370	0.250	0.000	0.000	0.000
Ballast, PS	9.000	3.980	-0.370	0.250	0.000	0.000	0.000
Entire Model	246.000	2.468	0.000	0.335	0.372	1.128	1.179

A.5 Locations of measurement equipment

The following figures present the positions of measurement equipment. Figure A.4 shows the longitudinal and transverse transducers where global structural loads were measured. Figure A.5 gives the positions of the three different measurement systems for motions and accelerations used in the experiments. Table A.3 gives the positions for the measurement equipment mentioned in Figs. A.4 and A.5. Figure A.6 illustrates the positions of the pin transducers used for slamming force measurement.

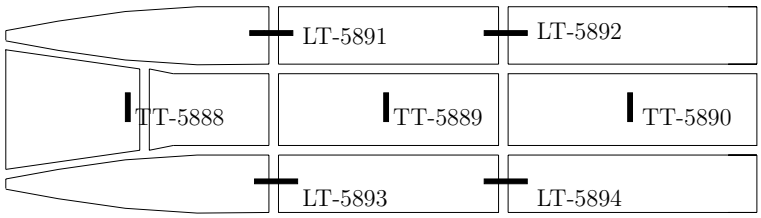

Figure A.4 Location of 5 degree-of-freedom transducers for measurements of global structural loads; LT – Longitudinal Transducer; TT – Transverse Transducer

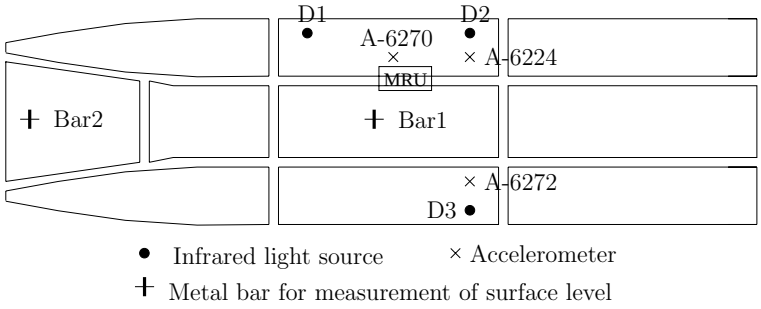

Figure A.5 Locations of measurements of relative vertical motions (Bar1 and Bar2) and the three different measurement systems for body motions and accelerations: MRU, Optical (D1,D2,D3) and Three-Accelerometer system (A-6224,A-6270,A-6272).

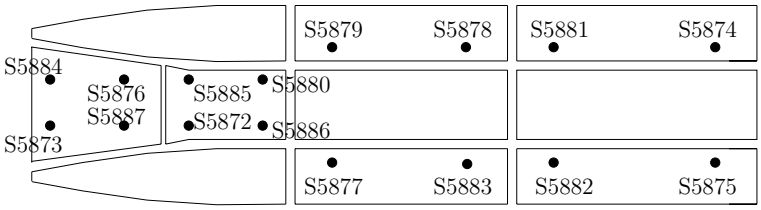

Figure A.6 Locations of pin transducers for measurement of slamming forces.

Table A.3 Positions of instrumentation of the model. x-coordinate is from the bow to stern with $x = 0$ at the bow. y is positive at the starboard side and z is from the base line of the catamaran. 'dof': degrees of freedom; 'tr.': transducer; 'Acc.': acceleration.

No	Component	Code	x [mm]	y [mm]	z [mm]	Figure
1	5 dof force tr.	TT-5888	770			A.4, A.7
2	5 dof force tr.	TT-5889	2080			A.4, A.7
3	5 dof force tr.	TT-5890	3390			A.4, A.7
4	5 dof force tr.	LT-5891	1480	330		A.4, A.7
5	5 dof force tr.	LT-5892	2680	330		A.4, A.7
6	5 dof force tr.	LT-5893	1480	-330		A.4, A.7
7	5 dof force tr.	LT-5894	2680	-330		A.4, A.7
8	Acc. (x,y,z)	A-6224	1930	320	375	A.5
9	Acc. (z)	A-6270	1635	315	377	A.5
10	Acc. (z)	A-6272	1930	-320	377	A.5
11	MRU	MRU	2020	210	305	A.5
12	Optical 1	D1	1760	435	770	A.5
13	Optical 2	D2	2570	470	770	A.5
14	Optical 3	D3	2570	-480	770	A.5
15	Relative motion	Bar1	2165	0	surface	A.5
16	Relative motion	Bar2	35	0	surface	A.5

A.6 Force transducers and elastic steel springs

Two adjacent rigid ship segments are connected longitudinally by five degree of freedom aluminum force transducers and steel springs, as shown in the Fig. 2.1. The same arrangement is used for transverse transducers at the center plane of the catamaran. Figure A.7 and Table A.4 present the detailed geometry and dimensions.

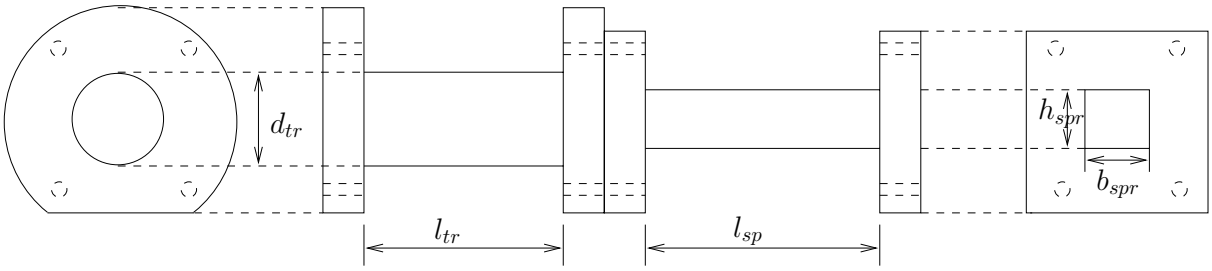

Figure A.7 Five degree freedom force transducer in aluminum connected with steel spring. Subscripts *tr* and *spr* refer to respectively transducer and spring.

Table A.4 Dimensions of longitudinal and transverse springs and force transducers illustrated in Fig. A.4. The names of the items are defined in Fig. A.7.

Type	d_{tr} [mm]	l_{tr} [mm]	h_{spr} [mm]	b_{spr} [mm]	l_{spr} [mm]
Longitudinal	35.0	80.0	18.2	31.0	100.0
Transversal	35.0	80.0	9.0	23.5	180.0

As shown in Table A.4, the spring has a rectangular cross-section with width $b = 0.031m$ and height $h = 0.0182m$. The area moment of inertia of the cross-section about its neutral axis is $I = bh^3/12 = 1.5574 * 10^{-8}m^4$. By using that the modulus of elasticity $E = 2.1 * 10^{11}N/m^2$ for steel and accounting for two hulls, we get $(EI)_{eq} = 2EI = 6.541 * 10^3 Nm^2$. The transducer has a diameter $d = 0.035m$. This gives $I = \pi d^4/64 = 7.3662 * 10^{-8}m^4$. With $E = 6.85 * 10^{10}N/m^2$ for aluminum, we find that $2EI = 1.009 * 10^4 Nm^3$. Since there are two holes in the transducer, we approximately estimated that the effective stiffness of the transducer is only about $60\% \sim 70\%$ of the value obtained without the holes. This finally leads to an equivalent beam between every two rigid bodies in our three-body model, with a stiffness $(EI)_{eq} = 6.541 \cdot 10^3 Nm^2$ and length $L_{eq} = 0.21m$.

A.7 List of tested forward speed cases in head sea

Table A.5 Regular wave tests with self propelled catamaran in head sea

Test No.	T(s)	H(m)	Time Window	$U'(m/s)$	H'(m)	Wetdeck slamming
1101	1.2s	0.03m	18-28s	1.92	0.03164	No
1102	1.0s	0.03m	18-28s	1.92	0.02874	No
1103	1.3s	0.03m	15-27s	1.89	0.02974	No
1104	1.4s	0.03m	14-27s	1.95	0.03560	No
1105	1.5s	0.03m	17-25s	1.97	0.03328	No
1106	1.6s	0.03m	15-26s	1.99	0.03066	No
1107	1.8s	0.03m	14-26s	1.90	0.02840	No
1108	2.0s	0.03m	13-25s	1.90	0.02910	No
1109	2.5s	0.03m	13-21.5s	1.88	0.03070	No
1110	1.3s	0.10m	13-21s	1.90	0.09506	No
1111	1.5s	0.10m	19-27s	1.84	0.10470	Yes (most severe)
1112	1.8s	0.06m	16-28s	1.86	0.05172	Yes (small)
1114	1.8s	0.10m	15-26s	1.80	0.08214	Yes (moderate)
1115	2.0s	0.10m	15-26s	2.00	0.09660	Yes (moderate)

In the table, T means the incident wave period and H is the intended or specified incident wave height. The measured wave heights are different and presented in column H'. U' is the calculated forward speed of the catamaran based on the optical surge measurements during the steady-state conditions. The time window shown in the table is the time period with steady-state response.

Appendix B

Slamming model details

B.1 Slamming model with Kutta condition

B.1.1 General solution of vortex distribution

This part will give detailed derivations of the vortex solution (Eq. (3.90)) for the Kutta condition slamming model.

We will first show that the boundary value problem for the slamming model with Kutta condition is equivalent to the 2D unsteady lifting problem of a thin foil in an infinite fluid. Kutta condition implies that the fluid velocity is finite at the trailing edge in the lifting problem and at the aft deck-free surface intersection point in the slamming problem. The mathematical equivalence between these two different physical problems was also shown by Ulstein (1995). However due to the completeness of the derivation of the solution and to be consistent with our notation and coordinate system, it is of advantage to show this equivalence here.

We then start with the 2D unsteady linearized lifting problem of a thin foil in an infinite fluid. Length dimensions will be made nondimensional with respect to c where $2c$ is the chord length of the foil. A Cartesian coordinate system (x, z) is introduced. There is an ambient fluid velocity of magnitude U along positive x-axis. The body boundary condition is transferred to the cut $-1 \leq x \leq 1$ on $z = 0$. This is consistent with linear thin foil theory . An unsteady wake is mathematically located between $x = 1$ and $x = 1 + Ut$ on $z = 0$. This is shown by Newman (1977) and follows by that the free vorticity in the wake is by linear theory convected with the velocity U. We will also later in the text show this. A vortex distribution with density $\gamma(x, t)$ along $-1 \leq x \leq 1 + Ut$ on $z = 0$ is used to represent the flow. The velocity potential caused by the presence of the foil is called ϕ. There is a zero pressure jump across the wake. This can mathematically be expressed as

$$\frac{\partial \phi^+}{\partial t} + U\frac{\partial \phi^+}{\partial x} = \frac{\partial \phi^-}{\partial t} + U\frac{\partial \phi^-}{\partial x} \qquad \text{on } 1 < x < 1 + Ut,\ z = 0 \tag{B.1}$$

Here the superscripts + and − refer to respectively the upper and lower side of the wake. Since $\phi^+ - \phi^-$ is directly related to circulation, there has to be a jump in the velocity potential across the wake. It follows by the vortex distribution (See Newman (1977)) that

$$\frac{\partial \phi^+}{\partial x} = -\frac{\partial \phi^-}{\partial x} \qquad \text{on } 1 < x < 1 + Ut,\ z = 0 \tag{B.2}$$

The vortex distribution implies that there is no horizontal velocity induced by ϕ along $z = 0$ outside $-1 < x < 1 + Ut$. This means that the velocity potential is constant along $z = 0$ outside $-1 < x < 1 + Ut$. This constant can be freely set as zero. By integrating Eq. (B.2) from $x = 1 + Ut$, $z = 0$ to x, we get

$$\phi^+ = -\phi^- \qquad \text{on } 1 < x < 1 + Ut,\ z = 0 \tag{B.3}$$

This gives by using Eq. (B.1) that

$$\frac{\partial \phi^+}{\partial t} + U\frac{\partial \phi^+}{\partial x} = 0 \qquad \text{on } 1 < x < 1 + Ut,\ z = 0 \tag{B.4}$$

If we now make the analogy to our slamming problem and define the wetted part of the deck to be between $-1 < x < 1$ and consider the fluid domain $z < 0$, Eq. (B.4) is then our dynamic free surface condition. In addition both the unsteady lifting problem and the slamming problem require a Kutta condition at $x = 1$. We can then directly use the solution of the unsteady lifting problem as presented by Newman (1977). Since we use a different coordinate system and Newman (1977) did not give all details in the derivation, we will elaborate more on the derivation of this solution.

By using the relationship

$$\frac{\partial \phi_\pm}{\partial x} = \mp\frac{1}{2}\gamma(x,t) \qquad \text{on } -1 < x < 1 + Ut,\ z = 0 \tag{B.5}$$

Eq. (B.1) can be written as

$$\frac{\partial \gamma}{\partial t} + U\frac{\partial \gamma}{\partial x} = 0 \tag{B.6}$$

The solution of this differential equation is simply

$$\gamma(x,t) = \gamma(x - Ut) \qquad \text{in the wake} \tag{B.7}$$

It means what already has been mentioned that the vorticity in the wake is convected with the velocity U and that the wake is between $1 < x < 1 + Ut$ on $z = 0$.

The body boundary condition on the wetted length (Newman (1977)) leads to

$$v(x,0,t) \equiv v_0(x,t), \qquad -1 < x < 1 \tag{B.8}$$

where $v_0(x,t)$ means the relative velocity component normal to the wetdeck.

We can start the derivation from Eq. (3.89). The integrals in Eq. (3.89) can be divided into two parts: one over the wetdeck and the other over the 'wake'. However the 'wake' in the slamming problem is not a physical wake, but a consequence of the dynamic free surface condition. This gives

$$v_0(x,t) + \frac{1}{2\pi}\int_1^\infty \frac{\gamma(\xi - Ut)}{\xi - x}d\xi = -\frac{1}{2\pi}\fint_{-1}^1 \frac{\gamma(\xi,t)}{\xi - x}d\xi \qquad \text{where } -1 < x < 1 \tag{B.9}$$

This is a singular integral equation for the vortex strength. It is identical to Eq. (3.51) except that the integral on the left hand side of Eq. (B.9) is unknown. This can later be decided by applying Kutta condition.

The general solution of Eq. (3.51) is given as (Eqs. (73-77) on pp.184 Newman (1977))

$$\gamma(x,t) = \frac{2}{\pi}\frac{1}{(1-x^2)^{\frac{1}{2}}}\left\{\fint_{-1}^1 \frac{v_+(\xi,t)(1-\xi^2)^{\frac{1}{2}}}{\xi - x}d\xi + \frac{\Gamma}{2}\right\} \tag{B.10}$$

Here $\Gamma(t) = \int_{-1}^1 \gamma(x,t)dx$.

Substituting Eq. (B.9) gives

$$\gamma(x,t) = \frac{2}{\pi}\frac{1}{(1-x^2)^{\frac{1}{2}}}\left\{\fint_{-1}^1 \left(v_0(\xi,t) + \frac{1}{2\pi}\int_1^\infty \frac{\gamma(\xi' - Ut)}{\xi' - \xi}d\xi'\right)\frac{(1-\xi^2)^{\frac{1}{2}}}{\xi - x}d\xi + \frac{\Gamma}{2}\right\} \tag{B.11}$$

The double integral in Eq. (B.11) can be reduced by interchanging the order of integration, using partial fractions and Hilbert transforms. The following gives the details.

We first introduce the so-called Hilbert transforms $H_n(x)$, defined as

$$H_n(x) = \fint_{-1}^1 \frac{\xi^n\, d\xi}{(\xi - x)(1-\xi^2)^{\frac{1}{2}}} \tag{B.12}$$

Since $(1-\xi^2)^{-1/2}$ is a homogeneous solution of the integral equation expressed in Eq. (3.51), we get

$$H_0(x) = \fint_{-1}^1 \frac{d\xi}{(\xi - x)(1-\xi^2)^{\frac{1}{2}}} = 0 \tag{B.13}$$

For $n \geq 1$, a recursion formula gives

$$H_n(x) = I_{n-1} + xH_{n-1}(x) \tag{B.14}$$

where

$$I_n = \int_{-1}^1 \frac{x^n}{(1-x^2)^{\frac{1}{2}}} = \begin{cases} \pi\frac{1\cdot3\cdot5\cdot\ldots\cdot(n-1)}{2\cdot4\cdot6\cdot\ldots\cdot(n)}, & n \text{ even}, \\ 0, & \text{otherwise.} \end{cases} \tag{B.15}$$

This implies for instance that $H_1(x) = \pi$, $H_2(x) = \pi x$ and $H_3(x) = \pi/2 + \pi x^2$. So far only $-1 < x < 1$ is considered. However in Eq. (B.11) the integration variable ξ' is outside of the wetted part of the deck. So it is necessary to evaluate the resulting Hilbert transforms for values of x outside of ± 1. The generalization can be easily done by replacing x by a complex variable $z' = x + iz$ in Eq. (B.12). The recursion formula Eq. (B.14) remains valid in this case, so it is necessary only to consider the generalization of Eq. (B.13) for complex z'. It takes the form

$$H_0(z') = \int_{-1}^{1} \frac{d\xi}{(\xi - z')(1-\xi^2)^{\frac{1}{2}}} = 0 \tag{B.16}$$

This gives consistent with Newman's definition of branches (See Section 3.5.4, Eq. (3.75))

$$H_0 = \mp\pi(x^2-1)^{-\frac{1}{2}}, \qquad \begin{matrix} x > 1, \\ x < -1. \end{matrix} \tag{B.17}$$

Here the case of $x > 1$ is of interest. We get for $x > 1$ that

$$\begin{aligned} H_1(x) &= I_0 + xH_0(x) = \pi - \pi x(x^2-1)^{-\frac{1}{2}} \\ H_2(x) &= I_1 + xH_1(x) = \pi x - \pi x^2(x^2-1)^{-\frac{1}{2}} \end{aligned} \tag{B.18}$$

The following partial fraction relationship will be used

$$\frac{1}{(\xi - x)(\xi' - \xi)} = \Big(\frac{1}{\xi - x} + \frac{1}{\xi' - \xi}\Big)\frac{1}{\xi' - x} \tag{B.19}$$

Now we are ready to simplify the second integral in the brackets of Eq. (B.11). It follows that

$$\begin{aligned} & \fint_{-1}^{1} \frac{(1-\xi^2)^{\frac{1}{2}}}{\xi - x} d\xi \cdot \frac{1}{2\pi} \int_{1}^{\infty} \frac{\gamma(\xi' - Ut)}{\xi' - \xi} d\xi' \\ &= \frac{1}{2\pi} \int_{1}^{\infty} d\xi' \fint_{-1}^{1} d\xi \frac{(1-\xi^2)^{\frac{1}{2}} \gamma(\xi' - Ut)}{(\xi - x)(\xi' - \xi)} \\ &= \frac{1}{2\pi} \int_{1}^{\infty} d\xi' \frac{\gamma(\xi' - Ut)}{\xi' - x} \fint_{-1}^{1} d\xi \Big[\underbrace{\frac{(1-\xi^2)^{\frac{1}{2}}}{\xi - x}}_{\text{part1}} + \underbrace{\frac{(1-\xi^2)^{\frac{1}{2}}}{\xi' - \xi}}_{\text{part2}} \Big] \end{aligned} \tag{B.20}$$

By using Hilbert transforms, the 'part1' integration gives

$$\begin{aligned} & \fint_{-1}^{1} \frac{(1-\xi^2)^{\frac{1}{2}}}{\xi - x} d\xi \qquad\qquad \text{where } -1 \le x \le 1 \\ &= \fint_{-1}^{1} \frac{1-\xi^2}{(\xi - x)(1-\xi^2)^{\frac{1}{2}}} d\xi \\ &= H_0(x) - H_2(x) = -\pi x \end{aligned} \tag{B.21}$$

Further the 'part2' integration in Eq. (B.20) gives by using Eqs. (B.18) that

$$\begin{aligned}\fint_{-1}^{1}\frac{(1-\xi^2)^{\frac{1}{2}}}{\xi'-\xi}d\xi &= -\fint_{-1}^{1}\frac{(1-\xi^2)^{\frac{1}{2}}}{\xi-\xi'}d\xi \\ &= -\big(H_0(\xi')-H_2(\xi')\big) \\ &= \xi'\pi-\pi(\xi'^2-1)^{\frac{1}{2}} \qquad \text{for } \xi'>1\end{aligned} \tag{B.22}$$

By adding the results due to 'part1' and 'part2', Eq. (B.20) can be expressed as

$$\begin{aligned}&\fint_{-1}^{1}\frac{(1-\xi^2)^{\frac{1}{2}}}{\xi-x}d\xi\cdot\frac{1}{2\pi}\int_{1}^{\infty}\frac{\gamma(\xi'-Ut)}{\xi'-\xi}d\xi' \\ &=\frac{1}{2\pi}\int_{1}^{\infty}\frac{\gamma(\xi'-Ut)}{\xi'-x}\Big[\underbrace{\pi(\xi'-x)}_{\text{parta}}\underbrace{-\pi(\xi'^2-1)^{\frac{1}{2}}}_{\text{partb}}\Big]d\xi'\end{aligned} \tag{B.23}$$

With the relationship given in Eqs. (B.7) and that the total circulation about the foil plus its wake by Kelvin's theorem is equal to zero, *i.e.* $\Gamma(t)+\int_1^\infty\gamma(x,t)dx=0$, integration related with 'parta' in Eq. (B.23) gives

$$\frac{1}{2}\int_{1}^{\infty}\gamma(\xi'-Ut)\,d\xi'=\frac{1}{2}\int_{1}^{\infty}\gamma(\xi',t)\,d\xi'=-\frac{\Gamma(t)}{2} \tag{B.24}$$

This will cancel the $\Gamma/2$ term in the largest brackets in Eq. (B.11).

So only 'partb' in Eq. (B.23) contributes to the final result of the γ-expression given by Eq. (B.11). This means

$$\gamma(x,t)=\frac{2}{\pi}\frac{1}{(1-x^2)^{\frac{1}{2}}}\left\{\fint_{-1}^{1}\frac{(1-\xi^2)^{\frac{1}{2}}}{\xi-x}v_0(\xi,t)d\xi-\frac{1}{2}\int_{1}^{\infty}\frac{(\xi^2-1)^{\frac{1}{2}}}{\xi-x}\gamma(\xi-Ut)d\xi\right\} \tag{B.25}$$

Dimensionalizing Eq. (B.25) in the X-Z coordinate system leads to Eq. (3.90).

B.1.2 Solution of vortex distribution with linear approximation of relative impact velocity

When $v_0(\xi,t)$ is expressed as

$$v_0(\xi,t)=V_1+V_2\xi \tag{B.26}$$

the first integration in Eq. (B.25) can be simplified as

$$\begin{aligned}\fint_{-1}^{1}\frac{(1-\xi^2)^{\frac{1}{2}}}{\xi-x}v_0(\xi,t)d\xi &= \fint_{-1}^{1}\frac{(1-\xi^2)(V_1+V_2\xi)}{(\xi-x)(1-\xi^2)^{\frac{1}{2}}}d\xi \\ &= V_1H_0(\xi)+V_2H_1(\xi)-V_1H_2(\xi)-V_2H_3(\xi) \\ &= -V_1\pi x+V_2(\frac{\pi}{2}-\pi x^2)\end{aligned} \tag{B.27}$$

by using real Hilbert transforms.

The final expression of $\gamma(x,t)$ is then

$$\gamma(x,t) = \frac{2}{(1-x^2)^{\frac{1}{2}}}\Big[-V_1 x + V_2(\frac{1}{2} - x^2)\Big] - \frac{1}{\pi(1-x^2)^{\frac{1}{2}}}\int_1^\infty \frac{(\xi^2-1)^{\frac{1}{2}}}{\xi - x}\gamma(\xi - Ut)d\xi \tag{B.28}$$

Dimensionalizing Eq. (B.28) in X-Z coordinate system leads to Eq. (3.91).

B.1.3 Derivation of velocity potential

The velocity potential on the wetted part of the deck will be derived in the following text. By using that $\partial\phi(x,t)/\partial x = \gamma(x,t)/2$, that $\phi = 0$ at $X = -c$ and integrating the vorticity expressed by Eq. (3.91) along the wetted part gives the velocity potential as

$$\begin{aligned}\phi(X_1\,,t) &= \int_{-c}^{X_1}\Bigg[\frac{1}{2(c^2-X^2)^{\frac{1}{2}}}\Bigg\{\underbrace{[-2V_1X + V_2(c^2-2X^2)]}\\ &\qquad \underbrace{-\frac{1}{\pi}\int_c^\infty \frac{(\xi^2-c^2)^{\frac{1}{2}}}{\xi - X}\gamma(\xi - Ut)\,d\xi}\Bigg\}\Bigg]dX \\ &= \phi_1 + \phi_2\end{aligned} \tag{B.29}$$

Here the integrated results associated with the first and second horizontal braces are denoted as ϕ_1 and ϕ_2. It is easily shown that ϕ_1 is exactly the same velocity potential as in Eq. (3.17) when Kutta condition is not applied. Further ϕ_2 can be expressed as

$$\phi_2(X_1\,,t) = -\frac{1}{2\pi}\int_{-c}^{X_1}\Bigg\{\frac{1}{(c^2-X^2)^{\frac{1}{2}}}\int_c^\infty \frac{(\xi^2-c^2)^{\frac{1}{2}}}{\xi - X}\gamma(\xi - Ut)\,d\xi\Bigg\}dX \tag{B.30}$$

$$= -\frac{1}{2\pi}\int_c^\infty (\xi^2-c^2)^{\frac{1}{2}}\gamma(\xi - Ut)\left\{\int_{-c}^{X_1}\frac{1}{(c^2-X^2)^{\frac{1}{2}}(\xi - X)}\,dX\right\}d\xi \tag{B.31}$$

Equation (B.31) follows from Eq. (B.30) by interchanging integration order. The integration in the brackets in Eq. (B.31) can then be evaluated first. Here $\xi > c$ and $-c < X_1\,, X < c$. Together with $X = c\cos\theta$ and $X_1 = c\cos\theta_1$, we have

$$\int_{-c}^{X_1}\frac{dX}{(c^2-X^2)^{\frac{1}{2}}(\xi - X)} = \int_{\theta_1}^{\pi}\frac{d\theta}{\xi - c\cos\theta} \tag{B.32}$$

$$= \left[\frac{2}{\sqrt{(\xi-c)(\xi+c)}}\arctan\frac{(\xi+c)\tan\frac{\theta}{2}}{\sqrt{(\xi-c)(\xi+c)}}\right]_{\theta_1}^{\pi}$$

$$= \frac{1}{\sqrt{\xi^2-c^2}}\Big(\pi - 2\arctan\Big(\sqrt{\frac{\xi+c}{\xi-c}}\tan\frac{\theta_1}{2}\Big)\Big) \tag{B.33}$$

Further by substituting Eq. (B.33) in Eq. (B.31), combining the results of ϕ_1 and taking into account that $\gamma(X_1\,,t)$ is zero when $c + Ut < X_1 < \infty$, we get the final expression of the velocity

potential as Eq. (3.92). For easy reference in the following derivations, it is also presented here as

$$\phi(X_1\,,t) = \underbrace{V_1\sqrt{c^2-X_1^2}+\frac{1}{2}V_2X_1\sqrt{c^2-X_1^2}}_{\phi_1}$$
$$\underbrace{-\frac{1}{2\pi}\int_c^{c+Ut}\gamma(\xi-Ut)\left[\pi-2\arctan\Big(\sqrt{\frac{\xi+c}{\xi-c}}\tan\frac{\theta_1}{2}\Big)\right]d\xi}_{\phi_2}$$
$$\text{for}\quad -c<X_1<c,\quad Z=0_- \tag{B.34}$$

with $\theta_1 = \arccos(\frac{X_1}{c(t)})$.

B.1.4 Derivation of vertical force and pitch moment

Consistent with the development of the Kutta condition model, the pressure should also include the spatial derivative term, *i.e.* $p = -\frac{\partial\phi}{\partial t} - \rho U\frac{\partial\phi}{\partial x}$. The vertical impact force F_3 can then be expressed as

$$\begin{aligned}F_3 &= B\int_{-c}^{c}(-pn_3)dX_1 = B\int_{-c}^{c}pdX_1\\ &= \underbrace{B\int_{-c}^{c}(-\rho\frac{\partial\phi_1}{\partial t})dX_1}_{\text{F3\_part1}} + \underbrace{B\int_{-c}^{c}(-\rho\frac{\partial\phi_2}{\partial t})dX_1}_{\text{F3\_part2}} + \underbrace{B\int_{-c}^{c}(-\rho U\frac{\partial\phi}{\partial X_1})dX_1}_{\text{F3\_part3}}\end{aligned} \tag{B.35}$$

Here ϕ_1, ϕ_2 and ϕ are defined in Eq. (B.34). It can easily be shown that the 'F3_part1' is the same as the vertical impact force when Kutta condition is not applied (Eq. (3.20)), *i.e.*

$$\text{F3\_part1} = B\int_{-c}^{c}(-\rho\frac{\partial\phi_1}{\partial t})\,dX_1 = -\frac{\partial}{\partial t}\Big(\frac{1}{2}\rho\pi c^2V_1\Big)\,B \tag{B.36}$$

The 'F3_part3' can be simplified by expressing the tangential velocity on the wetted deck in terms of γ and by using Kelvin's theorem to express the circulation $\Gamma(t)$. This means

$$\begin{aligned}\text{F3\_part3} &= B\int_{-c}^{c}(-\rho U\frac{\partial\phi}{\partial X_1})\,dX_1 = B\int_{-c}^{c}\Big(-\rho U\frac{\gamma(X_1,t)}{2}\Big)\,dX_1\\ &= -\frac{1}{2}\rho U\,\Gamma(t)\,B = \frac{1}{2}\rho U\,B\int_c^{c+Ut}\gamma(\xi-Ut)\,d\xi\end{aligned} \tag{B.37}$$

The 'F3_part2' in Eq. (B.35) requires a more lengthy derivation. By noting that γ, ξ, c and θ_1 are all time dependent parameters, it follows that $\partial\phi_2/\partial t$ can be expressed in terms of the

following three parts, *i.e.*

$$\begin{aligned}\frac{\partial\phi_2(X_1\,,t)}{\partial t} &= -\frac{1}{2\pi}\int_c^{c+Ut}\frac{\partial\gamma(\xi-Ut)}{\partial t}\left[\pi-2\arctan\Big(\sqrt{\frac{\xi+c}{\xi-c}}\tan\frac{\theta_1}{2}\Big)\right]d\xi\\ &\quad-\frac{1}{2\pi}\int_c^{c+Ut}\gamma(\xi-Ut)\left(\frac{\partial}{\partial t}\left[\pi-2\arctan\Big(\sqrt{\frac{\xi+c}{\xi-c}}\tan\frac{\theta_1}{2}\Big)\right]\right)d\xi\\ &\quad-\frac{1}{2\pi}\left(f(\gamma,c,U,\theta_1,\xi,t)\,\Big|_{\xi=c}\,\frac{dc}{dt}-f(\gamma,c,U,\theta_1,\xi,t)\,\Big|_{\xi=c+Ut}\,\frac{d(c+Ut)}{dt}\right)\\ &= \text{Parta}+\text{Partb}+\text{Partc}\end{aligned}\tag{B.38}$$

In 'Partc' in Eq. (B.38), the integrand $\gamma(\xi-Ut)\left[\pi-2\arctan\Big(\sqrt{\frac{\xi+c}{\xi-c}}\tan\frac{\theta_1}{2}\Big)\right]$ in the integral expression for ϕ_2 is notated as $f(\gamma,c,U,\theta_1,\xi,t)$. 'Partc' is the consequence of the time derivative of an integral where the lower and upper integration limits are time variables (*e.g.* Spiegel (1962)). Due to that the big square-bracket in $f(\gamma,c,U,\theta_1,\xi,t)$ is zero at $\xi=c$ and $\gamma(\xi-Ut)$ is zero at $\xi=c+Ut$, 'Partc' does not contribute.

Further in the integral in 'Partb', both c and θ_1 must be differentiated with respect time t, *i.e.* $\frac{\partial}{\partial t}=\frac{\partial c}{\partial t}\frac{\partial}{\partial c}+\frac{\partial\theta_1}{\partial t}\frac{\partial}{\partial\theta_1}$ with $\frac{\partial\theta_1}{\partial t}=\frac{\partial c}{\partial t}\frac{\cos\theta_1}{c\sin\theta_1}$. This gives finally

$$\text{Partb}=\frac{1}{2\pi}\frac{\partial c}{\partial t}\frac{1}{c\sin\theta_1}\int_c^{c+Ut}\frac{c+\xi\cos\theta_1}{\sqrt{\xi^2-c^2}}\,\gamma(\xi-Ut)\,d\xi\tag{B.39}$$

The time derivative of γ in 'Parta' can be related to the spatial derivative $\partial\gamma/\partial\xi$ by using Eq. (B.6). Then by doing a partial integration and accounting for that the integral vanishes at $\xi=c$ and $c+Ut$, 'Parta' can finally be simplified as

$$\text{Parta}=-\frac{U}{2\pi}c\sin\theta_1\int_c^{c+Ut}\frac{1}{(\xi-c\cos\theta_1)\sqrt{\xi^2-c^2}}\,\gamma(\xi-Ut)\,d\xi\tag{B.40}$$

Based on above derivations, Eq. (B.38) can be expressed as

$$\begin{aligned}\frac{\partial\phi_2(X_1\,,t)}{\partial t} &= \frac{1}{2\pi}\frac{\partial c}{\partial t}\frac{1}{c\sin\theta_1}\int_c^{c+Ut}\frac{c+\xi\cos\theta_1}{\sqrt{\xi^2-c^2}}\,\gamma(\xi-Ut)\,d\xi\\ &\quad-\frac{U}{2\pi}c\sin\theta_1\int_c^{c+Ut}\frac{1}{(\xi-c\cos\theta_1)\sqrt{\xi^2-c^2}}\,\gamma(\xi-Ut)\,d\xi\end{aligned}\tag{B.41}$$

The 'F3_part2' in Eq. (B.35) can then be found by integrating Eq. (B.41) with respect to X. By interchanging integration order, introducing $X_1=c\cos\theta_1$ and noting that

$$\int_0^{\pi}\frac{(\sin\theta_1)^2}{\xi-c\cos\theta_1}=\frac{\pi}{c}\left[\xi-\sqrt{\xi^2-c^2}\right]\qquad\text{for }\xi>c\tag{B.42}$$

it follows that

$$\begin{aligned}\text{F3\_part2} = &-\frac{\rho c}{2}\frac{\partial c}{\partial t}\,B\int_c^{c+Ut}\frac{\gamma(\xi-Ut)}{\sqrt{\xi^2-c^2}}\,d\xi \\ &+\frac{\rho U}{2}\,B\int_c^{c+Ut}\Big(\frac{\xi}{\sqrt{\xi^2-c^2}}-1\Big)\,\gamma(\xi-Ut)\,d\xi \end{aligned} \tag{B.43}$$

Summing up 'F3_part1' in Eq. (B.36), 'F3_part2' in Eq. (B.43) and 'F3_part3' in Eq. (B.37) gives the final result of vertical impact force on the wetted part as Eq. (3.93), *i.e.*

$$\begin{aligned} F_3 \;=\; &-\rho\pi c\frac{\partial c}{\partial t}V_1 B-\frac{1}{2}\rho\pi c^2\frac{\partial V_1}{\partial t}B \\ &-\frac{1}{2}\rho c\frac{\partial c}{\partial t}B\int_c^{c+Ut}\frac{\gamma(\xi-Ut)}{\sqrt{\xi^2-c^2}}d\xi \\ &+\frac{1}{2}\rho U B\int_c^{c+Ut}\frac{\xi}{\sqrt{\xi^2-c^2}}\gamma(\xi-Ut)d\xi \end{aligned} \tag{B.44}$$

The pitch moment F_5 about $X=0$ can be expressed as $F_5=-B\int_{-c}^{c}(l+X)p\,dX$. By using interchanging order of integration, applying real and complex Hilbert transforms, integrating term by term and noting that

$$\int_0^{\pi}\frac{(\sin\theta_1)^2\cos\theta_1}{\xi-c\cos\theta_1}=\frac{\pi}{2c^3}\left(\xi-\sqrt{\xi^2-c^2}\right)^2 \qquad \text{for } \xi>c \tag{B.45}$$

we can in a similar way as in deriving F_3 derive the expression for F_5 given by Eq. (3.94).

B.2 Numerical implementation of impact loads in the equations of motions

The terms that are explicitly proportional to accelerations $\ddot{\eta_3}^1, \ddot{\eta_5}^1$, velocities $\dot{\eta_3}^1, \dot{\eta_5}^1$ and motions η_3^1, η_5^1 in the vertical slamming force F_3 and pitch moment F_5 for the different slamming models (See Chapter 3) are moved to the left hand side of the equations of motions and included in the mass, damping and restoring coefficients of the dynamic system (Eq. 2.1). Here the superscript 1 refers to the forward segment of our three-body model, because the wetdeck slamming only happens in the forward ship segment in cases studied in this thesis. Since these terms are different from previously defined coefficients, they are denoted as a'_{ij}, b'_{ij} and k'_{ij}. The non-zero

terms are as follows

$$
\begin{aligned}
a'_{33} &= \frac{1}{2}\rho\pi c^2\, B \\
a'_{35} &= a'_{53} = -l \cdot a'_{33} \\
a'_{55} &= (l^2 + \frac{c^2}{8}) \cdot a'_{33} \qquad \text{(B.46)} \\
b'_{33} &= \rho\pi c \frac{\partial c}{\partial t}\, B \\
b'_{35} &= -(U + \frac{\partial l}{\partial t}) \cdot a'_{33} - l \cdot b'_{33} \\
b'_{53} &= -\frac{\partial l}{\partial t} \cdot a'_{33} - l \cdot b'_{33} \\
b'_{55} &= l\,(U + 2\frac{\partial l}{\partial t}) \cdot a'_{33} + (l^2 + \frac{c^2}{4}) \cdot b'_{33} \qquad \text{(B.47)} \\
k'_{35} &= -U \cdot b'_{33} \\
k'_{55} &= -U \cdot b'_{53} \qquad \text{(B.48)}
\end{aligned}
$$

Here l is the mid x-coordinate of the wetted length, as defined in Chapter 3. The coefficients presented above are applicable for all the slamming models in Chapter 3. When dealing with the slamming model with Fourier expansion of V_R, time derivatives of expressions with Bessel functions J_n of the first kind are needed. It is then used that

$$
\begin{aligned}
J'_0(z) &= -J_1(z) \\
J'_n(z) &= \frac{1}{2}\big[J_{n-1}(z) - J_{n+1}(z)\big] \qquad \text{for } n \geq 1 \qquad \text{(B.49)}
\end{aligned}
$$

This procedure improves the numerical stability in the time integration of the equations of motions.

Appendix C

Flow chart in numerical model

Figure C.1 illustrates briefly the flow chart of the numerical model. The blocks surrounded by the dashed lines are used when the Modal based method (See Section 5.4.2) is applied in solving the dynamic equations. The blocks with the dashed-dotted lines are activated when the Kutta conditions are accounted for. It should be noted that wetted length can be decided either by Von Karman method or Wagner based method (See Chapter 3). When Wagner based method is applied, the time steps are determined by prescribed change of the wetted length (Section 3.4).

In the figure, some abbreviations are used for easy expression. In details 'Hydro.' represents hydrodynamic and hydrostatic; 'seg.' for segment; 'sys.' for system; 'dyn.' for 'dynamic'; 'Rel.' for 'Relative vertical'; 'cond.' for condition and 'Coord.' for coordinate. Further 'FK' means Froude Krylov, 'HS' for 'hydrostatic', 'VSF' for vertical shear force and 'VBM' for 'vertical bending moment'.

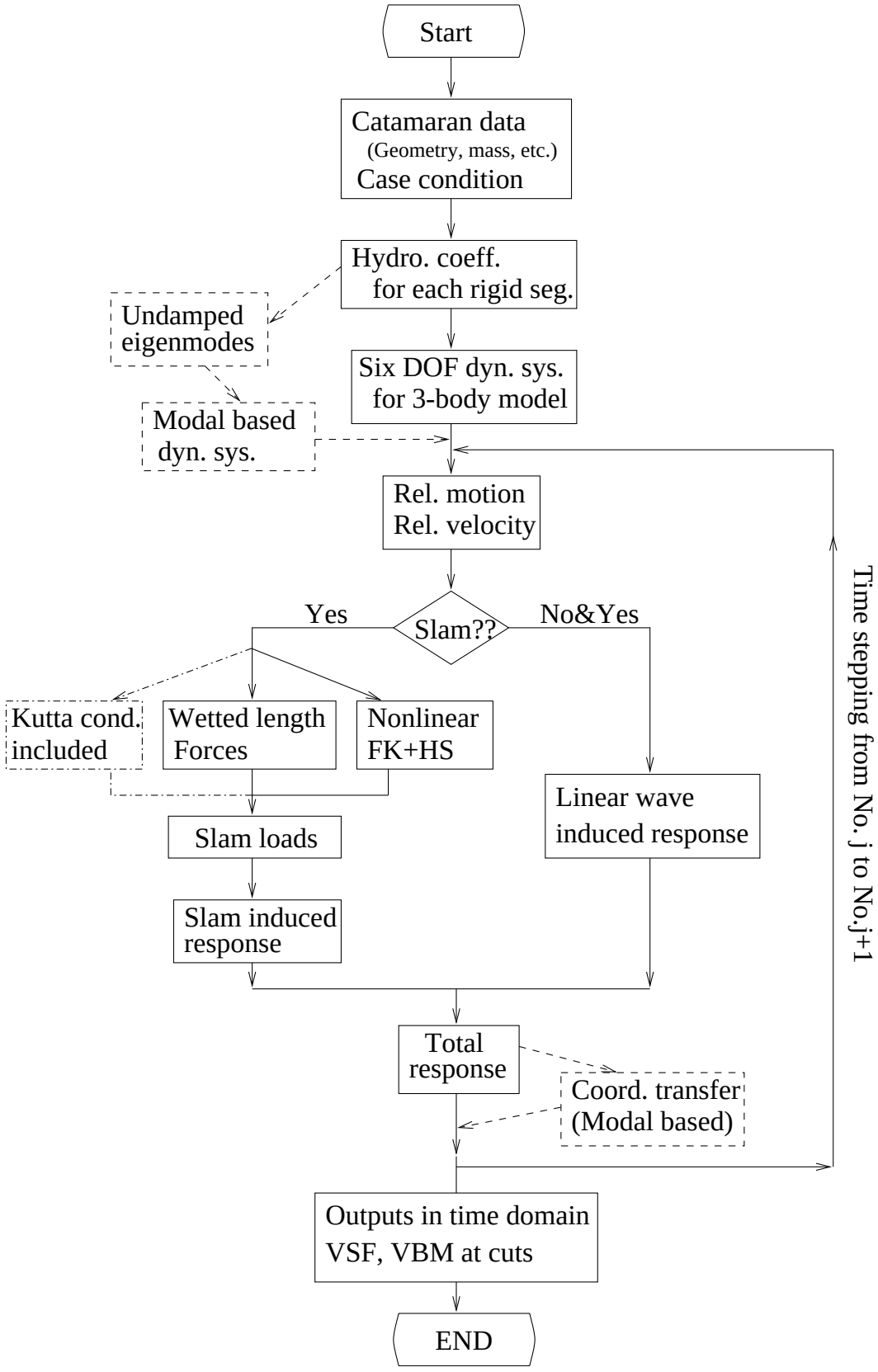

Figure C.1 Flow chart of the numerical model